Lifting the fog off fuel mist explosions : a new procedure to determine the ignitability and explosivity of mist releases

Stephanie El-Zahlanieh

▶ **To cite this version:**

Stephanie El-Zahlanieh. Lifting the fog off fuel mist explosions : a new procedure to determine the ignitability and explosivity of mist releases. Reactive fluid environment. Université de Lorraine, 2022. English. NNT : 2022LORR0280 . tel-04221814

HAL Id: tel-04221814
https://theses.hal.science/tel-04221814

Submitted on 28 Sep 2023

HAL is a multi-disciplinary open access archive for the deposit and dissemination of scientific research documents, whether they are published or not. The documents may come from teaching and research institutions in France or abroad, or from public or private research centers.

L'archive ouverte pluridisciplinaire **HAL**, est destinée au dépôt et à la diffusion de documents scientifiques de niveau recherche, publiés ou non, émanant des établissements d'enseignement et de recherche français ou étrangers, des laboratoires publics ou privés.

UNIVERSITÉ DE LORRAINE | BIBLIOTHÈQUES UNIVERSITAIRES

AVERTISSEMENT

Ce document est le fruit d'un long travail approuvé par le jury de soutenance et mis à disposition de l'ensemble de la communauté universitaire élargie.

Il est soumis à la propriété intellectuelle de l'auteur. Ceci implique une obligation de citation et de référencement lors de l'utilisation de ce document.

D'autre part, toute contrefaçon, plagiat, reproduction illicite encourt une poursuite pénale.

Contact bibliothèque : ddoc-theses-contact@univ-lorraine.fr
(Cette adresse ne permet pas de contacter les auteurs)

LIENS

Code de la Propriété Intellectuelle. articles L 122. 4
Code de la Propriété Intellectuelle. articles L 335.2- L 335.10
http://www.cfcopies.com/V2/leg/leg_droi.php
http://www.culture.gouv.fr/culture/infos-pratiques/droits/protection.htm

Laboratoire Réactions et Génie des Procédés, CNRS, UMR 7274
Sciences and Engineering of Molecules, Products, Processes, and Energy doctoral school

THESIS

Presented and defended publicly on:
November 4th, 2022

for obtaining the title of:

Doctor of the University of Lorraine in Process, Product, and Molecular Engineering

by

Stephanie EL-ZAHLANIEH

Chemical and Petrochemical Engineer

LIFTING THE FOG OFF FUEL MIST EXPLOSIONS: A NEW PROCEDURE TO DETERMINE THE IGNITABILITY AND EXPLOSIVITY OF MIST RELEASES

Thesis director:	Mr. Olivier DUFAUD	Pr. University of Lorraine, France
Thesis supervisor:	Mr. Alexis VIGNES	Dr. INERIS, France
Reviewers:	Mr. Philip BOWEN	Pr. Cardiff University, United Kingdom
	Mr. Fabien HALTER	Pr. University of Orléans, France
Examinators:	Mr. Simon GANT	Dr. Health and Safety Executive, United Kingdom
	Mr. Pierre-Alexandre GLAUDE	Dr. University of Lorraine, CNRS, France *(president of the jury)*
	Mrs. Agnès JANES	Dr. CRAMIF, France
	Mrs. Sabine ZAKEL	Dr. Physikalisch-Technische Bundesanstalt, Germany

“Individually, we are one drop. Together, we are an ocean.”
- Ryunosuke Satoro

Acknowledgements

I would like to start by thanking the Reactions and Chemical Engineering Laboratory (LRGP) and the French National Institute for Industrial Environment and Risks (INERIS) for making this thesis possible and for their technical and financial support.

I extend my gratitude to my thesis director, Olivier Dufaud, who was always present, supporting, and encouraging. I really appreciate your time and effort during these three years, and I thank you for believing in my abilities; a special thank you for all the dad jokes that always made us laugh! I would also like to express my appreciation and thanks to Alexis Vignes, my thesis supervisor, with whom I shared enriching conversations. Thank you for your contribution to this thesis and all the advice and encouragement.

A special thank you goes to my PhD committee members, to whom I had the pleasure to defend my work. Thank you for taking the time to read my dissertation and for your enriching comments.

I am also thankful for the collaborations made to complement this project, especially with the Health and Safety Executive (HSE), the PTB, and the BAM. I extend my thanks to the suppliers of the products tested in this thesis, including TotalEnergies CPE and Valtris Champlor.

These three years were made easier by the presence of my LRGP family. I am grateful for each and every one of you, especially the BJC and the SAFE team. I am happy I met you!

I would not have accomplished what I have today without the support and love of very important people with whom I was blessed. I would like to start by expressing my gratitude to my mother, who sacrificed a lot to provide a loving and encouraging environment and always pushed me to be the best I could be. I also extend my gratitude to my father, who has been my idol for as long as I can remember and has taught me that being a good person is the most rewarding in life. My brother, Khalil, and sister, Priscilla, have always been my constant source of laughter, love, and safety, and to them I am eternally thankful. The list goes on, and I am grateful for each member of my big family, but I would finally like to express my utmost gratitude to my aunt and uncle, Nicole and Fadi, who have made this journey possible and always showed me love and support.

Life has sent me loved ones who have supported me through many of my journeys and to whom I will remain grateful. Mahdi, you were there for me each step of the way. You supported my decisions, calmed me down in my hardest moments, and believed in me. Wherever life may take us, I am eternally grateful to have shared unforgettable memories with you. Jana and Siham, you have never left me alone. You always made sure that I felt supported, loved, and strong. Thank you! Suha and Marwa, you have played an important role in my life, and I am incredibly thankful that I met you on our first day of university. I know that our bond remains forever.

Abstract

In a world where fuels are indispensable and ubiquitous in nearly every industry, attention should be paid to the dangers they might cause. Indeed, numerous incidents have occurred throughout the years due to accidental fuel releases in the form of mists, resulting in explosions and human and material losses. Nevertheless, while standards and regulations for flammable gases/vapours and dust are well-established, those for liquid aerosols remain less so. This is mainly due to the lack of means of characterisation, available data, and scientific knowledge in such a matter. The objective of this study is hence to propose a complete procedure allowing the evaluation of the ignition sensitivity and explosion severity of fuel mist clouds. Suitable prevention, protection and mitigation measures can then be implemented in a harmonised and systematic way.

For this study, seven fuels of different physicochemical properties and industrial uses were chosen. A gravity-fed mist generation system, which is relatively easy to manufacture and controllable, was designed to mimic industrial leaks and ruptures while remaining adjustable to a laboratory-scale apparatus. Based on a Venturi junction, the system was equipped with twin-fluid nozzle sets with varying orifice diameters. Subsequently, modifications were made to the standardised 20 L explosion sphere used for dust explosion tests to accommodate the mist generation system. Moreover, a control and data acquisition system with customised software was specifically developed to ensure the safe operation of the test equipment and optimal interpretation of the experimental data. Once the test apparatus was ready and validated, characterisation tests took place. Three nozzle sets were chosen with a maximum attainable mist concentration of about 800 $g.m^{-3}$ and droplet diameters ranging between 5 µm and 100 µm. The mist cloud's droplet size distribution (DSD) was examined using an in-situ laser diffraction sensor. Moreover, Particle Image Velocimetry (PIV) was performed to determine the level of turbulence of the cloud inside the equipment throughout the injection process up to the moment of ignition. Experimental findings also allowed the proposition of a correlation that predicts the Sauter Mean Diameter (SMD) of a mist cloud generated using a twin-fluid nozzle based on the characteristics of the fluid and the injection conditions. Subsequently, a complete modus operandi was established and proposed after calibration and validation tests. The pre-characterised mist cloud would then be ignited under different conditions to determine the ignition sensitivity and explosion severity of the seven selected fuels in a single apparatus. It was seen that the fuels could be classified into four minimum ignition energy (MIE) categories ranging from less than 130 mJ to 5 kJ. The lower explosion limit (LEL) and the limiting oxygen concentration (LOC) were also determined. Moreover, it was observed that a smaller DSD, a higher initial temperature, and a more turbulent mist cloud all lead to higher explosion severities

to a certain extent. The influence of the chemical nature, the vapour content, the ignition energy, and the addition of flammable gases was also evaluated. This parametric analysis allowed the differentiation between distinct classes of fuels and was complemented by flame propagation studies conducted in a flame propagation tube. The flame speeds and burning velocities were determined, allowing the understanding of the phenomenology of mist explosions. An evaporation model was also developed to complement experimental findings.

This study proposed a liquid classification system, depending on which specific test procedures were recommended. It also put forward the application of such procedures in industrial cases to illustrate the importance of considering scenarios involving the generation of fuel mists, particularly those with high flashpoints, and the need to assess the safety parameters of mists through experimental means for standardisation.

RESUME

Dans un monde où les combustibles sont d'un usage indispensable et sont omniprésents dans l'industrie, il convient de prêter attention aux dangers qu'ils peuvent représenter. En effet, de nombreux incidents se sont produits au fil des ans en raison de rejets accidentels de combustibles liquides sous forme de brouillard, entraînant des explosions et des pertes humaines et matérielles. Néanmoins, si les normes et réglementations relatives aux gaz/vapeurs et aux poussières inflammables sont bien établies, celles relatives aux aérosols liquides le sont bien moins. Ceci est principalement dû au manque de moyens de caractérisations, de données disponibles et de connaissances scientifiques en la matière. L'objectif de cette étude est donc de proposer une procédure complète permettant d'évaluer la sensibilité à l'inflammation et la sévérité de l'explosion de nuages de brouillard d'hydrocarbures. Des moyens de prévention, de protection et de mitigation adaptés pourront alors être mis en œuvre de manière harmonisée et systématique.

Pour cette étude, sept combustibles aux propriétés physico-chimiques et aux usages industriels différents ont été choisis. Un système de génération de brouillard par gravité, relativement aisé à concevoir et à contrôler, a été développé pour simuler des fuites de liquide sous pression tout en restant adaptable à un équipement à l'échelle d'un laboratoire. Basé sur une jonction Venturi, le système a été équipé de jeux de buses à deux fluides dont les diamètres d'orifice peuvent varier. Par la suite, des modifications ont été apportées à la sphère d'explosion standardisée de 20 L utilisée pour les essais d'explosion de poussières afin d'accueillir ce système de génération de brouillard. En outre, un système de contrôle et d'acquisition de données avec un logiciel personnalisé a été spécifiquement développé pour assurer le fonctionnement sûr de l'équipement d'essai et l'interprétation optimale des données expérimentales. Une fois l'appareil d'essai prêt et validé, les essais de caractérisation ont eu lieu. Trois jeux de buses ont été choisis avec une concentration maximale de brouillard atteignable d'environ 800 $g.m^{-3}$ et des diamètres de gouttelettes compris entre 5 µm et 100 µm. La distribution de la taille des gouttelettes (DTG) du nuage de brouillard a été examinée à l'aide d'un appareil de diffraction laser in-situ. De plus, la vélocimétrie par image de particules (PIV) a été réalisée pour déterminer le niveau de turbulence du nuage à l'intérieur de l'équipement tout au long du processus d'injection jusqu'au moment de l'inflammation. Les résultats expérimentaux ont également permis de proposer une corrélation qui prédit le diamètre moyen de Sauter (DMS) d'un nuage de brouillard généré à l'aide d'une buse bi-fluide à partir des caractéristiques du fluide et des conditions d'injection. Par la suite, un mode opératoire complet a été établi et proposé après des tests de calibration et de validation. Le nuage de brouillard pré-caractérisé est ensuite enflammé dans différentes conditions afin de déterminer la sensibilité à l'inflammation et la sévérité de l'explosion des sept

combustibles sélectionnés dans un seul et même appareil. Il a été constaté que les combustibles pouvaient être classés en quatre catégories d'énergie minimale d'allumage (EMI) allant de moins de 130 mJ à 5 kJ. La limite inférieure d'explosivité (LIE) et la concentration limite en oxygène (CLO) ont également été déterminées. En outre, il a été observé qu'un DSD plus petit, une température initiale plus élevée et un nuage de brouillard plus turbulent conduisent tous à une sévérité d'explosion plus élevée dans une certaine mesure. L'influence de la nature chimique, de la teneur en vapeur, de l'énergie d'allumage et de l'ajout de gaz inflammables a également été évaluée. Cette analyse paramétrique a permis de différencier des classes distinctes de combustibles et a été complétée par des études de propagation de flamme réalisées dans un tube de propagation de flamme. Les vitesses de flamme ont été déterminées, permettant la compréhension de la phénoménologie des explosions de brouillard. Un modèle d'évaporation a également été proposé afin d'analyser plus avant les résultats expérimentaux.

Cette étude a proposé un système de classification des liquides, à partir duquel des procédures d'essai spécifiques sont recommandées. Les résultats de cette étude ont été également appliqués à des études de cas industriel afin d'illustrer d'une part l'importance de la prise en compte des scénarios impliquant la génération de brouillards d'hydrocarbures et particulièrement ceux présentant des points d'éclair élevés et d'autre part, la nécessité d'évaluer les paramètres de sécurité des brouillards au travers de moyens expérimentaux destinés à être normalisés.

TABLE OF CONTENTS

TABLE OF FIGURES

TABLE OF TABLES

NOMENCLATURE

Symbol	Unit	Meaning
a	$m.s^{-2}$	Acceleration
A	m^2	Surface area
C	$g.m^{-3}$	Concentration
C_p	$J.kg^{-1}.K^{-1}$	Heat capacity
d or D	m	Diameter
dP/dt_{ex}	$bar.s^{-1}$	Rate of explosion pressure rise
dP/dt_{max}	$bar.s^{-1}$	Maximum rate of explosion pressure rise
h	$W.m^{-2}.K^{-1}$	Convection heat transfer coefficient
K	-	Karlovitz factor
K_v	$m^2.s^{-1}$	Droplet evaporation rate
K_x	$bar.m.s^{-1}$	Deflagration index
P_{ex}	bar	Explosion overpressure
L_v	$kJ.kg^{-1}$	Latent heat of vaporisation
$\dot{m}$	$g.s^{-1}$	Mass flow rate
M	$g.mol^{-1}$	Molar mass
N	-	Number of droplets
P_{ex}	bar	Explosion pressure
P_{max}	bar	Maximum explosion pressure
r	m	Droplet radius
s	-	Mass stoichiometric coefficient
s_D	m	Inter-droplet distance
S_s	$m.s^{-1}$	Spatial velocity
S_u	$cm.s^{-1}$	Burning velocity
S_u^0	$cm.s^{-1}$	Unstretched burning velocity
t	s	time
t_v	s	Ignition delay time

T	°C	Temperature
u	$m.s^{-1}$	Horizontal velocity
U	$m.s^{-1}$	Velocity
v	$m.s^{-1}$	Vertical velocity
V	m^3	Volume
v_{rms}	$m.s^{-1}$	Root-mean square velocity
x	-	Molar fraction
Y	-	Mass fraction
z	m	Position of the flame front

Greek letter	**Unit**	**Meaning**
α	-	Significance level
γ	-	Ratio of specific heats ($C_{p,p}/C_{p,v}$)
ΔH_{comb}	$J.mol^{-1}$	Molar enthalpy of combustion
ΔH_v	$J.mol^{-1}$	Molar enthalpy of vaporisation
δ_M	m	Markstein length
δ_p	m	Preheating zone thickness
δ_r	m	Reaction zone thickness
ε		Emissivity
λ	$W.m^{-1}.K^{-1}$	Thermal conductivity
μ	Pa.s	Dynamic viscosity
ρ	$kg.m^{-3}$	Density
σ	$kg.s^{-2}$	Surface tension
$\tau_{ignition}$	s	Ignition time
τ_s	s	Relaxation time
φ	-	Volume fraction
ϕ	-	Fuel equivalence ratio

Dimensionless number	Unit	Meaning
B_M	-	Mass transfer Spalding number
B_T	-	Thermal transfer Spalding number
Da	-	Damköhler number
G	-	Combustion group number
Kn	-	Knudsen number
La	-	Laplace number
Le	-	Lewis number
Nu	-	Nusselt number
Oh	-	Ohnesorge number
Pr	-	Prandtl number
Re	-	Reynolds number
Sc	-	Schmidt number
Sh	-	Sherwood number
St	-	Stokes number
Sta	-	Stanton number
We	-	Weber number

Acronym	Unit	Meaning
AIT	°C	Auto-Ignition Temperature
CEA	-	Chemical Equilibrium with Applications
CFD	-	Computational Fluid Dynamics
DSD	-	Droplet Size Distribution
FP	°C	Flashpoint
HAC	-	Hazardous Area Classification
HELOS	-	Helium-Neon Laser Optical System
LEL	$g.m^{-3}$	Lower Explosion Limit
LOC	$\%_{v/v}$	Limiting Oxygen Concentration

MEC	$g.m^{-3}$	Minimum Explosible Concentration
µGC	-	Micro-Gas Chromatography
MHSIT	°C	Minimum Hot Surface Ignition Temperature
MIE	J	Minimum Ignition Energy
MIT	°C	Minimum Ignition Temperature
MMD	m	Mass Median Diameter
MSDS	-	Material safety Data Sheet
PDA	-	Phase Doppler Anemometry
PIV	-	Particle Image Velocimetry
SMD	m	Sauter Mean Diameter
UEL	$g.m^{-3}$	Upper Explosion Limit

Indices	**Unit**	**Meaning**
$_c$	-	characteristic
$_d$	-	droplet
$_g$	-	gas
$_{inj}$	-	injection
$_K$	-	Kolmogorov scale
$_l$	-	liquid
$_{M, m}$	-	mist
$_o$	-	orifice
$_{opt}$	-	optimal
$_s$	-	stoichiometry
$_{st}$	-	dust
$_v$	-	vapour
$_q$	-	quenching

Chapter I:
Introduction

1.1. Context and background

For centuries, the World has depended greatly on hydrocarbons which are ubiquitous, indispensable fuels used in nearly every existing industry. However, their use has led to numerous incidents along their value chain, i.e., during production, handling, storage, or transportation. Among these incidents, the chemical and petrochemical industries have witnessed a significant number of explosions triggered by involuntary mist releases (Santon, 2009; Lees et al., 2019). Such inadvertent releases can lead to the formation of a flammable mixture that can cause an explosion in the presence of an ignition source. Identifying the risk of formation of an explosive mist atmosphere in or around equipment dealing with flammable fluids in industrial sectors, such as production, processing, distribution, and retail sectors, therefore appears of importance to better manage fire and explosion risks. At the European level, two Directives are currently implemented to properly manage explosion risks in the workplace. The first directive, 1999/92/EC, provides minimum requirements for improving the safety and health protection of workers potentially at risk from explosive atmospheres. It clearly defines an explosive atmosphere as a mixture of flammable substances with air, under atmospheric conditions, having the form of gases, vapours, *mist*, or dust and through which combustion spreads after ignition has occurred. This directive also classifies the areas where explosive atmospheres may occur according to their frequency and duration of occurrence (Zones 0, 1, and 2 for gases, vapours, or *mist* and Zones 20, 21, 22 for combustible dust, with decreasing frequency of occurrence) (Directive 1999/92/EC, 2000). The second directive, 2014/34/EU, stipulates which equipment and protective systems are intended for use in potentially explosive atmospheres as it attributes equipment, which are categorised based on their level of protection, to each classified zone (Directive 2014/34/EU, 2014).

As mentioned, the so-called ATEX Directives recognise the possible threat posed by mists. However, there is still a lack of tools to assess explosion risks related to mists, and only a limited amount of information is available on how to estimate the degree of the threat posed by high-flashpoint fluid mists and the type of ATEX equipment to use. Furthermore, the International Electrotechnical Commission IEC 60079-10-1 (2020) clearly states that current standards and classifications do not apply to mist hazards generated at temperatures below the flashpoint. Nonetheless, it became evident that several mist explosions did actually occur at temperatures below the flashpoint of the aerosolised liquid (Eckhoff, 2005; Eichhorn, 1955; Gant et al., 2020) and that, although ATEX standards recognise the dangers of flammable mists, liquid categorisation is still limited to this flashpoint (see Section 2.3). Indeed, while the classification of flammable gases and dust is well-established, that of liquid aerosols remains less so. This is mainly due to a lack of scientific data and knowledge in such a matter, highlighted by the Energy

Institute (Energy Institute, 2015), which stated that *"there is little knowledge on the formation of flammable mists and the appropriate extents of associated hazardous areas"*. These concerns were also confirmed recently by Lees et al. (2019) and Yuan et al. (2021).

1.2. Gas and dust explosions: going back to the basics

The attention of prevention officers and legislators has long been focused on the risks presented by the generation of clouds of flammable vapours or gases, as well as on the formation of explosive dust atmospheres. One might wonder why current standards are this well-established and comprehensive for gases, vapours, and dust clouds and not for mist clouds. In fact, gases, vapours, and dust clouds are currently well-defined, and their involvement in accidents is clearly identified and assessed. On the other hand, the matter is more complex for mist incidents, as they were often mistaken for vapour explosions and treated as such, just like dust clouds before the first extensively investigated wheat flour explosion in Turin (Eckhoff, 2005). This lack of knowledge and clear regulations cause the risks of mist clouds to be rather misevaluated.

Numerous standards currently provide experimental methods to determine the ignitability and explosibility of combustible gases, vapours, and dust clouds (Table I-1). The existing standards detail the experimental setups and operating conditions to be used during tests measuring specific ignitability and explosibility parameters. The latter help in designing suitable safety equipment as advised by the ATEX directive 2014/34/EU and proper explosion prevention and protection systems (e.g., venting protective systems: EN 14491 (2012) for dust clouds, EN 14994 (2007) for gases and vapours).

Table I-1: Existing standards to determine the ignitability and explosibility of gases/vapours and dust clouds

	Dust clouds	**Gases and vapours**
Explosion severity (P_{max}, dP/dt_{max}, K)	EN 14034-1 (2004)+A1 (2011) EN 14034-2 (2006) ASTM E1226-19 (2019)	EN 15967 (2022)
Ignition sensitivity (LEL, MIE, MIT)	EN 14034-3 (2006) ASTM E2019-03 (2019) ASTM E1515-14 (2014) ASTM E1491-06 (2019) ISO/IEC 80079-20-2 (2016)	EN 1839 (2017) ASTM E681-09 (2015)

Hazardous areas linked to gases, vapours, and dust clouds can, therefore, be well-classified (IEC 60079-10-1, 2020; IEC 60079-10-2, 2015), and precautions to prevent or mitigate explosions can and should be taken. For instance, one of the most important conceivable ignition sources is a heated surface. As a result, the ***maximum surface temperature*** of the equipment is an important parameter to consider and must be included in the Ex-marking of ATEX equipment. Therefore, in line with EN 1127-1 (2019) and EN 13463-1 (2009), equipment for use in such atmospheres must have a safety margin to the auto-ignition temperature (AIT) (in the case of gases or vapours) and the minimum ignition temperature (MIT) (in the case of dust clouds).

In addition, the ***limits of flammability*** (the lower explosion limit, LEL, and the upper explosion limit, UEL) are crucial explosion risk prevention parameters. The gas/vapour or dust clouds concentration should be maintained outside this explosive range to ensure a non-explosive atmosphere at concentrations well below the LEL or well above the UEL. In a case where process condition adjustments fail to preserve substances out of the explosion range, inerting becomes a viable option. The available oxygen in the atmosphere is, here, replaced by an inert gas to reduce or prevent an explosion. The ***limiting oxygen concentration*** (LOC) is hence introduced as an important parameter below which flame propagation and, as a result, an explosion cannot take place (CEN/TR 15281, 2006). This parameter, which will depend on the nature of the inert gas, is determined following the EN 1839:2017 standard for gases and vapours and the EN 14034-4 (2011) standard for dust clouds. Moreover, as part of the risk assessment and hazardous area classification (HAC) parameters, the ***minimum ignition energy*** (MIE) of a flammable cloud should also be considered since it is the lowest stored energy upon which electrical discharge is sufficient to effect ignition of the most ignitable concentration under specific conditions. So far, there is little data on measured MIE of sprays and dispersed droplets (IEC TS 60079-32-1:2013+AMD1:2017). It should also be noted that the standard ISO/IEC 80079-20-1 (2020) provides guidance on the ATEX classification of gases and vapours (i.e., gas/vapour groups IIA, IIB, and IIC) through the measurement of the ignition minimum current (MIC) or the maximum experimental safe gaps (MESG) for gas/vapour-air mixtures so as to be able to select an appropriate group of equipment. The compatibility of such equipment located in ATEX areas against the risk of electrostatic ignition is based, in particular, on the comparison between the values recorded during the evaluation of MIC or MESG and the MIE thresholds not to be exceeded as given in the standard IEC 60079-32-2 (2015).

The selection of adequate equipment for dust relies as well on the determination of three dust groups (IIIa, IIIB and IIIC) based on the knowledge of the “combustibility” of the material, its nature (metallic or not), its size (flyings or not) and its resistivity. In any case, it appears of primary importance not only to control electrical hazards by limiting the current and voltage in

a circuit but also to manage electrostatic hazards by properly earthing/grounding, bonding, and avoiding electrostatic discharge. The latter can only be achieved by evaluating the MIE properly.

When preventing the formation of an explosive atmosphere or the presence of an ignition source proves difficult, mitigating measures to protect employees should be taken. Explosion suppression, isolation, relief venting, and containment are all viable options to ensure the safety of workers. The last two options rely on the ***maximum explosion overpressure*** (P_{max}) and the normalised ***deflagration index*** K_{st} (determined from the ***maximum rate of explosion pressure rise*** dP/dt_{max}). Indeed, from these two parameters of a confined explosion, a venting area can be calculated to reduce the explosion severity and allow part of the material to escape to a location where its emergence can be tolerated from a health and safety standpoint (Jespen, 2016). Moreover, when affordable, the equipment can be designed to withstand overpressure and contain the explosion without rupture, which can be considered an application of inherent safety principles.

The list goes on about parameters that can be identified and that permit preventing explosions, selecting equipment, taking mitigating measures, assessing risks, and classifying hazardous zones. Table I-2 comprises some of such parameters, the current standards used to determine and apply them, following the ATEX directives, and their applications through two examples:

- Example 1 considers an industrial pump which pumps benzene and is equipped with a mechanical seal and placed at ground level outdoors. The latter has a molar mass of 78.11 $g.mol^{-1}$ and an AIT of 498 °C. A leakage is found due to the rupture of the mechanical seal (secondary source of release according to EN 60079-10-1). Seen that the AIT of the vapour is greater than 450 °C and that the MIE is higher than 0.2 mJ, an electronic grounding system belonging to the equipment group IIA and temperature class T1 can be used.

- Example 2 studies a cyclone aluminium dust collector followed by a filter bag. The temperature of the surrounding surfaces must not exceed 475 °C (MIT of aluminium is about 550 °C, d_{50} = 23 µm) (BGIA GESTIS-DUSTEX, IFA). The MIE of very fine aluminium powder can be as low as 1 mJ. Aluminium powder is then combustible metal dust classing this material in dust group IIIC. The dedusting mechanism can create an electrostatic energy release of about 10 mJ, a value higher than the MIE. Therefore, the adequacy of such equipment against electrostatic risks requires electrical grounding of all apparatus and anti-static filters. Employees should also be equipped adequately.

These two examples illustrate succinctly the importance of safety parameters on the risk management of processes handling gases or powders, but...

Table I-2: Application of some risk assessment parameters on gases/vapours and dust clouds

Parameter	Gases and vapours	Dust clouds	Standards	Applications
Auto-ignition temperature (AIT)	○ Surfaces must be kept below 80 % the AIT of the mixture ○ Equipment temperature classes (T1 - T6)	-	○ ISO/IEC 80079-20-1 (2020) ○ ASTM E659-15 (2015)	Example 1: temperature class T1 (AIT > 450 °C) ➔ equipment with a maximum T of 450 °C should be selected
Minimum ignition temperature (MIT)	-	○ Surfaces must be kept below the adjusted MIT of the mixture $T_{max} \leq MIT_{adjusted}$ $MIT_{adjusted} = 2/3 \times MIT$ (°C) $MIT_{adjusted} = MIT_{5mm} - 75$ (°C)	○ NF/BS CEI EN 50281-2-1 (2000) ○ ISO/IEC 80079-20-2 (2016) ○ IEC 60079-10-2 (2015)	Example 2: equipment with a maximum T of 475 °C should be selected
Minimum ignition energy (MIE) or current (MIC)	Gas groups IIA, IIB, IIC	Dust groups IIIA, IIIB, IIIC	○ (ISO/IEC 80079-20-1, 2020) ○ ISO/IEC 80079-20-2 (2016) ○ ASTM E582-21 (2021) ○ ASTM E2019-03 (2019)	○ Example 1: Gas group IIA ○ Example 2: Dust group IIIC ○ Installation of grounding/earthing systems

1.3. But what about mists?

Accidental explosions are not limited to the two states of matter mentioned above, solid and gas. Liquids dispersed as mist clouds should also be taken into consideration. Agitation, splashing, oil lubrication, ruptures in vessels and pipelines due to accidental damages or corrosion, and evaporation then eventual condensation of the fuel into mist are all forms of unplanned releases of flammable hydrocarbon aerosols which make chemical and petrochemical industries prone to mist explosion hazards.

Of frequent occurrences in the industry, causing major accidents and being increasingly documented (see Section 2.2), such flammable mists are neither well classified nor subject to dedicated regulations. Qualitative guidance can be found in some standards, including the Energy Institute's model code of safe practice EI15 (Energy Institute, 2015) and IEC 60079-10-1 (2020), but there exists a lack of quantitative methods permitting to assess mist explosions and classifying linked hazardous areas correctly. As Gant (2013) pointed out, the matter is more complex for mists than for gases, vapours and dust clouds. Although heterogeneous as a dust cloud, the droplet size distribution of a mist cloud depends even more on time, turbulence level, and concentration. Mist releases are not usually uniform and stable, mostly due to eventual evaporation, droplet breakup, coalescence, or sedimentation. Moreover, with high flashpoint multi-component fuels, the presence of volatile fractions renders studying their flammability and explosivity rather challenging. Indeed, according to the IEC 60079-10-1 (2020) standard, if a mist hazard has been established, 'Zones 0, 1, or 2' cannot be used as hazardous area classifications since the types of protection used in such zones are not necessarily applicable for mist risks. Additionally, the standard mentions that, due to their complexity, mist clouds' risk assessment should preferably be supported by specific references or operating experiences so that judgements are based on pertinent data (IEC 60079-10-1, 2020). Therefore, standards are limited to qualitative methods since each release is strongly influenced by the handled liquid.

Many efforts were made in the previous decades to quantitively study mist hazards. For instance, Burgoyne and Cohen (1954) notably studied the effects of droplet sizes on the flammability of the mist cloud. Ballal and Lefebvre (1978) conducted several studies to measure and predict the ignition energy and quenching distance of quiescent and turbulent fuel mist clouds. In parallel, throughout the years, a considerable number of mist-related incidents have been reported. Eckhoff (2005) dedicated a chapter of his book to shed light on the explosions of liquid droplets and past related incidents. Other incident reviews were published by Santon (2009) and Lees et al. (2019). A liquid/area classification system was also proposed by the Health and Safety Executive (HSE), dividing industrially interesting fuels into four release classes according to their

volatility and their ease of atomisation (Gant et al., 2016). The list of dedicated studies is far from being exhaustive (which will be detailed in Section 2.4), but there is still no standard experimental test method to evaluate safety parameters for mist ignition and explosion assessment.

1.4. Main goals and objectives

The increased interest and concern in preventing and mitigating mist explosion incidents call for a standardised test method to evaluate such risks and a greater understanding of the influence of external conditions. This work, therefore, aims to propose a complete procedure allowing the evaluation of the ignition sensitivity and the explosion severity of fuel mist clouds. Hence, the main parameters of interest are the LEL, MIE, LOC, P_{ex}, dP/dt_{ex}, and K_M. The variability and complexity of a turbulent mist cloud are taken into account. They are studied experimentally and by using complementary modelling and simulations.

The core of the manuscript comprises five chapters presenting the experimental and modelling approaches taken to understand, assess, and prevent fuel mists explosions.

- **CHAPTER II** is dedicated to introducing a literature review on reported mist explosions, their classification, and some generalities on the formation and ignition of a mist cloud. A flammable mist cloud is defined along with the main factors influencing its turbulence level, concentration, and droplet size distribution. In addition, the parameters of interest linked to the ignition sensitivity and the explosion severity are discussed. Subsequently, a scientific look at the two-phase combustion of a mist cloud considering evaporation and group contribution phenomena is presented. The bibliographic approach in this chapter has been reduced to its fundamentals to meet the manuscript's needs.

- **CHAPTER III** offers a detailed description of the experimental methods followed to establish a complete procedure and a new experimental set-up to assess the ignitability and the explosibility of a mist cloud. The chapter starts off with a dimensional analysis highlighting the influencing parameters on the generation of the cloud. A selection of fuels is presented along with ex-situ characterisation of the physicochemical properties of the liquids of interest. The employed experimental vessels, as well as in-situ characterisation of the aerial behaviour of the fuel mist, are then put forward. Here, the turbulence level, the concentration, and the droplet size distribution of a generated mist cloud are quantified using different experimental and simulated techniques. This chapter ends with dimensional analysis of a mist cloud's ignition and the presentation of the used ignition sources.

- **CHAPTER IV** discusses the design and the validation of testing devices permitting the

completion of the opted procedure. The performance of the mist generation is evaluated for seven selected fuels. A CFD approach is presented to complement experimental findings. Ignition sources are also debated and compared as they may influence the turbulence level and the growth of a flame kernel when actuated inside the explosion vessel. In addition to calibration tests and uncertainty evaluations, a comprehensive modus operandi is proposed. The latter was then debated and compared with a standard dust configuration test.

- **CHAPTER V** offers an in-depth investigation of experimental results. The ignition sensitivity and explosion severity of the seven fuels were first presented. A parametric analysis of the influence of the fuels' chemical nature, the droplet size distribution, the level of turbulence, the ignition energy, the initial temperature, and the mist concentration allows benchmarking of the test procedure against different types of fuels. Moreover, the influence of fuel blending and varying the vapour fraction of an injected mist is communicated. A sneak peek at hybrid explosions is also offered, where methane and a fuel mist cloud are ignited, allowing the assessment of the contribution of each component.

- **CHAPTER VI** first discusses the theory of group combustion in mist clouds. It then proposes an approach to experimentally evaluate the flame speed and burning velocity in a flame propagation tube and a vented experimental vessel in order to eventually determine the laminar burning velocity. This velocity is an inherent, intrinsic parameter that may be employed in sophisticated simulations to assess the effects of a mist explosion under specified conditions. It was also determined by considering the pressure-time evolution and semi-empirical correlations. A mist evaporation model is finally suggested to complement experimental findings.

A general conclusion puts an end to the work performed in this thesis. This final chapter consists of a review of the implemented mechanisms, followed by a proposition of a general classification allowing the choice of a procedure based on industrial conditions. The impact of this study on the modalities of risk assessment, prevention, mitigation, and ATEX classifications is subsequently deliberated, followed by a presentation of some perspectives.

A final part appears at the end of this manuscript featuring the appendices, which support the general development of the thesis.

Chapter II:

From the generation to the ignition of mists

Properly identifying a mist cloud and acquiring sufficient knowledge of previous mist incidents, current standards, and ignition and explosion phenomenology are all prerequisites for a process safety professional treating any mist explosion hazard. This chapter, therefore, serves as a reference divided into four parts. A mist cloud is first defined according to its droplet sizes. The second part then includes an incident review and discusses reported mist explosions in transport, production, aviation, and other industries. Subsequently, a third section is devoted to the current standards and proposals applied to classify oil fluids and assess related risks. Finally, a literature review confers the key parameters to take into account in mist generation, ignition and explosion phenomena, as well as the efforts previously made to identify and study them. Measures to study the combustion kinetics and assess related risks are also conveyed.

2.1. How to define a mist

To better understand the phenomenon of fuel mist explosions, the mist cloud should be well defined and characterised. According to the Globally Harmonized System of classification and labelling of chemicals (GHS) (ST/SG/AC.10/30/Rev.8, 2019), ***mists*** are defined as liquid droplets, generally of sizes ranging from 1 to about 100 µm, of a particular substance or mixture suspended in a gas - usually air. The alternative term "smoke" is then used for aerosols with diameters lower than 1 µm (Fraser and Eisenklam, 1956), while "sprays" consist of dispersed droplets of diameters generally greater than 50 µm. Other definitions are also encountered. For instance, Ballal and Lefebvre (1981a) consider the term "mist" to be suitable for up to 100 µm (Gant, 2013), while the IEC 60079-10-1 (2020) standard identifies a diameter range from sub-micron to 50 microns. Figure II-1 depicts the variety of drop sizes that may be found in natural/accidental occurrences as well as those typically created by atomisers.

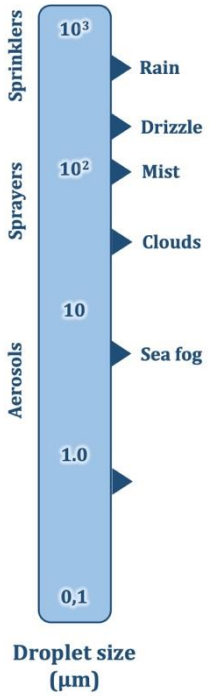

Figure II-1: Drop size spectrum - redrawn from Fraser and Eisenklam (1956)

This study concentrates on mist clouds of droplet diameters reaching 100 µm. It should be noted that this research is limited to process safety applications and does not encompass combustion engines for which sprays are generated.

Nevertheless, as proposed by Eckhoff (2005), the terms "spray" and "mist" are used arbitrarily in the following of this thesis as they are both relevant in this case.

2.2. What mist releases have caused

High flashpoint liquids tend to be considered intrinsically safer and less likely to ignite than liquids with low or moderate flashpoints (see Section 2.3). However, there are two exceptions to this rule. First, a liqwuid can be ignited at temperatures below its flashpoint if it soaks into a porous insulating substrate due to oxidative self-heating (Santon, 2009). Second, if, alternatively, this same liquid is scattered as a fine spray in the air, it can ignite and result in a fire or explosion, depending on the conditions.

Whilst acknowledging the risk, most articles and reviews on this topic point to a relatively low occurrence rate. For instance, Eckhoff (2005) stated that *"open reports of case histories of accidental spray/mist explosions in the process industries are scarce"*. Nonetheless, the consequences of such explosions are often underestimated and unforeseen, mostly due to the application of gas-phase flammable properties to the evaporated liquids underestimating the ignitability and explosion severity of mists (Yuan et al., 2021). In fact, numerous scenarios might contribute to the accidental formation of mist clouds from leaks at temperatures below the flashpoint. Indeed, the assumption that reactivity is lost as the fuel mixture becomes richer loses its accuracy in the presence of flammable mists, as their hazards may be unpredictable (Hansen et al., 2013). In addition to being underestimated, mist explosions might often be confounded with vapour explosions and their specificities neglected.

One explosion incident that has been doubted to be triggered by a mist release is the Buncefield explosion, which took place on the 11th of December 2005. This incident occurred due to the overflow of a gasoline tank after the failure of the safety systems initially fitted to prevent the tank from overfilling. This failure led to the spilling of large quantities of gasoline that then formed a fuel-air mixture igniting a few moments later. CCTV cameras and witnesses reported the appearance of a mist-like cloud (Yuan et al., 2021). According to Atkinson (2017), several incidents similar to the Buncefield explosion have occurred; nevertheless, none have caused such widespread damage. This incident has contributed to the process safety community by raising awareness of the significant impact such explosions can have and proving that more work and attention should be put into the risk assessment of oil storage. Yet, oil storage is not the only concern.

A mist incident survey conducted by the Health and Safety Executive shed light on several mist explosion incidents, which took place around the world and in different industries, including railway, manufacturing, refinery, offshore, and aviation. The authors used various databases such as the National Technical Information Service, Major Hazards Data Incidents Service (MHIDAS), and the Chemical Engineering and Biotechnology Abstracts (Santon, 2009). Thirty-seven

incidents were identified, including 20 explosions which resulted in 29 fatalities. Santon (2009) further stated that in all cases, the incidents arose from the ignition of mist at temperatures near or below the liquid's flashpoint. The leaks involved in such explosions were created by pressurised sprays or condensation aerosols of industrial high-flashpoint fuels such as kerosene, diesel, as well as lube and fuel oil.

Ten years later, Lees et al. (2019) analysed additional incident databases (UK HCRD Hydrocarbon Release Database, ARIA, and ZEMA) to institute common trends in flammable mists incidents (see Figure II-2). The authors stated that, as of 2016, with the increased interest in mist explosions, incident report forms for the HCRD, such as the Report of an Oil and Gas Incident Form (ROGI), began to include the question: "Did a liquid spray/mist release occur?", which was not the case for the ARIA and ZEMA databases. The HCRD findings demonstrated that around 10 % of reported releases on offshore oil and gas installations on the UK Continental Shelf between 2016 and 2018 involved sprays or mists. Diesel, hydraulic oil, and lubricating oil were found to be the most involved in the reported mist incidents, as they each formed 20 % of the latter. Most of these releases were greater than 10 kg and were considered "under pressure" (pressures ranging from 3.6 to 200 bar). Furthermore, the authors stated that the temperature was scarcely reported, and that the majority of the release hole sizes were between 1 mm and 10 mm (circular orifice equivalent diameter) with a circular, annular, or slit hole geometry.

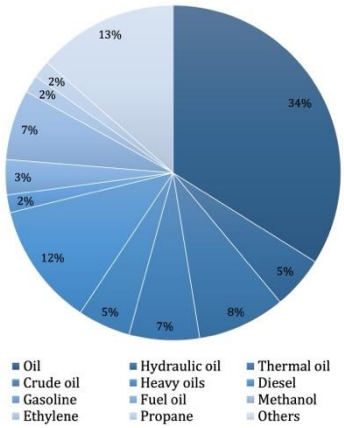

Figure II-2: Fluid spray releases from ZEMA and ARIA databases - reproduced from Lees et al. (2019)

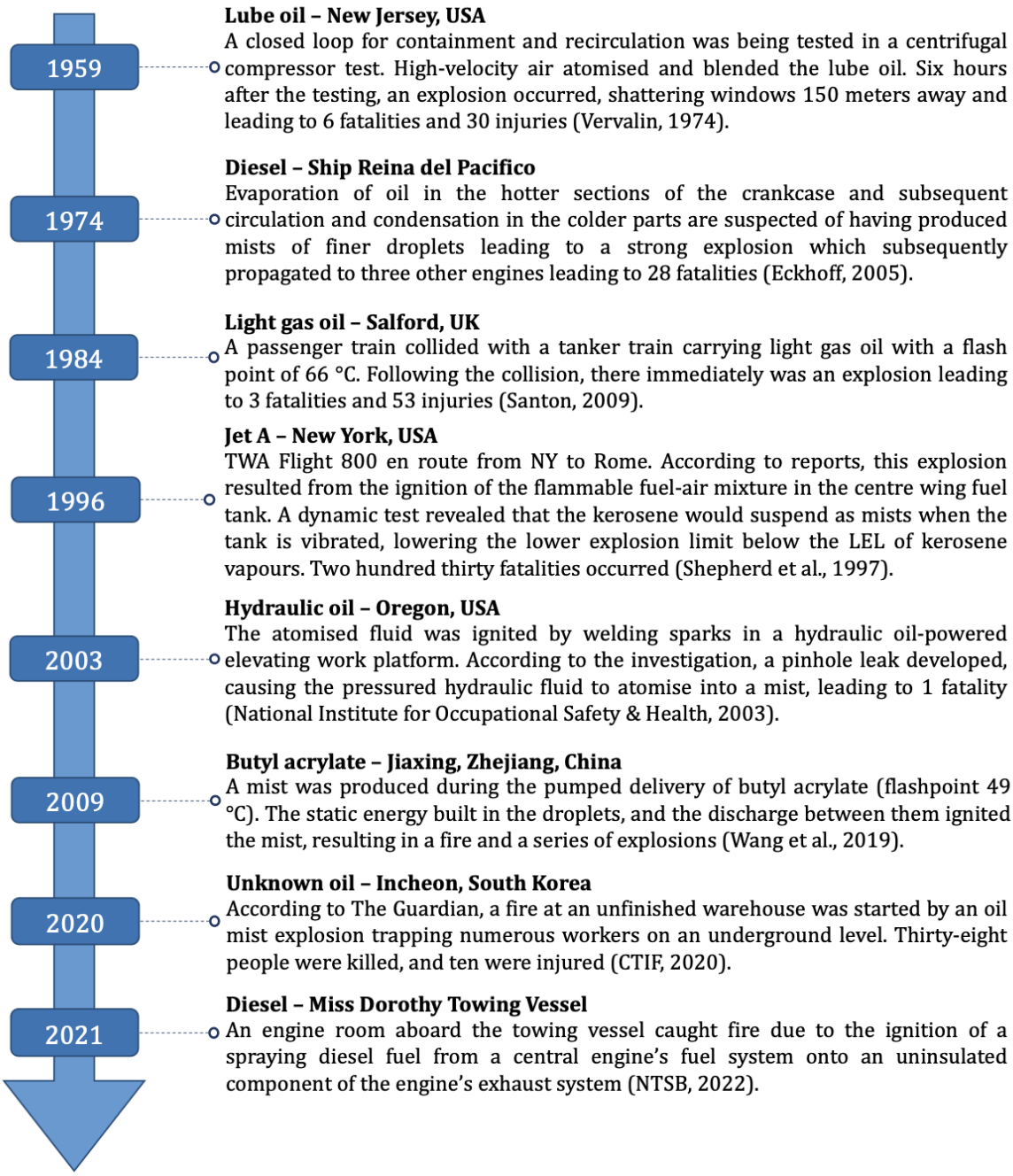

Figure II-3: Illustrative example of mist related incidents throughout the years - some are adopted from Santon (2009) and Yuan et al. (2021)

Figure II-3 depicts a historical timeline of some example mist accidents. It portrays explosions that took place throughout the years in different industries and were caused by different potential ignition sources (see Section 3.10). Such ongoing incidents highlight the importance of setting up means of prevention, protection, and mitigation for ATEX and accidental risks linked to mist explosions. The lack of knowledge and research in this field can be considered one of the numerous causes of the continuing occurrence of such incidents. It should be noted that many have gone non- or misreported due to the lack of exposure and guidance.

2.3. Classification of oil fluids

Jespen (2016) identifies five key terms to consider in zone classification for oil fluids. First, the ***zone*** should be identified according to the duration of occurrence of the explosive atmosphere and the type of explosive mixture. One must also be familiar with the notion of *the* ***grade of release*** when it comes to liquid (or gas) releases into the atmosphere from a point source. Generally, a continuous, primary (occurs periodically or occasionally), and secondary (unlikely to occur in normal operation) grade of release under air conditions will result in Zone 0, 1, and 2 classifications, respectively. The third and most difficult component of the zone classification work is determining the ***zone extension*** outside equipment, which is often caused by failure leaks and is highly influenced by the liquid's characteristics, the level of ventilation, and the release rate and volume. A point source (e.g., secondary grade) release requires the use of a basic dimension, the ***hazard radius***. This dimension is defined as the hazardous area's horizontal extent in the open air and predicted as the distance at which the flammable vapour concentration has reduced to the LEL. Finally, it is palpable that the ***degree of ventilation*** is a critical factor in establishing a correct zone classification as it influences the extent of a zone depending on whether the equipment is placed in an open, closed, or sheltered area. The five mentioned terms are crucial factors in zone classification. However, to appropriately implement this classification system and identify potential oil fluid ATEX areas, it is first necessary to know to which class this oil fluid belongs.

As mentioned previously, the flashpoint of an oil fluid is currently used as a key indicator of its volatility and the extent of rapid vapour formation from its release. Oil fluids are, therefore, generally classified according to their flashpoint and handling temperature. Adopted standards, such as the EI15, NFPA, GHS, and OSHA, all take into account these parameters but might differ by flashpoint boundaries or by including the boiling point as well. The Energy Institute's model code of safe practice EI 15 (Energy Institute, 2015) classifies oil fluids as seen in Table II-1. Under normal processing settings, however, the mentioned classification is generally insufficient for proper zone classification. As a result, the "fluid category" notion was introduced, which is now a critical aspect in calculating zone hazard radii. Fluid categories comprise five groups, including A, B, C, G(i), and G(ii) (see Table A-1 in Appendix A). The category of interest here is category C which contains any flammable liquid that does not evaporate quickly or boil upon release but can reach a temperature beyond its flashpoint or create a ***flammable mist or spray*** when released. However, when zone classification during processing is necessary, it is a requirement that the fluid fall into category C and no other category. A liquid belonging to Class II or III (1) can fall in category C if it is handled at conditions permitting the generation of a flammable mist (system pressures above 5 bar) or at temperatures above its FP but below its boiling point. Otherwise,

areas around Class II or III (1) equipment are generally not viewed as hazardous areas where zone classification is necessary. EI 15 recognises that the FP is not always a reliable indicator and recommends increasing hazard radii. Nonetheless, additional guidance on such a matter remains scarce.

Table II-1: Classification of oil fluids according to their flashpoint and handling conditions (Energy Institute, 2015)

Class	Oil fluids
Class 0	Liquified petroleum gases
Class I	FP < 21 °C
Class II (1) or (2)	21 °C ≤ FP ≤ 55 °C
Class III (1) or (2)	55 °C < FP ≤ 100 °C
Unclassified	FP > 100 °C

(1) Handled below FP, (2) Handled at or above FP

For the purpose of clarifying and enhancing existing guidelines, as of 2011, the Health and Safety Executive (HSE) has led a Joint Industry Project (JIP). The project has involved research on the formation of flammable mists of 12 common fuels, methods for predicting the extent of the flammable cloud, and concepts for protected equipment and equipment selection. Subsequently, in 2016, the HSE proposed a liquid classification system, categorising fluids according to their properties and operating conditions. The classification distributed different liquids into a restricted number of classes, a system similar to that used in the area classification of gases or vapours (Gas Group and Temperature Class). Influencing parameters were examined and taken into account, as the system was based on the liquid's flashpoint and its estimated ease of atomisation (Gant et al., 2016). The latter was represented by the ratio of the Ohnesorge number Oh to its critical value Oh_c for primary atomisation (other calculations were performed for secondary atomisation). This value represents the transition from a wind-induced break-up to an atomisation break-up, and it is calculated as a function of the Reynold number Re (equations II-1,2). It should be noted that the Ohnesorge ratio depends on the physicochemical properties of the fluid as well as the jet's velocity. A fluid can, therefore, be classified into different Release Classes depending on the dispersion conditions.

$$Oh = \frac{\mu_l}{\sqrt{\rho_l d_o \sigma_l}} \qquad \text{II-1}$$

$$Oh_c = 745 Re_l^{-1.22} = 745 \left(\frac{\rho_l U_l d_o}{\mu_l} \right)^{-1.22} \quad \text{II-2}$$

Where ρ_l, μ_l, and σ_l are the liquid's density, dynamic viscosity, and surface tension, respectively, d_o, the orifice diameter, and U_l the liquid's jet velocity.

Based on findings and the JIP's modelling, a categorisation system was created to classify fluids into four release classes bound by ***the flashpoint and the propensity to atomise*** (Oh/Oh_c), with comparable features related to mist formation and flammability as seen in Table II-2. Gant et al. (2016) concluded that fluids which belong to Release Class I tend to be more easily atomised and are more volatile such as commercial fuels. The authors suggested that these fluids should be treated as EI15 Category C fluids but with a more conservative mindset and care because releases between 1 and 5 bar can create a hazardous zone. Release Class II comprises fluids less likely to atomise and more volatile, such as viscous fuel oils. The authors mentioned that no flammable zone should be considered for hole sizes ≥ 1 mm and pressures < 20 bar, otherwise, fluids should be treated as Category C fluids. The same advice was given concerning Release Class III, which includes fluids less volatile and less prone to atomise, such as hydraulic and lubricating oils. Finally, fluids which are less volatile and more atomising (e.g., heated hydraulic or lubricating oils) and belong to Release Class IV should be treated as Category C fluids.

The authors insisted that any extrapolation of the results to general guidelines for all orifices, all pressures, and all fluids is unsuitable due to the small quantity of data gathered currently. More work is, therefore, required to establish a generic liquid classification system that facilitates the identification of hazardous zones and the installation of suitably ignition-protected equipment within these areas.

Table II-2: HSE liquid classification of flammable mists (Gant et al., 2016)

	***Oh* Ratio < 2**	***Oh* Ratio ≥ 2**
32 °C < FP < 125 °C	Release Class **II** More volatile, less atomising	Release Class **I** More volatile, more atomising
FP ≥ 125 °C	Release Class **III** Less volatile, less atomising	Release Class **IV** Less volatile, more atomising

Calculations were based on reference conditions (an orifice diameter of 1 mm and a pressure drop of 10 bar)

2.4. Still in the mist? A bibliographic study

The possibility of flammable mist forming during normal operation or due to an anticipated technical failure should be evaluated (Energy Institute, 2015). In most situations, safety professionals tend to resort to engineering judgements and operational experiences, a method considered rather qualitative, when faced with mist releases. This is due to the high complexity of mist formation. Moreover, a mist's ignitability and explosibility depend not only on the amount of vapour but also on droplet sizes, concentrations, orifice diameters, release pressures, etc. Numerous studies have been carried out to assess mist hazards and push for a more quantitative approach. This section discusses:

- Mist generation methodologies followed by fellow researchers
- Flammability and explosivity tests
- Two-phase combustion kinetics analyses
- Risk assessment studies based on previous tests and analyses

Relevant parameters to this research are pinpointed throughout this section.

2.4.1. Mist generation and characterisation

The industrial applications of sprays and mists include combustion and air conditioning due to their rapid vaporisation and controllable heat and mass transfer. They also include fire suppression and cleaning due to their high momentum impact (Ashgriz, 2011; Nasr et al., 2002). Sprays are likewise widely used in internal combustion engines and gas turbines. This extensive industrial use of sprays lays out various possible generation techniques that researchers have used to simulate mist releases due to leaks or ruptures. Indeed, a representative and reproducible generation methodology should be adopted to mimic, as much as possible, industrial accidents while maintaining a controllable mist cloud to study.

2.4.1.1. Existing generation methodologies

Williams (1990) described the process of atomisation as injecting a liquid through a narrow diameter or by increasing the surface area of a sheet of liquid until it becomes unstable and breaks down. The liquid's nature, as well as the type and form of the atomiser, play an essential role in the atomisation mechanism.

Researchers have used different mist/spray generation methodologies in the context of studying hazardous ignition or explosion scenarios. Many have categorised these methodologies, such as Eckhoff (2005), who classified the devices used for atomising and generating sprays into three main categories, including air-blast or aero-dynamical atomisers, generators depending on

centrifugal action, hydraulic/hydro-dynamical spray generators, in addition to one last category of special atomisers such as electrostatic or ultrasonic ones. Gant (2013) proceeded by listing the following four principal ways used to generate mists: spray discharge from a pressurised liquid reservoir, condensation of saturated vapour, agitation and splashing, and air stripping. More recently, Yuan et al. (2021) reported three main categories of spray generation methodologies: the Wilson cloud chamber, electrospray, and mechanical injectors.

Among these techniques, four categories, corresponding to the most discussed in the literature, will be described below:

Liquid pressurisation

This mist generation method encompasses both intentional (e.g., spray painting) and unintentional emissions (e.g., point release from damaged pipework). Spray breakup is the primary mechanism allowing mist formation in a jet release; however liquid droplets may collide with surrounding solid surfaces and fragment further. Researchers like Addai (2016) pressurised a specific volume of liquid in a solvent chamber and then evacuated it into a vacuumed test apparatus (mainly the 20 L explosion sphere), creating a mist cloud due to the pressure difference. Such a technique ensured a droplet size distribution (DSD) up to around 20 µm for tested liquids. Gant et al. (2016) and Giles et al. (2017) also used this method to study the flammability hazards of high-flashpoint liquid releases under different pressures. One downside of liquid pressurisation is the presence of a continuous liquid stream, ligaments, or non-spherical droplets at low pressures, rendering the measurement of the mist cloud's DSD rather difficult.

Electrospray

Mist generation is achieved by applying electrostatic forces to a liquid. A liquid with appropriate electric conductivity is fed through a tiny nozzle creating an electrostatic force which results in charged and uniform droplets. The nozzle's tip is kept at a few kilovolts relative to a ground electrode placed at a specified distance from the nozzle. Ashgriz (2011) explained that electrospray basically results from sending a high voltage power supply which causes electrophoresis and the creation of an electrostatic force overpowering that of the surface tension. The fluid is deformed into a conical shape extensively studied by Taylor (1964), who experimentally demonstrated that when a high enough electric field is given to the meniscus fluid/air interface, it develops into a conical shape. Such a method ensures high control of the flow rate and diameter range of the spray as the droplet size distribution tends to be narrow (low coalescence phenomena are observed due to the presence of charged droplets) (Jaworek, 2007). However, one main downside is its non-applicability to all types of liquids and its sensitivity to the electric field surrounding the emitter tip. For instance, electrospray modes may vary when

varying the electric field at the orifice capillary at constant fluid properties (Ashgriz 2011). Jaworek (2007) also stated that high surface tension liquids could not atomise using this method. Moreover, the conductivity and dipole moment of the liquid should not exceed certain limits. Lian (2011) also mentioned that it is challenging to theoretically determine the droplet size of the electrospray and increase its droplet concentration. This mist generation method has been used in studies on aerosol flammability. For instance, Lian et al. (2010) investigated the ignition of a heat transfer fluid aerosol generated by electrospray where droplet diameters were controlled between 70 µm and 110 µm. Lin et al. (2015) later proposed an improved electrospray method producing more uniform droplets, better dispersion, smaller DSD, and higher concentrations. The authors utilised their test method with a propane pilot flame to analyse the flame propagation of a heat transfer fluid and noticed better repeatability.

Condensation of a saturated vapor

Condensation can occur due to a sudden rapid pressure drop that lessens the temperature of the mixture and triggers condensation of the existing vapour, like in the case of the Wilson cloud chamber. Based on the mentioned phenomenon, Hayashi et al. (1975, 1977) developed a droplet-generating device, in which they characterised the propagation of flames in droplet-vapour-air mixtures. The authors were able to develop three types of chambers, ensuring three Sauter Mean Diameters (see Subsection 2.4.1.2) of 4-7 µm, 18-25 µm, and approximately 30 µm by varying the minimum and maximum volume of the chamber, the maximum stroke, and the expansion time and speed (Cameron and Bowen, 2001). Consequently, based on the methodology of Hayashi et al. and Wilson's cloud chamber principles, Cameron and Bowen (2001) designed a new integrated cloud chamber/combustor producing quasi-monodisperse aerosols. Burgoyne and Cohen (1954), and similarly Singh and Polymeropoulos (1988), employed equipment that cooled a saturated vapour in a nitrogen environment with a regulated nuclei concentration. The mist was then infused with oxygen to achieve the same nitrogen-to-oxygen ratio as air. Many subsequent studies were based on the condensation principle to generate aerosols, such as; Bradley et al. (2014), who studied laminar mass burning and entrainment velocities in the case of isooctane, ethanol and hydrous ethanol/air aerosols, and Thimothée (2017), who performed flame propagation tests in microgravity conditions on sprays generated in a spherical combustion chamber based on the Wilson cloud chamber. The advantage of such a technique is the relatively monodispersed mist cloud that can be generated; however, droplet diameters larger than about 50 µm are not yet attainable. It should be noted that, according to Freeston et al. (1956), condensed mists are one of the main causes of crankcase explosions.

Spray nozzles

These mechanical injectors require a high relative velocity between the encompassing air/gas and the liquid to be atomised. Lefebvre and McDonell (2017) stated that the kinetic energy of the fluid, exposure to high-velocity air or gas, or mechanical energy applied externally through a rotating or vibrating device all contribute to the disintegration of a liquid jet or sheet during the atomisation process. The resulting spray is frequently characterised by a broad spectrum of drop sizes, due to the random nature of the atomisation process. Spray nozzles vary in many different characteristics and are usually categorised based on their atomisation mode, specifically on how the energy imparts to the liquid (Dombrowski and Fraser, 1954). Some of the main nozzle categories include:

- Twin-fluid nozzle: its performance depends on the contact between a gas stream and a liquid stream and can generate fine droplets at low liquid flow rates. Such nozzles can be based on different mechanisms, such as liquid pressurisation, gravity, and the siphon principle. Air caps for twin-fluid nozzles can vary between flat fan, full cone, or hollow cone affecting the type and angle of generated spray.

- Swirl nozzle: a fast-swirling fluid in a swirl nozzle is subjected to centrifugal force as it rotates in the nozzle chamber. This centrifugal force causes a liquid sheet to develop and break into droplets.

- Ultrasonic nozzle: a thin film of liquid flows on a vibrating surface and breaks into fine droplets. According to Avvaru et al. (2006), more uniform DSDs can be obtained since regular finite-amplitude capillary waves are sent. Such nozzles can generate low-pressure low-velocity sprays, which can be controlled and shaped rather accurately. Nevertheless, the droplet size distribution of the generated sprays depends significantly on the rheological nature of the liquid.

Many more spray nozzle types exist, differing in their mode of operation. Table II-3 regroups some of the spray nozzles used in fuel spray explosion and ignition studies and shows that a great deal of mist-concerned studies has used this type of nozzles.

Ashgriz (2011) stated that the mass flow rate, liquid mass distribution, spray pattern, spray impact, spray angle, and droplet size are all factors that can be used to classify spray nozzles. Various parameters affect the factors listed above, such as the nozzle geometry, the nature of the fluid, and the feed pressure. Many studies were performed to investigate the effect of such parameters on the droplet size distribution and turbulence level obtained from spray nozzles (see Subsection 2.4.1.2).

Table II-3: Spray nozzles used in aerosol flammability/explosivity-related studies

Spray nozzle type	Authors
Copper hemispherical nozzle	(Sung and Zhang, 2021)
Rotary atomising nozzles	(Willauer et al., 2006)
Simplex swirl atomisers	(Ballal and Lefebvre, 1981a) (Rao and Lefebvre, 1976)
Single and twin fluid nozzles	(Puttick, 2008)
Solenoid fuel injector	(Yuan et al., 2019)
Spinning cup atomiser	(Ballal and Lefebvre, 1978)
Spinning disk atomiser	(Pande et al., 1984)
Twin-fluid nozzle	(Jones and Zabetakis, 1952) (Bowen et al., 1997)
Ultrasonic atomising nozzles	(Polymeropoulos and Das, 1975)

2.4.1.2. Characterisation techniques

Mist characterisation is a mandatory step to take while studying the flammability of oil mists. Gant (2013) stated that properly characterising a mist before its ignition is crucial since the droplet size distribution, the concentration, and the turbulence of mists can considerably influence their safety parameters. Moreover, Bowen and Cameron (1999) expressed the need to quantify particle sizes, total equivalence ratio, droplet equivalence ratio, and pre-ignition turbulence for aerosol fuel clouds. The authors also stressed the importance of temporal resolution for used characterisation techniques due to the rapid time evolution of mist properties. Lemkowitz and Pasman (2014) correspondingly stated that the DSD is the most important physical property that influences explosion parameters. According to the authors, turbulence is also a property that has a complex effect on mist explosions.

Droplet Size Distribution

As a mist is seldom monodispersed, it can be considered as a range of drop sizes spread around an arbitrary mean value. The droplet size distribution is then usually graphically represented by plotting a histogram of drop size, with each histogram bar indicating the number of droplets whose dimensions lie within the limits $D - \Delta D/2$ and $D + \Delta D/2$, providing an instructive picture of the DSD. The drop volume of the spray can also be plotted instead of the drop numbers, resulting in the skewness of the histogram to the right, as shown in Figure II-4.

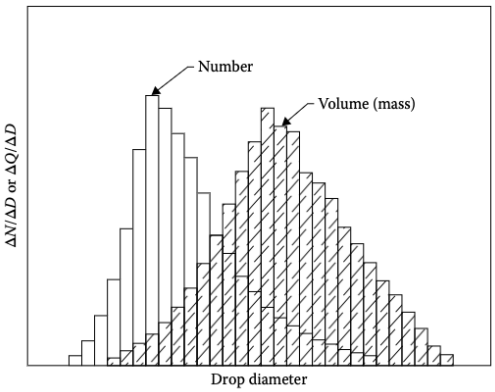

Figure II-4: Histograms presenting the drop size based on the number and volume of the spray (Lefebvre and McDonell, 2017)

Volume-based distributions are often employed in studies on spray characterisation as they illustrate the impact of changing operational conditions on the DSD (Lefebvre and McDonell, 2017). However, using number, surface area, or volume-based distributions may be acceptable and/or interesting depending on the application.

Many mathematical and empirical distribution functions can be employed to represent the entire DSD using a few parameters. Such functions are mainly used to compare modelling/theoretical results to experimental results. They generally comprise normal, log-normal, Nukiyama-Tanasawa, Rosin-Rammler, and upper-limit distributions, all described in detail by Lefebvre and McDonell (2017). Nonetheless, it is sometimes deemed more convenient to work with mean diameters rather than the entire DSD in many mass-transfer and flow calculations. Such diameters usually follow equation II-3:

$$D_{ab} = \left(\frac{\sum N_i D_i^a}{\sum N_i D_i^b}\right)^{\frac{1}{a-b}} \qquad \text{II-3}$$

Where i signifies the size range, N_i the number of droplets in the corresponding size range, and D_i the diameter of the centre of the size range.

Table II-4 demonstrates some diameters that can be of interest in mist combustion and their general applications. In addition, representative diameters are usually used for most engineering purposes. They are usually represented by d_x, where x % of the total liquid volume has smaller droplet sizes. For example, in the case of $D_{0.5}$ (or d_{50}), 50 % of the total liquid volume is in droplets smaller than this diameter (also known as the Mass Median Diameter MMD). Furthermore, as mean and representative diameters are insufficient to represent a spray's DSD (Tascón, 2018),

additional information may sometimes be required. Some factors can be calculated to supply a better representation and to determine the width and characteristics of the DSD curve. These factors include skewness, which measures the level of asymmetry of a distribution curve around the mean value, kurtosis, which indicates whether the data are light-tailed or heavily tailed relative to a normal distribution, and relative span factor, which indicates the range of the droplet sizes relative to the median diameter (level of polydispersity) (see equations II-4,6).

$$span\ factor\ \Delta = \frac{D_{0.9} - D_{0.1}}{D_{0.5}} \qquad \text{II-4}$$

$$skewness\ s = \frac{E(x-\mu)^3}{\sigma^3} \qquad \text{II-5}$$

$$kurtosis\ k = \frac{E(x-\mu)^4}{\sigma^4} \qquad \text{II-6}$$

Where μ is the mean of x, σ the standard deviation of x and $E(t)$ the expected value of quantity t.

Table II-4: Mean and representative diameters of mist clouds and their application (Lefebvre and McDonell, 2017)

Symbol	Name of the diameter	Equations (II-7,10)	Application
D_{20}	Surface area mean diameter	$\left(\frac{\sum N_i D_i^2}{\sum N_i}\right)^{\frac{1}{2}}$	Surface area controlling
D_{31}	Volume-length mean diameter	$\left(\frac{\sum N_i D_i^3}{\sum N_i D_i}\right)^{\frac{1}{2}}$	Evaporation, molecular diffusion
D_{32}	Sauter mean diameter (SMD)	$\frac{\sum N_i D_i^3}{\sum N_i D_i^2}$	Mass transfer, reaction
D_{43}	De Brouckere or Herdan mean diameter	$\frac{\sum N_i D_i^4}{\sum N_i D_i^3}$	Combustion equilibrium
$d_{0.1}$, d_{10}	-	10 % of the total liquid volume is in droplets smaller than this diameter	Representation of the persisting small droplets, choice of droplet separators
$d_{0.5}$, d_{50}	Mass Median Diameter	50 % of the total liquid volume is in droplets smaller than this diameter	Half the total aerosol mass
$d_{0.9}$, d_{90}	-	90 % of the total liquid volume is in droplets smaller than this diameter	Sedimentation, influence on flame propagation, complete evaporation and cooling processes

Optical drop size analysers differ in whether they apply imaging or non-imaging methods. However, one common factor between such analysers is that they are non-intrusive and do not impact or modify the DSD. Optical imaging, laser diffraction, optical array probes, and Phase Doppler particle analysers are all different apparatuses used for DSD measurements. Table II-5 summarises some studies on the flammability of aerosols and the techniques used to characterise their DSD. Many researchers, such as Lefebvre and McDonell (2017), recommend using only the SMD diameter for combustion applications. Indeed, the SMD is important when considering active surface reactions and is considered to best reflect the overall vaporisation behaviour of sprays for both diffusion-controlled and radiation-controlled vaporisation (Alkidas, 1981). Others, such as Aggarwal and Sirignano (1986), suggested that an alternate measure, notably the average surface area mean diameter D_{20}, was more suited for investigating the ignition behaviour of polydisperse sprays, as it is preferred for surface-controlled reactions.

Table II-5: Particle analysis techniques employed in mist ignition studies

Particle analysis technique	Representation	Reference
Laser Diffraction Particle Analyser (Malvern Instruments Ltd.)	SMD, span factor	(Yuan et al., 2019)
Light scattering technique	SMD	(Ballal and Lefebvre, 1978)
Mie extinction detection system	SMD	(Liu et al., 2016) (Bai and Wang, 2015) (Liu et al., 2014)
Phase Doppler anemometry (PDA)	SMD	(Maragkos and Bowen, 2002) (Gant et al., 2016)
The Malvern Mastersizer X™	SMD	(Cameron and Bowen, 2001)

Droplet velocity and turbulence level

The velocity, velocity profile, and level of turbulence all have a considerable effect on the primary and secondary atomisation of a liquid jet (Lefebvre and McDonell, 2017). Indeed, an increase in flow velocity promotes the jet's disintegration by increasing both the amount of turbulence in the liquid jet and the aerodynamic drag forces produced by the surrounding medium. This may lead to a fluctuation in the mist cloud's concentration causing it to fall into/out of the flammable range or modifying the droplet trajectory in the ambient environment. Not only does the turbulence level affect the process of jet breakup (primary and secondary atomisation of a liquid jet), but it also influences the level of violence of an explosion considerably (Dahoe et al., 2001; Skjold,

2003). It should also be noted that it may enhance coalescence/agglomeration and droplet-wall interaction phenomena as the cloud becomes denser in a confined vessel. Researchers, such as Bowen and Cameron (1999), therefore highlight the importance of quantifying the turbulence level of a mist cloud before ignition. Techniques like PDA and particle image velocimetry (PIV) can be used to calculate velocity vectors and fluctuations and turbulence intensity. Cameron and Bowen (2001), Bai and Wang (2015), Y. Wang et al. (2017), and Liu et al. (2016) all used the PIV technique. On the other hand, PDA was less used as it may be a source of error if droplets are not spherically shaped.

Mist concentration

The heterogeneous nature of a spray renders determining an exact concentration difficult. Such a parameter is important as its increase leads to a decrease in inter-droplet distances, increasing the chance of coalescence and sedimentation. For mist ignition studies, in order to specify the concentration of an ignited mist, different concentration zones should be identified. For instance, in conditions where sedimentation is plausible, concentrations expressed in weight per unit volume may give a vague impression of the relative flow rates of fuel and air into the propagating flame front. Burgoyne (1963) and Cook et al. (1977) differentiated between a suspended/static concentration (weight per unit volume) and a kinetic/flame-front concentration that depends on the former and both the sedimentation and upward flame speeds. While some researchers, such as Yuan et al. (2019), still use suspended/static concentrations, others, such as Sun et al. (2022) and Giles et al. (2017), use particle analysis techniques to quantify the kinetic mist concentration.

2.4.1.3. Influencing factors on the DSD

Kooij et al. (2018) studied the effect of spraying parameters, such as the injection pressure and the nozzle type, as well as fluid parameters (density, viscosity, surface tension), on the characteristics of sprays, more specifically on the droplet size. Their findings showed that the size of droplets is determined by a competition between fluid inertia and surface tension. This helped them conclude that it is possible to predict the droplet size from the calculation of the Weber ($We = (Oh.Re)^2$) number and the geometry of the nozzle. Additionally, Schick (2006) stated that droplet size and droplet size uniformity vary based on the following factors: fluid characteristics, fluid viscosity, the spray nozzle design, the flow through the spray nozzle, and the air pressure in the case of two-fluid nozzles. Influencing factors will be discussed in detail, divided into liquid properties and ambient and operating conditions as follows, and will then be grouped and implemented as dimensionless numbers in the rest of this manuscript:

Liquid properties

According to Lefebvre and McDonell (2017), the liquid properties that affect the size of droplets are mainly surface tension and viscosity. Kooij et al. (2018) validated the latter as they studied the effect of both parameters on the size of droplets.

- The surface tension, σ_l, is an important parameter in atomisation as it represents the capacity of a liquid to change its surface area under (shear) stress. In the case of hydrocarbon fuels in contact with air, it decreases as the temperature increases. Schick (2006) stated that increasing the surface tension increases the amount of energy required for atomisation, which will consequently lead to an increase in the droplet size for given operating conditions. The mentioned findings are in agreement with correlations developed by Krishna (2003), which exhibit that reducing the surface tension produces smaller droplets, i.e., increases the specific surface area of the atomised liquid.

- The viscosity, μ_l, affects not only the droplet size distribution in sprays, but it also affects the nozzle flow rate and the spray pattern. However, the effect of viscosity varies with the type of nozzle used (Lefebvre and McDonell, 2017). For instance, in the case of air blast nozzles, sensitivities towards variations in μ_l are lower than in pressure nozzles.

According to Schick (2006), as a liquid's viscosity and surface tension increase the amount of energy required to atomise it, an increase in any of these parameters will typically increase the droplet size. An increase in viscosity hence reduces the Reynolds number and prevents any inherent instability in the jet or sheet from developing. The combined impact is to slow down the breakdown of the spray and increase the size of the droplets.

Ambient and operating conditions

The ambient gas conditions in which the liquid is sprayed can vary extensively in pressure and temperature, leading to a significant influence on the cloud's characteristics. Operating conditions, as well as the employed nozzle's geometry, should also be considered.

- The increase in injection pressure improves the spray quality (fineness) as it decreases the droplet size diameter. In the case of twin fluid nozzles, increasing the air pressure increases the liquid suction rate affecting the initial spray velocity (Yao et al., 2013). This increase in pressure and acceleration hence increases the dynamic forces influencing the liquid jet and thus enhances the atomisation by increasing spray breakup. Schick (2006) similarly stated that an increase in injection pressure leads to a decrease in droplet size.

- If the ambient pressure is increased continuously above the normal atmospheric pressure, the mean drop size increases until reaching a maximum value and then slowly

declines (Lefebvre and McDonell, 2017). The ambient gas density can also influence the spray angle and droplet size. For instance, increasing the ambient gas density for a plain-orifice atomiser leads to a wider spray angle. This gas density is mainly affected by the ambient temperature. The ambient pressure also plays an important role when the spray is generated in a confined environment. For instance, in the case of a twin-fluid nozzle, as the spray is injected, the pressure gradient between the liquid reservoir and the confined environment decreases until reaching zero, inversely affecting the syphon phenomenon and stopping the liquid suction.

Various formulae and correlations exist in literature to relate the SMD to liquid properties and ambient and operating conditions and are detailed and implemented in Subsection 4.1.5 (Bowen and Shirvill, 1994; Elkotb et al., 1982; Lefebvre and McDonell, 2017).

2.4.2. Ignition sensitivity of fuel mists

The capacity of ignition sources to ignite flammable/explosive mixtures must be evaluated differently depending on the kind of discharge (Hattwig and Steen, 2004). Before determining such a capacity, one must quantify, if feasible, the ignitability of such mixtures. The goal of this section is to derive practical criteria for assessing the ignition hazards posed by ignition sources, contributing to a fundamental understanding of this phenomenon without delving into the technical details outlined by existing standards and regulations. Indeed, when a flammable mist cloud is exposed to specific conditions, its ignition sensitivity is an estimate, in the framework of risk analysis, of the likelihood that it will ignite. This responsiveness can then be determined under certain industrial conditions or worst-case scenarios and is affected by the type and power of the ignition source, the delivered energy, the fuel concentration, and the oxygen content.

2.4.2.1. Ignition sources

A source of ignition near a mist release can arise from electrical and non-electrical equipment in various forms, including sparks, stray currents, electrostatic discharge sparks, spontaneous heating, electromagnetic radiation, friction heating/sparks, exothermic reactions, and ultrasonic waves. EN 1127-1 (2019) also recognises flames and hot gases, hot surfaces, and lightning as susceptible ignition sources.

In practice, while performing aerosol flammability and explosivity studies, researchers intend to choose an ignition source that can represent a credible industrial situation where HAC is concerned (Gant et al., 2016). An ignition source can also be employed according to the intended purpose of the test. Various types are used, such as permanent sparks, pyrotechnical ignitors, exploding wires, and hot surfaces. Table II-6 summarises some experimental studies on mists and

the used ignition sources.

2.4.2.2. Balancing energy during ignition

Minimum Hot Surface Ignition Temperature (MHSIT)

One of the principal ways an oil mist explosion can occur is the generation of hot flammable vapours resulting from liquid hydrocarbon cracking when the mist is in contact with hot surfaces. In industries, fuels are also likely to be discharged while still in a liquid form against a hot surface. A hot surface can then be a strong ignition source, specifically in heat exchangers, exhaust pipes, turbines, etc. (Gant, 2013). The minimum hot surface ignition temperature (MHSIT) is, therefore, an important parameter to consider. It is the lowest hot surface temperature at which a fluid ignites once in contact. Ignition by a hot surface is highly influenced by many factors, such as the droplet size, the mist concentration, and the physical properties of the liquid (Yuan, 2006). The effectiveness of the hot surface is determined by its ability to generate a sufficient quantity of fuel vapours at a sufficient rate to attain a flammable concentration and temperature long enough to overcome the chemical ignition delay period. Surveys and studies on the ignition of oil mists by hot surfaces date back to the early 1950s (Freeston et al., 1956; Scull, 1951). Early findings showed that the MHSIT of kerosene, diesel, lubricating oil, and ethanol sprays was 650 °C, 718 °C, 430 °C, and 690 °C, respectively. Nonetheless, influencing factors, such as the experimental conditions, the mixtures' composition, the DSD of the spray, and the presence of a catalytic or inhibitory surface, should be considered. Yuan (2006) also measured the MHSIT of eight different non-fire-resistant hydraulic oils and diesel fuel sprays and found values between 330 and 480 °C. The author shed light on the MHSIT's dependence on the degree of atomisation and the direction of the spray relative to the hot surface. Additional studies, such as those performed by Shaw et al. (2010) on single fuel droplets, Davis et al. (2010) on high-performance fuels, and Motily et al. (2021) on high-pressure kerosene sprays are all relevant and give an estimate of values to take into consideration. It should be noted that when the MHSIT is unavailable, it is advised to assume that it is equal to the auto-ignition temperature (Gant, 2013), which will be detailed in the following section. There is currently no dedicated standard for the measurement of the MHSIT of flammable liquids or related mists.

Auto-Ignition Temperature (AIT)

The AIT is the lowest temperature at which the spontaneous ignition of a flammable mixture takes place. This ignition occurs with no help from an external energetic ignition source. Such property is important in fire and explosion safety measures as it is used to minimise the primary risk of ignition. Nevertheless, Nolan (2014) stated that the AIT is an extrinsic property as its value depends on the experimental method employed to determine it. For instance, an increase in

vessel volume will often result in a decrease in the AIT. Kuchta and Cato (1968) published AIT values of engine oils and lubricants of different classes and discussed the importance of such a parameter. A summary of the AITs of combustible gases and vapours was also published by Zabetakis (1964). Throughout the years, the autoignition of sprays has been studied under different conditions. Wong et al. (1993) notably investigated the auto-ignition processes of drops in non-dilute, non-convective, and monodisperse mist clouds. Snee et al. (2016) designed a lab-scale apparatus to assess the likelihood and consequences of fuel auto-ignition in gas turbines. The main goal of the authors' research was to learn more about the potential for flammable oil mists generated by regular operations of offshore gas turbines and old turbine lubricating oils to ignite in hot conditions. Liu et al. (2020) notably designed an aerosol shock tube to examine the auto-ignition of low-vapour-pressure fuels such as toluene. Wang et al. (2019) also determined auto-ignition characteristics of light naphtha, gasoline, and gasoline surrogate sprays in an optically accessible combustion chamber of constant volume. Currently, there are several test standards for the determination of the AIT of a flammable fluid (ASTM E659-15, 2015; DIN 51794, 2003; ISO/IEC 80079-20-1, 2020; …), but none for mists.

Minimum Ignition Energy (MIE)

The MIE is considered one of the most critical parameters necessary for assessing ignition risks. Any electrical spark generated in an explosive atmosphere with an energy greater than the MIE in an explosive atmosphere will trigger ignition with a high probability when the conditions met in the explosive atmosphere are similar to the conditions met during the determination of the MIE. This parameter is an ignition risk characteristic of mixtures and is essential data for electrostatic risk assessment. It is defined as the smallest amount of spark energy required to ignite the most easily ignitable mixture of a flammable substance in the air. As the MIE lowers, the risk of ignition increases, as even particularly weak ignition sources can trigger a fire and/or an explosion.

Conventionally, the MIE is determined using a modified Hartmann tube for dust clouds, as proposed in ASTM E2019-03 (2019) and ISO/IEC 80079-20-2 (2016). Different processes are used for gases and vapours, but, in most techniques, a charged capacitor is discharged across a spark gap (Hattwig and Steen, 2004). The ASTM E582-21 (2021) also suggests using an explosion sphere.

As for mist clouds, a variety of non-standardised approaches has been used over the years to determine their MIE. Rao and Lefebvre (1976) measured the MIE of kerosene sprays injected, under atmospheric conditions, into a flowing air stream and ignited using capacitance sparks. MIE values ranged between 3 and 100 mJ, varying with the level of turbulence, droplet size,

concentration, and spark gap. The droplet size was shown to be the most influencing factor on the MIE of kerosene sprays of 30 - 100 µm. A decrease in the MIE was observed, with a decrease in droplet size, an increase in the fuel-air ratio, or a decrease in air velocity. In addition, Ballal and Lefebvre (1981a, 1978) developed a model for predicting the MIE of both quiescent and flowing fuel mists. The authors found MIE values of heavy fuel oil, diesel, and isooctane mists below 500 mJ under different conditions, considering all physical, chemical, and dynamic effects present on the fuel-air mixture. Von Pidoll (2001) similarly stated that spark energies as low as 500 mJ were enough to ignite pure hydrocarbon mixtures when sprayed with coarse nozzles, whereas MIEs for gases and vapours lie between 0.02 mJ and 0.5 mJ and between 1 mJ and 1000 mJ for solid particles. Moreover, studies showed that as the volatility (the readiness of the liquid to vaporise, often linked to the liquid's boiling point and vapour pressure) of the fuel increases, the amount of energy required to vaporise the droplets decreases, requiring less energy to ignite (Peters and Mellor, 1980). The presence of any vapour thus reduces the MIE of a mist, but MIE graphs against the fuel equivalence ratio tend to adopt a parabolic shape limited between the LEL and the UEL. Nevertheless, Britton (2002) stated that it is more probable to overestimate the MIE, like in the case of many past data, which focused on the stoichiometric concentration rather than the optimal fuel concentration. An optimum droplet size should also be specified (Danis, 1987; Singh and Polymeropoulos, 1988). Additionally, it should be noted that MIE values tend to vary significantly depending on the optimum values of the electrode shape, circuit capacitance, spark gap and duration of the spark (Gant, 2013). This parameter is also easily influenced by several factors, one of which is the DSD. In fact, with small diameter droplets, the high surface-area-to-volume ratio leads to a faster evaporation process (Gant, 2013). Such an effect was also highlighted by Krishna (2003), who stated that igniting a mist becomes easier as the mean droplet diameter decreases. Optimal homogeneous and uniformly distributed mist clouds should, therefore, be generated to determine their MIE correctly.

Quenching distance (d_q)

Professionals are interested in flame quenching to prevent a flame from propagating and causing further damage. Indeed, equipment, such as flame arresters, can be employed to secure flammable vapours or gas handling systems. Passive flame arresters quench chemical reactions by absorbing heat from the flame (Guiberti et al., 2020). Due to heat losses to the surrounding surfaces, such flames cannot spread across very small spaces, which are characterised by the quenching distance d_q. This parameter can be defined differently depending on the configuration. For instance, in the case of flame propagation, it is a critical distance of an opening through which a flame can propagate. On the other hand, for flame impingement, such as in the case of Ballal and Lefebvre (1978), d_q is the critical size a flame must reach to propagate unassisted. Nevertheless,

the same physical considerations are taken for either definition. According to Ballal and Lefebvre (1978), the energy needed to achieve this critical size is referred to as the MIE described previously. Numerous models exist for predicting d_q as it is an important safety parameter in industrial processes (Ballal and Lefebvre, 1981a, 1978; Peters and Mellor, 1980). Research has shown that d_q is directly proportional to the droplet diameter and the liquid fuel density but inversely proportional to the squared root of the fuel equivalence ratio (ϕ) and the air density. Therefore, an increase in the mist concentration (remaining in the flammability range), meaning an increase in ϕ, or an increase in the fuel volatility, would result in a decrease in d_q. The effect of the pressure on d_q was also studied by Friedman and Johnston (1952), who showed that d_q was inversely proportional to the atmospheric pressure in the case of n-heptane, isooctane, benzene, and ethyl ether flames.

Furthermore, the influence of the quenching distance on the MIE has been extensively studied over the years. Ko et al. (1991) mentioned that, past the d_q, the MIE remains almost constant across a variety of gap sizes before increasing linearly as the gap dimension increases. Han et al. (2010) numerically investigated d_q and its effect on the MIE, which was shown to gradually increase below d_q and then take a sharp turn at d_q in a quiescent methane-air mixture. It should be noted that d_q is highly influenced by the turbulence level of the flammable cloud and is linked to the Karlovitz factor (Chomiak and Jarosiński, 1982), discussed in Subsection 2.4.3.4.

2.4.2.3. Lower Explosion Limit (LEL)

The Lower Explosion Limit (LEL) is defined as the lowest concentration that a flammable mixture should attain in order to support flame propagation away from an ignition source. This parameter is important because it can be used to determine the extent of a flammable cloud in HAC.

In 1955, the presence of the mist flammability zone was first conceptualised by Eichhorn (1955), as seen in Figure II-5(a), where the flammability zone depends on the fuel/air ratio and the temperature. More recently, as illustrated in Figure II-5(b), Yuan et al. (2021) extended the concept of the flammability zone of a mist under constant pressure by including the droplet size, concentration, and temperature as influencing factors. Indeed, the LEL is easily influenced by external factors. For instance, according to Burgoyne and Cohen (1954) and Zabetakis (1964), the LEL of a small-droplet mist cloud could be considered equal to that of the vapour since, due to high temperatures, very small droplets completely vaporise before the flame front's arrival, and then the flame propagation would be considered to take place in a simple vapour-air mixture. Larger droplets, however, behave differently as they would not have sufficient time to evaporate before the flame front reaches them. A combustion phenomenon then occurs depending on various parameters and is determined by the combustion group number G (see Subsection 2.4.4).

Moreover, many literature findings showed that the LEL tends to decrease with increasing droplet diameters (Burgoyne, 1963; Burgoyne and Cohen, 1954; Cook et al., 1977). However, the type of test apparatus and position of the ignition source could influence LEL values. Hence, the effect of the drop size on the LEL cannot be generalised. Wang et al. (2017) notably found an LEL of 218 $g.m^{-3}$ for nitroethane aerosols of 20 µm, a value which increases to 234 $g.m^{-3}$ as the SMD was increased to 34 µm. Other influencing parameters would be the nature of the flow of the mist cloud. For instance, the findings of Rao and Lefebvre (1976) showed that the LEL tended to decrease with increasing air velocities at constant fuel concentrations, which can probably be related to the improvement of the mass transfer coefficient. On the contrary, for a constant droplet size, LEL increased with increasing air velocities which was explained by the increase of heat lost from the spark kernel and the larger volumes heated by the spark. Another interesting finding is that of Yuan et al. (2019), who demonstrated that the LEL of the n-dodecane and n-octane aerosols was smaller than their corresponding vapour-air mixtures. The authors explain this result by relating it to the presence of a vapour film surrounding the droplet leading to a more concentrated zone near the ignitors.

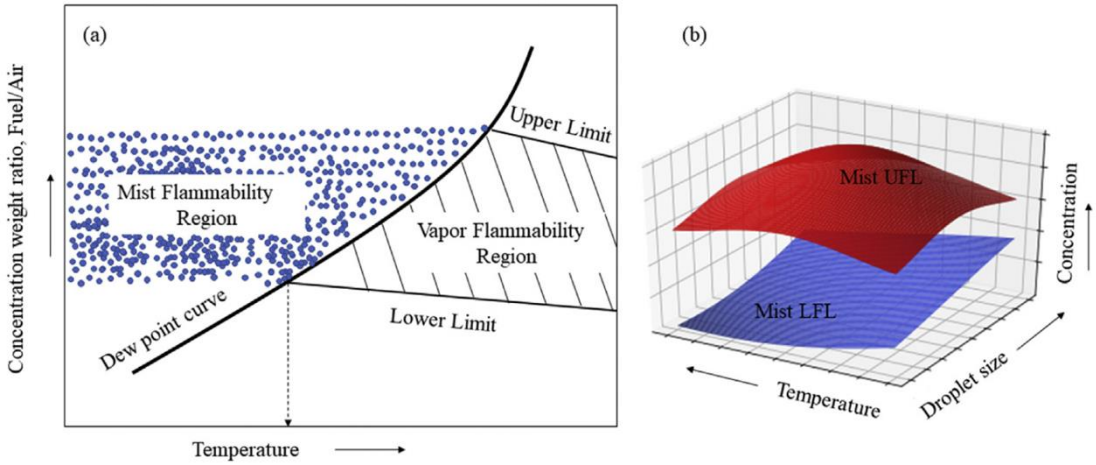

Figure II-5: (a) Flammability diagram at constant pressure (Eichhorn 1955, redrawn by Yuan et al. 2021); (b) Flammability region scheme as a function of drop size, concentration, and temperature (Yuan et al. 2021) Source: Journal of Loss Prevention in the Process Industries - Elsevier©

2.4.2.4. Limiting Oxygen Concentration (LOC)

The limiting oxygen concentration, LOC, is defined as the concentration of oxygen below which no flame propagation occurs. This parameter is usually measured under worst-case-scenario conditions, i.e., when the mixture is most flammable and is usually expressed in the percentage of oxygen (Addai et al., 2019). It is used as an explosion prevention measure to inert (decrease the oxygen content in) explosive atmospheres. Studies of LOCs associated with mists are recently scarce. Data are limited and come mostly from studies conducted in the twentieth century (Ballal and Lefebvre, 1978; Burgoyne, 1963; Sullivan et al., 1947). This parameter depends on the initial

temperature, the type of flammable mixture, the used inert gas, and the droplet size distribution.

2.4.3. Explosion severity of fuel mists

The explosion severity is an assessment of the explosion strength posed by combustible dust, vapour, or liquid aerosol in a confined vessel. It is generally used for explosion prevention and mitigating measures, especially in explosion relief venting and choosing appropriate pressure-resistant equipment when affordable. The explosion severity differs from the ignition sensitivity as the latter can be considered a parameter related to the probability that specific material ignites and gives rise to an explosion. At the same time, the former is connected to the aftermath of such explosions (Santandrea, 2020). Determining both characteristics provides a framework for explosion risk assessment and explosion safety management. Explosion severity indices comprise the maximum explosion pressure P_{max}, the maximum rate of pressure rise dP/dt_{max}, the maximum volume-normalised deflagration index K_x, and the flame propagation speed. These parameters are determined in closed vessels and are, therefore, volume-dependent (except for the deflagration index). The following sections discuss the determination techniques of the mentioned parameters, the test apparatuses used, and the influence of experimental conditions.

2.4.3.1. Experimental apparatus

Due to the presence of many factors influencing the explosion severity, it is generally suggested to carry out such tests in standardised conditions and apparatus. In the case of dust clouds and gases and vapours, standards mention two explosion vessels: a 1 m^3 vessel and a 20 L explosion sphere. Both apparatuses have advantages and disadvantages, but the 20 L is mainly used in process safety laboratories. This apparatus usually consists of a stainless-steel hollow sphere with an internal volume of 20 L. It is equipped with a water jacket to control its temperature, a vacuum pump to regulate its initial pressure, an injection system, whether for dust, vapours, or sprays, two electrodes to hold the ignition source are employed, pressure sensors to trace the pressure-time history, and a control and data acquisition system. Seen that no standard is available for determining the explosion characteristics of mists, investigators are constantly proposing modifications to existing explosion vessels or designing new apparatuses to perform such tests. For instance, Liu et al. (2016) and Sung and Zhang (2021) performed explosion severity tests on n-heptane, isopropyl nitrate, and JP-10 sprays using a confined 20 L cylinder. Yuan et al. (2019) used a 36 L dust apparatus when testing n-dodecane and n-octane mists, and Gieras et al. (2008) performed tests on hexane in chambers of four different volumes (5.6, 40, 150, and 1250 L). However, mist cloud characteristics were not controlled systematically for most of the previous studies, which hinders the reproducibility of the tests and the applicability of their results at the industrial level. These lab-scale experimental studies and others are detailed in

Table II-6, along with their findings.

2.4.3.2. Explosion overpressure and rate of pressure rise

To study aerosol explosion severity in confined vessels, the pressure-time curve helps finds the thermo-kinetic explosion parameters P_{max} and dP/dt_{max}. P_{max} is the ***maximum explosion pressure***, which mainly provides information on the thermodynamics of the explosion. dP/dt_{max} is the ***maximum rate of pressure rise***, which represents the kinetics of the explosion/combustion reaction. According to the European standard EN 15967 (2022), "Determination of the maximum explosion pressure and maximum rate of pressure rise of gases and vapours", P_{max} is the peak of the pressure-time curve, and dP/dt_{max} is the slope of the pressure rise, usually determined using specific methods between certain ranges. These parameters are essential in order to design protective equipment, compare the explosion severity of fuels or quantify the relative influence of the variation of specific operating parameters on this severity. However, it should be kept in mind that these parameters are determined in closed vessels and are volume-dependent, especially dP/dt_{max}.

2.4.3.3. Deflagration index

In order to take the volume dependency into account, the deflagration index is usually used as it normalises dP/dt_{max} by the volume of the vessel, as shown in equation II-11:

$$K = \left(\frac{dP}{dt}\right)_{max} . V^{\frac{1}{3}} \qquad \text{II-11}$$

Where K is the deflagration index, usually denoted K_{st} for dust and K_G for gases, and V is the volume of the experimental apparatus.

This deflagration index then allows the comparison of explosion severity results and usually the classification of flammable powders or gases. The cubic "law" for dust explosion states that regardless of the volume of the confined region, the same deflagration index will be attained for the same dust of similar concentration. The greater the deflagration index is, the more powerful the explosion. Regardless of its advantages, the deflagration index can sometimes be misused as the requirements for its validity are rarely fully met in practice (Santandrea, 2020). Although this index is generally used for dust and gases, some authors are recently applying it to aerosol explosions by applying the same formula but did not assess the reliability of such an approach for mists. For instance, Yuan et al. (2019) adopted K_a as a name and found a maximum of 24 barm.s^{-1} and 16 barm.s^{-1} for n-octane and n-dodecane aerosols, respectively.

2.4.3.4. *Flame propagation*

In addition to the maximum explosion pressure and the maximum rate of pressure rise (or the deflagration index), the "flame speed" is an important parameter for characterising the explosion severity. This section details this parameter and other factors to consider when examining flame propagation.

When an ignition source, specifically a spark, is actuated in a mist cloud of fine droplets, a small, somewhat spherical volume of gas and droplets is formed with rapidly increasing temperatures. This volume is known as the flame kernel. To properly develop a kernel in a flammable mixture, the energy stored in the mixture should be concentrated within a region the size of the laminar flame thickness, elevating the temperature to the adiabatic flame temperature (Spalding, 1979). Nevertheless, to sustain a flame kernel, the amount of energy generated by combustion must remain sufficient to exceed the rate of heat loss from said kernel to its surroundings. This allows the flame kernel to develop into a self-sustained propagating flame (Lewis and von Elbe, 1961). Indeed, as it is already known, combustion is a self-sustaining series of chemical reactions that occur along multiple complex reaction paths that include intermediate species. These species, along with produced heat, gradually diffuse towards the surrounding fresh gas phase by supplying enough energy to progressively reach ignition conditions. This reaction zone at the interface of the burnt and the oxygen-rich gas phases is the flame. The latter, hence, propagates through conduction, radiation, and radical propagation. The normal velocity at which the flame front travels relative to a given reference frame is defined as the ***flame propagation speed***. Nonetheless, the presence of droplets in the flow, their turbulence level, and their interactions with the flame and each other add to the complexity of this propagation-controlled phase and should therefore be taken into account (M. de Oliveira, 2019).

Although a complicated subject, many studies have been conducted until now to better understand and establish flame propagation in a mist cloud. Burgoyne and Cohen (1954) generated monodispersed tetralin aerosols and performed preliminary flame propagation characterisation for droplet diameters between 7 and 55 µm. The appearance of the flame was that of a premixed gas burner flame for diameters below 10 µm. It was also seen that the burning velocity in an aerosol of large drops is significantly higher than for a comparable aerosol of small drops. However, the method of aerosol generation precluded an independent study of fuel concentration and particle size effects. The mechanism of flame propagation was seen to change entirely over the drop-size range. Indeed, above 40 µm, drops burned individually, and each burning droplet ignited ones nearby, spreading combustion (Burgoyne and Cohen, 1954). Also, the behaviour of intermediate sizes was considered transitional. The authors finally confirmed

the presence of a critical drop diameter for homogeneous flame propagation of about 14 μm. Additional studies verified such presence by finding critical diameters ranging between 10 and 30 μm for different flammable liquids (Čekalin, 1961; Mizutani and Nishjmoto, 1972; Polymeropoulos and Das, 1975; Richards and Lefebvre, 1989). For instance, Polymeropoulos and Das (1975) later studied the effect of the droplet size on the burning velocity of kerosene-air sprays flowing upwards in a 25 mm stainless steel tube. Their findings showed that the burning velocity increases to a maximum value as the degree of atomisation in the spray increases (smaller particle size droplets) and then drops to a burning velocity approaching that of a premixed gas flow. Starting with relatively big droplets and maintaining a constant air-fuel ratio, a reduction in droplet size results in a more closely spaced suspension, a greater volumetric heat release rate, and, as a result, an increase in burning velocity. However, when the droplet size shrinks further, substantial amounts of fuel evaporate ahead of the flame and mix with the air between the droplets, resulting in the deceleration of the burning velocity. Hayashi et al. (1977) also proposed an optimum equivalence ratio that governs flame propagation, considering the fuel vapour available at the flame front only and ignoring the remaining fuel in droplets that survive the flame. Subsequently, Ballal and Lefebvre (1981a) designed a model for flame deflagration in quiescent flammable mist-air mixtures. The authors used Fuller's method (Fuller et al., 1969) of using acoustic devices, which create flat flames in tubes, in order to investigate aerosol flame propagation. Their results demonstrated that the burning velocity of mists was appreciably enhanced by a reduction in drop size to 30 μm and that the presence of fuel vapour in a multi-droplet environment was beneficial for flame propagation. Several investigations confirmed a reduction in flame speed in the presence of droplets compared to a gaseous mixture with the same equivalence ratio (Hayashi et al., 1977; Lawes and Saat, 2011; Mikami et al., 2009; Polymeropoulos and Das, 1975). This can be explained by the additional energy required to vaporise the fuel droplets near the flame front and, most importantly, the droplets' extended evaporation time scales (Ballal and Lefebvre, 1981b).

In addition to the flame propagation speed, the ***burning velocity*** is an important property for premixed flames as it encapsulates the core information of the combustible hydrocarbon mixture's diffusivity, exothermicity, and reactivity (Chong and Ng, 2021). It is the speed at which the flame front propagates relative to the unburnt mixture. The determination of this parameter is vital for hazardous explosion protection and fuel tank venting as it provides a prediction of an explosion's consequences (especially using CFD modelling). In order to determine the burning velocity, the ***laminar burning velocity*** should first be identified, as it is an intrinsic characteristic quantity of a fuel-air mixture. Undeniably, the flows are not laminar during an explosion, and the flame is not flat. Thus, to better link the burning velocity of the reactive mixture and the turbulent

flame velocity, it is possible to consider the idealised case of the laminar burning velocity, i.e., that of a flat/planar flame. The medium's thermodynamic conditions also play an essential role (Galmiche, 2014). The structure of a laminar preheated flame can be schematised as in Figure II-6 with the delimitation of the preheating and reaction zone. The heat flow from the burnt gases raises the temperature of the fresh gases upstream, over a thickness of δ_p. In this preheating zone, the chemical reactions can be considered negligible compared to the effects of thermal diffusion. In the reaction zone of thickness δ_r, the heat release peak is due to chemical reactions.

At a given pressure and temperature, the laminar burning velocity S_u^0 describes how a planar flame propagates into a quiescent unburnt mixture ahead of the flame. S_u^0 is usually maximal near the stoichiometric concentration and is determined in a fully laminar gas flow situation. Its order of magnitude usually ranges between 0.2 $m.s^{-1}$ for dust clouds and 0.4 $m.s^{-1}$ for common gases (Lemkowitz and Pasman, 2014). It should be added that, due to the necessary initial turbulence needed to disperse a powder, or more generally, an aerosol, the determination of S_u^0 is far more difficult and less common for binary mixtures than for gaseous reactants. In practice, the flame does not remain flat because the reactive zones are constantly subjected to local external pressures and heat loss, causing the flame to expand (Thimothée, 2017). The concept of flame stretching is, therefore, introduced. Many researchers have extensively studied this concept, notably Clavin (1985) and Markstein (1964). Depending on the composition of the mixture, stretching of the reactive zones can lead to a variation in the laminar burning velocity or even local extinctions. The burning velocity, therefore, mainly depends on a flame stretching factor K, which was presented by Williams (1975) and is also known as the Karlovitz factor (Karlovitz et al., 1951), and on the unstretched laminar burning velocity through either linear or non-linear relations (see Section 6.2).

Experimentally, determining a laminar burning velocity in a mist cloud, especially one intended to mimic a hazardous fuel release, proves rather tricky. Therefore, to attain low turbulence, some researchers performed tests in microgravity environments in parabolic flights or drop towers (Nomura et al., 2000; Nunome et al., 2002; Thimothée, 2017). Otherwise, the instabilities due to gravity forces, especially in the case of an upward propagating flame, should be taken into account. In addition, hydrodynamic instabilities may appear due to the deflection of the streamlines at the level of the flame front, as identified by Darrieus and Landau (Galmiche, 2014). Such instabilities modify both the local equilibrium of the thermodynamic parameters and the local concentrations of the species and cause the deformation of the flame front.

The laminar burning velocity can also be determined from experimental findings in confined explosion vessels (Bradley et al., 2014; Vukadinovic et al., 2013; Zhang et al., 2019b) or flame propagation tubes (mainly used for dust clouds). Nevertheless, due to the previously described

instabilities, the accuracy of the acquired values would be limited. The parameter can also be estimated using empirical correlations, such as that published by Neophytou and Mastorakos (2009), or a series of analytical equations such as those proposed by Rochette et al. (2019) for both weakly and fully evaporation-controlled flames. Flame propagation in fuel mist clouds is thoroughly discussed in Chapter VI.

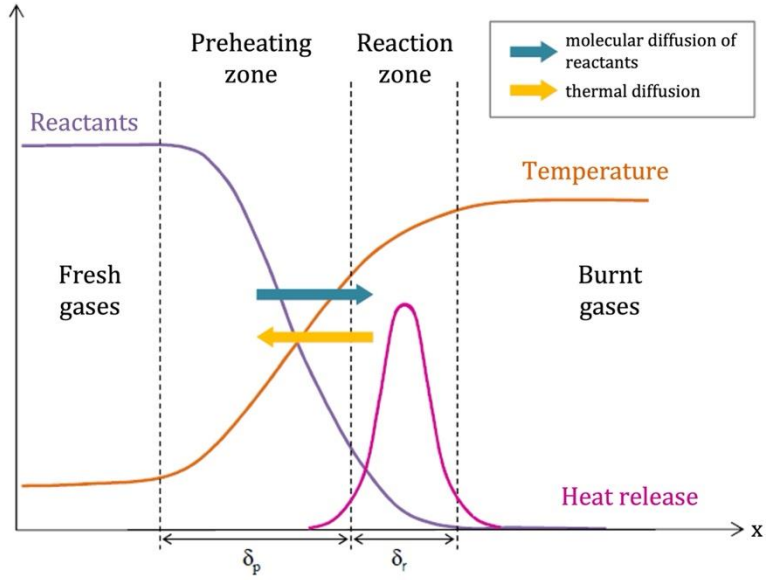

Figure II-6: Structure of a premixed laminar flame - translated from Galmiche (2014)

Table II-6: Aerosol explosion experimental studies and results in the literature

Liquid	Explosion vessel	Mist generation method	Mist cloud conditions	Ignition source & Energy	Results	Reference
Isopropyl nitrate	20 L confined cylinder	Double nozzle pneumatic atomisation system		High-temperature ignition source	Double-peak-explosion 1st: P_{max} 6.6 bar, dP/dt_{max}=604.6 bar.s^{-1} at Φ=2.4 2nd: P_{max} 15.4 bar, dP/dt_{max}=331.1 bar.s^{-1} at Φ=1.8	(Sung and Zhang, 2021)
n-heptane	20 L confined cylinder	Double nozzle pneumatic atomisation system	SMD between 7.07 and 7.11 µm	High-temperature ignition source	Double-peak-explosion 1st: P_{max} 6.2 bar, dP/dt_{max}=1253.4 bar.s^{-1} at Φ=3.6 2nd: P_{max} 13.4 bar, dP/dt_{max}=159.8 bar.s^{-1} at Φ=1	(Sun and Zhang, 2021)
n-octane & n-dodecane	36 L dust apparatus	Solenoid fuel injector	SMD of 110 µm and 117 µm for n-octane and n-dodecane respectively	Coil spark - 100 mJ	n-octane: P_{max} 6.23 bar, K_a about 24 barm.s^{-1} at Φ=1 n-dodecane: P_{max} 4.72, K_a about 16 barm.s^{-1} at Φ=1.1	(Yuan et al., 2019)
JP-10	20 L confined cylinder	Double nozzle pneumatic atomisation system	SMD of 20 µm and 35 µm - U_{rms} varies between 3.5 and 7 m.s^{-1}	Spark ignition - 40.32 J	20 µm: P_{max} 8.7 bar, dP/dt_{max} 1210 bar.s^{-1} at 435 g.m^{-3} 35 µm: P_{max} 8.4 bar, dP/dt_{max} 880 bar.s^{-1} at 626 g.m^{-3}	(Liu et al., 2016)
Diethyl ether	20 L spherical vessel	Double nozzle pneumatic atomisation system	SMD of 12.89 µm and 22.9 µm	Spark ignition - 40.32 J	12.89 µm: P_{max} 9.8 bar, dP/dt_{max} 3245.5 bar.s^{-1} at 285.36 g.m^{-3} 22.9 µm: P_{max} 7.8 bar, dP/dt_{max} 2091.3 bar.s^{-1} at 278.23g.m^{-3}	(Bai and Wang, 2015b)
RP-5 and RP-3	20 L spherical vessel	Spray nozzle	5 different injection pressures	Pyrotechnical ignitors - 2 kJ	RP-5: P_{max} 6.45 bar and dP/dt_{max} 32.8 bar.s^{-1} at P_{inj} = 3.43 bar RP-3: P_{max} 6.42 bar and dP/dt_{max} 35.1 bar.s^{-1} at P_{inj} = 17.17 bar	(Zheng et al., 2014)
-10 military diesel and -35 ordinary diesel	20 L spherical vessel	Spray nozzle	5 different injection pressures	Pyrotechnical ignitors - 2 kJ	-10 diesel: P_{max} 6.44 and dP/dt_{max} from 34.7 bar.s^{-1} at P_{inj} = 3.43 bar -35 diesel: P_{max} 5.92 bar and dP/dt_{max} 34.2 bar.s^{-1} at P_{inj} = 17.17 bar	(Lei et al., 2014)
Hexane	5.6, 40, 150, and 1250 L chambers	Compressed liquid dispersion system	Controlled droplet diameters between 0.25 and 0.7 mm	Electrical spark discharge of 5 J energy or chemical ignitors of 2 kJ energy	250 µm: P_{max} greater than 4 bar. 700 µm: P_{max} 2 bar	(Gieras et al., 2008)

2.4.3.5. Influence of the mist concentration

The significant influence of the mist concentration has been highlighted throughout the previous sections. As this study specifically concerns fuel mist, most of the fluids of interest are multi-component, which imposes the use of $g.m^{-3}$ units instead of the commonly-used fuel equivalence ratio. Nonetheless, an estimation of the fuel equivalence ratio can be employed via surrogate single component liquids. Moreover, theoretical mist concentrations are generally less than experimental ones. Due to the high fluctuations of a mist cloud, especially in a confined vessel, the estimation of the concentration involved in the explosion proves difficult. Indeed, the sedimentation of droplets, their mutual interactions, and the rain-out phenomenon (proportion of the liquid aerosol collected by contact with the wall of the vessel or the ground/floor in the case of an accidental release) play a significant role in varying the local concentration. The latter is of great importance as it affects the ignition sensitivity and the explosion severity (see Chapter V for more details). It should also be noted that a highly saturated mist cloud may cause flame quenching, which is rarely experienced due to the circulation of the injected mist in the confined vessel.

2.4.3.6. Influence of initial temperatures and pressures

Explosivity experiments are usually conducted at ambient temperatures and pressures, so their results can be extrapolated to most industrial cases. Nevertheless, several studies were carried out to study the influence of the initial temperature and pressure on the explosion severity of fuel-air mixtures as mist release conditions vary significantly. For instance, Zhang et al. (2019) employed a cylindrical vessel where the initial temperature was varied between 353 and 393 K and the initial pressure between 0.6 to 1 bar. Tests were conducted on n-hexane sprays. The authors acquired the thermo-kinetic explosion parameters P_{max} and dP/dt_{max}, as well as the laminar burning velocity. Their findings showed that P_{max} and dP/dt_{max} increased with increasing initial pressures. This influence was related to the increase in the amount of fuel involved in the combustion mixture, which increased the release of chemical energy and eventually led to an increase in explosion pressure. As a consequence, these experiments were not carried out at a constant fuel equivalence ratio. On the other hand, the thermo-kinetic parameters decreased with increasing initial temperatures. The authors explain this variation by relating it to the decrease in burning charge and thermal loss with increasing initial temperatures. They concluded that such an increase accelerates the droplets' evaporation, causing the phenomenon to turn into a gaseous explosion. As for the laminar burning velocity, it decreased with increasing initial pressures and with decreasing initial temperatures. Similar results were obtained by studies of pre-evaporated clouds (Cammarota et al., 2019; Kurata et al., 1994; Mitu and Brandes, 2017; Razus et al., 2011; Vukadinovic et al., 2013).

2.4.3.7. Influence of droplet diameters

In addition to the concentration and the initial experimental conditions, the droplet size distribution is one of the most influencing factors impacting the ignitability and explosivity of hydrocarbon aerosols. Indeed, Rao and Lefebvre (1976) indicated that improving atomisation and droplet size distribution is the most effective method to increase the fuel evaporation rate. Bowen and Shirvill (1994) also clearly highlighted the critical dependence of the ignition of aerosols on the droplet size for a fixed fuel/air ratio. The presence of a critical diameter that influences the evolution of the flame propagation speed was also highlighted in Subsection 2.4.3.4.

To study the influence of the droplet diameter, researchers disperse sprays under the same experimental conditions while varying the DSD, whether by changing the orifice diameter or by varying the injection pressure. Liu et al. (2016) demonstrated that the explosion severity decreases with increasing Sauter Mean Diameter (SMD) of JP-10 sprays. Y. Wang et al. (2017) confirmed the previous findings and added that as the mixture became denser, the influence of the DSD, i.e., the specific area of the droplets, on the peak pressure (P_{ex}) declined. A similar impact was observed on dP/dt_{ex}. The authors stated that the mean ratio of the vapour and liquid-phase concentration decreased with increasing SMD. It was then concluded that under the same conditions, the rate of evaporation of droplets with a higher SMD was lower than that with a lower SMD, which was most probably related to the increase in injection pressure hence an increase in turbulence. The DSD was also found to negatively influence the LEL (meaning that a DSD increase tends to decrease the LEL) (Burgoyne, 1963; Burgoyne and Cohen, 1954; Cook et al., 1977; Danis, 1987); however, such influence depends on experimental conditions and whether it is an upward or downward flame propagation. Indeed, contradictory conclusions were drawn by Liu et al. (2015) and Y. Wang et al. (2017), but further investigations should be carried out, which has been notably done within the framework of this study (see Section 5.4). In addition, Lewis and Elbe (2012) stated that larger droplets tend to become more distorted due to their increased inertia. This distortion may cause a non-symmetric expanding flame providing an imbalanced thrust force, accelerating large droplets, and promoting flame propagation.

2.4.3.8. Influence of initial turbulence levels

In a turbulent combustion environment, such as an engine, differences in laminar burning velocity across fuels can be observed. In theory, a fuel having a greater laminar burning velocity would thus be anticipated to burn quicker in an engine (Cracknell et al., 2013). The medium in which the flame propagates in an explosion on an industrial site has a level of turbulence which can accelerate the flame speed from a few $m.s^{-1}$ to near sonic speeds, increasing heat output via

promoting transport processes. The literature discusses several correlations between turbulent and laminar burning velocities (Dahoe and de Goey, 2003; Karlovitz et al., 1951) (Subsection 2.4.3.4). Turbulence's beneficial effect on flame propagation velocity, and therefore on the amount of energy released per unit volume, explains its widespread use in combustion industries. Generally, turbulence increases the reaction by increasing the flame surface, but it can also cause extinction in extreme cases. Previous mist explosion studies discussing the influence of the initial turbulence level are scarce. Wu et al. (2022) studied the influence of the mist injection pressure into an explosion vessel on the thermo-kinetic explosion parameters. The authors found that the increase of the injection pressure, which was accompanied by a decrease of the DSD, promoted the increase of both P_{ex} and dP/dt_{ex}.

2.4.4. Combustion kinetics

The ability to understand the behaviour of a single drop of fuel is the basis upon which practical research may be built. In a well-characterised environment, studying the evaporation of an isolated drop by raising the temperature of the surrounding gases or by combustion allows researchers to obtain first-rate information, such as evaporation speed and the influence of the medium. Godsave (1953) developed a simplified droplet evaporation model, the ***d²-law***, to understand the standard evaporation process of a single droplet. It demonstrates that the square of the droplet diameter decreases linearly with time in a diffusion-controlled process (see equation II-12). It is generally considered a well-established law to represent the evaporation of a spherically symmetrical droplet in a fixed environment where the interaction between droplets is considered negligible, and the temperature of the droplet is constant and uniform.

$$d^2(t) = d_0^2 - K.t \qquad \text{II-12}$$

Where d is the droplet diameter at time t, d_0 is the initial droplet diameter, and K is the evaporation rate constant of the fuel droplet. A more detailed approach will be developed in Section 6.3.

Grasping the entire precise structure of spray combustion by tracking every microscopic activity connected with each droplet that interacts with its surrounding gas is hard since spray combustion involves a large number of small liquid droplets. Consequently, from a practical standpoint, only averaged quantities are significant. The combustion of droplets can therefore adopt distinct combustion regimes that can be apprehended through the so-called “combustion group” theory, as well as the d^2-law of evaporation.

Group combustion is a theory developed by Chiu and Liu (1977) and Chiu et al. (1982) based on continuum theory and a quasi-steady-state assumption. The authors proposed distinct

combustion regimes according to a group number, denoted *G*, starting with a mist of droplets submerged in an oxidising atmosphere and at high temperatures. *G*, a dimensionless number, is the ratio between the droplet evaporation rate and the heat diffusion rate of the hot gases in the cloud and is expressed as shown in equation II-13. This parameter was demonstrated to have a significant impact on the temperature, oxygen, and vapour content distribution in a flame and its location.

$$G = 1.5Le\left(1 + 0.276Re^{\frac{1}{2}}\,Sc^{\frac{1}{3}}\right)\left(\frac{D}{s_D}\right)N^{\frac{2}{3}} \qquad \text{II-13}$$

Where *Le* is the Lewis number (often considered equal to unity), *Sc* is the Schmidt number, *Re* is the Reynolds number, *D* is the mean droplet diameter, s_D is the inter-droplet distance, and *N* the number of droplets inside the cloud.

According to the authors, droplet group combustion comprises four modes: single droplet combustion, internal group combustion, external group combustion, and external sheath combustion. The modes and their characteristics are detailed in Figure II-7. For instance, some physical models of the combustion of a dense droplet cloud and fuel sprays predict that droplets in a dense spray zone would not burn with individual flames, as indicated in a classical theory of single droplet combustion. Instead, the droplets in the cloud evaporate in the dense spray zone, and the resulting fuel vapour is carried radially outward, mixes with air, and burns with a global envelope flame that surrounds all the droplets in the cloud or dense spray region. The above-described combustion mode is known as external group combustion and is expected to occur in typical industrial burners.

The applicability of this theory was validated by steady-state and quasi-steady experiments. Labowsky and Rosner (1978) notably found similar results and added the Thiele modulus $\frac{r_c}{r}\sqrt{3\varphi}$ as a significant factor for determining the start of internal group combustion. φ, here, is the volume fraction of the droplets, *r* is the radius of the droplet, and r_c is the radius of a spherical mist cloud.

Such theories, however, are quasi-steady and do not take into account unsteady conduction in the gas phase across the cloud or transient droplet heating. These sorts of unsteadiness can be severe since the time and length scales for conduction and the time scale for droplet heating are both long. Indeed, the group combustion theory does not consider the hydrodynamic interactions between the mist cloud and the flame. The reaction zone's location depends only on the composition of the local mixture, and droplet-droplet interactions are only examined by their evaporation (Saat, 2010). According to Zhou et al. (1999), the assumption of stationary droplet evaporation in Chiu's group combustion theory is only justified for a spray of large droplets

because the relative motion between the surrounding gas phase and the droplets is significantly small due to the large inertia of such droplets, implying that convective effects on droplet evaporation are not negligible. On the other hand, in order to account for the influence of droplet movement on spray evaporation, the theory overestimates convective effects on the droplet evaporation rate for small droplets. As a result, rather than being a complete theory, the aforementioned theory serves as a foundation for additional research (Sirignano, 2014). Indeed, according to the author, even if significant deviations, such as forced or natural convection and transient liquid heating, were neglected, dense spray clouds instigated important variations of the expected behaviour of an isolated droplet. The use of the d^2-law is therefore disadvised in practical situations.

Numerous different approaches have been followed. Borghi and Champion (2000) and Chan (1996) incorporated the evaporation time t_v, the flame characteristic time t_f and its thickness δ_f. The authors stated that when $t_v << t_f$, the flame front propagates in a single-phase flow like a premixed gaseous flame where the drops had evaporated in the preheating zone. In the case where $t_v > t_f$, the situation becomes more complex. For δ_f greater than the inter-droplet average distance s_d, the flame front thickens due to dispersed droplets on its inside. On the contrary, the droplets burn in a secondary reactive zone, having crossed the primary premixing front. The authors also add an influencing parameter on the shape of this zone, the separation factor S (which is equal to the ratio of s_d and the flame radius that potentially envelops each droplet). For low values of S, a group combustion regime is followed, where the drops burn individually or in small groups surrounded by a flame. For higher values of S, a mode of percolating combustion, then of combustion in pockets is distinguished. Sirignano (2007) and Sirignano and Wu (2008) also developed a droplet array vaporisation and burning theory based on a non-unitary Lewis number taking into account the influence of neighbouring droplets on the Nusselt number, the Sherwood number, and the rates of vaporisation and heat release. Their theory is considered applicable in dense sprays but is still limited to assuming that all droplets have the same temperature and neglecting natural or forced convection.

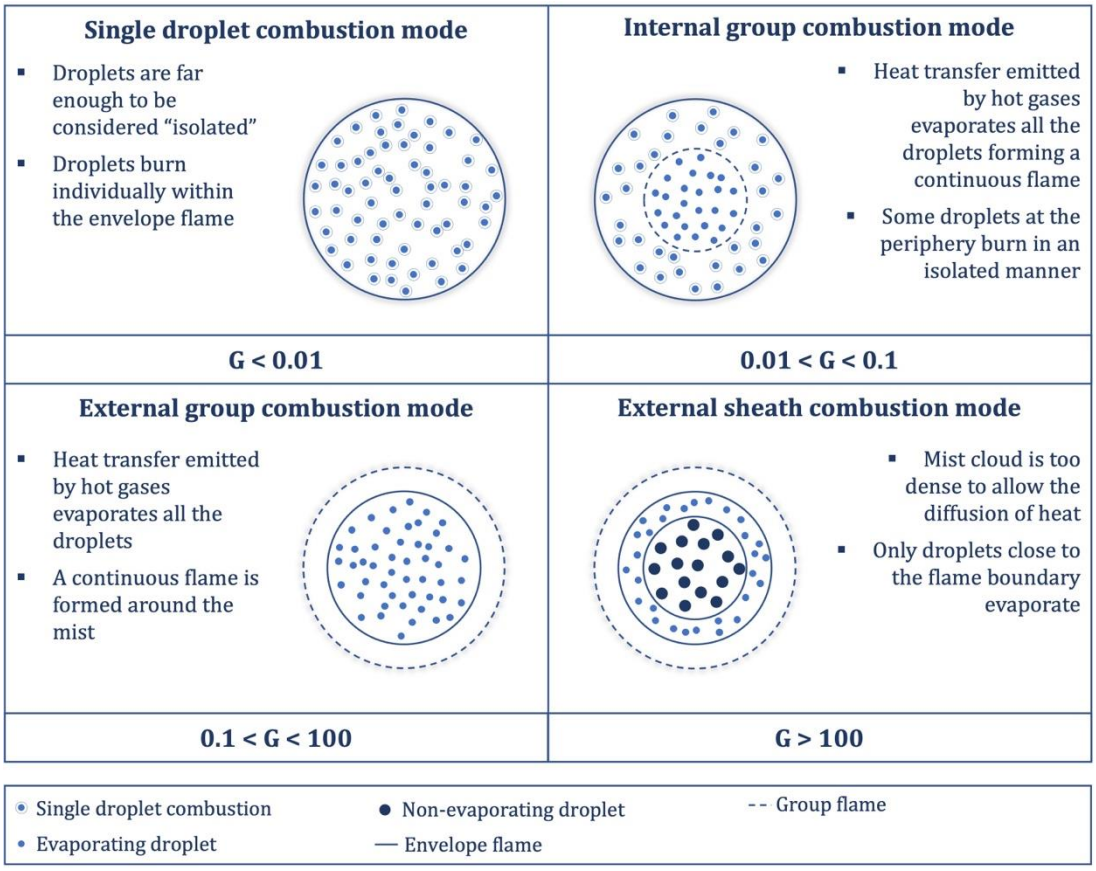

Figure II-7: Mist cloud combustion regimes proposed by Chiu and Liu (1977) - readapted from Nakamura et al. (2005) and Saat (2010)

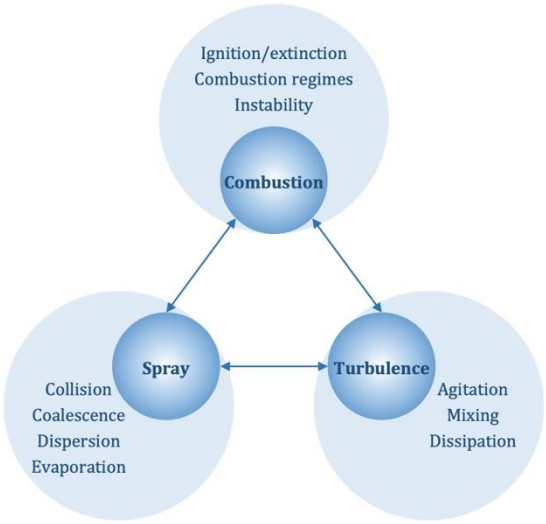

Figure II-8: Two-phase turbulent combustion - triple interaction between spray, turbulence, and combustion conditions - redrawn from Boileau (2007)

The complexity of two-phase combustion was expressed by Boileau (2007), who stated that it arises from the significant interaction of three major phenomena: combustion chemical reaction, two-phase flows, and turbulence. The author stated that the investigation of such a combustion process necessitates an interdisciplinary approach in which the examination of couplings is like that of phenomena taken separately.

Indeed, combustion-turbulence and spray-combustion interactions were discussed in the preceding sections. Moreover, the turbulence-spray interaction was conveyed in Subsection 2.4.1.3. The more interactions are taken into account, the more complex the two-phase combustion analysis becomes.

Figure II-9 depicts the potential combustion regimes that a spray can follow at the exit of a spray nozzle. Primary and secondary atomisation are taken into account, as well as group combustion with possible extinction or reignition regions.

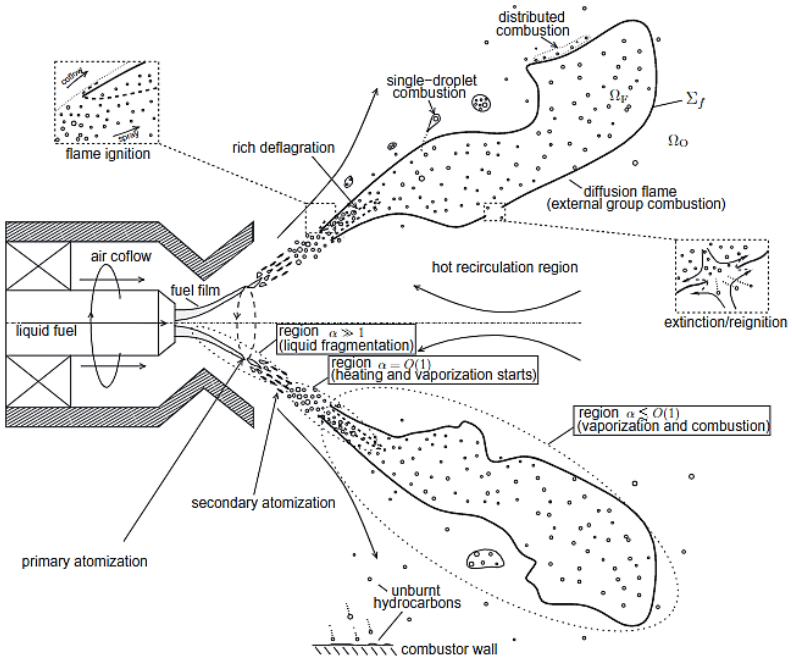

Figure II-9: Combustion regimes of a spray at the exit of a fuel injector (Sánchez et al., 2015)

2.4.5. Risk analysis

As seen from the previous discussions, numerous factors play a role in the ignition of a mist cloud. We are in an environment that might be considered controlled but is not sufficiently representative of the uncontrolled industrial conditions that may lead to an accident. This risk aspect of mist releases has begun to be addressed but is still limited by their high complexity.

Santamaría Ramiro and Braña Aísa (1998) described the word risk as an indication of the possibility of suffering loss or damage to people. The authors also shed light on the word "hazard", which describes a physical or chemical condition that can potentially cause damage to people, properties, or the environment. Risk analysis is a systematic approach followed to identify and assess factors that may put people or a certain project at risk. According to Santamaría Ramiro and Braña Aísa (1998), three stages of risk analysis for the prevention of accidents generally imply:

- Identifying all adverse events that could lead to a hazard. Asking "what could go wrong?"
- Analysing all mechanisms that could lead to such events. Asking "what consequences can be expected?"

- Estimating the unwanted consequences and their occurrence frequency. Asking "what is the expected frequency?"

To help reduce the likelihood of possible risks, the Risk Assessment Matrix (Figure II-10) is a visual representation tool that could be used. After identifying the risks, analysing them, and assessing their impact level, one can prioritise all risks by ranking them as critical, high, moderate, low, and extremely low. Each rank corresponds to a different colour, as seen in Figure II-10, and is placed in a cell according to its probability of occurrence as a function of its caused damage.

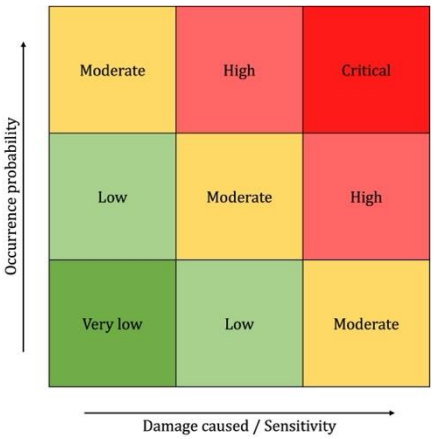

Figure II-10: Risk Assessment Matrix

Based on the operating pressure and the size of the emitted aerosol particles, Krishna et al. (2003) proposed a risk matrix to rate the risks of heat transfer fluid aerosols. Figure II-11 depicts this matrix and shows that a high pressure and a low Sauter Mean Diameter (SMD) form the highest hazard, while large droplet diameters at low operating pressures result in the lowest hazard.

Yuan et al. (2021) pinpoint a limitation of this matrix, stating that the authors only took into account the general quantities (operation pressure and droplet size), which are relatively hard to know before an incident takes place, seen that the droplet size depends on the operation pressure, the size of the orifice, and many other external conditions. Yuan et al. (2021) subsequently proposed a conceptual method allowing the risk analysis of flammable liquids. Figure II-12(a) depicts the risk matrix for aerosol deflagration severity based on the potential maximum explosion pressure and the deflagration index. These parameters form a thermo-kinetic representation of the explosion. Seen that studies in this field are limited, the authors proposed the use of Chemkin or Stanjan to predict the explosion pressure. As for the deflagration index, several models exist, allowing its prediction, such as those proposed by Dahoe and de Goey (2003) and Di Benedetto and Russo (2008). Figure II-12(b) presents the risk matrix related to the probability of atomisation. To predict such probability, several correlations relating the mean diameter of the SMD to the liquid's properties (specifically its viscosity and surface tension) exist. The influence of such parameters is discussed in Subsection 2.4.1.3. Based on these two risk matrices, the authors were able to propose a risk matrix for the risk assessment of aerosol explosions where, for instance, very high explosion severity along with a high probability of atomisation form the highest risk.

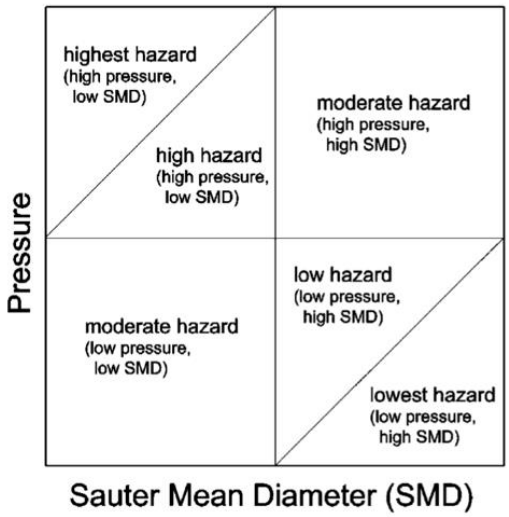

Figure II-11: Hazard levels of heat transfer fluids (Krishna et al. 2003)

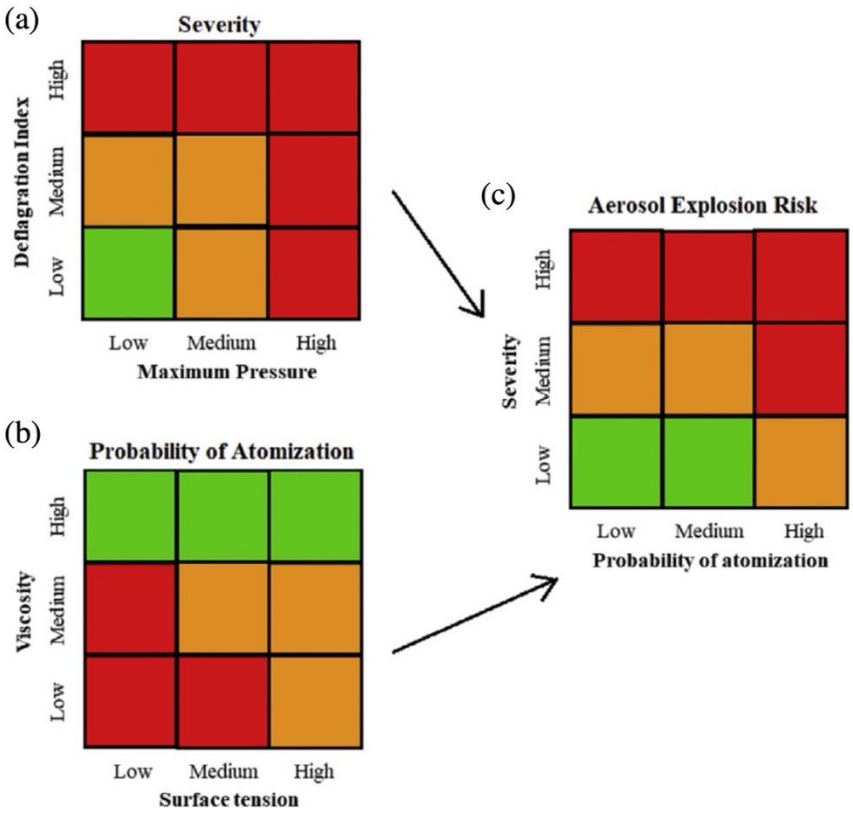

Figure II-12: Risk matrix for (a) aerosol deflagration severity (b) probability of atomisation (c) risk assessment for aerosol explosion (Yuan et al. 2021)

Summary

At present, an ATEX risk assessor is often at a loss when faced with the risk of an explosive mist atmosphere. This chapter provides essential elements for understanding what a mist cloud is and the associated phenomenology relating to the ignition and explosion of such a cloud. These aspects are put into perspective in relation to the accidentology of the subject. This chapter thus constitutes an essential basis for understanding the issues and problems relating to this study. A mist cloud principally consists of liquid droplets of sizes ranging from 1 to about 100 µm. The study of previous accidents revealed that mist explosions have taken place in manufacturing, transport, aviation, and other industries. Most of the releases were greater than 10 kg and occurred through release orifices with an equivalent diameter of between 1 mm and 10 mm and were considered "under pressure". Such ongoing incidents stress the importance of establishing means of prevention, protection, and mitigation for ATEX and better understanding the accidental risks associated with mist explosions.

A third part was then devoted analysing existing standards and proposals used to categorise petroleum fluids and evaluate associated hazards. Currently, the key indicator for such a categorisation is the flashpoint, boiling point, and handling temperature. Liquids that can create a flammable mist are comprised in Category C if they are used in systems with pressure above 5 bar or at temperatures above the flashpoint but below the boiling point. However, additional guidance on managing the risks associated with the formation of a flammable mist remains scarce. This section also mentioned a Joint Industry Project in which the HSE (UK) put forward a liquid classification system that categorises liquids according to their ease of atomisation and flashpoint.

Finally, a literature review highlighted the critical factors affecting mist generation and ignition, as well as elements relating to the phenomenology of the explosion. The different methods of mist generation, including liquid pressurisation, electrospray, condensation, and spray nozzles, were discussed in detail. Moreover, some characterisation techniques that form an essential step while studying the flammability of oil mists were mentioned in addition to influencing factors, such as the ambient conditions and the liquid properties. This section also helped derive practical criteria for assessing the ignition hazards and distinguished between the ignition sensitivity and the explosion severity of a mist cloud. Experimental apparatus, which are sometimes used by safety professionals to assess the ignition risks of fuel mists, were also listed along with influencing factors. This chapter then ended following a study of the aspects relating to the kinetics of droplet combustion, which is essential for a good understanding of the dangerous phenomena associated with mists.

Résumé

A l'heure actuelle, un évaluateur des risques ATEX est souvent démuni lorsqu'il est confronté au risque de formation d'une atmosphère explosive de brouillard. Ce chapitre fournit des éléments essentiels afin de comprendre ce qu'est un nuage de brouillard ainsi que la phénoménologie associée relative l'inflammation et l'explosion d'un tel nuage. Ces aspects sont mis en perspective par rapport à l'accidentologie recensée sur le sujet. Ce chapitre constitue ainsi une base essentielle pour la compréhension des enjeux et problématiques relatifs à cette étude. Dans une On retiendra qu'un nuage de brouillard consiste essentiellement en des gouttelettes de liquide dont la taille varie de 1 à environ 100 µm. L'étude de l'accidentologie a permis d'analyser les explosions de brouillard documentées dans les secteurs de la production, du transport, de l'aviation et d'autres industries. Les fuites impliquées dans ces incidents étaient le plus souvent créées par des pulvérisations sous pression ou des aérosols de condensation de carburants industriels à point d'éclair élevé tels que le kérosène, le diesel, des lubrifiants ou encore du fioul. La plupart des rejets étaient supérieurs à 10 kg et ont eu lieu à travers des orifices de rejet d'un diamètre équivalent compris entre 1 mm et 10 mm et ont été considérés comme "sous pression". Ces incidents répétitifs soulignent l'importance de mettre en place des moyens de prévention, de protection et de mitigation tant pour gérer les risques ATEX que pour mieux appréhender les risques accidentels liés aux explosions de brouillard.

Une troisième partie a ensuite été dédiée à l'analyse des normes et guides existants actuellement utilisés pour catégoriser les fluides pétroliers et évaluer les risques associés. L'indicateur clé pour une telle catégorisation est actuellement le point d'éclair, le point d'ébullition et la température d'utilisation. Les liquides qui peuvent créer un brouillard ou un spray inflammable sont compris dans la catégorie C s'ils sont utilisés dans des systèmes dont la pression est supérieure à 5 bars ou à des températures supérieures au point d'éclair mais inférieures au point d'ébullition. Les recommandations pour la gestion des risques associés à la formation d'un brouillard inflammable restent toutefois peu fournies. Ce chapitre mentionne également un Joint Industry Project dans lequel le HSE (UK) a proposé un système de classification des liquides en fonction de leur facilité d'atomisation et de leur point d'éclair.

Enfin, une revue de la littérature scientifique a permis de mettre en avant les facteurs importants conditionnant la génération d'un brouillard et son inflammation ainsi que les éléments relatifs à la phénoménologie de l'explosion. Les différentes méthodes de génération de brouillard, notamment la pressurisation de liquide, l'électrospray, la condensation et les buses de pulvérisation, ont été examinées en détail. En outre, certaines techniques de caractérisation qui constituent une étape essentielle dans l'étude de l'inflammabilité des brouillards d'huile ont été mentionnées, ainsi que les facteurs d'influence, tels que les conditions ambiantes et les propriétés

des liquides. Cette section a également permis d'établir des critères pratiques pour évaluer les risques d'inflammation d'un brouillard, en distinguant la sensibilité à l'inflammation de la sévérité d'explosion d'un nuage de brouillard. Les appareils expérimentaux, parfois employés par des acteurs de la sécurité pour évaluer les risques d'inflammation de brouillard des carburants, ont également été recensés ainsi que les paramètres expérimentaux d'influence. Ce chapitre se termine par une étude des aspects relatifs à la cinétique de combustion de gouttelettes, essentielle pour la bonne compréhension des phénomènes dangereux liés aux brouillards.

Chapter III:
Mists and methods

Following the literature review, a dimensional analysis allowed highlighting the main parameters that impact mist formation and should be examined to meet the objectives of this study (Section 1.4). Several experimental techniques were employed to pre-characterise a set of fuels selected according to their industrial interest and physicochemical properties. A mist generation system was chosen to disperse the liquid into a specific explosion vessel. Subsequently, the mist cloud would be ignited using a specifically-chosen ignition source. Flame propagation tests were also performed, and complementary in-situ mist characterisation measurements were carried out. All necessary details are explicitly discussed in this chapter. It should be noted that the design of the new set-up and the development of the experimental protocol are both discussed in Chapter IV.

3.1. Dimensional analysis of mist generation

After identifying the numerous factors that may influence the atomisation process of a mist, predictive correlations linking a mean droplet diameter to injection conditions and fluid properties follow. Because the inclusion of dimensionless groups reduces the quantity of experimental data and is more easily applicable, dimensional analysis is the most often adopted quantitative approach. Previous studies conducted by Elkotb et al. (1982), Inamura and Nagai (1985), Krishna (2003), Mandato et al. (2012), and others proposed numerous correlations linking important parameters to atomisation characteristics.

The selected influencing parameters are listed in Table III-1 for the current dimensional analysis. These eight parameters imply three different dimensions: M (mass), L (length), and T (time). Hence, five independent dimensionless numbers can be linked through a correlation to describe the mist atomisation process, according to the Vaschy-Buckingham theorem (Buckingham, 1914). The SMD was chosen because it represents the volume to surface area ratio of the spray and is the most commonly used mean diameter in fuel droplets combustion systems and other applications requiring heat and mass transfer to liquid droplets (Lefebvre and McDonell, 2017). The equivalent diameter of the outlet orifice, d_o, was chosen to characterise the influence of the nozzle geometry on the atomisation process; other geometrical parameters related to the nozzle body could have been evoked but were discarded because their influence is less direct. This dimensional analysis will be applied to propose relationships linking the DSD to the injection conditions and influential fluid properties (see Subsection 4.1.4). It will also help classify fluids according to the ease of atomisation.

Table III-1: Influencing parameters used for the dimensional analysis of mist generation

Notation	Definition	SI unit	Dimension
SMD	Sauter mean diameter	m	L
d_o	Equivalent orifice diameter	m	L
v	Injection velocity	$m.s^{-1}$	$L.T^{-1}$
ρ_g	Air density	$kg.m^{-3}$	$M.L^{-3}$
ρ_l	Liquid density	$kg.m^{-3}$	$M.L^{-3}$
σ	Surface tension	$N.m^{-1}$	$M.T^{-2}$
μ_g	Air dynamic viscosity	Pa.s	$M.L^{-1}.T^{-1}$
μ_l	Liquid dynamic viscosity	Pa.s	$M.L^{-1}.T^{-1}$

3.1.1. Dimensionless numbers

From the listed parameters, three were designated as basic parameters (μ_g, v, and d_o), which contain all three units. The five remaining parameters were then coupled with the basic ones to form a dimensionless number, as shown in equation III-1:

$$\pi_1 = \mu_l . {\mu_g}^a . v^b . {d_o}^c \qquad \text{III-1}$$

The dimensions were raised to unknown powers, ensuring a dimensionless result:

$$0 = M.L^{-1}.T^{-1}.M^a.L^{-a}.T^{-a}.L^b.T^{-b}.L^c \qquad \text{III-2}$$

Consequently, the three coefficients were verified:

Dimension M: $1 + a = 0$

Dimension L: $-1 - a + b + c = 0$

Dimension T: $-1 - a - b = 0$

The first dimensionless number π_1 can therefore be expressed as follows:

$$\pi_1 = \frac{\mu_l}{\mu_g} \quad \text{III-3}$$

A similar approach yielded the four remaining dimensionless numbers:

$$\pi_2 = \frac{\rho_l v d_o}{\mu_g} \quad \text{III-4}$$

$$\pi_3 = \frac{\sigma}{\mu_g v} \quad \text{III-5}$$

$$\pi_4 = \frac{\rho_g v d_o}{\mu_g} \quad \text{III-6}$$

$$\pi_5 = \frac{SMD}{d_o} \quad \text{III-7}$$

A comparison with existing dimensionless numbers was applied to assess the physical significance of those numbers. For instance, a combination among π_1, π_2, and π_3 led to finding the Laplace number:

$$La = \frac{\rho_l \sigma d_o}{{\mu_l}^2} = \frac{\pi_2 \pi_3}{{\pi_1}^2} = {\pi_2}' \quad \text{III-8}$$

Similarly, the Weber number was found through a ratio between π_4 and π_3:

$$We = \frac{\rho_g v^2 d_o}{\sigma} = \frac{\pi_4}{\pi_3} = {\pi_3}' \quad \text{III-9}$$

A density ratio was also obtained from π_2 and π_4:

$$\frac{\rho_l}{\rho_g} = \frac{\pi_2}{\pi_4} = {\pi_4}' \quad \text{III-10}$$

The dimensionless number π_5 can consequently be expressed as a function of the other dimensionless numbers as seen in equation III-11. A correlation linking these parameters can be acquired using coefficients A to E as seen in equation III-12.

$$\frac{SMD}{d_o} = f(\pi_1, \pi_2', \pi_3', \pi_4') = f\left(\frac{\mu_l}{\mu_g}, La, We, \frac{\rho_l}{\rho_g}\right) \quad \text{III-11}$$

$$\frac{SMD}{d_o} = A\left(\frac{\mu_l}{\mu_g}\right)^B (La)^C (We)^D \left(\frac{\rho_l}{\rho_g}\right)^E \quad \text{III-12}$$

Coefficients A to E can then be estimated experimentally as shown in Subsection 4.1.4.

3.1.2. Physical significance

Each dimensionless number has a physical significance showing its influence on the atomisation process of a certain liquid:

Viscosity ratio

The viscosity ratio, $\left(\frac{\mu_l}{\mu_g}\right)$, represents the ratio of the fuel's viscosity to that of the air.

Laplace number

The Laplace number (equation III-8), which is the ratio of surface tension forces to viscous forces within the liquid, represents the contribution of liquid characteristics to the atomisation process.

Weber number

The Weber number, expressed in equation III-9, is the ratio of the dynamic forces produced by the surrounding air to the surface tension, and it exhibits the influence of external forces on the development of droplets and stream breakup. When dynamic forces dominate, a higher Weber number is attained. It should be noted that We and Oh (Section 2.3) are related through equation III-13:

$$Oh = \frac{\sqrt{We}}{Re} \qquad \text{III-13}$$

Density ratio

The density ratio, $\left(\frac{\rho_l}{\rho_g}\right)$, similarly signifies the ratio of the fuel's density to the density of air.

3.2. Fuel selection

The dimensionless numbers previously listed will help differentiate fuels and classify them according to their atomisation characteristics. For this study, fuels were chosen to cover a wide range of physicochemical properties and industrial use, as explosive mist atmospheres can occur in various sectors (Figure II-3). Five complex fuels, including aviation kerosene jet fuel - Jet A1, diesel, light fuel oil, biodiesel, and Mobil DTE VG 68 Heavy Medium (later called Mobil DTE) were chosen after being listed in the existing classification of HSE discussed in Section 2.3. These fuels are all multi-component high-flashpoint liquids with increasing dynamic viscosity. Ethanol and isooctane, two liquids largely used in numerous chemical processes, were also added to this study not only for their industrial interest but also for being single-component liquids of well-known properties and combustion behaviours.

Ethanol

The industrial value of ethanol has been continuously growing throughout the years with its emergent use as an engine fuel or an oxygenated fuel additive for automobiles. Such demand for ethanol or ethanol-fuel blends is and will keep leading to an increase in its production and transport, hence increasing the requirements to manage fire or explosion risks. Moreover, the high volatility of ethanol leads to its rapid evaporation (Pinheiro et al., 2019) near the flame front when dispersed in small droplets, which justifies the comparison with ethanol vapour explosion results as done by Thimothée (2017).

Isooctane

Isooctane is commonly used as a gasoline surrogate and is typically added in relatively high proportions to improve fuel's knock resistance. It has been extensively used in droplet and vapour mixture combustion studies, including Dombrowski et al. (1974), Sulaiman (2006), and Saat (2010).

Kerosene Jet A1

In 2009, Santon showed that 7 incidents, over 29 detailed in his review, were related to kerosene mists. They were mostly related to transportation activities, from cargo accidents to aviation kerosene explosions (Santon, 2009). Filling or emptying (voluntarily or accidentally) of storage must also be carefully examined with regard to aerosols generation. For instance, kerosene explosions occurred in Cilacap (1995) and Mombasa (2013) during tank refuelling and storage leaking, respectively. Bowen and Shirvill (1994) also pointed out the risks behind the potential atomisation of kerosene.

Diesel

In their incident review, Lees et al. (2019) mentioned that data from the UK Hydrocarbon Release Database (HCRD) showed that 20 % of mist-related incidents occurred from diesel sources. In fact, the authors stated that out of 48 mist/spray release flash fires reported between 2000 and 2005, 11 involved diesel releases. For this study, diesel B7 was used.

Light Fuel Oil

LFO is usually used as a heating fuel for homes and industrial buildings. It was the subject of many studies conducted by the HSE in their MISTS1 joint industry project (Gant et al., 2020). The LFO used in this study was supplied by CPE, Total Energies (Maxeville, France).

Biodiesel

Biodiesel mists, although industrially interesting, have seldom been studied. This fuel was

recommended by the HSE for testing in the current work due to the range of substance properties for different biodiesels. The biodiesel used for this study was of type B100 supplied by Valtris Champlor (Verdun, France).

Mobil DTE Heavy Medium VG68

This fluid is a high-performance circulating lubricating oil specifically designed to lubricate steam and hydraulic turbines, and other systems that demand long useful lubricant life. It may be used under pressure and be released as a mist, especially for gas turbine applications.

3.3. Ex-situ characterisation

Commercialised fuels can behave differently depending on petroleum cuts, ageing, or suppliers. Their multi-component nature can also influence and lead to discrepancies in their characteristics which calls for a pre-characterisation phase. Characterisation tests were carried out on all seven fluids under ambient conditions.

In addition to density re-evaluation, viscosity measurements were performed using the Hoeppler Falling-Ball Viscometer (Brookfield KF30 model) according to the German norm DIN 53015 (2019). Furthermore, surface tension measurements were executed following the Pendant Drop method at 20 °C. As for the flashpoint, tests were performed using the Setaflash Series 3 flashpoint tester following the ASTM D3278-21 (2021) standardised test method. The measured physicochemical properties were determined at ambient temperatures and are demonstrated in Table III-2.

The HSE Release Classes, mentioned in Section 2.3, can consequently be recalculated, assuming the reference conditions of a release pressure drop of 10 bar through an orifice diameter of 1 mm. Figure III-1 exhibits the repartition of 5 out of the 7 fuels. Ethanol and isooctane do not enter this classification due to their high volatility. It should be noted that, according to the HSE, Release Class II comprises fuel oils. Nevertheless, the supplied LFO differed significantly from that tested by the HSE (Gant et al., 2016).

Table III-2: Experimentally measured physicochemical properties of the seven selected fluids

Fluid	Isooctane	Ethanol 96%	Kerosene Jet A1	Diesel B7	LFO	Biodiesel B100	Mobil DTE
Density (kg.m^{-3})	690	870	850	880	880	920	930
Dynamic viscosity (mPa.s)	0.45	1.31	1.23	2.95	2.88	6.3	154.28
Surface tension (kg.s^{-2})	0.018	0.022	0.026	0.027	0.025	0.031	0.03
Flashpoint (°C)	-12	17	40	65	58	250	220

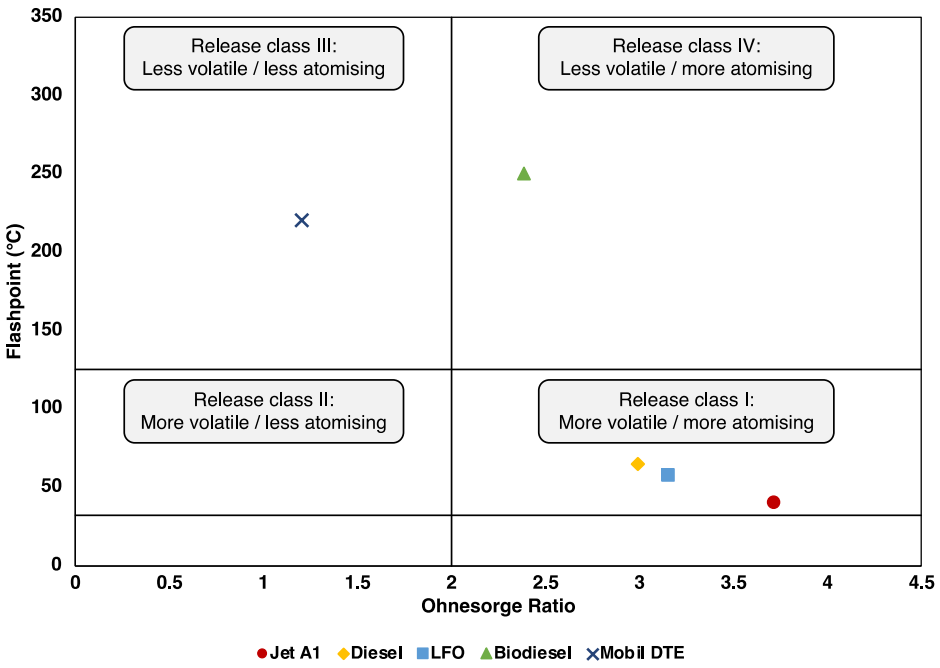

Figure III-1: HSE liquid classification of selected fuels - adapted from Bettis et al. (2017) for the current study

3.4. Explosion vessel

As discussed previously, there is no existing standard to evaluate the flammability and explosivity of fuel mists. For this study, several steps were taken in order to choose the right tools and complete protocol, to check the accessibility to the equipment and the repeatability and reproducibility, and to verify the relevance of the benchmark.

While there are other experimental tools available for their evaluation, the ***20 L explosion sphere*** was chosen for this thesis study. It is a standardised vessel and has been subject to numerous

well-documented investigations. It can be found in most process safety laboratories and is accepted by many explosion safety stakeholders. This vessel is a spherical stainless-steel chamber fitted with a double jacket allowing the circulation of a heat transfer fluid which controls and maintains a constant temperature during experiments (cooling the sphere to temperatures lower than the external temperature is not possible). Figure III-2(a) depicts the sphere in dust configuration, as proposed by the EN 14034 standards series, where a 0.6 L tank connected to the chamber accommodates a known mass of a dust sample and is pressurised with air under a pressure of 20 bar. A fast-acting valve allows the dust dispersion in the partially evacuated sphere (initial pressure of 0.4 bar) by a jet of compressed air. An ignition source, placed in the centre of the enclosed vessel, is then triggered after a fixed ignition delay t_v. The latter is defined as the time between the start of the dust dispersion and the actuation of the ignition source. This delay can be associated with a specific degree of cloud turbulence at the ignition time. During the explosion, two piezoelectric pressure sensors are used to record the pressure-time evolution. The 20 L explosion sphere also comprises an inlet for purging air and two outlets for exhaust gases and vacuuming.

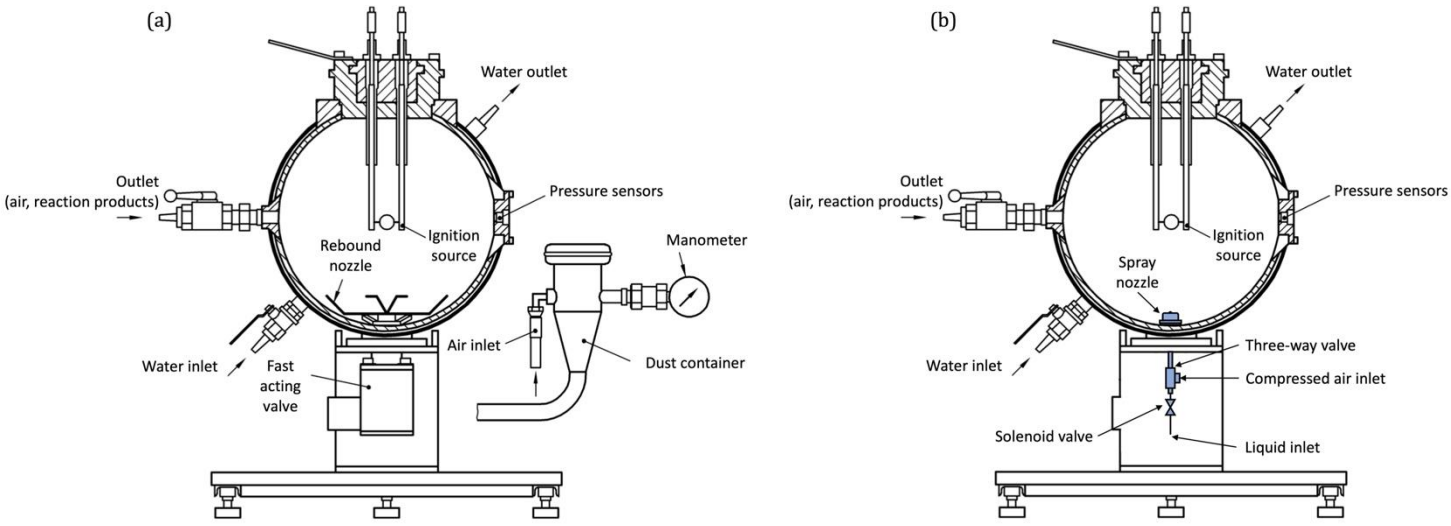

Figure III-2: The 20 L Siwek explosion sphere – (a) dust configuration, adapted from EN 14034-1 (2004)+A1 (2011), (b) modified version, mist configuration

In order to accommodate the mist generation system described in Section 3.5, the dust container, the fast-acting valve, and the rebound nozzle were removed (see Figure III-2(b)). While remaining inspired by the EN 14034 standards series, the test method was modified to adapt to the complexity of an injected mist cloud in a confined test vessel. A specific liquid is placed in a temperature-controlled metallic reservoir and then injected in the form of a mist into the sphere. A pre-determined injection time is calculated according to the desired sample concentration and allows the determination of the initial sphere pressure. The mist cloud is ignited after a defined

time of a few milliseconds after injection, and the rest of the procedure follows that of dust clouds.

Another apparatus that could be used for the same purposes is the 1 m^3 sphere. Considering the lack of experience on the cubic law applied for mist explosions, the latter would undoubtedly produce data that are more representative of industrial-scale accidents due to its larger size, provided that adequate modifications of the injection system are carried out. Nonetheless, the 20 L vessel is more available in laboratories and is easier to manipulate due to its dimensions.

3.5. Mist generation method

The choice of the mist generation system is of significant importance as it should be versatile, easily supplied/manufactured, adaptable, and controllable. Nonetheless, sufficient concentrations (Subsection 2.4.2.3) should be attained with suitable DSDs and turbulence levels to mimic an industrial leak as much as possible while remaining adjusted and convenient to a confined, relatively small vessel. Taking into account these considerations and the pros and cons of the aforementioned mist generation systems (Subsection 2.4.1), a ***twin-fluid spray nozzle*** was chosen for this study. Indeed, electrospray cannot be chosen because it would be necessary to control the electrical conductivity of each fluid to be tested. Condensation does not allow to reach a wide range of DSD, and liquid pressurisation limits the possibility of controlling the sphere's initial temperature and pressure and testing hybrid mixtures, thus justifying the choice of a spray nozzle. Such a nozzle comes in different configurations, where the liquid can be pressurised and then atomised with an air stream or can be supplied by a siphon or gravity-fed system.

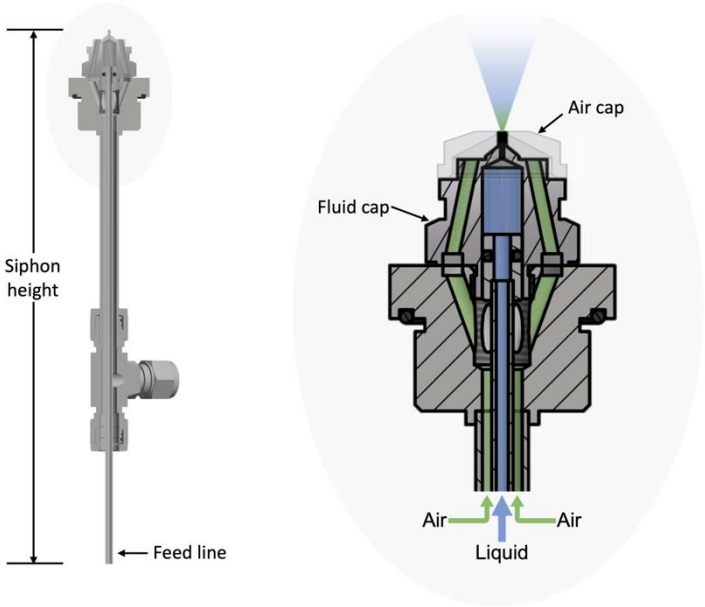

Figure III-3: Mist generation system based on a Venturi junction

An exemplary scheme of a twin-fluid spray nozzle is portrayed in Figure III-3. This nozzle functions due to a Venturi junction. Compressed air passes through a three-way ball valve and draws the liquid, which is placed in a temperature-controlled reservoir, up through a feed line towards the nozzle. The liquid would, therefore, be atomised by the airflow. Such a setup consists of an air cap and a fluid cap (supplied by Spraying Systems®), ensuring an internal or external mixing of the fluids to generate a fine spray pattern. Both caps come in different orifice diameters allowing the creation of hundreds of combinations. The caps should be locked together using a specific locknut to avoid vibrations. The spray flow rate, angle, pattern, and coverage can, therefore, be controlled by varying combinations. For the current study, many combinations have been tested. Nevertheless, three nozzle sets, shown in Figure III-4, were mainly used. Nozzle set N1 represented the smallest orifice diameter and slot width (air cap: 1.8 x 0.51 mm), while nozzle set N2 was that with the largest orifice diameter (air cap: 0.3 mm). An intermediary nozzle set N' was also chosen (air cap: 3.09 x 0.89 mm).

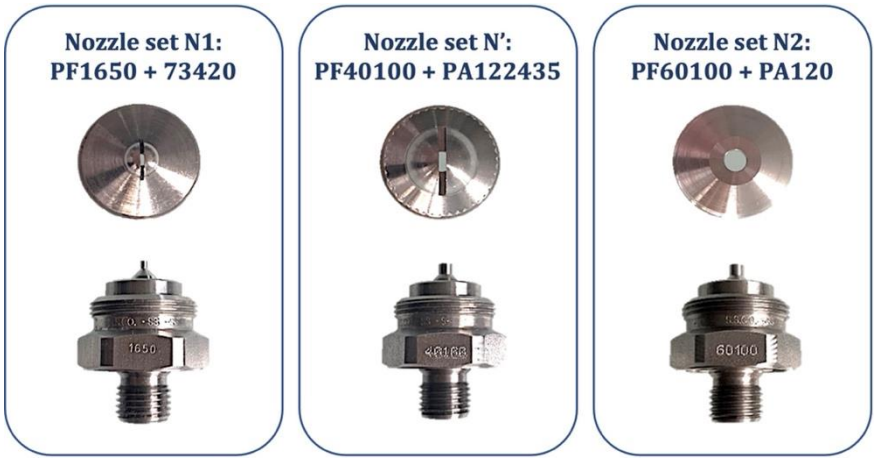

Figure III-4: Three mainly-used air cap and fluid cap nozzle combinations (Spraying Systems®) for this study

Two electronic solenoid valves (see Figure III-5) were placed on the liquid and the compressed air inlets to control the injected concentration and the liquid/air ratio and prevent potential backflow due to the explosion. The body of the nozzle spray was specifically designed to fit into the explosion sphere's support ring already used for dust explosion tests (for the rebound nozzle). The height of the vertical sphere's support was also modified from 16 to 27 cm to allow the mist injection system to fit underneath the explosion sphere. This system was, hence, placed at the base of the sphere, with the nozzle set mounted inside the vessel allowing upward mist injection. The setup can tolerate air injection pressures that reach about 10 bar depending on the orifice diameter. Nevertheless, to avoid significant complexities caused by spray impingement and fragmentation due to the strong wall impacts, injection pressures were limited to a range of 2 to 5 bar (values determined experimentally). Occasional tests with higher pressures were carried out. Evidently, imitating the pressure of an actual industrial mist release is rather difficult

inside the 20 L confined explosion sphere. Almost half of the accidental releases reported by Lees et al. (2019) occurred at pressures higher than 100 bar (with more than half occurring with a release hole equivalent diameter between 0.56 and 10 mm). Local concentrations, flow rates, and spatial heterogeneity are seldom reported. However, the selected mist generation system allows full control of the DSD and the injected concentration, simultaneously or independently. For instance, according to the supplier, for an air injection pressure of 3 bar, water flow rates as low as 0.4 and as high as 4.6 $g.s^{-1}$ (nozzle set N2) can be reached. Therefore, for an injection duration of 8 seconds, mist concentrations ranging from about 170 to 1855 $g.m^{-3}$ are attainable in the 20 L sphere. The orders of magnitudes of both the concentration and the DSD attained by this system are coherent with other studies and will be detailed in Section 4.1, justifying the choice of this mist generation system.

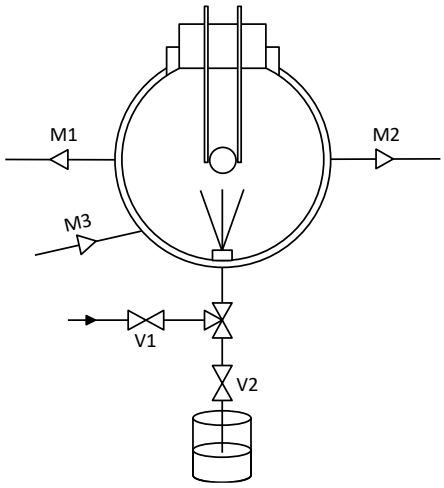

Figure III-5: Schematic drawing of the manual (M) and solenoid (V) valves used.
M1: evacuation valve, M2: vacuum valve, M3: water inlet valve
V1: compressed air inlet valve, V2: liquid inlet valve

3.6. In-situ characterisation

In order to define the phenomena related to the interaction of the liquid and gas phases, numerous techniques have been taken into consideration in this work. The tools used to experimentally examine the primary characteristics of the mist cloud are covered in this section. The mist concentration, the DSD, and the level of turbulence being the most influencing factors on a mist cloud have been characterised under different conditions in an identical replica of the 20 L sphere allowing visual access.

3.6.1. Droplet Size Distribution

Figure III-6: DSD analysis experimental set-up in the 20 L open sphere - adapted from Murillo (2016)

An in-situ laser diffraction sensor (HELOS/KR-VARIO by Sympatec GmbH) was used to assess the time evolution of droplet size distributions. The experimental vessel used was a replica of the 20 L sphere designed by Murillo (2016). The ***"open" sphere*** was equipped with four lateral windows and one on top (borosilicate glass), each with a diameter of 9.7 cm (see Figure III-6). This vessel allows visual access to the generated mist cloud while remaining comparable to the actual 20 L explosion sphere.

The HELOS laser sensor measures the DSD directly through the transparent windows using three high-resolution measuring ranges (R1, R3, and R5) from 0.5 µm to 875 µm. For this study, the droplets were assumed spherical (if necessary, it is possible to modify the shape factor in the mentioned apparatus), denoting that the measured diameter remains the same, regardless of stresses and particle orientation. The R3 lens was mainly used as it covers a range of droplet diameters, from 0.5/0.9 µm to 175 µm, which correspond to those generated by the three nozzle sets. The acquisition frequency was set to 2000 Hz. d_{10}, d_{50}, $d_{90,}$ and SMD, detailed in Subsection 2.4.1.2, are among the measurements provided by the sensor, in addition to the optical concentration. The height of the sensor was set to match the ignition source's location (i.e., the centre of the sphere) in order to assess the DSD of the mist just before ignition. The sensor is based on the Fraunhofer enhanced diffraction theory (FREE, parameter-free Fraunhofer evaluation), which is valid down to the submicron regime and does not require any complex refractive index.

3.6.2. Particle Image Velocimetry

Under particular conditions, Particle Image Velocimetry was performed to determine the level of turbulence reached by a mist generated in the sphere in the vicinity of the ignition source. In order to conduct these nonintrusive tests, a continuous wave (CW) Neodym-Yttrium-Aluminum-

Garnet (Nd:YAG) laser sheet (RayPower 2000 CW DANTEC DYNAMICS) with a wavelength of 532 nm was emitted. The dispersed droplets in a region of interest would then be illuminated, allowing their movement to be followed (see Figure III-7). The flow of the droplets was recorded with a high-speed video camera (Phantom VEO 410L) at 2000 frames per second with a resolution of 512 x 512 pixels. PIVlab 2.45, an open-source MATLAB program, was then used to conduct image pre-processing, PIV analysis utilising interpolation techniques, calibration, post-processing, and data validation on the recorded videos (Thielicke, 2021). The mean velocities $\bar{u}$ and $\bar{v}$, as well as the horizontal and vertical velocity fluctuations u_i' and v_i' (equations III-14 and III-15), were estimated from the data collected from PIVlab, allowing the calculation of the root-mean-square velocity (v_{rms} – equation III-16), which physically portrays the turbulence kinetic energy.

$$u_i' = u - \bar{u} \qquad \text{III-14}$$

$$v_i' = v - \bar{v} \qquad \text{III-15}$$

$$v_{rms} = \sqrt{\frac{1}{N}\sum (u_i')^2 + \frac{1}{N}\sum (v_i')^2} \qquad \text{III-16}$$

Where u_i' is the horizontal velocity fluctuation, v_i' is the vertical velocity fluctuation and N is the number of droplets detected for the velocity estimation.

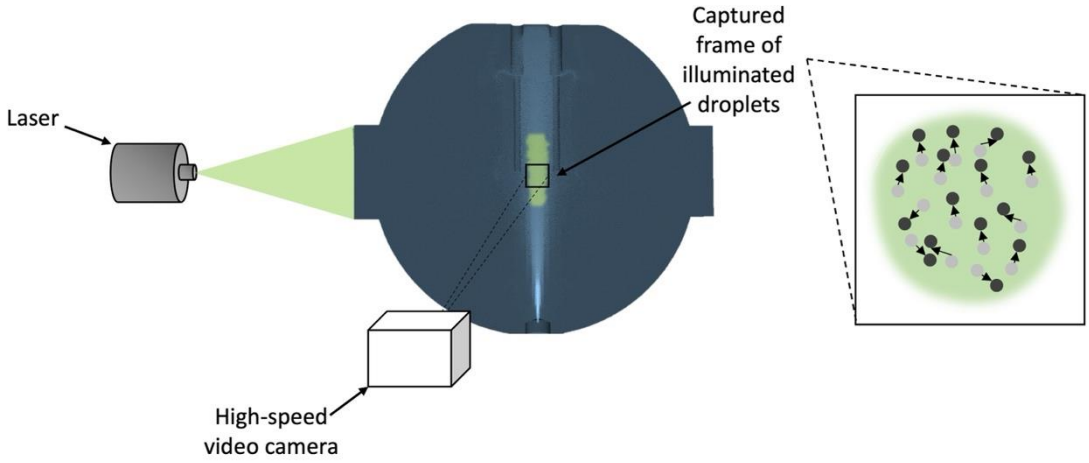

Figure III-7: Particle Image Velocimetry experimental set-up with the 20 L open sphere

The generated mist droplets are considered as the flow tracer due to their relatively short relaxation time and sufficient visibility (see Subsection 4.1.3). There was, therefore, no need to seed the liquid with small solid particles.

3.6.3. Concentration

As mentioned in Subsection 2.4.1.2, different concentration zones should be identified for a mist ignition in a confined vessel. The suspended mist concentration, expressed in weight per unit volume, was used for this study as a primary quantitative characteristic. The fuel mass was weighted along the time systematically during every mist injection. Wide ranges of mist concentrations are available, depending on the fluid and nozzle type as well as on the injection pressure. Repeatability and concentration fluctuations will be discussed in Section 4.7. Nevertheless, using this suspended concentration may give a vague impression of the relative flow rates of fuel and air into the propagating flame front. Experimental findings were therefore coupled with exhaust gas chromatography, simulated equilibrium reactions, and CFD modelling to estimate a local concentration.

3.7. Simulated characterisation

By detecting the fluctuations in the circumstances of the gas-liquid interaction throughout the course of a series of tests, the results provided a crucial foundation for the creation of computational analysis and helped direct the following stages of this research project.

A computational fluid dynamic modelling (CFD) has been developed at INERIS to complement the experimental approach followed in this study. The CFD model was based on an Euler-Lagrange method and was conducted on a SprayFoam solver. Modelling and meshing were carried out on Ansys 2021. This approach is a preliminary study aimed at examining the biphasic flow development inside the test apparatus and assessing conditions (e.g., turbulence, droplet-droplet or droplet-wall interactions, rain-out phenomena, etc.) prevailing in the fragmentation and the coalescence of the dispersed phase. The determination of local concentrations in the vicinity of the ignition source is also an envisaged result of this model (Chot-Plassot et al., 2022).

3.8. Dimensional analysis of mist ignition

Similar to the preceding dimensional analysis (Section 3.1), another one was conducted to characterise the ignition of a mist cloud and highlight the relevant dimensionless numbers that portray a forced ignition (e.g., spark ignition). This dimensional analysis will be used in Chapters V and VI to understand better and interpret the results obtained. A mist release would have a specific jet velocity v, dispersed in air, characterised by its density, ρ_g, and dynamic viscosity, μ_g. In general terms, to ignite the flammable mist cloud, sufficient energy, IE, must be applied to raise a region of characteristic size, d_c, proportional to the laminar flame thickness (or, to be more precise, the quenching distance) to the adiabatic flame temperature (Spalding, 1979). The spark kernel will expand, and a self-sustaining flame will begin to spread through the mist if the rate of

heat release caused by the evaporation of the fuel droplets is greater than the rate of heat loss from the spark kernel to the surrounding unburned gas (see Subsection 2.4.3.4). This, hence, calls for the following parameters: the thermal conductivity, λ, the enthalpy of vaporisation, ΔH_{vap}, the enthalpy of combustion, ΔH_{comb}, the specific heat, C_p, and the convection coefficient, h. This energy, which is sufficient to support the ignition process, is known as the minimum ignition energy, *MIE*. In addition, igniting a mist cloud is only possible if its concentration, C_m, is higher than its lower explosion limit. Finally, for simplicity, the ignition process will be considered as an irreversible fuel oxidation reaction with a characteristic chemical time, t_c. The listed parameters are presented in Table III-3.

Table III-3: Influencing parameters used for the dimensional analysis of a mist cloud ignition

Notation	Definition	SI unit	Dimension
ρ_g	Air density	$kg.m^{-3}$	$M.L^{-3}$
μ_g	Air dynamic viscosity	Pa.s	$M.L^{-1}.T^{-1}$
v	Injection velocity	$m.s^{-1}$	$L.T^{-1}$
IE	Delivered energy	J	$M.L^2.T^{-2}$
d_c	Characteristic cloud size	m	L
λ	Thermal conductivity	$W.m^{-1}.K^{-1}$	$M.L.T^{-3}.\theta^{-1}$
ΔH_{vap}	Enthalpy of vaporisation	$J.mol^{-1}$	$L^2.T^{-2}$
ΔH_{comb}	Enthalpy of combustion	$J.mol^{-1}$	$L^2.T^{-2}$
C_p	Specific heat capacity	$J.kg^{-1}.K^{-1}$	$L^2.T^{-2}.\theta^{-1}$
h	Convection coefficient	$W.m^{-2}.K^{-1}$	$M.T^{-3}.\theta^{-1}$
MIE	Minimum ignition energy	J	$M.L^2.T^{-2}$
C_m	Mist concentration	$kg.m^{-3}$	$M.L^{-3}$
t_c	Characteristic chemical time	s	T

3.8.1. Dimensionless numbers

With 13 parameters and 4 dimensions, 9 dimensionless numbers were found:

$$\pi_1 = \frac{\rho_g}{C_m} \quad \text{III-17}$$

$$\pi_2 = \frac{\mu_g}{v d_c C_m} \quad \text{III-18}$$

$$\pi_3 = \frac{IE}{v^2 {d_c}^3 C_m} \quad \text{III-19}$$

$$\pi_4 = \frac{\lambda}{v d_c C_p C_m} \quad \text{III-20}$$

$$\pi_5 = \frac{\Delta H_{vap}}{v^2} \quad \text{III-21}$$

$$\pi_6 = \frac{\Delta H_{comb}}{v^2} \quad \text{III-22}$$

$$\pi_7 = \frac{h}{v C_p C_m} \quad \text{III-23}$$

$$\pi_8 = \frac{MIE}{v^2 {d_c}^3 C_m} \quad \text{III-24}$$

$$\pi_9 = \frac{t_c v}{d_c} \quad \text{III-25}$$

A comparison and exploitation of existing dimensionless numbers were similarly applied here:

Reynolds number:
$$Re = \frac{\rho_g v d_c}{\mu_g} = \frac{\pi_1}{\pi_2} = {\pi_2}' \quad \text{III-26}$$

$$\frac{IE}{MIE} = \frac{\pi_3}{\pi_8} = {\pi_3}' \quad \text{III-27}$$

Lewis number:
$$Le = \frac{k}{v d_c \rho_g C_p} = \frac{\pi_4}{\pi_1} = {\pi_4}' \quad \text{III-28}$$

Spalding number:
$$B_T = \frac{IE}{\Delta H_{vap} {d_c}^3 C_m} = \frac{\pi_3}{\pi_5} = {\pi_5}' \quad \text{III-29}$$

$$\frac{\Delta H_{comb} {d_c}^3 C_m}{IE} = \frac{\pi_6}{\pi_3} = {\pi_6}' \quad \text{III-30}$$

Stanton number:
$$Sta = \frac{h}{v \rho_g C_p} = \frac{\pi_7}{\pi_1} = {\pi_7}' \quad \text{III-31}$$

Nusselt number:
$$Nu = \frac{h d_c}{\lambda} = \frac{\pi_7}{\pi_4} = {\pi_8}' \quad \text{III-32}$$

Damköhler number:
$$Da = \frac{t_c h}{\rho_g d_c C_p} = \frac{\pi_7 \pi_9}{\pi_1} = {\pi_9}' \quad \text{III-33}$$

The dimensionless number π_3' can consequently be expressed as a function of the other dimensionless numbers as seen in equation III-34.

$$\pi_3' = \frac{IE}{MIE} = f(\pi_1, Re, Le, B_T, \pi_6', Sta, Nu, Da) \qquad \text{III-34}$$

3.8.2. Physical significance

Dimensionless number π_1

This dimensionless number, $\left(\frac{\rho_g}{C_m}\right)$, represents the ratio of air density to the mist concentration.

Reynolds number

The Reynolds number (equation III-26) expresses the ratio of the inertial forces to the viscous forces of air in the mist cloud.

Dimensionless number π_3'

This dimensionless number, $\left(\frac{IE}{MIE}\right)$, symbolises the ratio of the delivered energy to the MIE, which can represent overdriving.

Lewis number

The Lewis number, expressed in equation III-28, is the ratio of the thermal diffusivity to the mass diffusivity.

Spalding number

This heat transfer number (equation III-29) is usually expressed as follows: $\frac{C_p \Delta T}{\Delta H_{vap}}$ to compare available energy to that required for droplet evaporation. The increase in temperature ΔT can be associated with the available energy IE via the mist concentration and the characteristic diameter of the cloud's volume: $\Delta T = \frac{IE}{\frac{\pi}{6} {d_c}^3 C_m C_p}$ (Ballal and Lefebvre, 1978).

Dimensionless number π_6'

This dimensionless number, $\left(\frac{\Delta H_{comb} {d_c}^3 C_m}{IE}\right)$, conveys the ratio of the produced energy by combustion to the delivered energy *IE*.

Stanton number

The Stanton number, expressed in equation III-31, measures the ratio of the heat transferred to the mist cloud by convection to its thermal capacity. It is generally used in thermal runaway prevention/studies.

Nusselt number

The Nusselt number, shown in equation III-32, is the ratio of the convective heat transfer to the conductive heat transfer across the boundary of the mist cloud volume of diameter d_c.

Damköhler number

The Damköhler number (equation III-33) compares the characteristic chemical time to the characteristic diffusion time.

3.9. Flame propagation tube

It is of interest to visualise eventual flame deformations by the presence of droplets on the flame front and any change to the flame front surface and the flame propagation speed. Moreover, the laminar burning velocity of a fuel-air combination is an inherent, intrinsic parameter that may be employed in sophisticated simulations (CFD modelling, e.g., FLACS code - Gexcon) to assess the effects of an explosion under specified conditions (Skjold, 2014). This parameter was evaluated via flame propagation visualisation in a 1-meter-long flame propagation tube with a square cross-section of 7 cm^2 (see Figure III-8). The latter was coupled with a high-speed video camera (MotionBLITZ EoSens® mini) to analyse the first moments of the flame kernel growth before touching the tube's walls. The mist would be injected at the bottom of the tube and ignited in the middle using a spark ignition source. A coloured background (complementary to the flame's colour) was added on the rear window of the tube in order to distinguish the flame more easily. Video analyses were carried out, and the propagation speed was first estimated supposing that the flame expands spherically and is driven by a one-step exothermic process with the mixture's thermodynamic parameters, such as molecular weight, specific heat, and thermal conductivity, remaining constant and allowing the estimation of the unstretched burning velocity. It should be noted that the flame propagation tube is equipped with a relief valve, which opens at 1.15 atm, and is therefore not considered a confined vessel. Measurements were, subsequently, extended to the open sphere described in Section 3.6 to provide a larger analysis window.

Values found using the flame propagation tube were also compared to calculations of the laminar burning velocity S_u^0 obtained by Silvestrini's correlation (Silvestrini et al., 2008) (equation III-35):

$$S_u^0 = 0.11 \frac{\left(\frac{dP}{dt}\right)_{max} V^{\frac{1}{3}}}{P_{max}\left(\frac{P_{max}+1}{P_0}\right)^{0.14}\left(\frac{P_{max}}{P_0}\right)^{\frac{1}{\gamma}}} \qquad \text{III-35}$$

Where dP/dt_{max} is the maximum rate of pressure rise, P_{max} the maximum explosion overpressure at a specific concentration, P_0 the atmospheric pressure, and γ the ratio of specific heats.

Such comparisons may permit the evaluation of the appropriate method supplying reliable values of the laminar burning velocity of a mist cloud. More details are provided in Chapter VI.

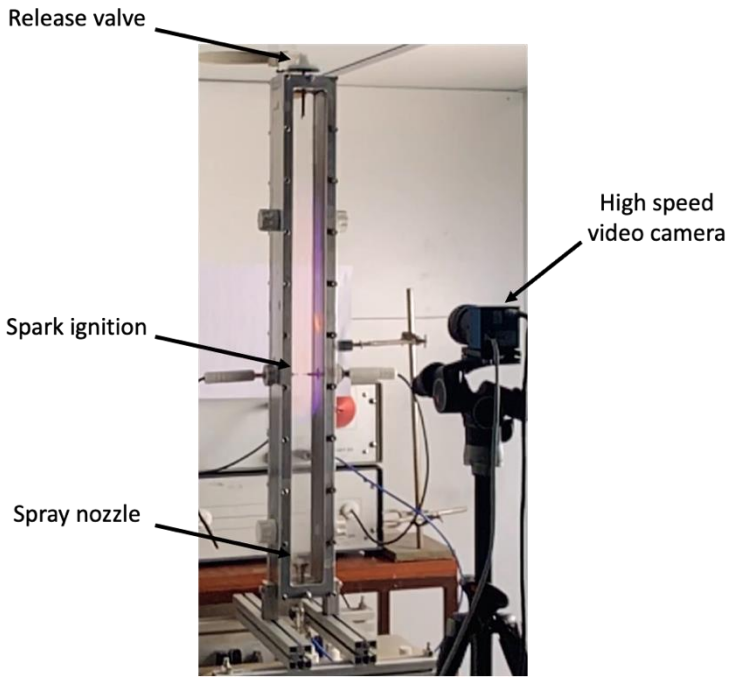

Figure III-8: Flame propagation tube equipped with a spray nozzle and a spark ignition system

3.10. Ignition sources

Several ignition sources, such as exploding wire ignitors, spark ignition, pyrotechnical ignitors, and hot spot ignitors, have been employed in past investigations on explosion limits and deflagration pressures. The ignition source proposed by the EN 14034 standard comprises two chemical ignitors, each of 5 kJ. Such an ignitor contains zirconium metal, barium nitrate, and barium peroxide (Spitzer et al., 2021; Szabová et al., 2021).

In order to widen the range of ignition energies available, two types of ignition sources were tested: ***chemical ignitors*** of energies ranging from 100 J to 10 kJ (Sobbe GmbH) and ***spark ignition*** (see Figure III-9). The *spark ignition* used delivers a maximum power of 225 W, i.e., 225 $J.s^{-1}$. Thus, a permanent spark would be generated during 444 milliseconds to deliver an energy of 100 J. Therefore, for higher energies, in order not to generate for a long duration and cause the droplets to sediment or/and to diffuse the ignition energy to a too large volume of mist, chemical pyrotechnical ignitors were used. The permanent spark was generated following a signal sent from the KSEP 320 high voltage unit (Cesana AG), which was connected to the electrodes. To control the generation time, hence the ignition energy, the unit was bypassed by a custom control system (Section 4.4). Similarly, a low-voltage electrical signal was supplied by the bypassed KSEP 310 unit to actuate the chemical ignitors. Both ignition sources were examined at 100 J to guarantee that they both provide similar results (Section 4.3).

In addition, a high-voltage spark ignition system was specifically developed at the LRGP to test lower ignition energies starting from about 130 mJ. This system consisted of a Brandenburg 3590-1320 DC/DC converter 12 V to 10 kV voltage with a total power of 5 W and a maximum input current of 0.5 mA. The output of this converter is adjustable, allowing the variation of the delivered energy to the mist cloud (more details in Figure A-2). The real spark duration, as well as the continuous delivered current, is then calculated to obtain an accurate estimation of the delivered ignition energy (see Figure A-1). The spark tungsten electrodes were placed at a separating distance of 6 ± 0.1 mm on stainless-steel electrodes which were insulated from the sphere's wall using Teflon plugs.

Throughout this manuscript, it will be seen that the choice of the ignition source would depend on the type of liquid tested and the intention of the test. The ignition source, whether chemical or spark ignitors, would be placed in the centre of the sphere, with a separation distance of 13.3 cm to the injection system, and be actuated by a new control system (detailed in Section 4.4).

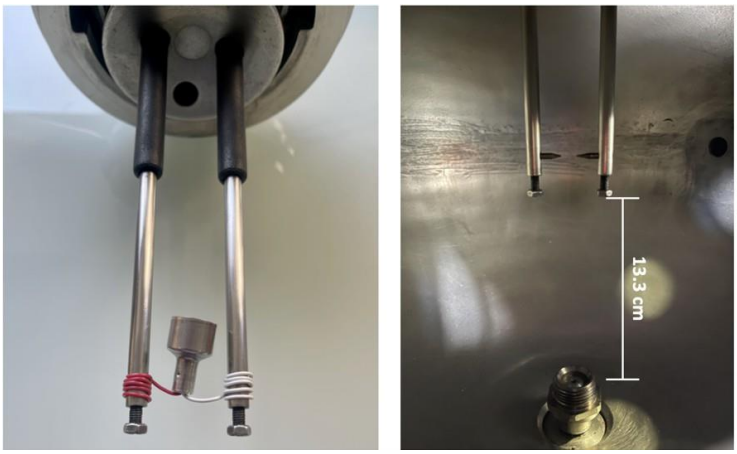

Figure III-9: Employed ignition sources - left: 100 J chemical ignitors (Sobbe GmbH), right: spark ignitors mounted in the 20 L sphere

Summary

Chapter III discussed the fuels selected for this study and the methods followed to assess the flammability and explosivity of mist clouds. First, dimensional analysis was conducted to highlight the key factors that influence mist formation. The identified parameters were divided into five dimensionless numbers that would allow the establishment of a correlation linking the operating conditions of the 20 L sphere and the liquid properties to the obtained Sauter Mean Diameter (SMD).

Seven fuels were selected to cover a wide range of physicochemical properties and industrial sectors potentially impacted by the risk of flammable mist formation. Kerosene Jet A1, diesel, light fuel oil, biodiesel, and Mobil DTE VG 68 Heavy Medium were chosen as five multi-component fuels. In addition, ethanol and isooctane were selected mainly for their simple composition (single-component liquids) and the numerous studies conducted on their physicochemical properties and combustion behaviour. Each fuel was deliberated briefly according to its importance in industrial sectors and its involvement in accidental mist releases. Accordingly, the selected fuels were characterised using ex-situ techniques, such as the Hoeppler Falling-Ball Viscometer and the Setaflash Series 3 flashpoint tester.

A section was then devoted to the test vessel used for explosion testing. As there is no standardised test to evaluate the flammability and explosivity of fuel mists, numerous steps were taken to choose the right tools. The 20 L explosion sphere, a standardised vessel subject to numerous well-documented investigations, was chosen as the main apparatus for this study. Some modifications to the sphere were then discussed. The mist cloud injected into the 20 L sphere was generated using a twin-fluid spray nozzle that functions due to a Venturi junction. This generation system was chosen as it is versatile, easy to manufacture, adaptable, and controllable.

The chapter was then complemented with in-situ characterisation methodologies to examine the primary characteristics of the mist cloud in the 20 L sphere experimentally. These techniques allowed the measurement of the droplet size distribution using an in-situ laser diffraction sensor, which allows the evaluation of the temporal evolution of droplet size distributions, the measurement of the turbulence level within the sphere by Particle Image Velocimetry, and the measurement of the actual fuel concentrations injected into the 20 L sphere. Experimental values were subsequently used as inputs to a CFD model that will be discussed in detail in Chapter V.

Finally, the ignition of the mist cloud, first discussed through dimensional analysis, revealed nine dimensionless numbers. In addition to the tests carried out in a 20 L sphere, further tests were carried out in a flame propagation tube in order to evaluate and visualise the flame propagation.

Résumé

Le chapitre III traite des liquides combustibles sélectionnés pour cette étude et des méthodes suivies pour évaluer l'inflammabilité et l'explosivité des nuages de brouillard. Tout d'abord, une analyse dimensionnelle a été menée et a mis en évidence les paramètres clés influençant la formation des brouillards. Ces paramètres ont été divisés en cinq nombres sans dimension qui ont permis d'établir une corrélation liant les conditions de fonctionnement de la sphère de 20 L et les propriétés du liquide au diamètre moyen de gouttelettes (DMS) obtenu.

Sept carburants ont été sélectionnés afin de couvrir une large gamme de propriétés physico-chimiques et de secteurs industriels potentiellement impacté par les risques de formation de brouillards inflammables. Le kérosène Jet A1, le diesel, le fioul léger, le biodiesel et le Mobil DTE VG 68 Heavy Medium ont été choisis comme cinq hydrocarbures multi-composants. En outre, l'éthanol et l'isooctane ont été sélectionnés comme substances de référence en raison de leur constitution simple (mono-constituant) et des nombreuses études menées sur leurs propriétés physico-chimiques et leur comportement à la combustion. Chaque hydrocarbure a fait l'objet d'une réflexion succincte par rapport à leur importance dans les secteurs industriels et de leur implication dans la formation accidentelle de nuage de brouillard. Les combustibles sélectionnés ont été caractérisés à l'aide de techniques ex-situ, telles que le viscosimètre à chute de bille Hoeppler et le testeur de point d'éclair Setaflash Series 3.

Une section a ensuite été consacrée au récipient d'essai utilisé pour les tests d'explosion. Comme il n'existe pas d'essai normalisé pour évaluer l'inflammabilité et l'explosivité des brouillards, de nombreuses mesures ont été réalisées afin de sélectionner un système d'injection adapté. La sphère d'explosion de 20 L, un récipient standardisé ayant fait l'objet de nombreuses recherches bien documentées, a été choisie comme appareil principal pour cette étude et les modifications apportées à la sphère ont été discutées. Le nuage de brouillard injecté dans la sphère de 20 L a été généré à l'aide d'une buse de pulvérisation à deux fluides qui fonctionne grâce à une jonction Venturi. Ce système de génération a été choisi car il est polyvalent, facile à construire, adaptable et contrôlable.

Ce chapitre présente ensuite les techniques de caractérisation in situ employées afin d'évaluer expérimentalement les principales caractéristiques du nuage de brouillard généré dans la sphère de 20 L. Ces techniques permettent la mesure de la distribution de la taille des gouttelettes par diffraction laser in-situ, permettant ainsi d'évaluer l'évolution temporelle des distributions de taille des gouttelettes, la mesure du niveau de turbulence à l'intérieur de la sphère par vélocimétrie par image de particules et la mesure des concentrations de combustibles effectivement injectées dans la sphère de 20 L. Les valeurs expérimentales ont ensuite été

utilisées comme données d'entrées dans un modèle CFD qui sera discuté en détail au chapitre V.

Enfin, l'inflammation du brouillard, discuté dans un premier temps au travers d'une analyse dimensionnelle, a permis de mettre en évidence neuf nombres sans dimension. Au-delà des essais réalisés en sphère de 20 L, des essais complémentaires ont été réalisés dans un tube de propagation de flamme afin d'évaluer et visualiser la propagation de la flamme.

Chapter IV:
Design and validation of a new test device

The proposition of a new test method requires thorough designs and hundreds of calibration and validation tests. This chapter is based on the outline of the EN 14034 standards series. It covers all the points of interest put forward by the standard that helped develop the device. Subsequently, it demonstrates the ranges of concentration, droplet sizes, and turbulence levels attained by the proposed mist generation system. A preliminary CFD model then complemented the findings. A characterisation and a comparison of the available ignition sources were carried out. The pressure measurement system and the control and data acquisition system are discussed in this chapter which ends with a proposed modus operandi. Throughout the chapter, examples will be provided mainly for ethanol and kerosene Jet A1, but several tests were also performed on the five other fuels.

4.1. Mist generation system

Similar to the EN 14034 standards series section 4.3 entitled "Dust dispersion system", this section comprises the characterisation of the mist generation system's performance, specifically its generated concentrations, flow rates, DSDs, and turbulence levels. Attainable ranges of the parameters were measured for the three chosen nozzle sets and air injection pressures ranging between 2 and 5 bar (Section 3.5).

4.1.1. Concentration, flow rate, and pressure increase

A weighing scale was used in situ to measure the injected liquid mass for each injection duration. Therefore, the liquid flow rate ranges were determined for each fluid, injection pressure, and nozzle set. Measurements were performed at least three times per condition, allowing the determination of the system's accuracy (see Section 4.7). As the least viscous and least dense liquid, isooctane was used to demonstrate the maximum attainable liquid flow rates, as shown in Table IV-1. Injection durations were limited to 10 or 12 seconds (depending on the tested liquid) to avoid excessive recirculation and liquid pool formation. Prior to each mist injection, the sphere would be partially vacuumed to a calculated pressure so that the pressure in the confined vessel would equal 1 atm after injection. The calculated pressure depends on the pressure increase accompanying each nozzle set. This increase was measured and is demonstrated in Table IV-1.

It should be noted that values may differ by changing the siphon distance (position of the feed line shown in Figure III-3). Moreover, in order to avoid using a weighing scale for each experiment, it is advised to use a flowmeter if feasible.

Throughout this manuscript, results will be presented as a function of a ***nominal mist concentration*** determined through the ratio of the injected mass and the volume of the test vessel. For an injection duration of 10 seconds, nominal concentrations of about 120 $g.m^{-3}$,

575 g.m^{-3}, and 790 g.m^{-3} can be reached using nozzle sets N1, N', and N2, respectively, for an air injection pressure of 3 bar.

Table IV-1: Maximum attainable liquid flow rates and pressure increase as a function of the nozzle set and air injection pressure

	Injection pressure	2 bar	3 bar	4 bar	5 bar
Liquid flow rate (g.s^{-1})	**Nozzle set N1**	0.28	0.24	0.24	0.23
	Nozzle set N'	1.32	1.15	1.15	1.13
	Nozzle set N2	1.68	1.58	1.68	1.67
P increase (mbar.s^{-1})	**Nozzle set N1**	29.3	36.9	45	49
	Nozzle set N'	32.6	39.7	50.5	57.6
	Nozzle set N2	28.4	40.3	54.4	59.5

It should be noted that it is not possible to infinitely increase the mist concentration in the 20 L sphere due to a saturation phenomenon that could take place following several factors:

1- The recirculation and rain-out of the spray jet limit the local concentration.

2- The coalescence of the droplets is inevitable (if the Stokes number, St_K, on the Kolmogorov timescale is < 1, a low coalescence rate of monodispersed droplets should be expected (Wunsch, 2009). Eventual coalescence would come from turbulence where shear forces in the fluid would push the droplets towards each other. If St_K >> 1, coalescence occurs by droplet-droplet and droplet-wall collision).

3- With the increase in the droplets' abundance, droplets and their vapour phase reach equilibrium as the pressure is increased to the vapour pressure of the liquid.

4.1.2. Droplet Size Distribution

4.1.2.1. Diameter range

Five-second DSD measurements were performed based on a full-factorial design of experiments (Antony, 2014) (3 factors: A = equivalent orifice diameter, B = air injection pressure, C = fluid type). Each test comprised an injection duration of 4 seconds and 1 additional second to visualise the influence of sedimentation on the DSD. Measurements were performed with intervals of 50 ms (2 DSD per millisecond and an average value each 50 ms). Droplet diameters, ***as low as 5 µm***

and as high as 100 µm, were reached with the predetermined generation configurations. Higher droplet diameters were reachable when using the twin-fluid nozzles with larger orifice diameters.

As seen in Figure IV-1, ***three droplet diameter ranges*** are attainable for mist clouds generated using the three nozzle sets at an air injection pressure of 2 bar. The figure depicts the DSD for an ethanol mist at 3000 ms, but similar behaviour was observed during the whole injection duration and for the other fuels. The DSD obtained with nozzle set N1 exhibits a monomodal, uniform, and relatively narrow distribution. On the other hand, nozzle set N2 distributions tend to be larger in width with small peaks of smaller diameters. The appearance of small peaks depended on the type of fuel and the ease of fragmentation. Nozzle set N' exhibited an intermediary distribution with persisting primary droplets.

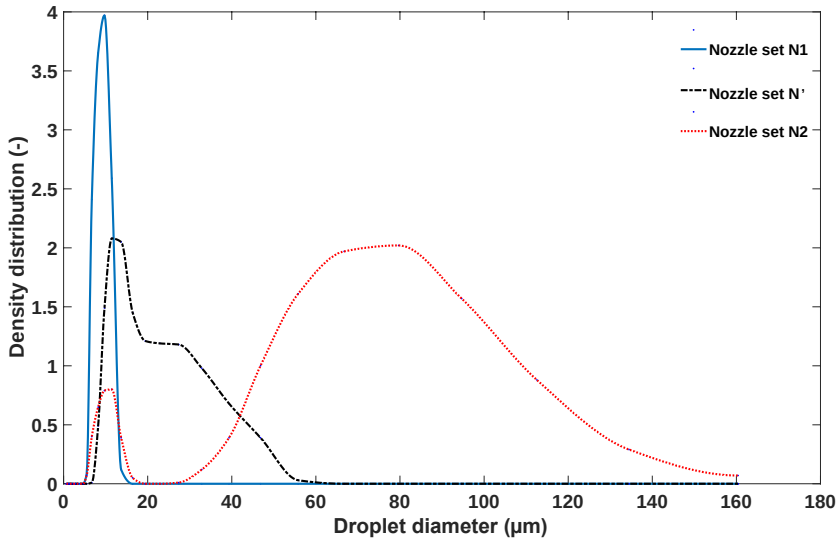

Figure IV-1: Droplet size distribution (volume/mass) at t = 3000 ms of ethanol mist generated at P = 2 bar using the three nozzle sets (El-Zahlanieh et al., 2022c)

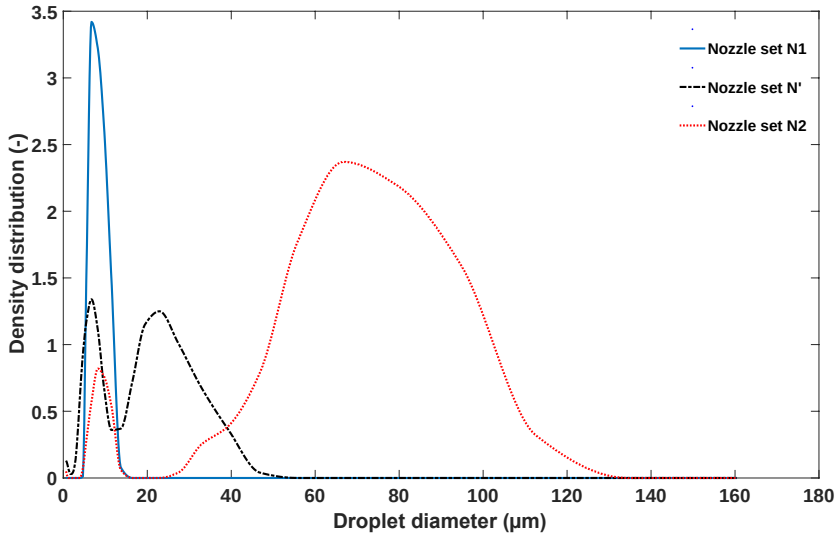

Figure IV-2: Droplet size distribution (volume/mass) at t = 4000 ms of kerosene Jet A1 mist generation at P = 3 bar using the three nozzle sets (El-Zahlanieh et al., 2022b)

Similar distributions were also obtained for the other fuels with slight discrepancies as the physicochemical properties differed. Figure IV-2 exhibits the same 3-range DSD for Jet A1 mist under similar operating conditions just before ignition.

4.1.2.2. DSD time evolution

With the three diameter ranges validated for all fuels, the evolution of the DSD with time was studied to evaluate the effect of potential coalescence. Jet A1 mists were generated into the open sphere using nozzle set N2 with an injection pressure of 3 bar. The time employed for measuring the diameter ranges (4 s generation) was also used to measure the time evolution of droplets. Figure IV-3 presents distributions starting from t = 1950 ms, corresponding to the beginning of the second half of the generation step (so as not to overload the figure), and ending at t = 3950 ms, corresponding to 50 ms before the closure of the injection valves. A time step of 400 ms was used. As it can be seen, the peak corresponding to primary droplets of a median diameter of 8 µm persisted all along the last 2 seconds. However, this peak tends to decrease in height (the log density distribution decreases from about 1.5 to 0.75). A shift towards the large diameters was also observed with increasing time showing the likely presence of a coalescence phenomenon. Nevertheless, it should be stressed that the time evolution of the DSD does not call into question the validity of the 3 ranges of diameters.

Table IV-2 also demonstrates the evolution of d_{10}, d_{50}, d_{90}, and SMD diameters after stopping the injection, which allowed the evaluation of the stability of the mist cloud. A slight increase (a maximum of 8 % of the initial value) in the four diameters was observed, justifying the shift of the distribution curves to bigger diameters, and confirming the coalescence hypothesis. Moreover, the span factor, skewness, and kurtosis of each distribution curve were calculated (equations II-4,6 in Subsection 2.4.1.2). The span factor, which quantifies the distribution width, remained constant at a value of 1.4, showing that the distribution around the mean diameter did not vary a lot in the last second of measurement. Similarly, change in skewness and kurtosis values can be considered negligible, demonstrating that, other than a change in mean diameters, the distribution curves do not change considerably after stopping the injection and that the ***mist cloud remains rather stable*** before ignition occurs.

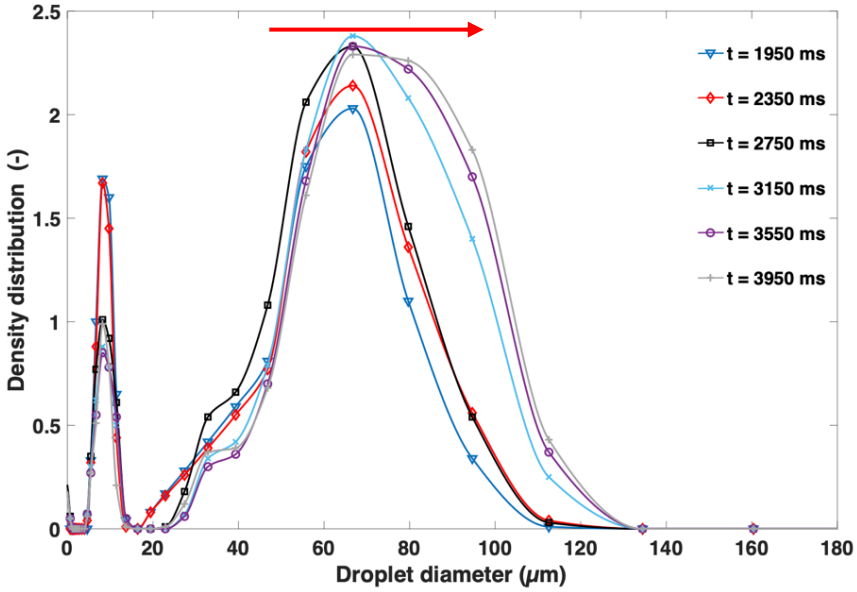

Figure IV-3: Droplet size distribution (volume/mass) of Jet A1 mists generated at P = 3 bar using nozzle set N2 - time step 400 ms starting from t_{inj} = 1950 ms

Table IV-2: Variation of droplet size parameters as a function of time for Jet A1 mist generated using nozzle set N2 after stopping the mist injection

Time (ms)	d_{10} (µm)	d_{50} (µm)	d_{90} (µm)	SMD (µm)	Span factor	Skewness	Kurtosis
t_f – 50 ms	7.3	58.6	90.4	15.6	1.41	1.76	5.01
t_f + 150 ms	7.6	60.5	92.3	16.7	1.39	1.81	5.16
t_f + 350 ms	7.6	61.2	93.8	16.5	1.40	1.80	5.10
t_f + 550 ms	7.7	61.9	94.3	17.4	1.39	1.75	4.92
t_f + 750 ms	7.7	62.2	95	16.6	1.40	1.77	4.93
t_f + 950 ms	7.7	61.9	94.3	17.4	1.39	1.75	4.92

4.1.2.3. Parametric analysis

Experimental data were analysed using a MATLAB program and the Minitab Statistical Software. The latter allowed drawing Pareto charts, showing the absolute values of standardised effects, from the largest to the smallest (Figure IV-4). Repeatability tests were carried out in the centre of the study area, defined by the design of experiments, which made it possible to determine the standard deviation. The significance level, α, of the tests was set at 0.05. A reference line

corresponding to a critical t-value of 1.993 was determined, where it is the $\left(1-\frac{\alpha}{2}\right)$ quantile of a Student's t-distribution with degrees of freedom equal to those for the error term. By comparing the effects relative to the reference line, being the critical value above which parameters have a statistical significance, the following conclusions can be drawn:

a) Factor A, the orifice diameter: this factor showed a significant effect on both d_{50} and d_{90}; however, its effect on the other parameters is low. The orifice diameter, therefore, mainly affects the skewness of the distribution curve, leading to a negatively skewed distribution and indicating the presence of larger droplets but the persistence of smaller ones.

b) Factor B, the air injection pressure: this factor has the most significant influence on the presented diameters as well as on the skewness and kurtosis of the distribution curves. Indeed, injecting with a higher air pressure enhances fragmentation, not only leading to the presence of smaller droplets, but also increasing the turbulence level, which leads to an increased chance of coalescence, droplet-droplet interaction, or rainout.

c) Factor C, the fluid type: although its influence is lower than that of factor B, this factor affects all the chosen responses.

d) The span factor is neither significantly affected by the three chosen factors, nor by the persistence time, as shown in Table IV-2.

e) The d_{50} diameter, which is the most common diameter used to characterise a mist or a dispersion, is the most affected by the three factors.

In addition to the listed conclusions, attention should be paid to the influence of the interactions. From the charts above, interactions, such as those between factors B and C (air injection pressure and fluid type), were shown to have an important influence on d_{50} and d_{90}. Such interactions should be studied in detail since their influence on the concentration and turbulence of the mist cloud is not negligible.

Another influencing factor to be considered is the electrodes that were not present when conducting the series of DSD experiments. Such a type of measurement demonstrates the limitations that could be present when increasing the mist concentration or turbulence. Nevertheless, the DSD experiments show that it is possible to characterise a mist cloud when considering the experimental difficulties related to in-situ measurements in a confined vessel, but also demonstrate that choosing the input parameters one by one (type of nozzle, pressure, fluid) does not ensure to predict the DSD with accuracy.

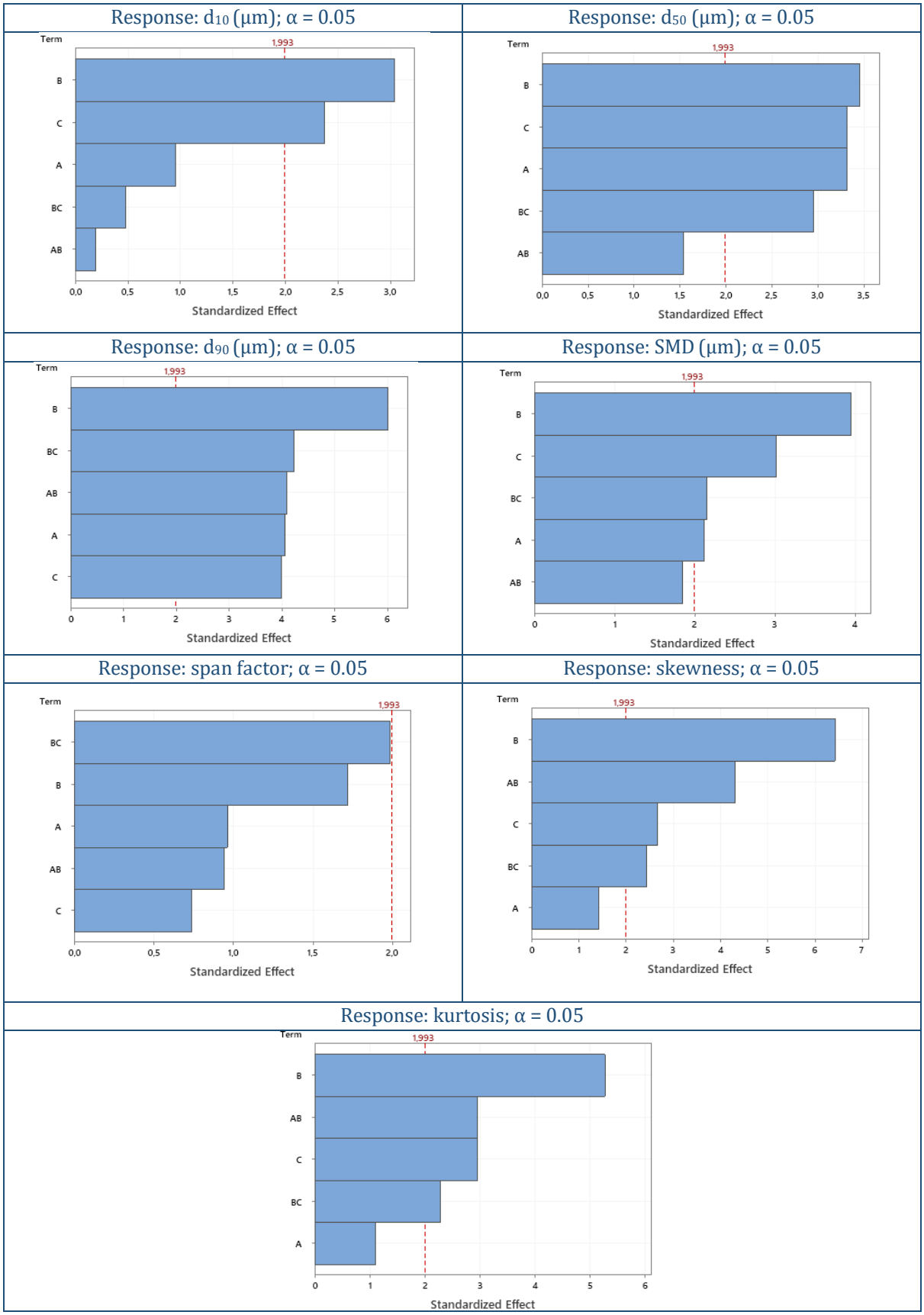

Figure IV-4: Pareto Charts of the Standardised Effects for d_{10}, d_{50}, d_{90}, SMD, span factor, skewness, and kurtosis (Factors A = orifice diameter, B = air injection pressure, C = fluid type)

4.1.2.4. *Influence of a blast*

Determining the initial DSD is essential in order to be able to benchmark between aerosols, correctly interpret the observed trends, and model them. However, does the DSD remain unchanged during an explosion (as can be assumed for powders)? It is obvious that this parameter varies during the vaporisation phase upstream of the flame front, but can the DSD also be modified by the overpressure wave generated by the explosion?

In order to anticipate eventual DSD modification induced by a blast or a shock wave, a balloon was placed at the top centre of the open sphere and was pierced at the end of a four-second water mist injection (using nozzle set N2) (see Figure IV-5). As seen in Figure IV-6, a relatively weak blast triggers a decrease in the optical concentration accompanied by larger droplets. The presence of the latter can be explained by enhanced coalescence, caused by the wave. Coalescence is undeniably not the only aftermath of a shock wave; droplets may be deformed and/or may stick to the vessel's walls.

Although this does not truly imitate a propagating flame, it can give an idea of droplets present near the flame front. Small droplets of diameters lower than 20 µm persisted in the same volume density throughout the measurement, though they usually are more sensitive to changes in the gas phase, especially due to their very low relaxation time (discussed in the following Subsection 4.1.3). Nevertheless, they would evaporate much faster than larger droplets and have minimal effects on the propagating flame. Larger droplets, on the other hand, may act as obstacles. They evaporate slower and may cool combustion products, causing momentum and energy losses and deforming the flame front.

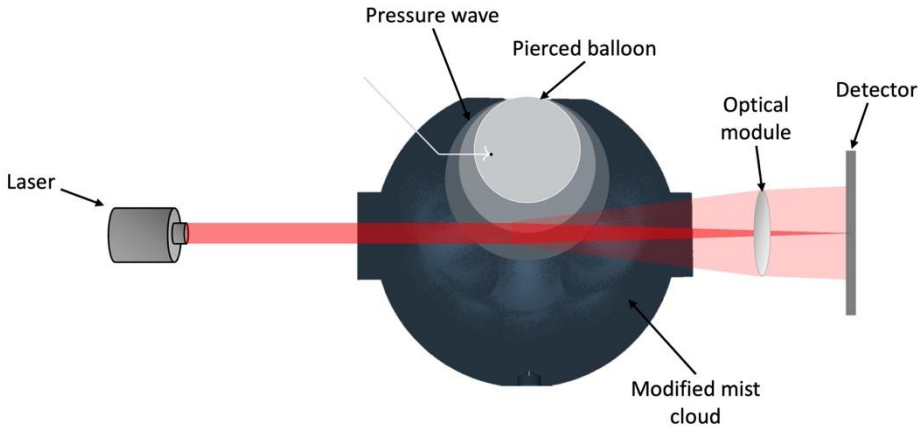

Figure IV-5: Schematic drawing of the blasted balloon - DSD measurements using the in-situ laser diffraction sensor

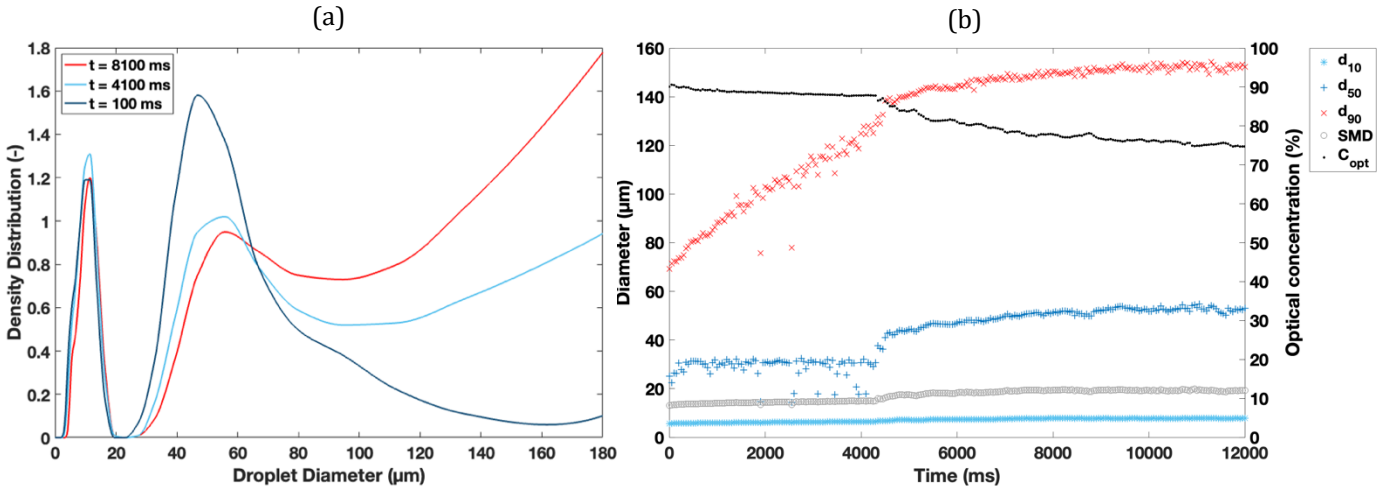

Figure IV-6: Influence of a balloon blast on the droplet size distribution of a mist cloud generated using nozzle set N2: (a) time evolution of the volume DSD, (b) time evolution of representative and mean diameters and the optical concentration

4.1.3. Particle Image Velocimetry

The dispersion of the selected fuels' mist clouds was tracked for a series of experiments, which were limited to one-second injections. Analyses were carried out for only one second as the clarity of the videos decreased with the increase of droplets in the 20 L sphere. The 2000 fps videos were converted to high-quality images, which were treated using PIVlab 2.45 (Thielicke, 2021). Nevertheless, if the carrier fluid (air) and droplet densities differ, gravitational forces can have a significant impact on the results (Raffel, 2007). An estimate of the droplet velocity lag v_{lag} in a continuously accelerating fluid should, therefore, be determined. This velocity can be derived from Stoke's drag law and be expressed as follows (equation IV-1):

$$v_{lag} = v_d - v_g = d_d^2 \frac{(\rho_d - \rho_g)}{18\mu_g} a \qquad \text{IV-1}$$

Where d_d is the droplet diameter, ρ_d and ρ_g are the droplet and air density, respectively, μ_g is the air dynamic viscosity, v_g is the air velocity, v_d is the droplet velocity and a is the acceleration.

As the density of all the fuels is much greater than that of air, the droplet velocity v_d should follow an exponential law (Raffel, 2007) (equation IV-2):

$$v_d = v_g \left[1 - \exp\left(-\frac{t}{\tau_s}\right)\right] \qquad \text{IV-2}$$

With τ_s being the relaxation time, which is expressed following equation IV-3:

$$\tau_s = d_d^2 \frac{\rho_d}{18\mu_g} \quad \text{IV-3}$$

The equations of the droplet's motion become more challenging to solve, and the result is no longer a straightforward exponential decay of the velocity if the fluid acceleration is not uniform or if Stokes drag does not apply. However, τ_s continues to be a useful indicator of a droplet's tendency to reach fluid velocity equilibrium (Raffel, 2007). For instance, for an ethanol droplet (ρ_d = 870 kg.m^{-3}) of a diameter of 9 µm, the relaxation time would be equal to 2.15.10^{-4} s for air properties at 20 °C and 1 atm (μ_g = 1.82.10^{-5} Pa.s). Such a low value shows that the droplets can be considered tracers and only take 0.2 ms to follow the turbulent flow. τ_s was similarly calculated for each fluid for three different median diameters and maintained rather low values (Table A-2, Appendix A).

With that established, images of the droplets' movements were first pre-processed on PIVlab. Unwanted zones were excluded, and contrast limited adaptive histogram equalisation (CLAHE) and auto contrast stretch enhancements were applied to improve their quality. The droplets now have stronger contrast and are more detectable, helping obtain a more precise velocity field. For a PIV analysis, each image is usually divided into a network of interrogation areas, which should overlap and correspondingly increase in size. The flow patterns would then be determined using FFT window deformation (Windowed fast Fourier transform) as an algorithm (see Figure A-3 for more details). Calibrating and post-processing would then result in establishing the mean velocity and mean horizontal and vertical fluctuations, which were used to calculate the root-mean-square velocity v_{rms} (equations III-14,16).

Most calculations were performed 3 ms after the end of each injection to visualise the turbulence level just before ignition. Results showed that vertical velocity vectors could reach up to 15 m.s^{-1} during the mist injection. With an increase of the air injection pressure from 3 to 5 bar, the v_{rms} of ethanol mist, generated with nozzle set N', was found to double in value, reaching about 2 m.s^{-1} (Table IV-3). With the same liquid, the v_{rms} obtained with each nozzle set was compared. With increasing orifice diameters (hence increasing DSD), the level of turbulence was seen to decrease slightly (Table IV-4). It should be noted that PIV experiments were part of an exploratory study to draw a preliminary picture, and further investigations are needed. Nevertheless, the performed tests were enough to provide orders of magnitude of the turbulence level attained in the 20 L sphere.

Table IV-3: Influence of the air injection pressure on the mist cloud turbulence level (1 s injection - nozzle set N' - ethanol)

P_{inj} (bar)	**3**	**4**	**5**
v_{rms} (m.s^{-1})	1.07	1.55	2.09

Table IV-4: Variation of the turbulence level with the change nozzle set (1 s injection - P_{inj} = 4 bar - ethanol)

Nozzle set	**N1**	**N'**	**N2**
v_{rms} (m.s^{-1})	1.74 ± 0.02	1.55 ± 0.07	1.27 ± 0.04

The evolution of v_{rms} with the injection time is depicted in Figure IV-7 for a Jet A1 mist cloud. v_{rms} values of about 1.1 m.s^{-1} were reached at the end of the mist generation with nozzle set N1 and P_{inj} = 3 bar, hence the instant at which the ignitors would be actuated. This v_{rms} reached a maximum of 1.5 m.s^{-1}at t_{inj} = 450 ms. A decrease in v_{rms} occurs after stopping the mist injection at t = 1000 ms as the level of turbulence decreases in the absence of compressed air injection and droplet-droplet interaction. Here, the sedimentation phenomenon takes the lead. Nevertheless, experimental explosion tests were only performed instantaneously after injection when the mist cloud was still considered turbulent. Figure IV-7 also comprises the spatial variation of the velocity magnitude of Jet A1 droplets at the end of the mist generation. Velocity magnitudes, ranging from 0.5 to 5 m.s^{-1}, were attained at the end of the injection. PIV findings not only served as indicators of the turbulence level but also were used as indicators for the CFD approach detailed in Section 4.2, for the proposal of a correlation linking the SMD to operating conditions and physicochemical properties, and for the calculation of several dimensionless numbers.

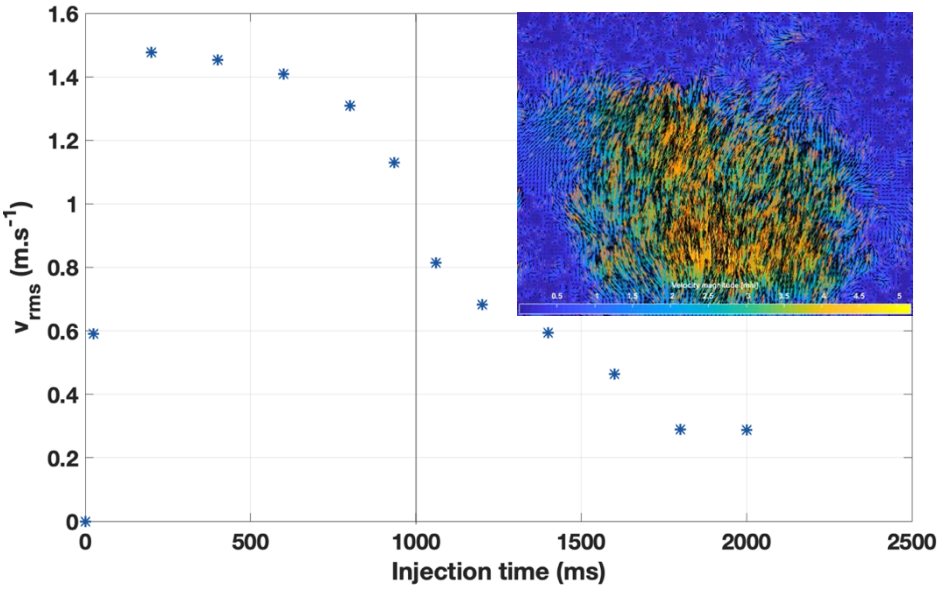

Figure IV-7: Evolution of the root-mean-square velocity with the Jet A1 mist injection time - spatial variation of the velocity magnitude (from 0 to 5 m.s^{-1}) of kerosene Jet A1 droplets at the end of the generation using nozzle set N1 and P_{inj} = 3 bar

4.1.4. Proposal of a correlation linking the SMD to influencing factors

The dimensional analysis of mist atomisation, detailed in Section 3.1, was coupled with 107 experimental DSD and PIV findings to estimate the coefficients A to E of equation III-12. The SMD of each DSD was extracted using a MATLAB program at 500 ms representing the initial stages of mist generation after a transitory phase prior to 500 ms. In addition, the following parameters were used to calculate the dimensionless numbers for each of the 107 cases: the physicochemical properties of air, those of the fuels (measured and shown in Section 3.2), and the mean velocity found by PIV at the corresponding injection time. This was carried out on experimental findings corresponding to a minimum and maximum Reynolds number of 14 and 28000, respectively, and a minimum and maximum Weber number of 0.34 and 7, respectively.

The correlation was first converted into a linear equation by applying its natural logarithm:

$$\ln\left(\frac{SMD}{d_o}\right) = \ln(A) + B\ln\left(\frac{\mu_l}{\mu_g}\right) + C\ln(La) + D\ln(We) + E\ln\left(\frac{\rho_l}{\rho_g}\right) \qquad \text{IV-4}$$

The coefficients A to E could therefore be estimated using multiple linear regression and are presented in Table IV-5:

Table IV-5: Correlation coefficients of mist generation in the 20 L sphere

$$\frac{SMD}{d_o} = A\left(\frac{\mu_l}{\mu_g}\right)^B (La)^C (We)^D \left(\frac{\rho_l}{\rho_g}\right)^E$$

A	B	C	D	E
$3.7.10^{-3}$	-1.15 ± 0.26	-0.58 ± 0.13	-0.35 ± 0.12	1.74 ± 0.7

Not being able to experimentally separate the liquids' physicochemical properties and experimentally study their influence independently, the influence of the dimensionless numbers is discussed here. As it can be seen in Table IV-5, the viscosity ratio, the Laplace number, and the Weber number have negative coefficients, showing that their increase leads to a decrease in the SMD (hence an increase in the atomisation efficiency). The density ratio, on the other hand, has a positive influence on the increase of SMD.

If we were to expand the correlation to examine the significance of each parameter, we would find the following (equation IV-5):

$$\frac{SMD}{d_o} = A(\mu_l)^{0.0038}(\mu_g)^{1.15}(\rho_l)^{1.16}(\rho_g)^{-2.1}(\sigma)^{-0.23}(d_o)^{0.08}(v)^{-0.7} \qquad \text{IV-5}$$

As it can be seen in equation IV-5, the exponent for the liquid viscosity is positive yet very close to zero, meaning that higher viscosities lead to slightly larger SMDs. A higher liquid density can similarly increase the SMD. On the other hand, the exponent for the surface tension is negative, which indicates that low surface tensions promote atomisation in twin-fluid nozzles (producing a finer spray). The liquid velocity also has a negative exponent. Indeed, higher velocities are produced by higher air injection pressures which cause finer droplet generation. Finally, smaller orifice diameters tend to form more constraints on the liquid-air stream, resulting in more break-ups and confirming the positive exponent. It should be noted that the properties of the air should not be neglected as their influence on the atomisation process is significant. These correlations are in good agreement with the experimental findings, and physical considerations can explain their implications.

4.1.5. Validation of the correlation

Following the validation of the correlation based on the physical significance of its exponents, additional experimental data was gathered and compared to the correlation. This demonstrates the reliability of the correlation and offers an assessment of the correlation performance. Arbitrarily-chosen experimental DSDs were used for several fuels while maintaining conditions

for the validity of the correlation. The SMD of each experimental DSD was retrieved and compared to that calculated using acquired correlation. As seen in Figure IV-8, the measured and correlated SMD values are in rather good agreement as points remain inside or at the border of the red zone. The latter was determined by calculating a 15 % uncertainty for both sides. Calculated errors did not exceed 21 %. Nevertheless, limitations (higher errors) were observed for diameters surpassing about 25 µm. It was seen that the correlation is only valid for low values of SMDs.

If we were to compare with existing correlations, empirical correlations expressing a mean droplet diameter for air-assist nozzles are numerous. One similar correlation is that established by Elkotb et al. (1982), expressed as follows:

$$SMD = 51 d_o Re^{-0.39} We^{-0.18} \left(\frac{\dot{m}_l}{\dot{m}_g}\right)^{0.29} \quad \text{IV-6}$$

Where *Re* is the Reynolds number, *We* is the Weber number, and $\dot{m}_l$ and $\dot{m}_g$ are the liquid and air mass flow rates, respectively.

It should be noted that the Reynolds number, which denotes the ratio of the liquid inertial to the viscous forces (as seen in equation IV-7), can be replaced by equation IV-8. The negative effects of both the Laplace and the Weber numbers, seen in both correlations, hence demonstrate the consistency with previous findings.

$$Re = \frac{\rho_l v d_o}{\mu_l} \quad \text{IV-7}$$

$$Re = \left(We.La.\frac{\rho_l}{\rho_g}\right)^{0.5} \quad \text{IV-8}$$

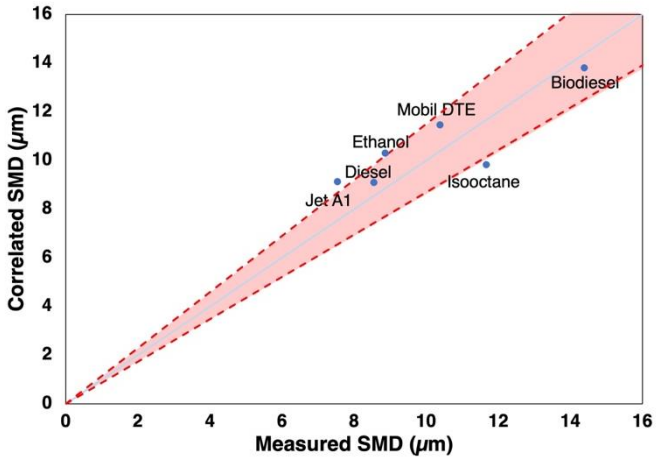

Figure IV-8: Comparison between the correlated and measured SMD at 500 ms after the start of the mist injection in the 20 L sphere

4.2. CFD approach

The mist injection was modelled into the confined vessel according to the design specifications of the 20 L sphere used in the experimental approach. This approach was carried out and communicated by Chot-Plassot et al. (2022) in a master's research internship.

The preliminary CFD study simulated an experimental configuration with an injection pressure of 3 bar. The input data for this case was 1 g of Jet A1 injected during 4 s with nozzle set N1. The PHAST software was used to calculate the air mass flow at the orifice, the pressure drop coefficient, the velocity at the orifice, and the air ejection velocity in the expansion zone. This resulted in an outlet jet velocity of 313 $m.s^{-1}$. It was chosen to simulate the flow at the interface of the orifice and the sphere from a given experimental DSD (considered at the nozzle orifice's exit, although measurements were performed at the centre of the sphere). This avoids modelling the complex geometry inside the nozzle where the primary atomisation of the liquid occurs. The post-orifice DSD was assumed to be monomodal and equal to the mean diameter d_{50}, but solely for these dimensionless computations. In order to assess the evolution/behaviour of this monomodal spray in the 20 L sphere, a simulation based on a Lagrangian grid for the dispersed phase (droplets) and an Eulerian grid for the continuous phase (air) was carried out. The Lagrangian method consists of tracking droplets along their trajectories, while the Eulerian method describes the velocity field, which associates a velocity vector with each point.

The flow was characterised by dimensionless numbers in order to implement adequate models in the numerical configuration. From the values of the dimensionless numbers (Table IV-6), the following considerations were taken:

- The spray is fine, but the four-way coupling is still necessary because the jet is confined, the flow is highly turbulent, and droplet-droplet interactions cannot be neglected (liquid volume fraction << 1 % and mass fraction ≈ 50 %)
- The flow is turbulent ($Re > 3000$)
- The droplets fragment catastrophically ($We > 350$ and $Oh < 1$)
- The droplets can evaporate (Sherwood number $Sh > 1$)
- The droplets follow the air trajectory (Stokes number $St < 1$)
- The regime is collisional (Knudsen number $Kn < 1$).

Table IV-6: Characteristic dimensionless numbers for the generation of a Jet A1 mist in the 20 L sphere at the injection orifice

Dimensionless number	Volume fraction	Re_{air}	*We*	*Oh*	*St*
Value (-)	0.02 %	52000	21500	0.13	2.4×10^{-4}

The dimensionless numbers were then used to select the appropriate solver. SprayFoam was chosen because it takes into account fragmentation and allows the modelling of the evolution of the droplet size distribution. Theoretical models were also chosen based on the dimensionless numbers (see Table IV-7). It should be emphasised that this preliminary approach did not take into account wall-droplet interactions, which were configured to a droplet stick model. The type of utilised turbulence model was RANS, which means that only the large scales of the turbulence will be numerically solved while the small and medium scales will be modelled. The k-ω sst model was used in relation to the high *Re* and the confined environment. It entails using both the traditional k-ε model distant from walls and the k-ω model near to walls. The O'Rourke model was chosen to depict the collision of two drops (O'Rourke, 1981). This model is based on a statistical approach and assumes that two droplets can only collide if they are in the same cell. Therefore, droplets can coalesce for a head-on collision, and droplets will rebound for an oblique collision.

Table IV-7: Theoretical models used for CFD modelling of a Jet A1 mist in the 20 L sphere

Phenomena	Turbulence	Droplet Forces	Fragmentation	Heat transfer	Evaporation	Collisions	Wall Interactions
Models	k-ω sst	Gravity, drag force	Reitz-Diwakar	Ranz-Marshall	Droplet evaporation	O'Rourke	Standard Wall Interaction: droplet stick

Figure IV-9, which displays the global view of the modelled 20 L sphere as well as the meshing of the injection system and the 20 L sphere, describes the structure of the simulation. At least six meshes per dimension were placed in the nozzle orifice area to obtain sufficient accuracy. Simulations were performed using a Crank-Nicholson semi-implicit time scheme. To minimise the number of fluid parcels and maintain a uniform mass of injected liquid, the fluid parcels used to simulate the mist injection consisted of several droplets of the same physical size. Following a sensitivity analysis, which sought to establish the appropriate calculation time to accurately represent the liquid mass flow rate, 10^5 parcels per second containing an average of 10000 droplets have been configured. Subsequently, a system of ordinary differential equations was solved to predict the evolution of mass, velocity, and temperature.

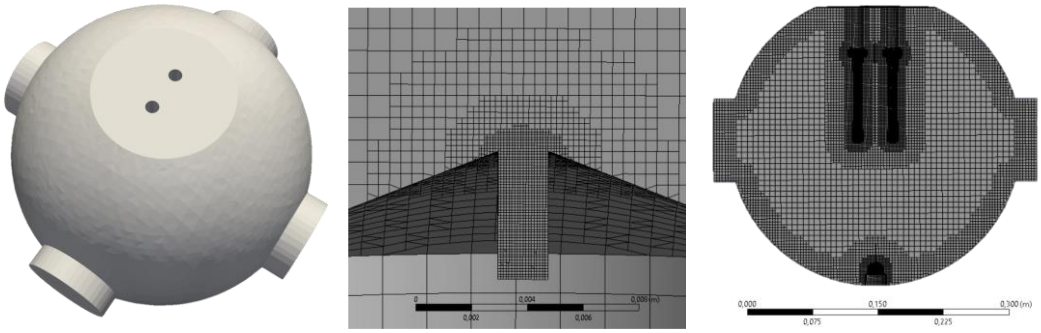

(a) (b) (c)

Figure IV-9: 20 L sphere modelled and meshed on Ansys Meshing using the CutCell meshing algorithm (a) global view, (b) focus on the injection orifice, (c) lateral view

Preliminary findings (Figure IV-10) showed the vertical dispersion of the ejected fluid, hitting the upper part of the sphere at around 400 ms. Recirculation zones would then be formed in the middle of the sphere where the turbulent kinetic energy and the velocity are high.

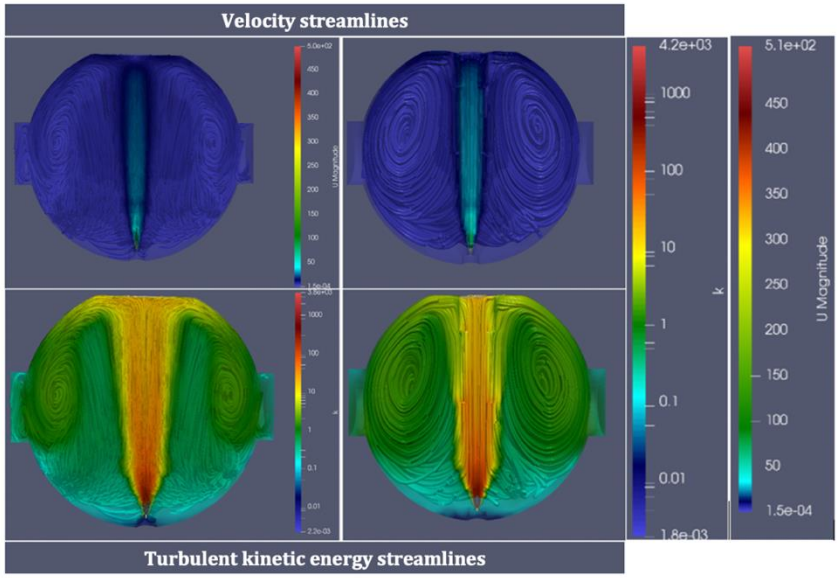

Figure IV-10: Representation of streamlines and iso-contour lines of the velocity and turbulent kinetic energy in two lateral views

Figure IV-11 demonstrates the evolution of the droplet size distribution between the nozzle exit (experimental red curve) and the sphere's centre (CFD simulated distribution). The DSD shape was seen to be conserved; nevertheless, a decrease was observed, showing the presence of fragmentation. Experimental findings at the sphere's centre will serve as reference distributions towards which simulations will be refined and adapted. Future steps will also include the determination of local concentrations, especially in the vicinity of the ignition sources. Moreover, the rain-out phenomenon should be quantified as some drops may leave the jet in the entrainment zone to form the "rain-out". These parameters are very important since they directly influence the combustion of mist clouds.

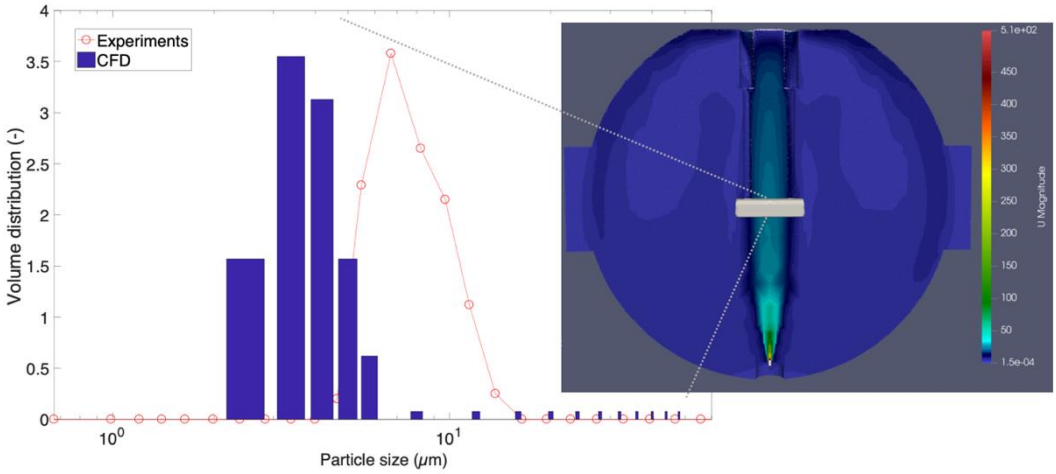

Figure IV-11: Comparison between the DSD at the orifice and the centre of the sphere after 1.5 s of mist generation using CFD modelling

4.3. Choosing the right ignition source

Equivalent to the EN 14034 standards series section 4.4 entitled "ignition source", this section comprises the comparison of the ignition sources, their characterisation, and their use in this study.

4.3.1. Comparison

A comparison of both the chemical ignitors and the permanent spark (generated using KSEP 320) ignition system was performed on ethanol and Jet A1 mist clouds. Both ignition sources were tested at 100 J and under similar operating conditions (t_v = 3 ms, T = 27 °C). Figure IV-12 shows that both ignition sources can deliver rather coherent values of both P_{ex} and dP/dt_{ex} for ethanol mists generated with nozzle set N1. For instance, at a mist concentration of 101 g.m^{-3}, the explosion overpressure reached 6.2 bar for both ignition sources. As for the rate of pressure rise, a minor difference in value was observed. This shift in values can be linked to the different initial flame kernel volumes created by both ignition sources. However, when taking into account the calculated repeatability errors, such a difference in value can be considered negligible. Another

difference between the two curves is the LEL (the lowest concentration at which ignition occurred) of the ethanol mist cloud, which appears to be lower in the case of spark ignition. Indeed, flammability limits are not absolute and depend on the type and strength of the ignition source. Here, spark ignition appears more conservative at low concentrations near the lower flammability limit. Indeed, the turbulence generated by the chemical ignitors can quench the flame propagation on a local scale. On the contrary, using spark ignition provides lower levels of turbulence and renders it easier for the flame to propagate as its stretching increases and the mass transfer phenomena are enhanced.

Table IV-8 demonstrates similar explosivity results performed at three different Jet A1 mist concentrations generated by nozzle set N1. As it can be seen, both ignition sources exhibited similar behaviour with the change of fluid.

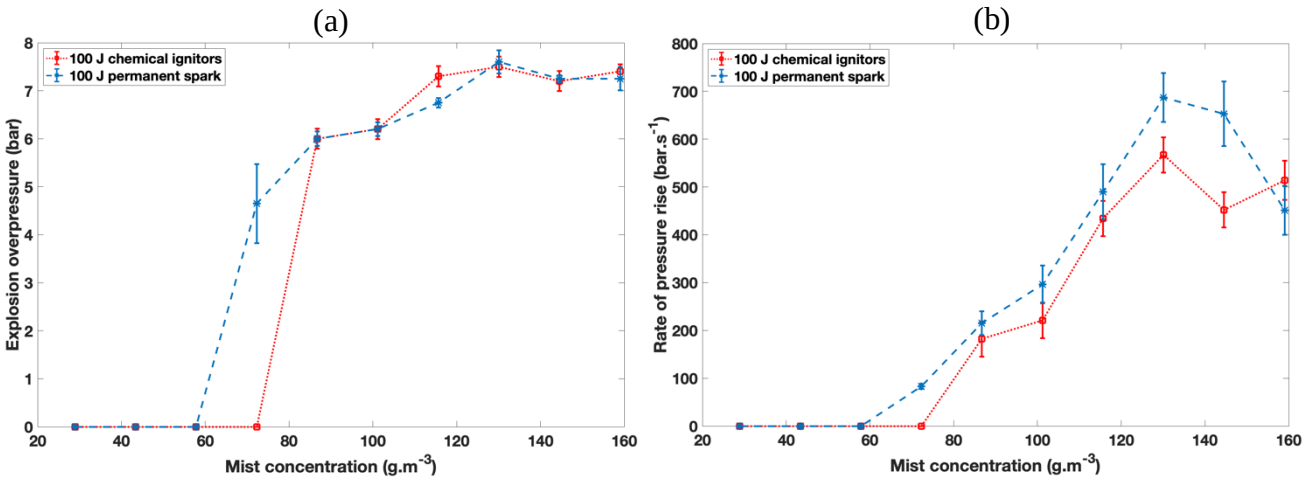

Figure IV-12: Comparison of the explosion severity of ethanol mists measured at 27 °C using Nozzle set N1 and 100 J chemical ignitors and permanent sparks

Table IV-8: Comparison of spark and chemical ignitors of 100 J on Jet A1 mist explosions

	P_{ex} (bar)			dP/dt_{ex} (bar.s^{-1})		
Mist concentration (g.m^{-3})	**102**	**116**	**130**	**102**	**116**	**130**
Spark ignition (100 J)	5 ± 0.2	5.3 ± 0.2	5.5 ± 0.2	107 ± 28	125 ± 28	158 ± 28
Chemical ignitors (100 J)	4.9 ± 0.2	5.5 ± 0.2	5.1 ± 0.2	80 ± 28	88 ± 28	170 ± 28

4.3.2. Characterisation and calorimetry

During a discharge of electrical energy, the energy used by the flame core to develop is lower than the energy delivered by the spark, which is itself lower than the available energy (P = U.I). Based on the idea that the available energy was potentially not the delivered energy, Spitzer et al. (2021) shed light on the possibility that this difference may also occur for pyrotechnical ignitors. It seemed interesting to be able to evaluate, even in an approximate way, the energy that is really available when using the ignition systems employed for the current study. Calorimetric measurements were, therefore, performed following the procedure proposed by Spitzer et al. (2021) (see Figure IV-13). The used calorimeter was composed of brass with a 2-cm inner diameter and a 6.5-cm outer diameter. The apparatus was well-isolated and was connected to a high-precision semiconductor thermistor and a resistance-voltage transformer allowing to track the recorded voltage's increase and thus the released energy. The authors performed calibration measurements on a 100-W lamp and were able to obtain a calibration sensitivity of about 0.07 $mV.J^{-1}$.

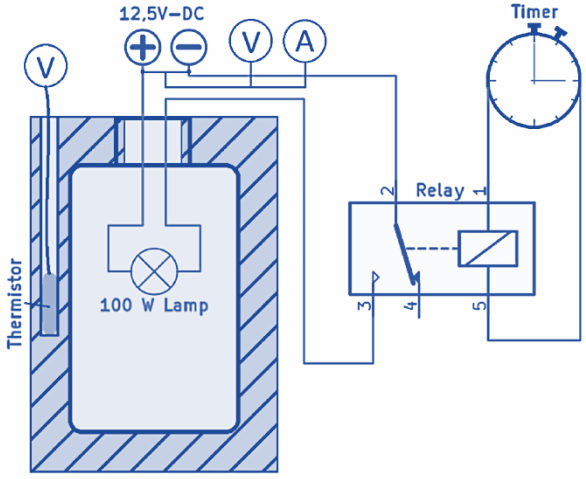

Figure IV-13: The adiabatic brass calorimeter used to assess delivered energies – calibration set-up (Spitzer et al., 2021)

The same set-up was used to double-check the net energy delivered by the developed high-voltage spark ignition system. Electrodes were placed 6 mm apart, and the spark was generated following a signal from the control and data acquisition system. As the energies generated by this ignition system, being very weak (hundreds of millijoules), fell out of the calibration range, spark durations were increased to attain energies of about 90 J. Thermistor measurements lasted for about 20 minutes each, and voltage-time evolution curves were treated to obtain the delivered energy. Figure IV-14 shows the voltage-time evolution curve after treatment (gradient clean-up and offset removal). As the curve has a positive slope, a specific procedure was followed, as advised by Spitzer et al. (2021), to determine point A. The latter corresponds to a point at which the grey and purple shaded areas are equal, leading to the estimated delivered voltage. The same

procedure was followed for all performed measurements, which were found to be lower than the expected delivered energy (current and voltage, 633 µA and 5 kV, respectively), but remained in the same order of magnitude. The spark, being generated for longer durations than usual, exhibited a discontinuous behaviour triggering heat losses and lower delivered energies than expected (about 50 % loss). In addition, these current findings cannot be considered scientifically indicative because we cannot accurately identify this method's uncertainty, especially when working with weak energies. Nonetheless, the approach did show that it is not the efficient energy we deliver and that real discharge energies are weaker than the former.

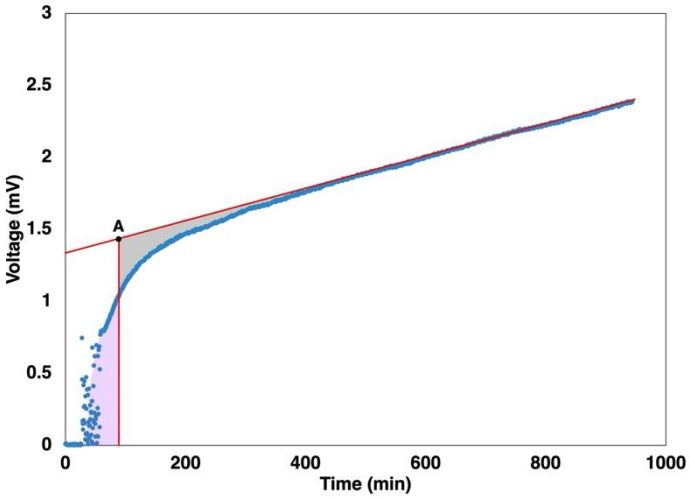

Figure IV-14: Voltage-time evolution of a 45-second spark ignition in the calorimeter

4.3.3. Application

For this study, the ignition source actuation command is sent instantaneously (t_v = 3 ms) after the end of the injection. This value is related to the valves' closing time and was established as the most appropriate to perform instantaneous ignitions. As for selecting the suitable ignition source, the KSEP 100 J permanent spark was specifically chosen to determine flammability limits, and the high-voltage spark ignition system was used to measure MIEs (Subsection 5.1.1). For explosion severity experiments and other parametric analyses, both the chemical ignitors and the permanent sparks were used, depending on the experimental conditions and the type of the tested fuel. Undeniably, the ignition source type will impact the ignition zone's temperature, the initial reaction volume, the radical generation mode, and the propagation of the flame kernel. Nevertheless, all these influences are taken into account while performing tests and switching between two types of ignition sources was not arbitrary (more details in Chapter V).

4.4. Control and data acquisition system

This section is similar to section 4.5 of the EN 14034 standards series, which defines a control unit as a unit that *"sequences the start of the dust injection, the activation of the ignition source and the start of the recording system"*.

A control and data acquisition system was developed at the LRGP, allowing operation under different chosen conditions and ensuring a safe manoeuvre. This system was based on a Mbed NXP LPC1768 type microcontroller as well as on a National Instruments NI-USB 6002 acquisition card. A software, specifically developed on LabVIEW (Figure VI-15) was used to allow the control of the electronic valves, hence the mist injection duration, the ignition delay t_v, the actuation of the ignition sources, and the start of the recording system. The program allows to automatically launch a test sequence determined in advance (manually by filling the table with valve opening/closing delays and ignitions delays or automatically using the Mist/Mist hybrid interface). An electromechanical relay ensures authorisation of system operation only if the sphere's safety switch is closed. As for the data recording, the USB acquisition card allows the visualisation of pressure data and real-time monitoring of the output signal of the low-energy spark ignition source described previously (current, voltage, and ignition duration values). When performing a sequence, the microcontroller sends a synchronisation signal to the acquisition card. For this application, the acquisition frequency was limited to 5000 Hz per channel.

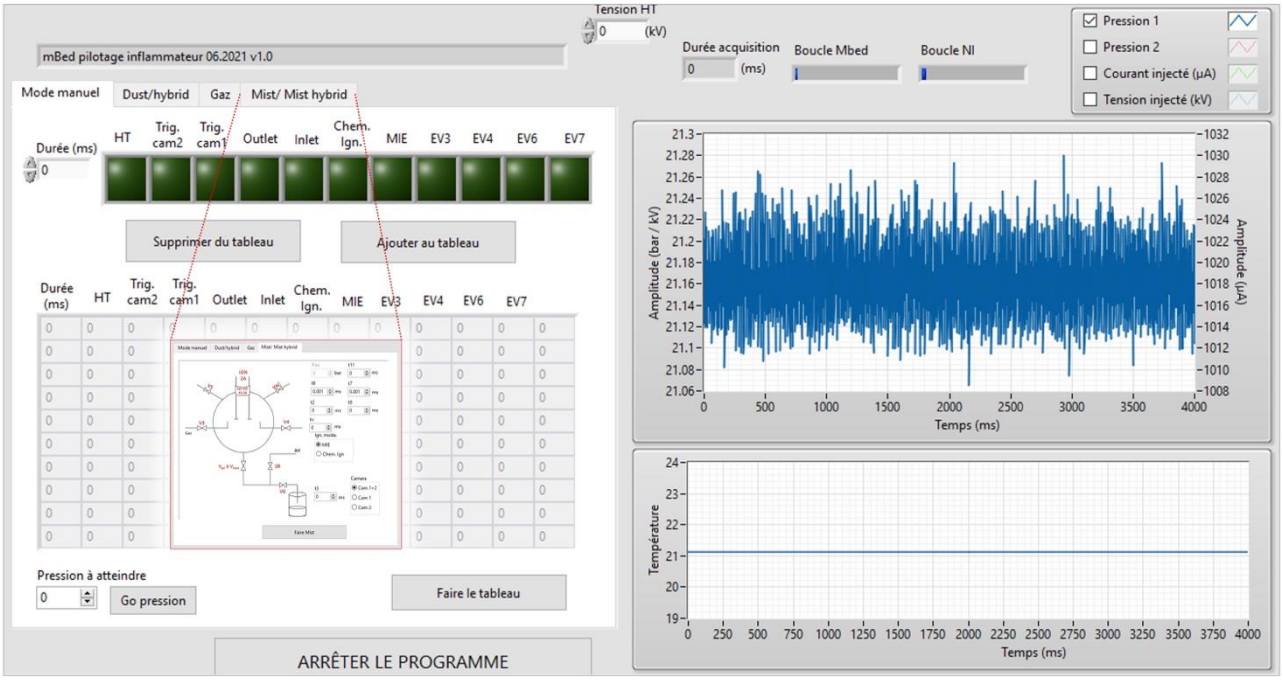

Figure IV-15: Control and data acquisition system LabVIEW interface for mist configuration testing

4.5. Pressure measurements and analysis

This section is homologous to section 4.6 of the EN 14034 standards series. Following the standard, two temperature-protected piezoelectric pressure sensors (Kistler Type 701A) recorded the pressure-time evolution during an explosion. In order to determine the explosion thermo-kinetic parameters, the explosion overpressure (P_{ex}) as well as the rate of explosion pressure rise (dP/dt_{ex}), a MATLAB program was prepared in agreement with the European standard EN 15967 (2022) "Determination of the maximum explosion pressure and maximum rate of pressure rise of gases and vapors". Figure IV-16 depicts an example of a pressure-time evolution during an ethanol mist explosion. The explosion overpressure was determined as the peak of the pressure-time curve, while dP/dt_{ex} was concluded using both two-point and five-point derivatives. Five-point derivatives were mainly exploited in this study as they provide more accurate data.

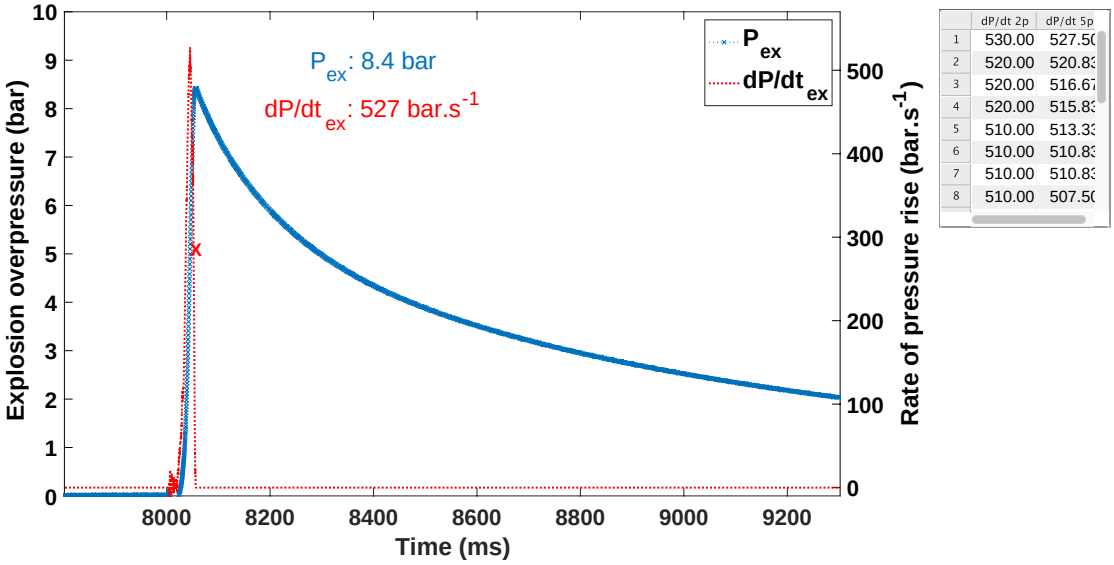

Figure IV-16: Time evolution of the explosion pressure of an ethanol mist cloud in the 20 L explosion sphere (generation at ambient temperature using nozzle set N1)

4.6. Proposed modus operandi

As proposed in the 6th section of the EN 14034 standards series, this study puts forward a detailed modus operandi, summarising all the previously discussed steps to perform a mist explosivity series of experiments. This procedure is also accompanied by a detailed timeline (Figure IV-17) of a typical experimental cycle composed of two phases: mist generation and mist ignition, permitting the visualisation of the following modus operandi more clearly:

1. The fuel of interest is placed in the metallic reservoir under ambient conditions.

2. The temperature of the sphere is controlled to the required predetermined temperature and recorded along with the atmospheric pressure.

3. The nozzle set and air injection pressure (P_{inj}) are chosen according to the needed DSD, turbulence level, and concentration range.

4. The injection time, t_{inj}, and evacuation pressure, P_0, are calculated according to the required testing concentration, atmospheric pressure, and turbulence level.

5. The 20 L sphere is vacuumed to the calculated evacuation pressure, P_0.

6. The fuel is injected into the sphere during the specified injection duration, t_{inj}, and then ignited by the chosen ignition source after an ignition delay time (t_v = 3 ms in standard conditions).

7. The pressure-time evolution is recorded using the two piezoelectric pressure sensors and visualised on the specifically developed data acquisition program.

8. An ignition is considered to have taken place when an overpressure, P_{ex}, of at least 0.5 bar relative to the initial atmospheric pressure, P_i, occurs.

9. The procedure is repeated for a concentration range, starting with at least a 1-second injection and increasing by steps of 1 s.

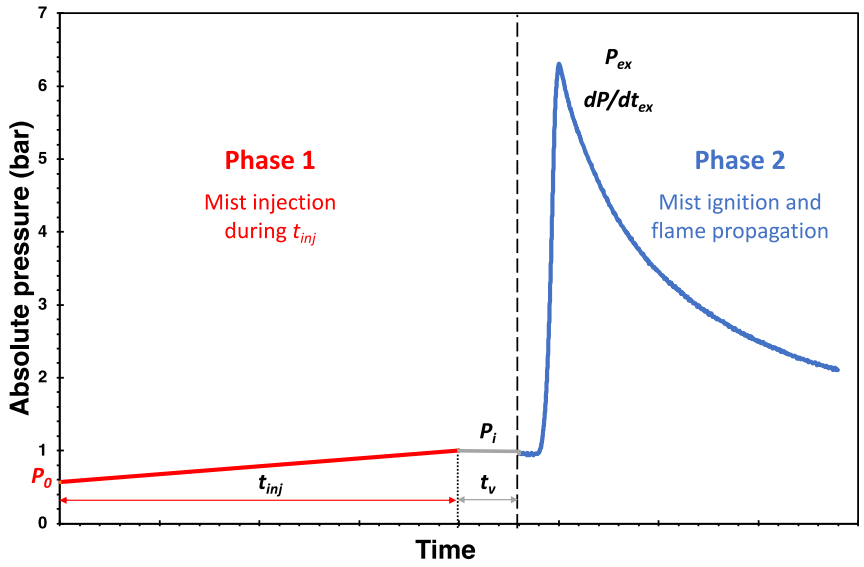

*Figure IV-17: Progress of a typical experimental cycle of two phases: **Phase 1**, mist injection, and **Phase 2**, mist ignition, separated by a delay time t_v*

4.7. Calibration, reproducibility, deviations

This section follows section 7 of the EN 14034 standards series. As proposed by the mentioned standard, the 20 L should be verified (explosion severity parameters, P_{max} and dP/dt_{max}) with at least one reference dust. In our case, ethanol vapours were tested in the 20 L sphere at 80 °C (> ethanol's boiling point) as a reference fluid. Chemical Equilibrium with Applications (CEA), a NASA computer program, was used as a comparison tool between the experimental results and theoretical calculations of ethanol's explosion overpressure (Figure IV-18) (McBride and Gordon, 1996). Results were consistent as the explosions performed in the 20 L sphere are not entirely under adiabatic conditions; therefore, it is normal to obtain an experimental overpressure lower than the theoretical adiabatic overpressure. Experimental findings were also compared with those found by Mitu and Brandes (2017) in the 20 L sphere and were found to exhibit similar overpressures near stoichiometry (100 – 125 g.m^{-3}). As the mixture shifted to the rich side, a sharper decrease in P_{ex} was seen by Mitu and Brandes (2017). Nevertheless, as it can be seen, experimental findings follow a similar trend as the numerical and literature data and can be used to verify the apparatus and test equipment.

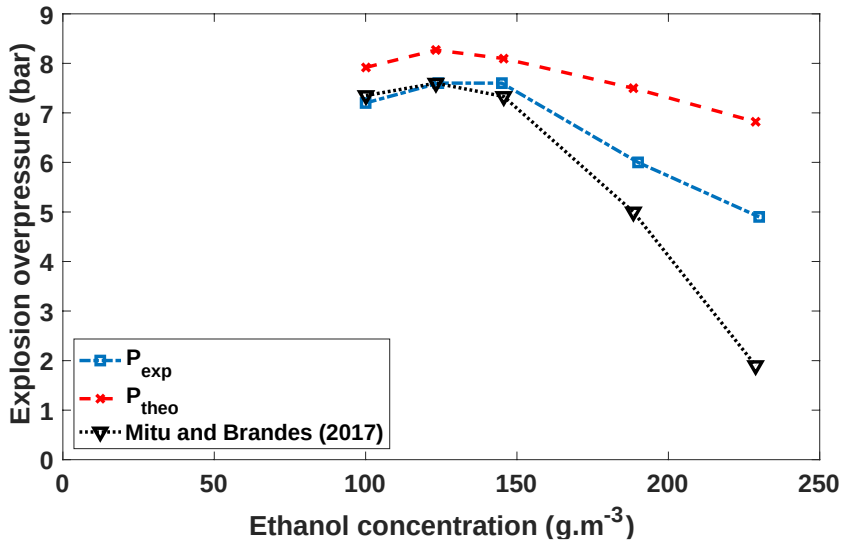

Figure IV-18: Comparison between experimental, literature, and theoretical ethanol combustion overpressures at 80 °C

Prior to each series of experiments, a set of calibration tests was performed. The mass of the injected liquid was measured at least three times per injection duration and under the predetermined conditions. This allowed identifying the mist injection system's accuracy, which will be represented using standard errors as it depends on the injected fuel and several other conditions. Standard errors, as low as ± 1 g.m^{-3} and as high as ± 12.98 g.m^{-3}, were found for nozzle set N1. Table IV-9 summarises the maximum concentration error attained for some of the selected fuels, most of which were reached at relatively long injection durations. For instance, for an injection of 10 seconds, these errors do not exceed a 10 % deviation from the 120 g.m^{-3}

associated mist concentration. It should be noted that the accuracy of the weighing scale and the solenoid valve should also be considered.

Table IV-9: The maximum attained mist concentration standard error (Nozzle set N1 - P_{inj} = 3 bar)

	Ethanol	Jet A1	Diesel	LFO	Biodiesel
Maximum concentration error ($g.m^{-3}$)	± 7.24	± 11.02	± 10.22	± 12.98	± 10.52

The repeatability of the explosion severity tests was also assessed as each was performed at least three times. As errors are condition-specific, they will be portrayed in the form of error bars in explosion severity curves. The EN 14034-1 (2004)+A1 (2011) standard suggests repeatability of a maximum deviation of 5 % and a reproducibility of 10 % of the P_{max} of a reference dust. Current findings have not exceeded, in terms of repeatability, a 12 % of the average P_{ex} value, which can be considered acceptable for a newly developed method. These variations are associated not only with the operating and environmental conditions but also with the design of the apparatus. Indeed, with a two-phase flow comes a lot of uncertainties, which shows the importance of understanding the evolution of a mist cloud and determining local concentrations and mist distribution inside the 20 L sphere. Reproducibility tests have not yet been carried out.

The EN 14034-2 (2006) standard evokes a table of the maximum permissible deviations obtained per range of rates of pressure rise of a reference dust. Table IV-10 compares these deviations with the maximum ones obtained experimentally for mist cloud explosions.

Table IV-10: Maximum permissible deviations for dust clouds explosions (EN 14034) and experimental findings for mist clouds

dP/dt_{max} ($bar.s^{-1}$)	Relative deviation for dust clouds (%)	Relative deviation for mist clouds (%)
< 50	± 30	± 18
> 50 to 100	± 20	± 27
> 100 to 200	± 12	± 7
> 200	± 10	± 15

4.8. It's about time for a standard

As seen until now, a well-established standard is required to assess mist ignitability and explosibility. The proposed test method supplies repeatable data that can serve in explosion prevention, protection, and mitigation measures.

This test method has, without a doubt, some limitations, all of which the previous sections have mentioned, and that can occur in actual mist releases, including droplet-wall interaction, ambiguous local concentrations, and upper limits of mist concentration in the confined and relatively small vessel. Nevertheless, every standard has some limitations and can be useful under a restricted set of conditions.

If we were to maintain the sphere in the dust configuration shown in Figure III-2(a) and test mist explosions following the EN 14034 standards series without any modification, more limitations would come our way. Figures IV-19 and IV-20 compare Jet A1 mist explosions performed following the dust configuration (P_{inj} = 20 bar) and the proposed test method mentioned in Section 4.6 (P_{inj} = 3 bar). Both sets of experiments were carried out at 27 °C using 100 J chemical ignitors by the same operator and on the same day. As seen in Figure IV-19, the LEL of Jet A1 mists is overestimated when using the dust configuration, showing that experiments using the mist configuration are more conservative in terms of safety. The same goes for the explosion severity for concentrations lower than 600 $g.m^{-3}$. Indeed, when a liquid is injected arbitrarily using the rebound nozzle, neither the DSD nor the mist concentration in the vicinity of the ignition source is controlled. At relatively low concentrations, pressurising the liquid to 20 bar and then injecting it through the rebound nozzle might not ensure a well-dispersed mist into the 20 L sphere, and the high turbulence might lead to quenching. On the other hand, at concentrations higher than 600 $g.m^{-3}$, P_{ex} values obtained using the dust configuration are higher, but the difference is less "dramatic", and the highest P_{ex} was obtained using the mist configuration, which is more conservative. As for the rate of pressure rise portrayed in Figure IV-20, a similar trend is followed even though, to some extent, the higher turbulence from the dust configuration is expected to lead to much higher combustion kinetics. The mist configuration also underestimates dP/dt_{ex} at higher concentrations, but higher values can be reached using the mist nozzles with higher injection pressures. This sheds light on an important positive point to the mist configuration. Using the proposed spray generation system allows the control of the level of turbulence and DSD; however, in a dust configuration at 20 bar, only a specific range of turbulence and DSD will be covered. The latter restricts the ranges of testing and leads to less cautious measures.

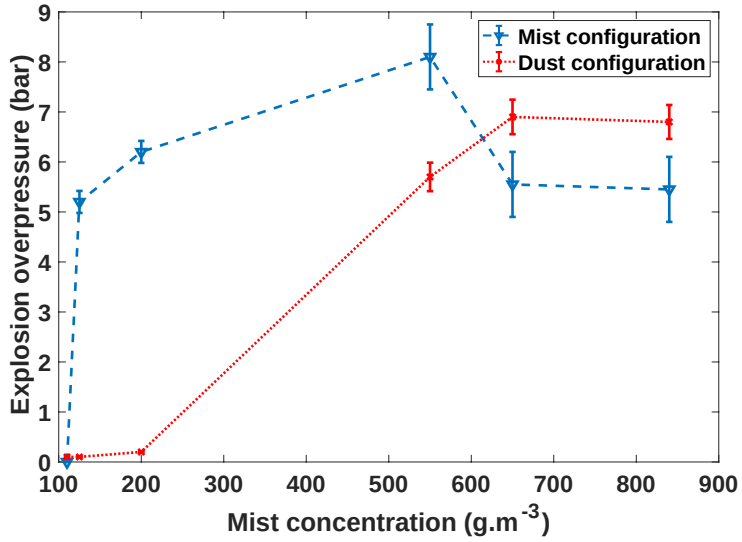

Figure IV-19: Comparison of the explosion overpressure obtained using dust and mist configurations for Jet A1 mists at T = 27 °C

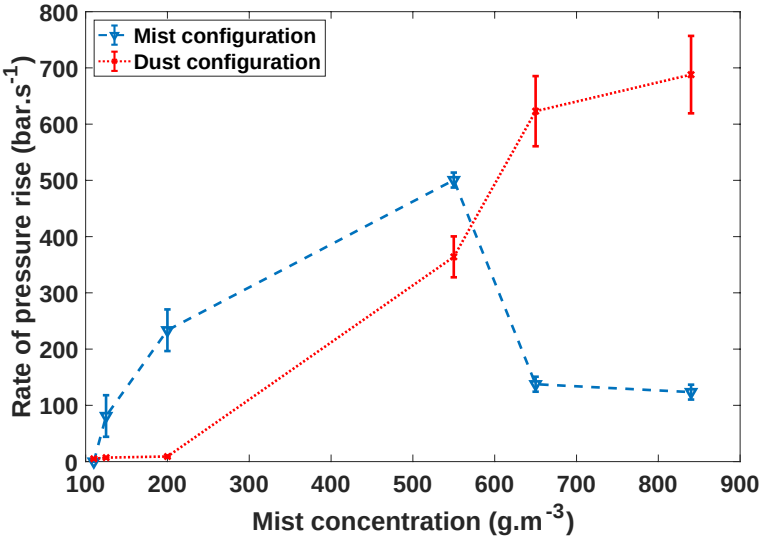

Figure IV-20: Comparison of the explosion rate of pressure rise obtained using dust and mist configurations for

Summary

The proposal of a new approach for the assessment of the ignition and explosion risks of a mist cloud necessitates the design of a new experimental tool and the performance of numerous calibrations. The focus of this chapter was the design and validation of the new test method and was based on the EN 14034 standards series. It covered all the points of interest addressed by the standard to develop the device.

First, the characteristics and performance of the mist generation system were presented. The spraying system had several configurations, allowing the change of the orifice diameter and the mist characteristics. Therefore, three nozzle sets of increasing equivalent orifice diameter were chosen and assessed, N1, N', and N2. The attainable concentrations, flow rates, and pressure increase were first evaluated using an in-situ weighing scale and a manometer. For instance, for an injection duration of 10 seconds, nominal concentrations of about 120 $g.m^{-3}$, 575 $g.m^{-3}$, and 790 $g.m^{-3}$ were attained using nozzle sets N1, N', and N2, respectively, for an air injection pressure of 3 bar. DSD measurements then followed, and a full-factorial design of experiments was performed. It was seen that using the proposed mist generation system, three droplet diameter ranges were attainable, ranging from 5 µm to 100 µm. The most monomodal distribution was obtained using nozzle set N1. It was also observed that the mist cloud remains rather stable, in terms of DSD, for about one second after injection. A parametric analysis was then performed with the help of Pareto charts to evaluate the significance of the influence of the air injection pressure, the orifice equivalent diameter, and the fluid type on the DSD. The factor that had the most significant influence on the DSD was the air injection pressure, which, when increased, favoured the fragmentation of the droplets and the increase in the turbulence level. The influence of a blasting balloon inside the sphere was also evaluated in order to assess the impact of a pressure wave on the granulometry of the droplets. Enhanced coalescence was perceived, especially for larger droplets which were most affected as their initial density distribution decreased after the blast with the creation of larger diameters, which may cool combustion products, causing momentum and energy losses and deforming the flame front. In addition, PIV measurements allowed the evaluation of the root-mean-square velocity (v_{rms}). It was seen that vertical velocity vectors could reach up to 15 $m.s^{-1}$ during injection, and v_{rms} varied between 1 and 2 $m.s^{-1}$, depending on the injection pressure. The experimental findings allowed the proposition of a correlation that predicts the SMD of a mist cloud (at the beginning of injection) with not more than a 21 % error. This section was subsequently followed by a CFD preliminary approach that predicted a DSD and will be used to analyse the behaviour of the biphasic flow.

In this chapter, the ignition sources were characterised using a calorimeter and were compared by performing ethanol explosions in order to select the most relevant ignition system. It was

found that the spark ignition was preferable to measure ignition sensitivity parameters as it delivered more conservative findings. On the other hand, for explosion severity tests and other parametric analyses, both ignition sources were proposed with an ignition delay of 3 ms after the end of the injection.

Following the choice of the ignition source, a control and data acquisition system were put forward. A detailed modus operandi was then suggested, outlining all the previously discussed steps to perform a mist explosivity series of experiments. Deviations in the mist concentration and the explosion thermo-kinetic parameters were also presented. The proposed procedure was calibrated and validated by theoretical and experimental findings.

Finally, a comparison between the proposed 20 L sphere test configuration for mists and the standard configuration used for dust explosivity assessment was performed, showing that the "mist" configuration could be more conservative in terms of safety for mist concentrations up to 600 $g.m^{-3}$.

Résumé

La proposition d'une nouvelle approche d'évaluation des risques d'inflammation et d'explosion d'un brouillard nécessite de concevoir un nouvel outil expérimental et la réalisation de nombreux étalonnages. Ce chapitre, consacré à la conception et à la validation de la nouvelle méthode d'essai, s'est appuyé sur la série de normes EN 14034. Il couvre tous les points abordés par ces normes permettant de développer le dispositif.

Dans un premier temps, les caractéristiques et les performances du système de génération de brouillard ont été présentées. Le système possède plusieurs configurations, permettant de modifier le diamètre de l'orifice et les caractéristiques du brouillard. Ainsi, trois jeux de buses, N1, N', et N2, de diamètre équivalent d'orifice croissant, ont été choisis et évalués. Les concentrations, débits et augmentations de pression atteignables ont d'abord été évalués à l'aide d'une balance et d'un manomètre in-situ. Par exemple, pour une durée d'injection de 10 secondes, des concentrations nominales d'environ 120 $g.m^{-3}$, 575 $g.m^{-3}$, et 790 $g.m^{-3}$ ont été atteintes en utilisant les ensembles de buses N1, N', et N2, respectivement, pour une pression d'injection d'air de 3 bar. Des mesures de granulométrie ont ensuite été effectuées, et un plan d'expériences factoriel complet réalisé. Il a été constaté qu'en utilisant le système de génération de brouillard proposé, trois gammes de diamètre de gouttelettes peuvent être atteintes, allant de 5 µm à 100 µm. La distribution la plus monomodale a été obtenue en utilisant le jeu de buses N1. Il a également été observé que le nuage de brouillard reste plutôt stable, en termes de distribution de taille, pendant environ une seconde, après la fin de l''injection. Une analyse paramétrique a ensuite été réalisée à l'aide de diagrammes de Pareto pour évaluer l'importance de l'influence de la pression d'injection d'air, du diamètre équivalent de l'orifice et du type de fluide sur la distribution de taille. Le facteur qui a eu l'influence la plus significative sur distribution granulométrique est la pression d'injection d'air qui, lorsqu'elle est augmentée, favorise la fragmentation des gouttelettes et l'augmentation du niveau de turbulence. L'influence de l'explosion d'un ballon à l'intérieur de la sphère a également été évaluée afin d'évaluer l'impact d'une onde de pression sur la granulométrie des gouttelettes. Une coalescence accrue a été perçue, en particulier pour les plus grosses gouttelettes qui ont été les plus affectées car leur distribution de densité initiale a diminué après l'explosion avec la création de plus grands diamètres, ce qui peut refroidir les produits de combustion, entraînant des pertes de momentum et d'énergie et déformant le front de flamme. En outre, des mesures de PIV ont permis d'évaluer la vitesse moyenne quadratique (v_{rms}). Les vecteurs de vitesse verticale pouvaient atteindre jusqu'à 15 $m.s^{-1}$ pendant l'injection, et la v_{rms} variait entre 1 et 2 $m.s^{-1}$, en fonction de la pression d'injection. Les résultats expérimentaux ont permis de proposer une corrélation qui prédit le diamètre moyen en surface (DMS) d'un nuage de brouillard avec une erreur maximale de 21 %.

Ces travaux ont ensuite été complétés par une approche préliminaire CFD permettant de prédire la granulométrie du nuage de gouttelettes et qui a permis de faire une première analyse du comportement de l'écoulement biphasique.

Les sources d'inflammation ont ensuite été caractérisées à l'aide d'un calorimètre et comparées entre elles en réalisant des explosions d'éthanol afin de choisir le système d'inflammation le plus pertinent. Il a été constaté que l'inflammation par étincelle était préférable pour mesurer les paramètres de sensibilité à l'inflammation car elle donnait des résultats plus conservateurs. En revanche, pour les tests de sévérité d'explosion et autres analyses paramétriques, les deux sources d'inflammation ont été proposées avec un délai de 3 ms après la fin de l'injection.

En second lieu, un système de contrôle et d'acquisition de données a été proposé. Un modus operandi a été détaillé, retraçant les étapes à suivre pour réaliser une série d'expériences d'explosivité de brouillard. La procédure proposée a été calibrée et validée par des considérations théoriques et expérimentales. Les caractéristiques thermocinétiques d'explosion de brouillards générés à partir des différents produits sélectionnés sont présentés.

Enfin, une comparaison entre la configuration d'essai proposée en sphère de 20 L pour les brouillards et la configuration normalisée utilisée pour l'évaluation de l'explosivité des poussières a été réalisée et montre que la configuration « brouillard » pourrait être plus conservatrice en termes de sécurité pour des concentrations allant jusqu'à 600 $g.m^{-3}$.

Chapter V:
Parametric analysis and 'benchmarking'

Now that a test method has been proposed following a standardised pathway, the seven selected fluids will go through a parametric analysis where the influence of several factors will be evaluated. This chapter provides potent insight into the behaviour of mist clouds under varying conditions. The sensitivity to ignition is first discussed by determining the minimum ignition energy, the lower explosion limit, and the limiting oxygen concentration. Second, the explosion severity of the fluids is examined. Subsequently, the influence of fluids' chemical nature, the initial temperature, the mist cloud's DSD and turbulence level, the ignition energy, the vapour content, and the presence of flammable gases is discussed in detail using specific examples. This benchmark will then be exploited to classify industrial liquids opting to help industries meet ATEX and DSEAR regulations requirements.

5.1. Ignition sensitivity

Determining the ignition sensitivity parameters (i.e., MIE, LEL, and LOC) is of paramount importance to evaluating the risk of formation of an explosive atmosphere, its ease of ignition and the means of inerting. Ignition sensitivity measurements were performed under ambient conditions, using the nozzle set N1 and an ignition delay t_v of 3 ms after the end of the mist injection into the 20 L explosion sphere.

5.1.1. Minimum Ignition Energy

For this section, the MIE is defined as the lowest electrical spark energy necessary to ignite a specific concentration of a mist cloud. MIE tests were first performed using the KSEP 320 permanent spark ignition system. However, it was perceived that the latter did not deliver low-enough energy and was limited to a minimum of 2.5 J (corresponding to a spark duration of 11 ms, which is the time needed to send the signal to the KSEP unit). Hence, the high-voltage spark ignition system was developed as discussed in Section 3.10, allowing the use of lower energies (minimum deliverable energy of about 130 mJ) with shorter spark durations. More accurate MIE tests were subsequently performed.

An essential factor to consider beforehand is the stochastic behaviour of mists towards spark ignition. Indeed, igniting a turbulent non-premixed cloud is accompanied by randomness arising due to the eventual local fluctuation of the fuel-air fraction (Birch et al., 1981), in addition to velocity fluctuations in the vicinity of the spark. Clearly, an ignition occurring at a specific timing, following spark initiation, can be easily impacted by the spark power, the volatility of the droplets in addition to their density and size, and the fluids' thermophysical nature. It will also rely on the turbulent flow's velocity and length scale, which may result in more heat diffusion from the spark and more vapour mixing than in a quiescent flow. The spark ignition is a complex question. To

consider a successful ignition, not only must a flame kernel be successfully generated after the spark has deposited its energy into the mist cloud, but also must the flame propagate and remain stable overall, accompanied by a pressure rise in a confined vessel, which in our case was determined by the two piezoelectric pressure sensors.

A series of MIE experiments was performed on the seven selected fuels generated with the N1 nozzle set (8 – 10 µm) and at an initial temperature of 27 °C (see Table V-1) (El-Zahlanieh et al., 2022a). Tests were based on Go/No-Go ignition, and no ignition was considered after at least ten consecutive tests. The tested fuels can be divided into ***four different (preliminary) groups***, including group I (MIE ≤ 0.1 J), group II (0.1 J < MIE ≤ 1 J), group III (1 J < MIE ≤ 100 J), and group VI (100 J < MIE ≤ 5000 J). It is supposed that isooctane and ethanol mists belong to group I. A distinction was made between groups II and III because 0.3 J were sometimes insufficient to ignite diesel and LFO mist due to ageing or supplier change. Moreover, it should be noted that a noticeable influence of the ambient conditions was perceived as the spark ignition was highly affected by the initial temperature and the relative humidity, which were maintained as constant as possible.

Table V-1: Minimum ignition energy of the seven selected fuels under ambient conditions and a droplet size distribution around 8 - 10 µm (nozzle set N1)

Fluid	Isooctane	Ethanol	Jet A1	Diesel	LFO	Biodiesel	Mobil DTE
MIE (J)	< 0.13	< 0.13	0.2	0.3	0.3	5000*	> 10000*

** Measured using chemical ignitors*

In order to study more in detail the evolution of the MIE with the concentration, measurements were carried out on Jet A1 mist (El-Zahlanieh et al., 2022b). At different mist concentrations, the energy was decreased with a spark duration step of 30 ms (corresponding to approximately 95 mJ) till the minimum deliverable energy of 130 mJ. Figure V-1 depicts the variation of the MIE of Jet A1 mist with average concentrations ranging between 110 and 160 $g.m^{-3}$. This variation exhibits a nearly ***parabolic behaviour***, as the fuel concentration shifts from lean to rich, with a minimum of about 200 mJ. It is common for hydrocarbon fuels to exhibit the lowest ignition energy on the fuel-rich side of the stoichiometric fuel-air ratio (Lee et al., 2001). Indeed, Lewis and Elbe (2012) linked this phenomenon to rapid fuel depletion near the ignition point and the comparatively slow fuel diffusion into this region. This depletion could take place by thermophoretic effect or due to the generated pressure wave. As a result, a fuel-rich environment is required to maintain the spark-generated flame kernel developing during the first ignition phase to keep providing fuel molecules to the kernel. Therefore, as discussed by Lee et al. (2001), an optimum equivalence ratio is maintained within the ignition kernel. Nevertheless, it is

noteworthy that, because of the multi-component nature of Jet A1 fuels, determining the equivalence ratio under specific conditions is difficult. In reality, for over 300 hydrocarbon species in such a fuel, a precise initial liquid phase composition and all of the Antoine coefficients must be determined. Basing the calculation of the fuel equivalence ratio on n-dodecane, a well-known surrogate of Jet A1, and supposing that all the mist evaporated once ignition occurs, a mist concentration ranging between 130 and 140 $g.m^{-3}$ can be represented by a theoretical equivalence ratio between 1.5 and 1.75. A local and a global fuel equivalence ratio should be distinguished here. Indeed, the ignition source is actuated 3 ms after the end of the mist injection. At that instant, there are potential heterogeneities in concentration due to turbulence and concentration modification phenomena due to the pressure wave generated by the ignition or thermophoresis phenomena. The MIE over the range of tested concentrations is on the fuel-rich side if a local fuel equivalence ratio in the vicinity of the ignition source is considered. On the other hand, increasing concentrations make it harder for the flame kernel to be sustained. MIE values for Jet A1 mist clouds are very scarce in the literature, where studies primarily focused on Jet A1 vapours (Bane et al., 2013; Lee et al., 2001; Shepherd et al., 1997).

These uncertainties reveal the need for a better understanding of the concentration distribution inside the 20 L sphere and call for more CFD simulations to visualise the mist cloud's repartition and predict any eventual fluctuation.

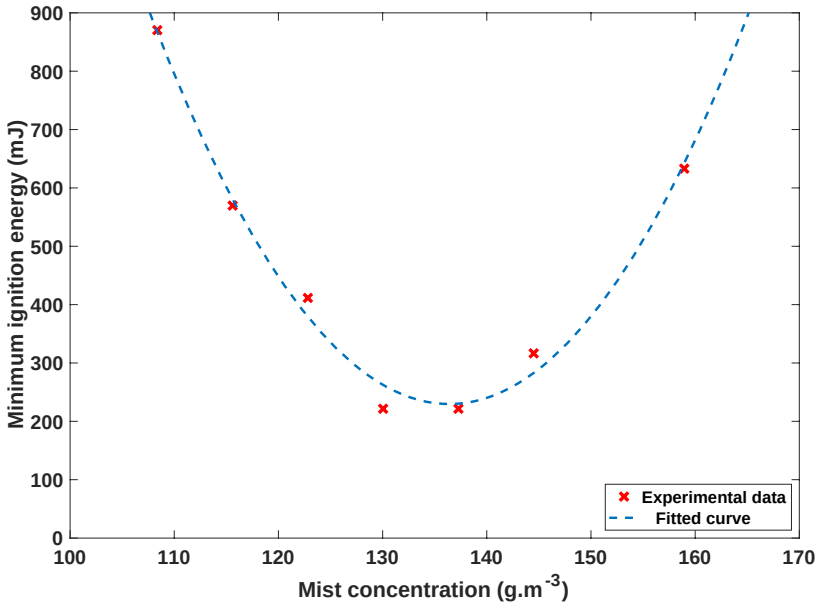

Figure V-1: Variation of the minimum ignition energy as a function of Jet A1 mist concentrations generated using nozzle set N1 at T = 27 °C

5.1.2. Lower Explosion Limit

In this study, the lowest concentration at which a mixture's flame propagates away from the ignition source is considered the LEL. Such a value was determined depending on whether an overpressure occurred. Table V-2 comprises the LEL of the seven fuels at standard conditions using 100 J KSEP spark ignition. This ignition source was chosen following its comparison with the 100 J chemical ignitors (Subsection 4.3.1). The latter exhibited higher values of LEL. Spark ignition was, therefore, chosen to obtain more conservative results.

Compared to literature, the orders of magnitude of the measured mist LEL are relatively coherent. Burgoyne (1957) found LEL values of hydrocarbon mists, specifically tetralin, around 50 $g.m^{-3}$. Similarly, Britton and Harrison (2018) indicated a value of 40 $g.m^{-3}$. Eckhoff (1995) concluded that the LEL of a spray would generally range between 100 $g.m^{-3}$ and 500 $g.m^{-3}$ regardless of the fuel volatility. Dufaud et al. (2015) also found an LEL in the order of 250 $g.m^{-3}$ for lube oil mists. It should be noted, however, that LEL values are very dependent on the placement of the ignition source used as well as on the apparatus in which the ignition takes place (Gant, 2013).

Table V-2: Lower explosion limit LEL_{mist} of fuels at T = 27 °C using nozzle set N1 (d_{50} < 10 µm), compared to LEL_{vapour}

Fluid	Isooctane	Ethanol	Jet A1	Diesel	LFO	Biodiesel	Mobil DTE
LEL_{mist} ($g.m^{-3}$)	42	64	65	80	88	103 *	No ignition
LEL_{mist} ($\%_{v/v}$)	0.9	3.3	0.88	0.98	1.1	0.85 *	No ignition
LEL_{vapour}• ($\%_{v/v}$)	1	3.1	0.6	1	0.5	-	-
$\%_{deviation}$ from LEL_{vapour}	- 10	+ 6.8	+ 46.7	- 2	+ 114	-	-

** Determined using 5 kJ chemical ignitors* *• Determined from fuels' MSDS*

As it can be seen in Table V-2, LEL_{mist} was also compared with the LEL_{vapour} of each fuel's vapour phase, which was obtained from the fuels' MSDS. To do so, the mist was considered to completely vaporise before ignition in order to calculate its volume percentage (also assuming that the ideal gas law is applicable here). One interesting observation is that perceived on biodiesel mists, a fluid considered non-volatile, which started to explode as of 5 kJ. As for Jet A1 and LFO, the statement that $LEL_{mist} \approx LEL_{vapour}$ for droplet sizes < 10 µm loses its validity as the deviation from the LEL_{vapour} is significant (about 47 % increase from the LEL_{vapour} of Jet A1, and 114 % increase

from the LEL_{vapour} of LFO). Nevertheless, the presence of larger droplets in the vicinity of the ignition source during ignition can cause such an increase. In order to investigate this phenomenon further, the influence of the DSD on LEL_{mist} was examined more specifically for Jet A1, as seen in Table V-3, at T = 20 °C. LEL_{mist} tended to increase with increasing DSD (from 94 $g.m^{-3}$ for d_{50} = 9 µm to 220 $g.m^{-3}$ for d_{50} = 60.5 µm), a finding rather coherent with that of Zabetakis (1964) but incoherent with that obtained by Burgoyne (1963). The latter author demonstrated that in upward flame propagation tests, LEL values tend to decline as the droplet diameter increases due to the flame stretching induced by the falling droplets. Nevertheless, such an effect becomes harder to identify when dealing with a spherical or quasi-spherical flame growth as in the 20 L sphere. Moreover, with a downward flame propagation, such indications become harder to pinpoint with increasing drop diameters due to the presence of droplets falling vertically downwards. Additionally, it can be noticed that the LEL of Jet A1 with nozzle set N1 are 94 $g.m^{-3}$ at 20 °C and 65 $g.m^{-3}$ at 27 °C. This highlights the influence of the initial sphere temperature on the LEL. This point will be reviewed and developed in Section 5.5.

As the nature of a mist release varies from one incident to another, a more conservative approach would be to take LEL_{vapour} as a reference to evaluate the extent of a hazardous zone and to choose the appropriate equipment. Nevertheless, as in the case of biodiesel, such values may not exist as the fluids are not considered flammable, hence showing the ***importance of measuring the LEL of high-flashpoint mists***.

Table V-3: LEL_{mist} of Jet A1 mists as a function of the DSD at T = 20°C

Nozzle set	DSD range (µm)	SMD (µm)	d_{10} (µm)	d_{50} (µm)	LEL_{mist} ($g.m^{-3}$)	LEL_{mist} ($\%_{v/v}$)	$\%_{deviation}$ from LEL_{vapour}
N1	8-10	7	9.2	9	94	1.2	+ 100
N'	40-60	10	15	14.5	127	1.6	+ 167
N2	80-100	16.7	7.6	60.5	220	2.8	+ 367

5.1.3. Limiting Oxygen Concentration

For this study, the LOC is considered the oxygen concentration below which no flame propagation occurs. Only preliminary tests on ethanol and Jet A1 mist clouds have been performed. In order to maintain a worst-case scenario, the mist clouds were injected into the explosion sphere using the nozzle set N1 at 27 °C. 100 J chemical ignitors were used to ignite the clouds. Nitrogen was used as the inert gas and injected into the sphere before the mist, reducing the oxygen percentage

inside the sphere. The vacuuming of the sphere depended on the desired oxygen concentration. The LOC was determined using Go/No-Go ignition at least three times per oxygen and mist concentration. Determining the LOC depends on the used ignition energy and the propagation criteria (Schwenzfeuer et al., 2001). An overestimation of the LOC, for instance, could occur if a weak ignitor is used, which shows the importance of using relatively high energy (with respect to the MIE, Table V-1) to remove its influence. Nevertheless, because of this reliance, the experimental data must be taken as relative values rather than absolute ones. Furthermore, the test vessel should be thoroughly cleaned, and the oxygen/nitrogen percentages should be very well-controlled to ensure precise and repeatable findings.

Findings showed that Jet A1 mists generated with nozzle set N1 have a LOC of 15.8 $\%_{v/v}$, corresponding to a mist concentration of 144 $g.m^{-3}$; whereas ethanol mists have a LOC of 13.1 $\%_{v/v}$, corresponding to a mist concentration of 110 $g.m^{-3}$ (see Table V-4). Determining these concentrations can serve as a complementary identification of the optimal mist concentration, which will be discussed further in this chapter.

Table V-4: Variation of the limiting oxygen concentration with Jet A1 and ethanol mist concentrations at 27 °C (nozzle set N1, 100 J chemical ignitors)

Kerosene Jet A1		**Ethanol**	
Mist concentration ($g.m^{-3}$)	**Oxygen concentration ($\%_{v/v}$)**	**Mist concentration ($g.m^{-3}$)**	**Oxygen concentration ($\%_{v/v}$)**
116	18.5	90	14.7
130	16.6	100	14.1
144	**15.8**	110	**13.1**
160	16.5	120	13.3
174	17	130	13.9

5.2. Explosion severity and mist concentration

After determining the ignition sensitivity of the seven fluids to support explosion prevention, the explosion severity is the next step in designing protection equipment. This section deals with determining the thermo-kinetic explosion parameters (P_{ex} and dP/dt_{ex}) at different concentrations. It is followed by discussions on many factors' influences, such as the DSD or the initial temperature, on such evolution. Throughout this chapter, explosion severity values may

differ from one section to another for a specific fluid. Such differences might have occurred mostly due to the ageing of the fuel in question and the change in petroleum cut.

Figure V-2 exhibits the evolution of P_{ex} and dP/dt_{ex} with the mist concentration of ethanol, diesel, and kerosene Jet A1 at T = 27 °C, generated with nozzle set N1 and ignited with 100 J chemical ignitors (t_v = 3 ms). A first noticeable observation is a rapid increase in the explosion overpressure at low concentrations for the three fuels. Such a rise may decrease the concentration accuracy at which the transition between ignition and no ignition occurs. Nevertheless, more concentration refinement can be made with the control system developed at the LRGP. Another observation is the plateau-like explosion overpressure curves for the three fuels. This behaviour was often perceived for the other fuels and can be explained by the recirculation of the mist in the 20 L confined sphere. It can also be caused by the saturation in the vessel, limiting the production of additional fuel vapours. The UEL can therefore be difficult to pinpoint. It can also be seen that an ***optimal mist concentration***, corresponding to the concentration at which the greatest explosion severity is achieved, is rather challenging to identify in the case of mists, a situation different from that of gases which usually attain an optimal concentration close to that corresponding to stoichiometry. The explosion thermo-kinetic parameters usually start to decrease as of such a concentration due to lack of oxygen. Indeed, Lemkowitz and Pasman (2014) stated that this optimum occurs in a fuel-rich mixture of dust (or mist), due to reduced conversion rates. As the optimal concentration usually corresponds to P_{max} and dP/dt_{max}, in the cases where no clear maximum can be identified, the average P_{ex} and dP/dt_{ex} attained on the plateau are usually appointed, and the smallest mist concentration providing these values is assumed to be the optimal mist concentration.

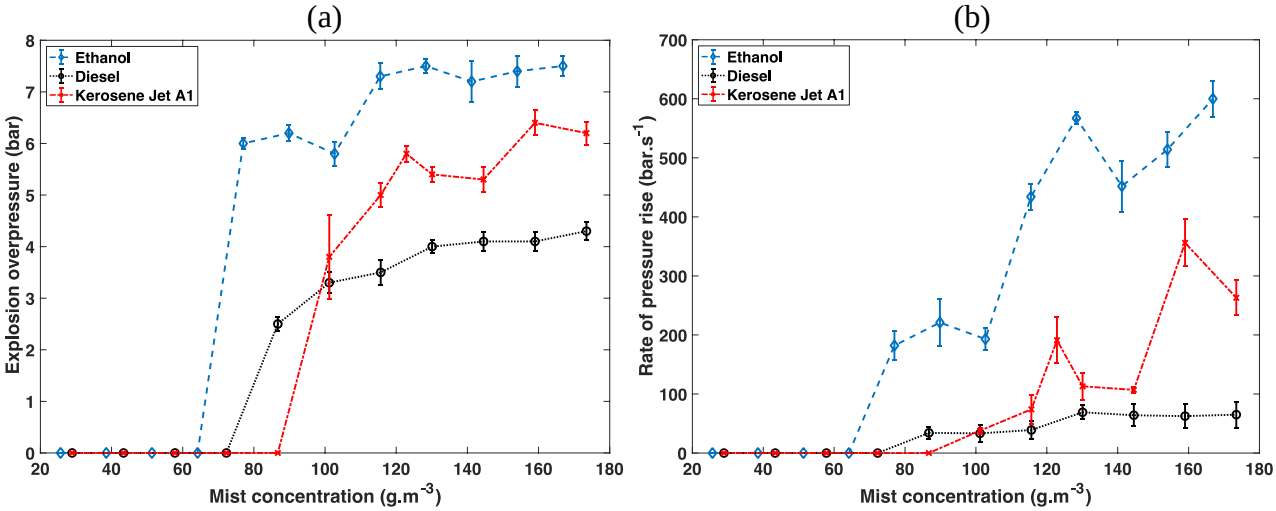

Figure V-2: Evolution of the explosion severity (a) P_{ex} and (b) dP/dt_{ex} with ethanol, diesel, and kerosene Jet A1 mist concentration at T = 27 °C – Nozzle set N1 – 100 J chemical ignitors

5.3. Influence of the chemical nature of the fluid

Another observation from Figure V-2 is the difference in the explosion severity of the three fuels. A first link can be made to the difference in the physicochemical properties of the fuels. Nonetheless, this is not the only explanation for such a difference. Table V-5 summarises the maximum explosion overpressures and the maximum rates of pressure rise as a function of the fluid in question. It should be noted that such values were extracted without taking into account the type of ignition source used (chemical or spark ignition) but were all found using nozzle set N1 under ambient conditions and using a 100 J ignition energy.

As it can be seen, both thermo-kinetic parameters decrease as the volatility of the fuel, which is represented by its vapour pressure and/or boiling point, decreases (fuels are listed by increasing order of boiling point, see Table A-3). Moreover, the overall amount of heat released during an explosion may be less than anticipated because part of the energy in the system is used to evaporate the less volatile liquids. The flame temperature will, therefore, decrease, which consequently lowers the maximum explosion overpressure.

Table V-5: Influence of the chemical nature of the fluid under standard conditions (T = 27 °C, t_v = 3 ms, Nozzle set N1)

Fuel	Ignition energy (J)	Optimal mist concentration ($g.m^{-3}$)	P_{max} (bar)	dP/dt_{max} ($bar.s^{-1}$)	K_M ($bar.m.s^{-1}$)
Isooctane	100	110	7.8	692	188
Ethanol	100	115	7.6	687	187
Kerosene Jet A1	100	159	6.4	356	97
Diesel B7	100	115	3.6	70	19
Light Fuel Oil	100	100	3.1	45	12
Biodiesel B100	5000	103	3	40	10
Mobil DTE VG68	10000	-	-	-	-

Four different behaviours can be pinpointed by comparing the seven fuels' explosion severity. Ethanol and isooctane exhibit the severest deflagration with respect to the others, while diesel, LFO, and biodiesel were the least severe. Mobil DTE did not exhibit any ignition, even when using

energies as high as 10 kJ, but further investigation is required by preheating the liquid and/or the sphere. Finally, Jet A1 was perceived as intermediately severe with a relatively high P_{max} and an intermediate dP/dt_{max}. Table V-5 allows a general comparison between the seven fuels. Indeed, by applying the cubic law (equation II-11) and by similarity with the classification applied for powders (Kst), ***four different deflagration classes*** can be proposed: M-0: K_M (bar.m.s^{-1}) = 0 non-explosible, M-1: 1 < K_M (bar.m.s^{-1}) ≤ 50, M-2: 50 < K_M (bar.m.s^{-1}) ≤ 150, and M-3: K_M (bar.m.s^{-1}) > 150. This operation will be discussed in more detail in Section 5.10.

5.4. Influence of the DSD

In addition to the energy used and the fluid's chemical nature, the DSD significantly influences the explosion severity of fuel mist clouds. Indeed, accidental releases can occur in different forms, most of which are caused by irregular orifice shapes and sizes and by different turbulence levels. In order to accurately assess the influence of the pre-characterised dispersions (Chapter IV) on the ignition sensitivity and the explosion severity, mist clouds were generated using the three nozzle sets and compared under similar operating conditions.

Figures V-3 and -4 show the evolution of the explosion severity parameters as a function of Jet A1 mist concentration using the three nozzle sets N1, N', and N2 (with d_{50} of 9 µm, 14.5 µm, and 60.5 µm, respectively) (ignition using 100 J chemical ignitors). As seen, a shift towards higher concentrations, accompanied by a decrease in the explosion severity, occurred as the orifice diameter was increased, hence the DSD. Indeed, as shown in Table V-3, the LEL was almost doubled from 94 g.m^{-3}, for nozzle set N1, to 220 g.m^{-3}, for nozzle set N2, which shows that smaller droplets are more sensitive to ignition.

For a specific concentration, in the case of nozzle set N1, the smaller the droplets, the larger the surface area, facilitating heat transfer and causing more complete evaporation and combustion of the droplets. More energy is therefore released, translated by a higher explosion overpressure. In addition, as the droplet size increases, in the case of the nozzle set N2, its relaxation time increases which may cause early sedimentation or a higher probability of not following the flow. This will consequently cause more droplet-wall interactions and would likely decrease the local concentration, hence affecting both thermodynamic and kinetic sides of the explosion. As for nozzle set N', the domination of the smaller droplets in its generated mist clouds (see Figure IV-1 and Figure IV-2) allows for obtaining a relatively strong explosion severity as the mist concentration increases. However, the explosion severity remains weaker than that obtained using nozzle set N1 for concentrations between 100 and 150 g.m^{-3}, probably due to the insufficient quantity of smaller droplets and the thermal inhibition caused by the larger ones.

Here, a limitation can be observed. As discussed before, the long injection durations are disadvised in order to avoid recirculation, the creation of liquid pools, rain-out phenomena, and uncertainties of the local ignited concentrations. That being said, the concentrations attained by nozzle set N1 within the injection duration limit cannot always intersect with those attained by nozzle sets N' and N2.

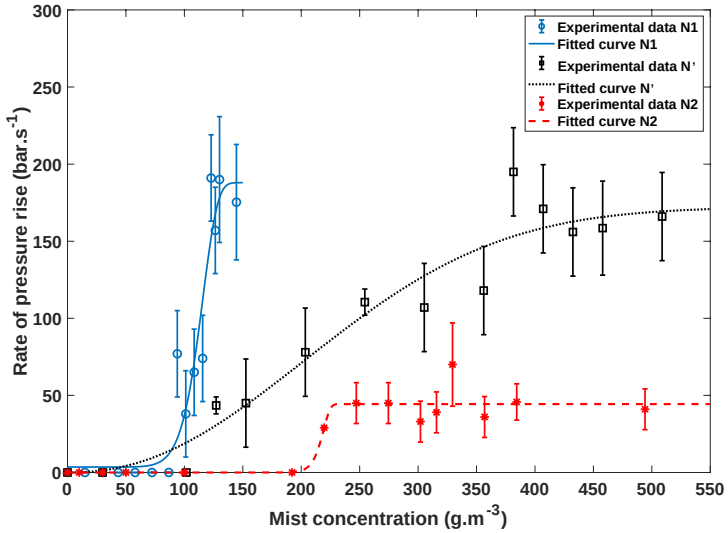

Figure V-3: Variation of the explosion overpressure P_{ex} as a function of Jet A1 mist concentrations for nozzle sets N1, N', and N2 ignited using 100 J chemical ignitors at T = 27 °C

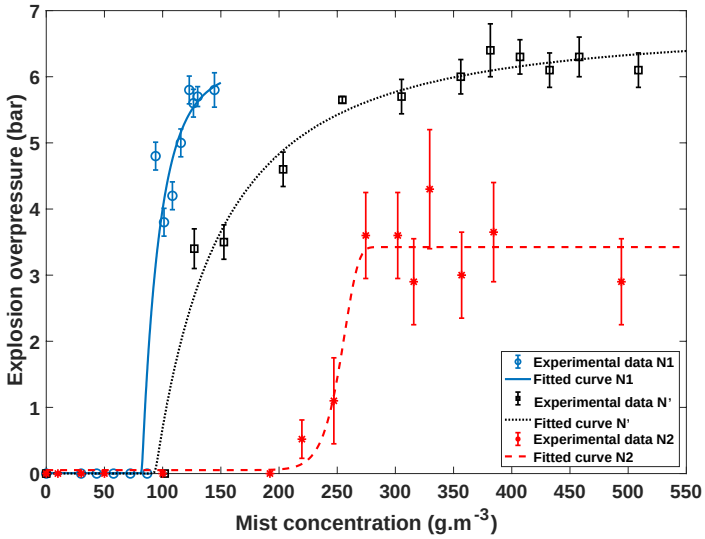

Figure V-4: Variation of the rate of pressure rise dP/dt_{ex} as a function of Jet A1 mist concentrations for nozzle sets N1, N', and N2 ignited using 100 J chemical ignitors at T = 27 °C

Table V-6 compares the optimal mist concentration, P_{max}, and dP/dt_{max} for ethanol, isooctane, Jet A1, diesel, and LFO mist clouds generated by nozzle sets N1 and N' with P_{inj} = 3 bar and t_v = 3 ms. As it can be seen, a shift of the optimal mist concentration is observed with nozzle set N'. The maximum explosion overpressure increased in the case of ethanol, isooctane, and Jet A1, but was not accompanied by an increase of dP/dt_{ex}. The increase of P_{ex} can clearly be explained by the

additional amount of injected fuel, while the decrease of dP/dt_{ex} was affected by the dynamics of the mist flow (v_{rms} decreases from about 1.74 m.s^{-1} to 1.55 m.s^{-1}). As for diesel and LFO, the contrary was perceived for P_{ex}. The latter either slightly decreased or remained rather constant when taking into account a maximum deviation of ± 12 %. This shows that approximately the same amount of fuel has been burnt. It also sheds light on the extra mass injected into the sphere that has not been burnt, hence explaining the lower rates of pressure rise. Indeed, some of the experiments performed with N' and N2 were accompanied by an increase of soot and some remaining liquid at the bottom of the sphere, as visually observed after each experiment.

Table V-6: Influence of the DSD on the explosion severity parameters of five tested fluids under ambient conditions

Fluid	Nozzle set	SMD (µm)	Optimal mist concentration (g.m^{-3})	P_{max} (bar)	dP/dt_{max} (bar.s^{-1})
Ethanol	N1	8.3	115	7.6	687
	N'	17.1	298	9.6	599
Isooctane	N1	9.6	110	7.8	692
	N'	12.0	130	8	459
Jet A1	N1	8.3	125	5.8	240
	N'	15.9	380	6.4	195
Diesel B7	N1	9.5	115	3.6	70
	N'	12.8	350	3.1	45
LFO	N1	10.4	100	3.1	45
	N'	11.1	345	3.1	47.5

5.5. Influence of the initial temperature

The possibility of fuel leaks in a heated environment cannot be neglected. Indeed, mist releases can take place in hot crankcase engines, which can heat up to about 100 °C, and also in turbines or heat transfer systems. For instance, in their literature review, Yuan et al. (2021) mentioned an explosion caused by a heat transfer fluid leak at a high temperature in LaGrange, USA. Moreover, the vapour/liquid ratio is greatly influenced by the mist temperature. To assess such incidents, experiments were performed by preheating the 20 L sphere and the liquid under examination.

This section will be complemented by an evaporation model proposed in Section 6.3.

5.5.1. Preheating of the sphere

5.5.1.1. Kerosene Jet A1

Using the surrounding water jacket, the sphere's temperature was set to 27 °C, 40 °C, and 60 °C (± 2 °C) to study the impact of the initial temperature on the mist explosion severity. The liquid was maintained at ambient temperature for this series of experiments. Mist concentrations varied from about 25 $g.m^{-3}$ to about 180 $g.m^{-3}$, with nozzle set N1, and from 40 $g.m^{-3}$ to about 700 $g.m^{-3}$, with nozzle set N2, at an injection pressure of 3 bar. An electrical spark-ignition source of 100 J was then activated (t_v = 3 ms) at an initial sphere pressure of 1 bar.

Figure V-5 shows that heating the sphere to a temperature higher than the flashpoint of Jet A1 (40°C, Table III-2) can indeed alter both the explosion overpressure and the rate of pressure rise. It should then be highlighted that, in general, the temperature of the mist is an essential parameter controlling its explosion severity. The gradual increase of the vapour concentration surrounding the droplet before ignition until reaching the LEL of Jet A1 vapours explains the changes observed in the figures. Indeed, with the increase of vapour concentration, droplet evaporation does not remain the only limiting regime of the ignition step which becomes gradually dominated by a gas combustion regime.

Nozzle set N1

Experiments performed with this nozzle set (low droplet diameters) showed that explosion overpressures were slightly increased from an average value (at the plateau) of 6 bar at T = 27 °C to about 7 bar at both 40 °C and 60 °C, which can be linked to the decrease of the initial number of moles contained in the 20 L sphere with increasing temperatures. Stoichiometry is therefore reached more rapidly, and transfers are enhanced. Nonetheless, a slight increase suggests that most of the Jet A1 injected into the 20 L sphere burnt, even at T = 27 °C. On the other hand, results showed that the temperature influence is more noticeable on the rate of pressure rise, hence on the limiting combustion regime and the combustion kinetics of the mist-vapour cloud. In the case of nozzle set N1, dP/dt_{ex} increased from 145 $bar.s^{-1}$ at T = 27 °C to about 285 $bar.s^{-1}$ at T = 40 °C, and then to 540 $bar.s^{-1}$ at T = 60°C for a mist concentration of 87 $g.m^{-3}$. It should also be underlined that the effect of the temperature is less perceptible at high mist concentrations, notably starting at a concentration between 115 $g.m^{-3}$ and 130 $g.m^{-3}$, where the behaviour of both the explosion overpressure and the rate of pressure rise tends to alter at constant temperatures of 40 °C and 60 °C. In fact, when the temperature increases from 27 °C to 60 °C, the vapour pressure of kerosene rises from 4 to 18 mbar (Shepherd et al., 2000). This suggests that kerosene cannot be

entirely vaporised at 60 °C for concentrations greater than 125 $g.m^{-3}$, at which saturation occurs (demonstrated using the evaporation model developed in Section 6.3). Furthermore, when the flame kernel has developed sufficiently, and the temperature of the sphere has increased considerably, the influence of the initial temperature of the mist is obviously less significant.

Nozzle set N2

As seen in Figure V-5, the behaviour of the ignited mist clouds generated by nozzle set N2 is very similar to that found using N1. Overpressures measured at 40 °C and 60 °C remain alike (7 bar), starting from a concentration of about 200 $g.m^{-3}$ (beginning of the plateau). However, those measured at 27 °C are much lower (4 bar) due to the concentration fluctuations that can be caused by larger droplets (as explained in the previous Section 5.4). As for the rate of pressure rise, the orders of magnitude at T = 40 °C were very close to those obtained by nozzle set N1 (both maximums reaching about 620 $bar.s^{-1}$). For T = 60 °C, on the other hand, plateau averages reached about 520 $bar.s^{-1}$ and 410 $bar.s^{-1}$ for N1 and N2, respectively. This marked difference can be directly linked to the DSD. Indeed, after saturation at 60 °C, the significant difference between both measurements is the presence of larger droplets (d_{50} = 62 µm, d_{90} = 103 µm for N2).

Lower explosion limit vs. initial sphere temperature

Another noticeable influence of the initial sphere temperature is that on the LEL of Jet A1 mist. Table V-7 shows that LEL values decrease with increasing temperatures which is logical as it is well known that lower flammability limits tend to decrease while upper limits increase as the temperature is increased (Ma, 2015). For kerosene vapours, Coward and Jones (1952) stated that their lower flammability limit, determined in an upward flame propagation tube and at a temperature sufficient to vaporise kerosene, lies around 0.7 $\%_{v/v}$. This value is coherent with those obtained in the 20 L sphere at elevated temperatures for nozzle set N1.

Table V-7: LEL of Jet A1 mists as a function of initial sphere temperature using nozzle sets N1and N2

Nozzle set	**N1**		**N2**	
Initial temperature (°C)	**LEL_{mist} ($g.m^{-3}$)**	**LEL_{mist} ($\%_{v/v}$)**	**LEL_{mist} ($g.m^{-3}$)**	**LEL_{mist} ($\%_{v/v}$)**
20	94	1.2	220	2.8
27	65	0.8	195	2.5
40	58	0.7	111	1.5
60	51	0.6	71	1

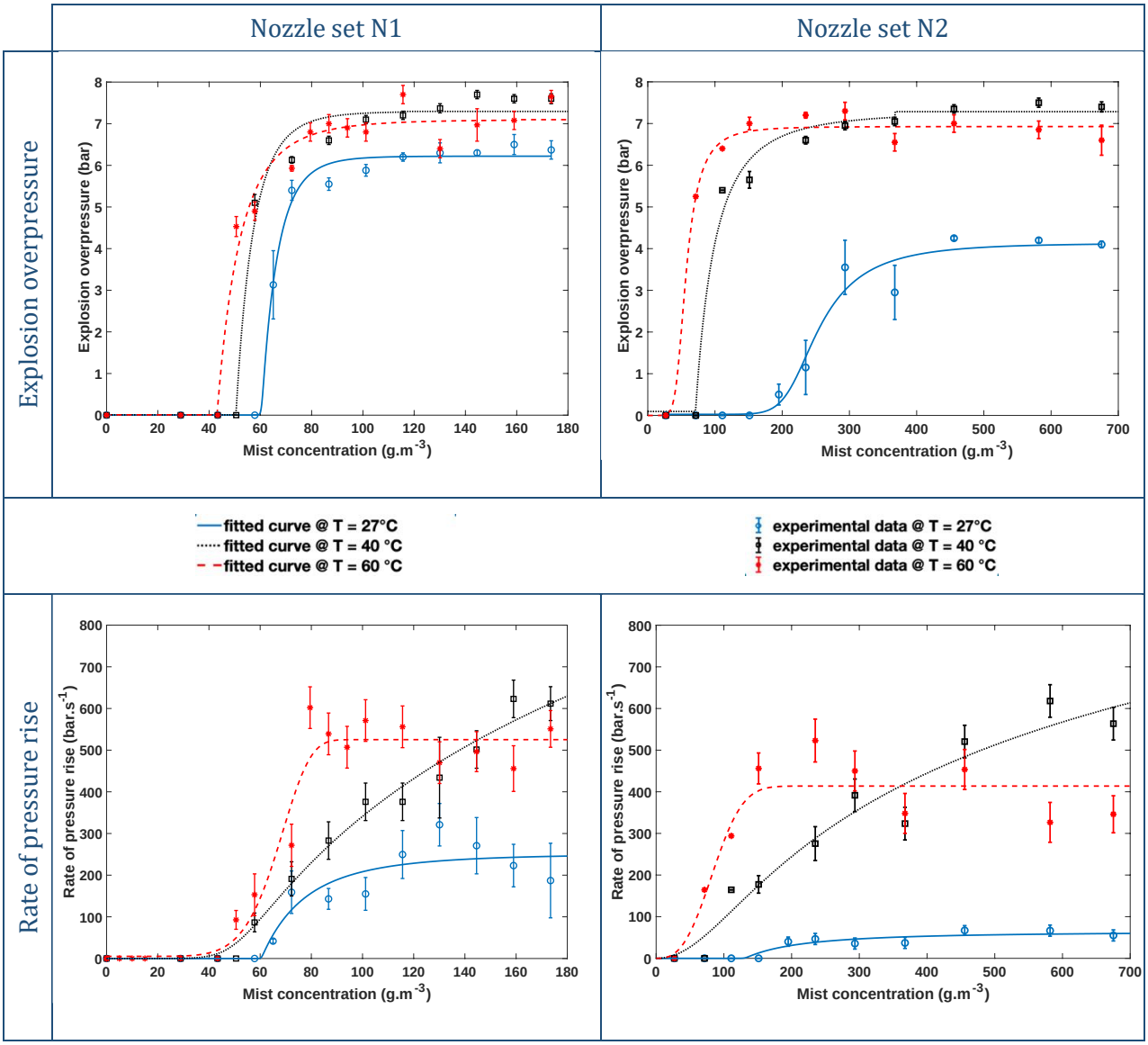

Figure V-5: Influence of the initial sphere temperature and the kerosene Jet A1 mist concentration on the explosion severity - using nozzle sets N1 and N2 at P_{inj} = 3 bar ignited used 100 J spark ignition

Experimental vs. theoretical

As already stated, the vapour concentration in the mist plays a significant role in the rate-limiting step determination. In order to highlight some specificities of Jet A1 mist explosions with regard to gas-phase explosions, theoretical calculations were performed for Jet A using the NASA Computer program CEA (Chemical Equilibrium with Applications). Figure V-6 shows a slight decrease in the explosion overpressure when the temperature increases for CEA simulations, which is not the case for the Jet A1 mist. This trend is probably due to the reduction in the initial number of total gas molecules in the closed vessel at a higher temperature, which is confirmed by various studies showing that the explosion overpressure of vapours tends to decrease with increasing temperatures while the rate of pressure rise remains rather insensitive to such variations (Li et al., 2015; Mitu and Brandes, 2017; Razus et al., 2011). It should also be noted that

as CEA considers a Jet A gas phase, a shift at the level of the LEL is observed. Indeed, Jet A1 mists require a greater concentration to vaporise and reach this LEL. The uncertainty of the exact concentration should also be reminded here to explain the difference in overpressures.

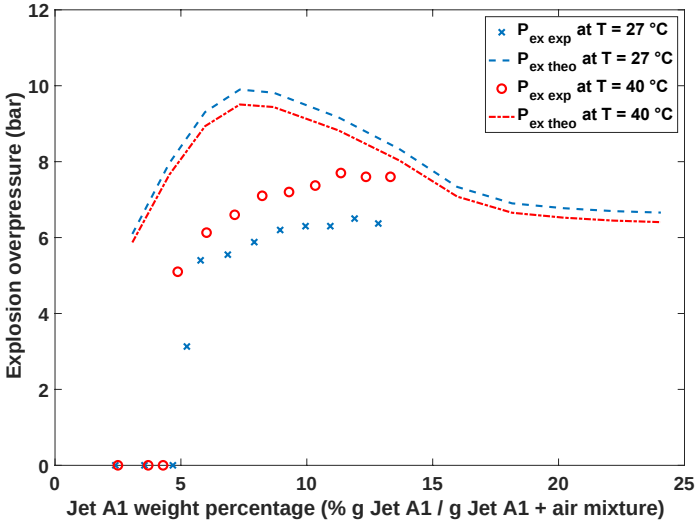

Figure V-6: Comparison of theoretical adiabatic explosion overpressure and experimental results for Jet A1 mists at T = 27 and 40 °C

The experiments performed at 27 °C were also proceeded by the composition analysis of exhaust gases by micro-gas chromatography (SRA 3000 µGC Analyer equipped with a thermal conductivity detector). Results showed the continuous but decreasing presence of O_2 was accompanied by the appearance of CO as of a mist concentration of 151 $g.m^{-3}$ (corresponding to about 3 g of injected Jet A1). This quantity of Jet A1, if all droplets were assumed to evaporate and if calculations were carried out on n-dodecane as a suitable Jet A1 surrogate, corresponds to a global theoretical fuel equivalence ratio (ϕ) of about 2 ($\%fuel_{w/w} \approx 11$). On the other hand, comparing the molar fractions *x* of the exhaust gases ($x_{CO} = 10^{-3}, x_{CO2} = 0.1$, and $x_{O2} = 0.05$) to those found by CEA for a wide range of Jet A1 concentrations showed that the molar fractions correspond to a fuel-air mixture of a global experimental ϕ of about 0.75. Such a finding validates that the injected mist concentration does not correspond to the actual quantity in suspension due to rainout and sedimentation phenomena, which also explains the presence of a plateau in explosion overpressure curves. Nevertheless, it can be seen that micro-gas chromatography tests of explosion exhaust gases, coupled with CEA simulations, could provide a reasonable estimation of the actual mist concentration inside the explosion vessel.

5.5.1.2. Diesel and LFO

Similar experiments were also performed on diesel and LFO mist clouds using 100 J spark ignition for concentrations reaching about 155 $g.m^{-3}$ using nozzle set N1. Initial sphere temperatures were increased from 30 °C to 80 °C.

Figure V-7 illustrates the influence of this temperature increase on both P_{ex} and dP/dt_{ex} of diesel mist. The LEL similarly decreased from 123 $g.m^{-3}$ at 30 °C to 93 $g.m^{-3}$ at 40 °C and 77 $g.m^{-3}$ at 60 °C and 80 °C. However, it can be seen that between 60 °C and 80 °C, no change in the LEL was observed. In fact, once the initial temperature exceeded the flashpoint, minimal changes were observed in the ignition sensitivity and on P_{ex} (comparing results obtained only at such high temperatures), which is similar to the previous observations on Jet A1 mist. Nevertheless, the influence on dP/dt_{ex} remained noticeable, showing that the kinetics of the mist combustion reaction, and especially the growth of the initial flame kernel, continue to be influenced by the initial surrounding temperature.

When compared with the previous Jet A1 experiments, it can be seen that even preheating the sphere to an intermediary temperature ($T = 40\ °C < FP_{diesel}$) significantly influences the explosion severity.

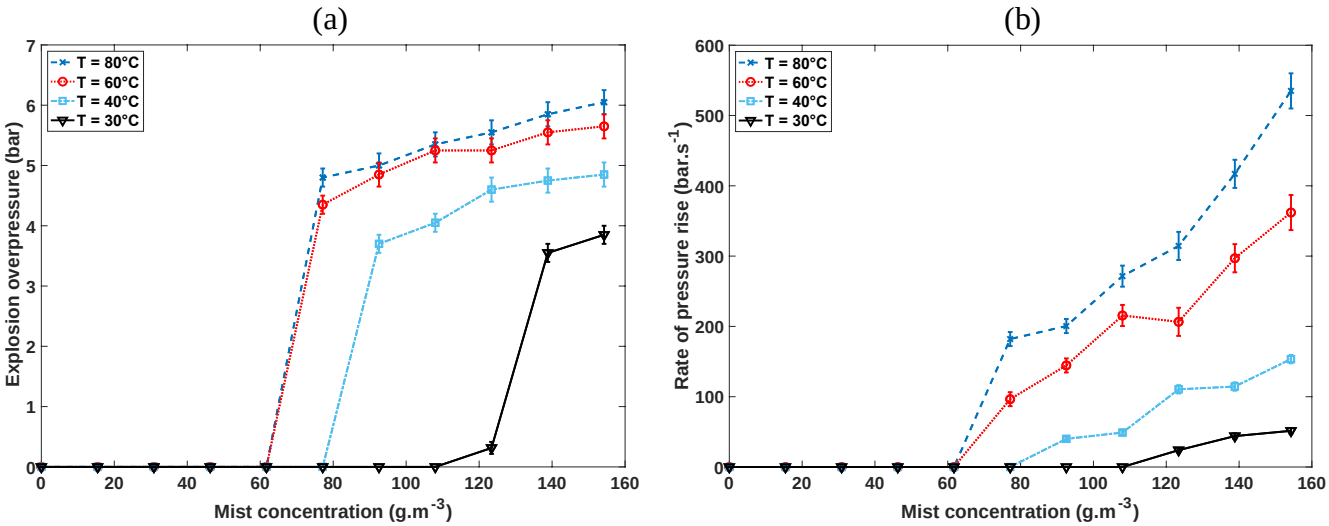

Figure V-7: Influence of the initial sphere temperature and the diesel mist concentration on (a) the explosion overpressure P_{ex} and (b) the rate of pressure rise dP/dt_{ex} – nozzle set N1, 100 J spark ignition

Similar tests were performed on LFO for mist concentrations reaching about 160 $g.m^{-3}$ with a DSD very similar to that of diesel. Table V-8 summarises the P_{ex} and dP/dt_{ex} values obtained during this series of experiments. Results were consistent with those obtained previously with diesel mists in that both P_{ex} and dP/dt_{ex} increased gradually with mist concentration and initial temperature accompanied by a decrease of LEL.

Table V-8: Influence of the initial sphere temperature and LFO mist concentration on both thermo-kinetic explosion parameters – nozzle set N1, 100 J spark ignition

	P_{ex} (bar)			dP/dt_{ex} (bar.s^{-1})		
C_{mist} (g.m^{-3})	T = 40 °C	T = 60 °C	T = 80 °C	T = 40 °C	T = 60 °C	T = 80 °C
65	0	0	0	0	0	0
81	0	0	4.6	0	0	135
97	3.8	4.8	5.1	49	182	262
114	4.1	5.2	5.5	57	220	334
130	4.4	5.2	5.6	88	214	369
146	4.6	5.4	5.9	122	277	454
162	4.6	5.6	5.9	121	359	515

5.5.1.3. Biodiesel

Biodiesel (FP = 250 °C) mist explosions were also evaluated; however, no explosions took place at the studied concentration range with 100 J ignitors. 5 kJ chemical ignitors were therefore used at initial sphere temperatures of 27°C, 60°C and 80 °C (see Table V-9). The difference between biodiesel and previously-tested fuels can be highlighted here. As it can be seen, minimal influence on P_{ex} and dP/dt_{ex} was perceived due to the very low volatility of biodiesel.

Table V-9: Biodiesel mist explosion at T = 60 °C and 80 °C using an ignition energy of 5 kJ

	P_{ex} (bar)			dP/dt_{ex} (bar.s^{-1})		
C_{mist} (g.m^{-3})	T = 27 °C	T = 60 °C	T = 80 °C	T = 27 °C	T = 60 °C	T = 80 °C
80	0	2.6	3	0	39	56
91	0	2.8	3.5	0	40	56
103	3	2.9	3.1	40	45	50
114	1.5	2.9	3	41	36	48

5.5.2. Preheating of the liquid and the sphere

The influence of the temperature of the mist on its explosion severity has just been demonstrated. However, from the point of view of the operating protocol and industrial applications, it is interesting to determine whether this effect is analogous if the fluid is preheated.

In the previous part of this section, the liquid fuel was placed in a reservoir at ambient temperature before injection into the heated sphere. Since compressed air was used to generate and break up the liquid droplets, there were concerns that these conditions could affect the initial temperature before ignition and the explosion severity. Temperature measurements were, therefore, conducted using a K-thermocouple with an acquisition frequency of 20 Hz and a temperature measurement precision of ± 0.2 %. The thermocouple was placed at the centre of the sphere in the vicinity of the ignition source. The sphere was heated to a specific temperature for at least 30 minutes. Then, a mist was injected, passing through the thermocouple. The temperature decreased by a few degrees (not more than 5 °C) and then quickly increased to the initial set temperature.

In order to assess the possible effect of this brief temperature drop, diesel fuel was heated in the metallic reservoir to 40 °C and 80 °C before injection into the sphere to match the temperature of the sphere. Figure V-8 illustrates the influence of this preheating of the fuel on the explosion severity at T = 80 °C. It can be seen that, taking into account the error bars, preheating the diesel fuel did not have a significant effect on the explosion severity tested in a preheated explosion sphere. However, a slight shift was observed in the rate of pressure rise.

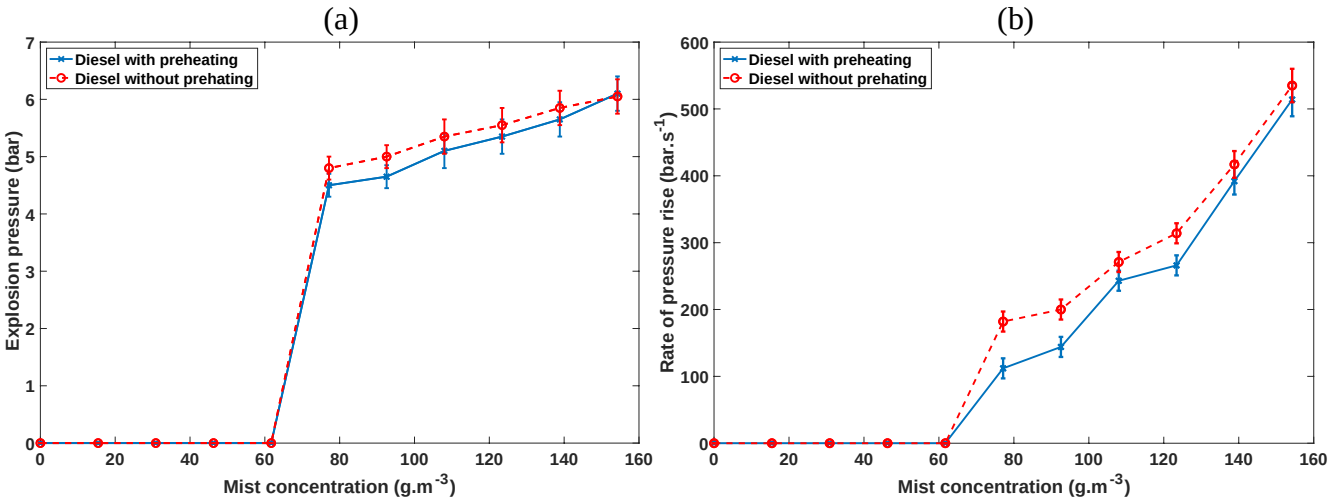

Figure V-8: Influence of the diesel mist concentration on (a) the explosion pressure P_{ex} and (b) the rate of pressure rise dP/dt_{ex} with and without preheating the fuel before injection, T_{sphere} = 80°C – nozzle set N1

Table IV-10 shows the results obtained at T = 40 °C, which confirm the mild influence of liquid preheating. However, it can be seen that the LEL did change from 93 g.m^{-3}, without preheating, to 108 g.m^{-3}, with preheating. This finding was rather hard to explain and could be linked to a potential change in the DSD arising from the temperature change due to the change in the liquid's physical properties, especially the viscosity. Therefore, complementary tests should be performed to assess the influence on the sensitivity to ignition and the kinetics of the explosion.

Table V-10: Comparison of P_{ex} and dP/dt_{ex} of diesel explosions at T = 40 °C with and without fuel preheating – nozzle set N1

	P_{ex} (bar)		**dP/dt_{ex} (bar.s^{-1})**	
C_{mist} (g.m^{-3})	**with preheating**	**without preheating**	**with preheating**	**without preheating**
77	0	0	0	0
92	0	3.7	0	40
108	3.8	4.1	51	49
123	4.5	4.6	88	111
138	4.6	4.7	108	115
154	4.6	4.8	111	154

5.6. Influence of the turbulence level

In a system where a mist is formed, turbulence plays an important role. It is responsible for droplet dispersion, mixing, and keeping droplets in suspension. According to Gant (2013), turbulence can lead a mist cloud, with a mean concentration lower than the LEL, to momentarily create zones within the explosive range due to concentration fluctuations. The additional effects and the importance of the initial turbulence level in the test vessel have been mentioned and discussed throughout this manuscript. However, it should be noted that too intense turbulence can lead to flame kernel quenching. This section comprises experiments performed to assess the influence of such level on the explosion severity of mist clouds, using two methods: changing the ignition delay time, t_v, and changing the air injection pressure, P_{inj}.

5.6.1. Changing the ignition delay time

The ignition delay time, t_v, defined in Section 3.4, is known to be related to the initial turbulence level and, consequently, has a significant effect on the explosion severity thermo-kinetic parameters. Siwek and Cesana (1995) described t_v as the simplest measure of turbulence, and the lower it is, the more turbulent the dispersion.

A diesel mist concentration of 123 g.m^{-3} ± 2 g.m^{-3} was injected into the 20 L sphere, which was heated to 40 °C. Tests were performed at six different ignition delay times, starting from ignition at 3 ms (to verify the closing of the inlet valve) after injection to a delay of 500 ms. Figure V-9 depicts the variation of the P_{ex} and dP/dt_{ex} as the ignition delay time increased. It can be seen that both thermo-kinetic parameters tended to decrease as t_v increased until reaching a time where no explosion occurred (t_v = 400 ms). This behaviour can be explained by the sedimentation phenomenon, which resulted in droplets depositing on the sphere's walls over time, decreasing the average mist concentration present in the ignition zone until it fell below the LEL. During this period, when sedimentation took place, the turbulence level represented by v_{rms} (determined by PIV – Subsection 4.1.3) decreased from 1.78 m.s^{-1} to about 0.6 m.s^{-1} at 400 ms. A similar trend has previously been observed in dust explosion experiments (Torrado, 2017).

The dP/dt_{ex} showed a steeper decrease with the ignition delay time than the P_{ex} curve. This is because the combustion kinetics are strongly influenced by the turbulence level. Therefore, a "worst-case scenario" can be expected at t_v = 3 ms, except for quenching phenomena.

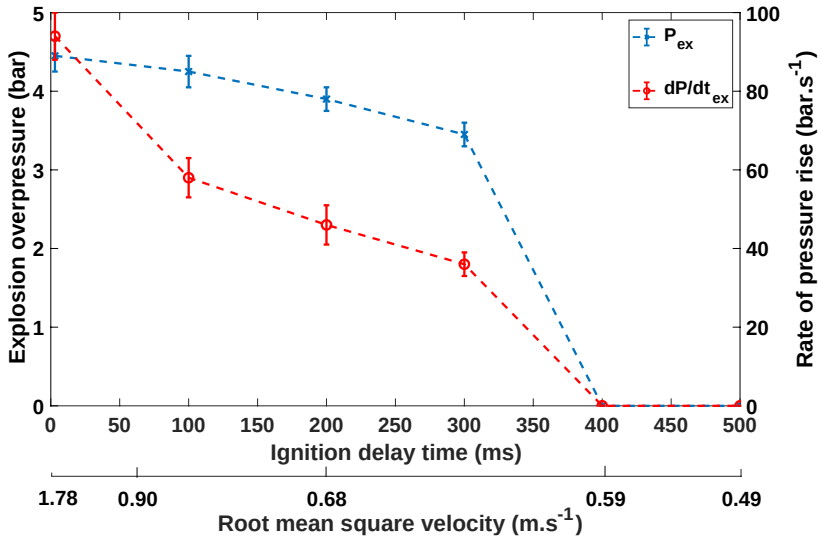

Figure V-9: Influence of the ignition delay time t_v on both P_{ex} and dP/dt_{ex} at T = 40 °C for a diesel mist concentration of 123 g.m^{-3} – nozzle set N1

5.6.2. Changing the air injection pressure

The explosivity of isooctane was assessed at two air injection pressures, 2 bar and 3 bar, using nozzle set N1. 100 J spark ignition was used with a t_v equal to 3 ms. Table V-11 compares the DSD at both injection pressures. As it can be seen, the increase in pressure is accompanied by a very minimal decrease in the DSD, which implies that the increase in both P_{ex} and dP/dt_{ex}, as seen in Figure V-10, is predominantly due to the higher level of turbulence. The LEL also decreased with increasing P_{inj}, broadening the explosion severity curves, and widening the flammability ranges. Though, this is generally not only due to the level of turbulence. Due to the nature of the chosen mist generation system, the variation of the air injection pressure will remain accompanied by a variation of the droplet size distribution, which has also proven to have a considerable effect on the explosion severity.

The extent of the influence also has to do with the physicochemical nature of the fluid:

- In the case of ***isooctane and ethanol***, an increase of P_{inj} slightly affected their P_{max} and LEL due to their relatively high volatility. Nevertheless, increasing P_{inj} from 3 to 8 bar, in the case of ethanol mist generated using N2, led to a 34 % increase of dP/dt_{max} (from 522 $bar.s^{-1}$ to 700 $bar.s^{-1}$) for a mist concentration of 550 $g.m^{-3}$.

- For ***Jet A1***, for instance, an increase of P_{inj} from 3 bar to 4 bar for nozzle set N1 shifted its explosivity curve to the left by decreasing the LEL from 94 $g.m^{-3}$ to 61 $g.m^{-3}$, respectively. The same P_{max} and dP/dt_{max} were attained, but that measured at 4 bar corresponded to a lower optimal concentration. The same product was tested with nozzle set N2 for 3 bar and 8 bar (liquid mass flow rate = 2.2 $g.s^{-1}$). A similar influence was perceived as the LEL was shifted from 220 $g.m^{-3}$ to 41 $g.m^{-3}$ (81 % decrease).

- For ***diesel and LFO***, the increase of P_{inj} for nozzle set N2 had an inverse effect on their explosivity as both P_{max} and dP/dt_{max} decreased. However, the increase in turbulence maintained its effect on the LEL by decreasing it.

Although turbulence sometimes seems to randomly influence the explosion severity and ignition sensitivity due to its high complexity and fluctuations, its effects can be predictable when taking into account all the parameters that can be affected when changing its level. Nonetheless, by decoupling the air injection pressure and the DSD and maintaining a constant droplet size while increasing the jet velocity, an adverse effect would be perceived on the flammability range (an increase of LEL), according to Rao and Lefebvre (1976), due to the increased heat loss from the spark kernel towards the fluctuating exterior (intense flame stretching leading to potential quenching).

Table V-11: Variation of droplet size parameters as a function of time for isooctane mist generated using nozzle set N1 at 2 and 3 bar

P_{inj} (bar)	d_{10} (µm)	d_{50} (µm)	d_{90} (µm)	SMD (µm)	Span factor	Skewness	Kurtosis
2	6.1	8.6	12.6	8.4	0.8	1.9	4.9
3	5.8	8.5	12.2	8.2	0.8	1.9	4.9

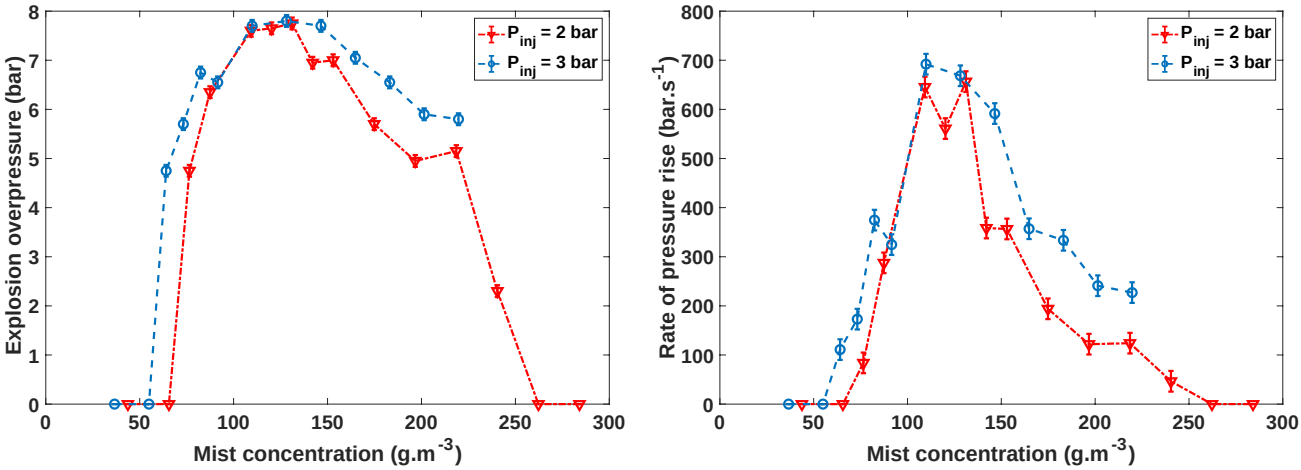

Figure V-10: Influence of the air injection pressure on the explosion severity of isooctane mist generated using nozzle set N1 at T = 27 °C

5.7. Influence of the ignition energy

As discussed before, the type and power of the ignition source have significant effects on the initiation and progress of the explosion. When chemical ignitors are used, they can alter the turbulence and flame propagation immediately after the ignition. Due to their multipoint ignition and/or volumetric effects, this occurs because they may overdrive the explosion and increase the burning velocity by increasing the total or effective flame front area. For gas and dust explosions, strong chemical ignitors have a comparable effect on the initial turbulence, which can increase the explosion overpressure, P_{ex}, and the rate of pressure rise, dP/dt_{ex}.

Taking these influences into consideration, experiments were performed on diesel, LFO, and biodiesel mist clouds at 60 °C using nozzle set N1 (t_v = 3 ms). It can be expected that as the energy of the chemical ignitors is increased, the surface temperature of the fuel droplets increases, accelerating the evaporation process and increasing the amount of vapour that participates in the combustion reaction. Nevertheless, as seen in Figure V-11, in the case of LFO, P_{ex} was faintly influenced by the increase of the ignition energy, while dP/dt_{ex} differed at low concentrations. This can be explained due to the influence of several parameters. First, at 88 g.m^{-3} and 100 g.m^{-3}, lower P_{ex} values were obtained when using the 5-kJ ignitors, meaning that less LFO took part in

the explosion process. The difference in concentration, therefore, affects both thermo-kinetic explosion parameters and leads to a lower dP/dt_{ex}. The same was noticed for diesel at 103 $g.m^{-3}$, where a 5 % decrease of P_{ex} led to a 19 % decrease of dP/dt_{ex}. Second, the use of much higher energy (multiplied by a factor of 50) implies a higher evaporation rate at a particular time and hence a richer vapour-air mixture. This mixture can be a rich fuel mixture where the limiting reactant is oxygen, hence explaining the lower explosion severity values obtained for both LFO and diesel when using 5-kJ ignitors. Finally, and most importantly, the high turbulence of the 5-kJ ignitor may have caused quenching of the propagating flame, especially at relatively low concentrations that mean a higher inter-droplet distance. Indeed, the concentrations at which LFO exhibited different dP/dt_{ex} are relatively close to its LEL, which is about 84 $g.m^{-3}$ at 60 °C.

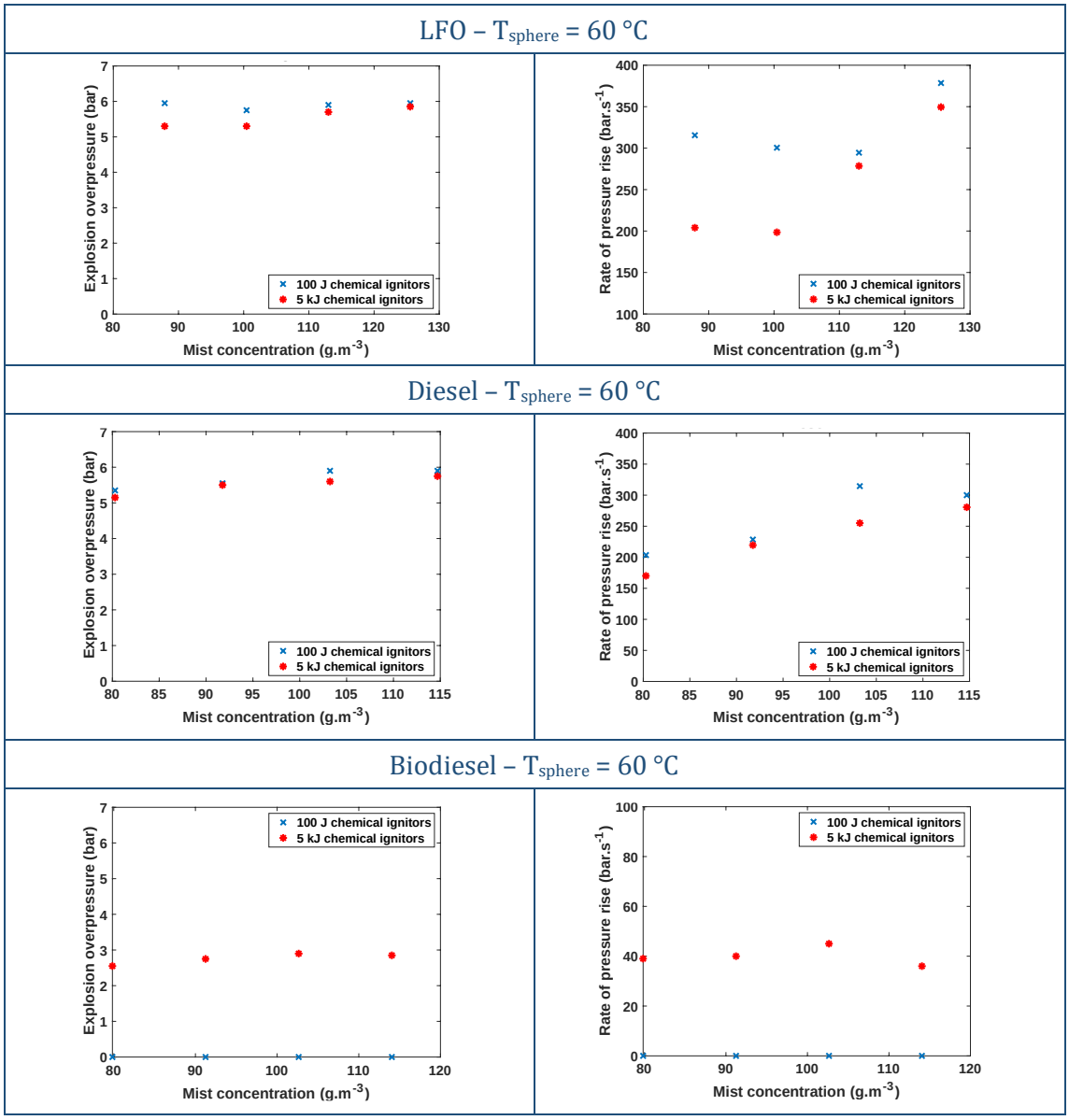

Figure V-11: Influence of the ignition energy on the explosion severity of LFO, diesel, and biodiesel at T = 60 °C - nozzle set N1

The contrary was perceived for biodiesel mists. In fact, the very low vapour pressure of biodiesel and its higher liquid heat capacity are two main factors contributing to its slow rate of evaporation. It, therefore, requires higher energies than diesel and LFO to evaporate. 100 J ignitors were insufficient to ignite the biodiesel cloud at 60 °C; however, the sphere was heated to 80 °C, and ignition occurred for both tested energies (Figure A-4). 5 kJ still exhibited higher explosion severities in the case of biodiesel and for the tested mist concentrations. This can also be due to the fact that 80 °C is still a low temperature relative to biodiesel's flashpoint (250 °C), while 60 °C is very close to both diesel's and LFO's flashpoints (65 and 58 °C, respectively).

5.8. Influence of the vapour content

Explosion severity and ignition sensitivity

As mentioned before, some discrepancies were noticed due to the multi-component nature of the fuels as fuel suppliers were changed or with the ageing of the fuels. Even a very slight change of temperature led to a big difference in ignitability and explosivity. Indeed, evaporation rates of constituent fuels can differ significantly in a multi-component liquid, resulting in a non-uniform distribution of the fuel inside the vessel and, thereby, changing the ignition and flame stability processes. The ignition behaviour is, hence, governed by the initial composition of the fuel, the volatility differential between its components, and the liquid-phase Lewis number $\left(Le = \frac{\lambda}{\rho C_p D}\right)$ (Aggarwal, 1998).

For this series of experiments, in the light of studying the influence of the vapour fraction on fuel mist ignitability and explosivity, experiments were carried out on binary isooctane-Jet A1 blends with varying volatilities. As seen in Figure V-12, the addition of isooctane to Jet A1 increased its explosion severity considerably. Another observed influence would be on the LEL, which shifted from about 80 $g.m^{-3}$ for Jet A1 only to about 45 $g.m^{-3}$ for Jet A1 + 25 $\%_{v/v}$ isooctane. Indeed, the presence of an increased vapour fraction surrounding the droplets facilitated the ignition of the mist cloud. As it can also be seen, the most noticeable difference was observed in the rates of pressure rise at relatively high mist concentrations, showing the influence of a substantial vapour fraction on the kinetics of the mist explosion. The higher volatility of isooctane leads to the presence of a higher percentage of fuel mixed with air before the start of combustion. This leads to an increased combustible mixture volume, thereby resulting in a more intense premixed burn and higher heat release, providing that the fuel-air mixture does not pass to the fuel-rich side, limiting this heat release.

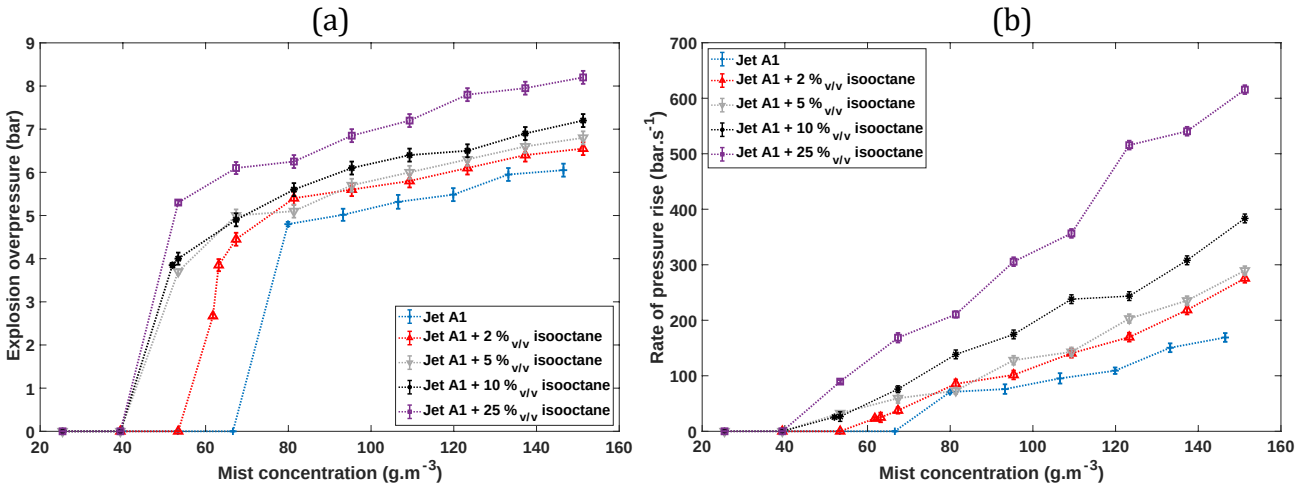

Figure V-12: Evolution of the (a) explosion overpressure, (b) rate of explosion pressure rise, as a function of Jet A1 + isooctane mist concentrations – nozzle set N1, 100 J spark ignition

Delay to ignite

In addition to the explosion severity, the time needed for mist clouds to ignite after the actuation of the ignition source can be affected. Here, the ignition delay time, t_v, defined in Section 3.4, should be differentiated from the ignition time, $\tau_{ignition}$, which is defined as the time needed for the mist cloud to ignite and reach a maximum rate of pressure rise after the actuation of the ignition source in the 20 L sphere (see Figure V-13a). $\tau_{ignition}$ is usually a crucial parameter used by engine designers and can usually be measured at high temperatures and pressures in a shock tube. This parameter is an essential macro indicator of a fuel's reactivity.

For a total mist concentration of about 125 g.m^{-3}, the time necessary to ignite the mist cloud of the five blends was compared (Figure V-13b and Table V-12). The decrease in $\tau_{ignition}$ is evident as the isooctane volume percentage increased, showing a significant acceleration and an enhancement of the reactivity with faster rates of pressure rise. The ignition behaviour is, hence, governed by the volatility differential between the constituent fuels. The variation of $\tau_{ignition}$ with the initial volume fraction of isooctane clearly indicates that the ignition behaviour of a multi-component fuel spray is strongly sensitive to the initial fraction of the most volatile components. This is indicative of the fact that the ignition process is vaporisation-controlled rather than kinetically controlled.

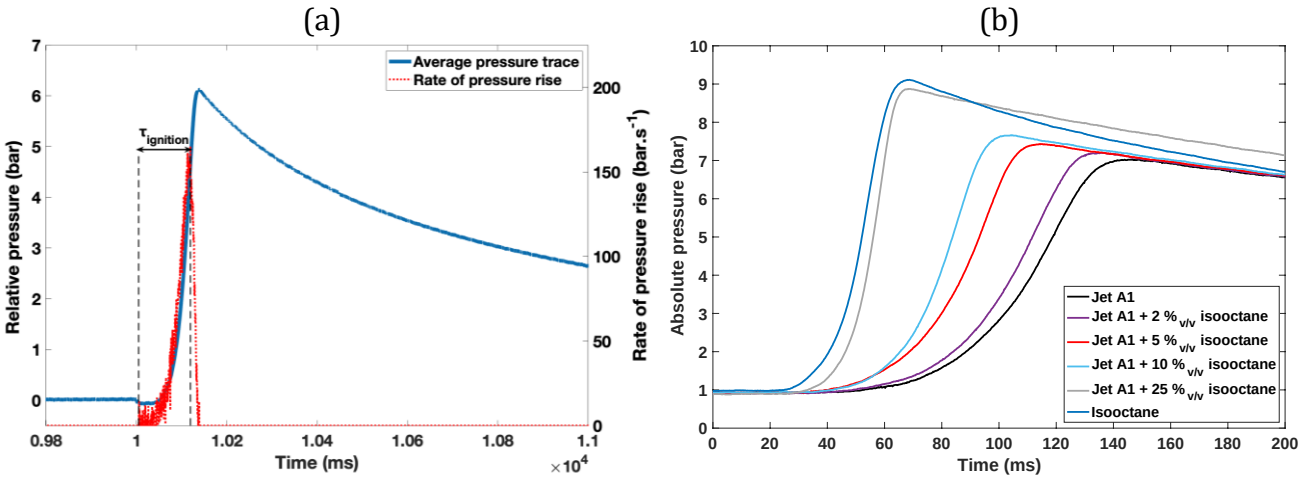

Figure V-13: (a) Ignition delay time identification (b) Pressure-time evolution for Jet A1 and isooctane mixtures for a total mist concentration of 125 g.m^{-3}

Table V-12: Evolution of the ignition time $\tau_{ignition}$ as a function of isooctane volume percentage in Jet A1 + isooctane blends for a total mist concentration of 125 g.m^{-3} – nozzle set N1

Fuel blend	**$\tau_{ignition}$ (ms)**	**P_{ex} (bar)**	**dP/dt_{ex} (bar.s^{-1})**
Jet A1	121	5.9	161
Jet A1 + 2 %$_{v/v}$ isooctane	113	6.1	170
Jet A1 + 5 %$_{v/v}$ isooctane	94	6.3	203
Jet A1 + 10 %$_{v/v}$ isooctane	85	6.5	244
Jet A1 + 25 %$_{v/v}$ isooctane	59	7.8	516
Isooctane	53	8	458

Ignition energy

As it can be seen in Table V-13, increasing isooctane in the mist cloud rendered it easily ignitable. It should be noted that the MIE here is not used in the strict sense of the standard but represents the least energy required to ignite the mist cloud at a specific concentration. The MIE decreased from a value greater than 900 mJ for Jet A1 mist to less than 160 mJ when the mixture contained 25 %$_{v/v}$ of isooctane. This can be explained by the help of isooctane molecules in facilitating the flame kernel's growth and propagation within the mist cloud. Indeed, the addition of isooctane increases the mixture's vapour pressure from 4 mbar for Jet A1 to 21 mbar for Jet A1 + 25 %$_{v/v}$ isooctane, supposing an ideal mixture of the liquids. Nevertheless, as the MIE lowers, the risk of

fire and explosion increases, as even particularly-weak ignition sources can cause fires and/or explosions. Therefore, any potential trace of a solvent residue in industries can significantly change the ignitability, or even a change in a petroleum cut where the lower volatility can lead to easily ignitable mist clouds.

Table V-13: Minimum ignition energy required for 65 g.m^{-3} of Jet A1 + isooctane blends

Fuel blend	IE (mJ)
Jet A1	> 900
Jet A1 + 2 %$_{v/v}$ isooctane	630
Jet A1 + 5 %$_{v/v}$ isooctane	380
Jet A1 + 10 %$_{v/v}$ isooctane	250
Jet A1 + 25 %$_{v/v}$ isooctane	< 160
Isooctane	< 130

5.9. Influence of a flammable gas

The role of the vapour content presented previously raised interest to go further and test the influence of a flammable gas on the explosion characteristics of a mist cloud. Therefore, experiments were first performed using nozzle set N1 at a sphere temperature of 27 ± 0.5 °C while varying Jet A1 mist concentrations between 67 and 120 g.m^{-3} to quantify the explosion severity of hybrid mixtures containing 3%$_{v/v}$ of methane. As seen in Table V-14, the addition of a low percentage of methane first influenced the LEL of the mist cloud by facilitating ignition at a concentration lower than 80 g.m^{-3}. Rates of pressure rise also accelerated by at least 3.6 times their initial values, even though the percentage of CH_4 did not exceed its LEL, which is about 5.5 %$_{v/v}$. An explosion that occurred when both components were found in lower quantities than their LEL shed light on the importance of understanding the explosion behaviour of gas-mist hybrid mixtures and determining the explosion driving regime. It is indeed important to determine whether a mist is sufficient to drive an explosion even when the gas content is not enough. Methane concentrations were therefore varied between 0 and 12 %$_{v/v}$ and Jet A1 mists between 0 and 120 g.m^{-3}. The same level of turbulence was maintained throughout the series of experiments to ensure that no influence, other than the Jet A1 – CH_4 mixture composition, occurred on the explosivity.

Table V-14: Influence of adding methane gas to Jet A1 mist clouds on the explosion severity at T = 27 °C

	P_{ex} (bar)		dP/dt_{ex} (bar.s^{-1})	
Mist concentration (g.m^{-3})	**Jet A1**	**Jet A1 + 3%$_{v/v}$ CH_4**	**Jet A1**	**Jet A1 + 3%$_{v/v}$ CH_4**
67	0	6.5	0	264
80	4.8	6.7	71	274
93	5	7	76	379
107	5.3	7.2	95	350
120	5.5	7.4	109	416

Figure V-14 represents a bubble chart expressing the rates of pressure rise obtained for various concentration to explosive limit ratios, as inspired by Russo et al. (2012), who evaluated the explosion severity of methane and nicotinic acid. Here, the LEL of CH_4 expressed in volumetric percentage, experimentally measured to be 5.5 %$_{v/v}$, and the minimum explosion concentration (MEC) of Jet A1 mist expressed in g.m^{-3}, experimentally predetermined to be 80 g.m^{-3} in this series of experiments, are differentiated. As can be seen in Figure V-14, the diameter of dP/dt_{ex} circles is proportional to their values ranging between 52.5 bar.s^{-1} to 613 bar.s^{-1}. The figure also demonstrates the existence of five different explosion regimes. A "mist-driven explosion" zone can first be identified for explosions taking place at mist concentrations above the MEC and CH_4 concentrations below the LEL. The explosion characteristics of the mist hence dominated the explosion. Inversely, when the CH_4 concentration is maintained above its LEL, and the contrary for Jet A1, the explosion becomes more "gas-driven". On the other hand, when both concentrations are above the lower limits, both fuels are considered to have contributed to the explosion leading to a "dual-fuel explosion" zone. Note that explosions with the same CH_4 concentration were more severe when more Jet A1 was introduced to the mixture, demonstrating the contribution of the mist cloud and the possible effect of the droplet presence on the flame propagation (radiation and potential stretching). Finally, the last two zones were seen to be divided into a "no explosion" zone and a "synergic explosion" zone. The latter was identified because the interaction of the two components resulted in a total impact more significant than the sum of their individual effects, even when below both their explosion limits. The former can be separated from the explosion regime by either Le Chatelier's mixture flammability limit rule (Mashuga and Crowl, 2000), usually applied for homogeneous gas mixtures, or the Bartknecht curve (Addai et al., 2016), usually applied for hybrid dust-gas mixtures.

Le Chatelier's law, which shows a linear relationship between the MEC of the mist and the LEL of the gas both weighed by their concentrations, is expressed as follows:

$$LEL_{mixture} = \frac{1}{\frac{C_{mist}}{MEC_{mist}} + \frac{x_{CH_4}}{LEL_{CH_4}}} \qquad \text{V-1}$$

Bartknecht curve, which shows that, by a second order equation, the MEC of the hybrid mixture decreases with increasing gas concentrations, is expressed as follows:

$$MEC_{mixture} = MEC_{mist}\left(\frac{x_{CH_4}}{LEL_{CH_4}} - 1\right)^2 \qquad \text{V-2}$$

Figure V-14 shows that the Bartknecht curve may better delimit the two zones as no explosions occurred under the curve. Nevertheless, complementary tests are required to better quantify and understand liquid-gas explosions. However, preliminary experiments on hybrid mixtures have highlighted the role that mists can take in an explosion, while complex simultaneous phenomena, including heat transfer, turbulence-combustion interaction, and combustion kinetics remain vague. Complementary tests could also include studying the influence of the DSD as the stability, turbulence, and sedimentation phenomena of the mist cloud could modify the burning velocity and the flame front, creating perturbations and possible stretching and radiation phenomena.

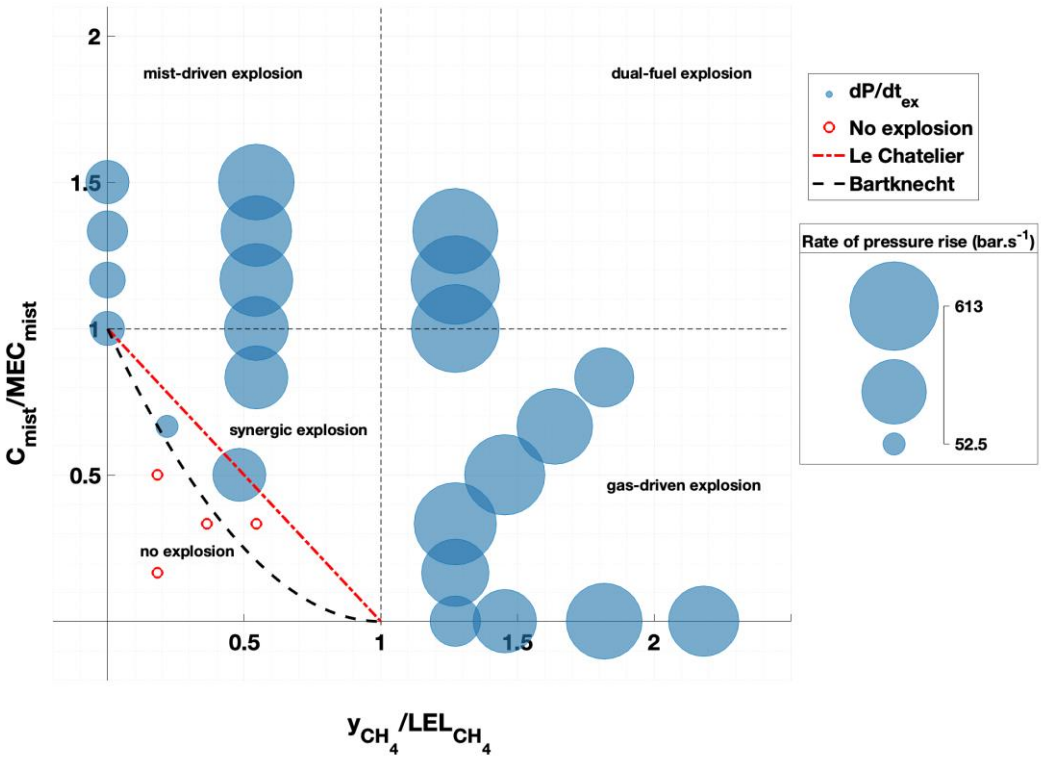

Figure V-14: Explosion experimental rates of pressure rise as a function of Jet A1 mist and methane concentrations

5.10. Off to standardisation?

With this chapter coming to an end, it is safe to say that it is time to standardise a complete procedure to evaluate mist explosion safety parameters. The followed procedure allowed the determination of the ignition sensitivity of mist clouds, as well as their explosion severity. The influence of many parameters was also taken into account, showing the versatility of the proposed modus operandi. This chapter has proven that scientific data can finally be supplied to move on to standardisation. Figure V-15 summarises the current situation of mist explosion risk assessment, the main points to cover, and the benefits of this study.

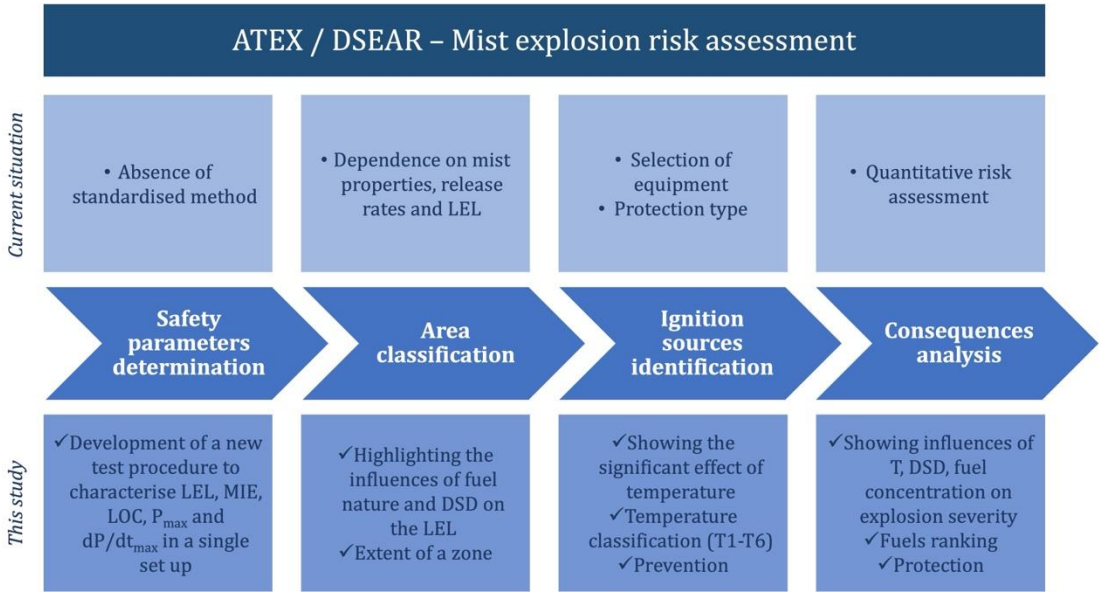

Figure V-15: Summary of the practical applications of this study in terms of mist explosion risk assessment

Although some discrepancies were observed due to storing, change of suppliers, and ageing, the previous sections revealed different mist behaviours and responses to ignition depending on the chemical nature of the fuel in question. The fuels were divided into four MIE categories (Figure V-16) as a function of their MIE, which was determined using the newly developed high-voltage spark ignition system. As for their explosion severity, it was proposed in Section 5.3 to use the deflagration index as a classification factor. However, if the assumptions taken for this law were revised (homogeneous and quiescent gas mixture, point ignition source, laminar spherical flame shells, perfect insulation, identical burning velocities (Eckhoff, 1984)), the applicability of the cubic law appears to be very restricted. Such an index has several inherent assumptions and limitations, and many of its requirements should be met to apply it to mist explosions. Nonetheless, it is still considered a universal characteristic that allows the comparison of the relative explosivity hazards and their violence (NFPA 68, 2018), and some professionals use it to quantify the explosion severity of liquid aerosols (Yuan et al., 2019). It is then of interest to

classify the tested liquid into four mist deflagration classes (Table V- 15) as a function of their calculated deflagration index K_M, similar to what was done in the case of dust deflagration classification.

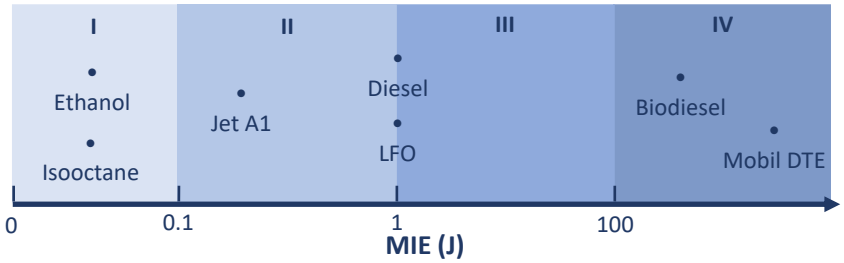

Figure V-16: Classification of the seven fuels into four MIE groups

Table V-15: The dust deflagration classification and the newly-proposed mist deflagration classification

Dust deflagration classes		**Mist deflagration classes**	
St class	**K_{st} (bar.m.s^{-1})**	**M class**	**K_M (bar.m.s^{-1})**
St-0	0 (non-explosible)	M-0	0 (non-explosible)
St-1	$1 < K_{st} \leq 200$	M-1	$1 < K_M \leq 50$
St-2	$200 < K_{st} \leq 300$	M-2	$50 < K_M \leq 150$
St-3	$K_{st} > 300$	M-3	$K_M > 150$

Still, it will not be sufficient to classify the tested fuels according to their MIE and K_M. For example, misestimations can take place due to changes in the turbulence level. It was also observed that the volatility and the DSD explained discrepancies from one fuel to another tested under the same conditions. A liquid classification system based on all the parameters mentioned will be established at the end of this manuscript, providing a fundamental basis to propose a standard covering many situations.

It should be kept in mind that standards are essential, but they should not be viewed as an absolute or unchangeable value or a precise representation of the industrial settings where explosions might arise. In order to be capable of determining the consequences of explosion scenarios, an intrinsic parameter must be established because possible deviations can occur with the cubic law as the flame thickness is non-negligible. Therefore, it is of interest to study the flame propagation in a mist cloud to understand the influence of radiative phenomena, stretching, and other phenomena that might occur and eventually determine the inherent laminar burning velocity…

Summary

After establishing a standard test procedure, the seven chosen fluids underwent a parametric analysis in which the impact of various parameters was assessed. This chapter offered insightful information on how mist clouds behave under different circumstances.

The ignition sensitivity was explored in the first section by calculating the MIE, LEL, and LOC. It was observed that the seven fluids could be divided into four MIE groups. With an MIE lower than 100 mJ, ethanol and isooctane were the easiest to ignite. Kerosene Jet A1, diesel and LFO showed intermediary behaviour, depending on their ageing and storing conditions, but the three fuels exhibited ignition with MIEs less than 1 J. Finally, with MIEs higher or equal to than 5 kJ, biodiesel and Mobil DTE were the hardest to ignite. Mobil DTE has not exhibited any ignition until now. Nevertheless, slightly preheating the liquids and the explosion vessel facilitated the ignition of the other fluids.

Concerning the risk of forming an explosive atmosphere, it was seen that, in the majority of cases, it might be more conservatory to consider the LEL of the fuel's vapours as a reference to evaluate the extent of a hazardous zone. However, some fuels that are supposed to unlikely form an explosive atmosphere, such as biodiesel, ignited with an LEL of 103 $g.m^{-3}$. Therefore, evaluating the LEL of mists in all cases is interesting. The LOC was an additional parameter evaluated for ethanol and Jet A1 mist clouds. The results showed that the LOC of Jet A1 mists, produced with nozzle set N1, was 15.8 $\%_{v/v}$ for 144 $g.m^{-3}$. In comparison, ethanol mists have a LOC of 13.1 $\%_{v/v}$ for 110 $g.m^{-3}$.

Using concrete examples, the remainder of this chapter covered in depth how the chemical nature of the fluids, the initial temperature, the droplet size distribution and turbulence of the mist cloud, the ignition energy, the vapour content, and the presence of flammable gases all affect the ignition and explosion process. It was first observed that for most of the fuels, concentration-dependent severity curves were obtained that showed a plateau from a certain concentration onwards, showing that it is not possible at present with this type of apparatus to determine the upper explosion limit (UEL) due to the probable recirculation of the injected mist. Moreover, the chemical nature of the fuels had a significant effect on explosivity measurements, directing toward a classification based on the deflagration index of the seven fuels into four deflagration classes (M-0: K_M $(bar.m.s^{-1})$ = 0 non-explosible, M-1: $1 < K_M (bar.m.s^{-1}) \leq 50$, M-2: $50 < K_M (bar.m.s^{-1}) \leq 150$, and M-3: K_M $(bar.m.s^{-1}) > 150$).

The influence of the DSD was subsequently studied. It appeared that the explosion severity, as well as the ignition sensitivity, decreased with increasing droplet diameters. The rate of pressure rise was the most impacted, demonstrating how the dynamics of the mist flow could readily affect

the reaction kinetics. The initial temperature also modified the explosion severity to a certain extent. In fact, its impact on the explosion overpressure diminished with rising temperatures higher than the flashpoint. Nonetheless, a more significant influence continued to occur on the rate of pressure rise. In addition to preheating the sphere, the liquid was preheated to assess the influence of an eventual temperature drop during the mist injection or any change in the liquid's physicochemical properties with the temperature change. A minimal influence was observed from preheating the liquid. The impact of the level of turbulence was also evaluated by increasing the ignition delay time up to 500 ms and by increasing the air injection pressure. It was seen that, in the case of diesel, both thermo-kinetic parameters tended to decrease as t_v increased until reaching a time where no explosion occurred (t_v = 400 ms). This behaviour was linked to the droplets' sedimentation, decreasing the mist concentration in the vicinity of the ignition source. An increase in the injection pressure shifted isooctane, ethanol, and Jet A1 explosivity curves to the left while having inverse effects on LFO and diesel. Increasing the turbulence in this manner might create more uncertainties and fluctuations.

Further on, by comparing chemical ignitors with ignition energies of 100 J and 5 kJ, the impact of the ignition energy on the explosion severity was evaluated. It was observed that raising the energy to 5000 J resulted in equal or lower severity parameters for fuel mists that had already ignited at 100 J. It was attributed to the strong turbulence of the 5-kJ ignitors, which most certainly changed the concentration distribution in the mist cloud. Nevertheless, no ignition took place while utilising 100 J as opposed to 5 kJ in the case of biodiesel, for instance. This suggested that the ignition energy must indeed be increased in cases where there was no ignition at 100 J.

Other contributing factors, such as the amount of vapour and the presence of flammable gas, were also investigated and significantly influenced the explosion severity. Therefore, it is essential to guarantee a tightly controlled environment when conducting such experiments. All the experiments in this chapter were performed in a single apparatus, the 20 L sphere. This chapter is the core of this study as it shows the high versatility of the 20 L sphere. Finally, it has allowed a better understanding of the factors influencing the phenomenology of the mists in a closed explosion chamber with various injection conditions.

Résumé

Après avoir établi une procédure d'essai standard, les sept fluides choisis ont fait l'objet d'une analyse paramétrique dans laquelle l'influence de divers paramètres a été évalué. Ce chapitre fournit des informations utiles sur le comportement des nuages de brouillard sous différentes conditions.

La sensibilité à l'inflammation a été explorée dans une première partie en évaluant l'EMI, la LIE et la CLO. Sur cette base, les sept fluides testés ont pu être divisés en quatre groupes d'EMI. Avec une EMI inférieure à 100 mJ, l'éthanol et l'isooctane étaient les plus faciles à enflammer. Le kérosène Jet A1, le diesel et le LFO ont montré un comportement intermédiaire, dépendant de leurs conditions de vieillissement et de stockage. Ces trois hydrocarbures ont présenté une inflammation avec des EMI inférieures ou égales à 100 J. Enfin, avec des EMI supérieures ou égales à 5000 J, le biodiesel et Mobil DTE étaient les plus difficiles à enflammer. Le Mobil DTE n'a pas présenté d'inflammation dans les conditions d'essai. Néanmoins, un léger préchauffage des liquides et du récipient d'explosion facilite l'inflammation des autres fluides.

En ce qui concerne le risque de formation d'une atmosphère explosive, il a été constaté que, dans la majorité des cas, il est plus prudent de considérer la LIE des vapeurs du combustible comme une référence afin d'évaluer l'étendue d'une zone dangereuse. Cependant, certains carburants considérés comme non susceptibles de former une atmosphère explosible, comme le biodiesel, se sont enflammés sous forme de brouillard avec une LIE de 103 $g.m^{-3}$. Il est donc intéressant d'évaluer la LIE d'un brouillard dans tous les cas. La CLO d'un brouilard de Jet A1 a été également évaluée. Les résultats ont montré que la CLO des brouillards de Jet A1, produits avec le jeu de buses N1, était de 15,8 $\%_{v/v}$ obtenue à une concentration optimale de 144 $g.m^{-3}$. En comparaison, les brouillards d'éthanol ont un CLO de 13,1 $\%_{v/v}$ obtenue à une concentration optimale de brouillard de 110 $g.m^{-3}$.

En considérant des exemples concrets, la suite de ce chapitre a permis d'étudier en profondeur comment la nature chimique des fluides, la température initiale, la distribution granulométrique et la turbulence du nuage de brouillard, l'énergie d'inflammation, la teneur en vapeur et la présence de gaz inflammables influencent le processus d'inflammation et d'explosion. Il a été d'abord observé que pour la plupart des combustibles, on obtenait des courbes de sévérité en fonction de la concentration qui présentait un plateau à partir d'une certaine concentration, ce qui montre qu'il n'est pas possible à l'heure actuelle, avec ce type d'appareillage, de déterminer la limite supérieure d'explosion (LSE) en raison de la probable recirculation du brouillard injecté. De plus, la nature chimique des combustibles a un effet significatif sur les mesures d'explosivité, orientant vers une classification basée sur un indice de déflagration normalisé des sept

combustibles en quatre classes de déflagration (M-0 : K_M (bar.m.s^{-1}) = 0 non-explosible, M-1 : 1 < K_M (bar.m.s^{-1}) ≤ 50, M-2 : 50 < K_M (bar.m.s^{-1}) ≤ 150, et M-3 : K_M (bar.m.s^{-1}) > 150).

L'influence de la distribution granulométrique a ensuite été étudiée. Il est apparu que la sévérité de l'explosion, ainsi que la sensibilité à l'inflammation, diminuaient avec l'augmentation du diamètre des gouttelettes. La vitesse de montée en pression a été la plus affectée, démontrant la manière dont la dynamique de l'écoulement du brouillard pouvait affecter la cinétique de la réaction. La température initiale a également modifié la sévérité de l'explosion dans une certaine mesure mais l'influence de la température sur la surpression d'explosion, au-delà du point d'éclair, tend à être relativement faible tandis qu'elle reste importante sur la vitesse de montée en pression. En plus du préchauffage de la sphère, le liquide a été préchauffé afin d'évaluer l'influence d'une éventuelle chute de température pendant l'injection du brouillard ou de tout changement des propriétés physico-chimiques du liquide avec le changement de température. Une influence minime a été observée du fait du préchauffage du liquide. L'impact du niveau de turbulence a également été évalué en augmentant le délai d'inflammation jusqu'à 500 ms et en augmentant la pression d'injection d'air. Il a été constaté que, dans le cas du diesel, la sévérité d'explosion tend à diminuer lorsque t_v augmente jusqu'à un t_v critique à partir duquel aucune explosion ne se produit (t_v = 400 ms). Ce comportement est lié à la sédimentation des gouttelettes, diminuant la concentration de brouillard à proximité de la source d'allumage. Une augmentation de la pression d'injection a déplacé les courbes d'explosivité de l'isooctane, de l'éthanol et du Jet A1 vers des concentrations plus importantes, tout en ayant des effets inverses sur le LFO et le diesel. Augmenter la turbulence de cette manière pourrait créer plus d'incertitudes et de fluctuations de turbulence.

Par la suite, en comparant des inflammateurs chimiques avec des énergies d'inflammation de 100 J et 5 kJ, l'impact de l'énergie d'inflammation sur la sévérité de l'explosion a été évalué. Il a été observé que l'augmentation de l'énergie à 5 kJ entraîne une sévérité d'explosion égale ou inférieure pour les brouillards de carburant qui s'enflamment à 100 J. Cela peut être attribué à la forte turbulence induite par des inflammateurs de 5 kJ, qui modifient très certainement la distribution de la concentration dans le nuage de brouillard. Néanmoins, aucune inflammation n'a eu lieu en utilisant 100 J par rapport à 5 kJ dans le cas du biodiesel, par exemple. Ceci suggère que l'énergie d'inflammation doit effectivement être augmentée dans les cas où il n'y a pas eu d'allumage à 100 J.

D'autres facteurs contributifs, tels que la quantité de vapeur et la présence de gaz inflammable, ont également été étudiés et ont influencé de manière significative la sévérité de l'explosion. Par conséquent, il est essentiel de garantir un environnement étroitement contrôlé lors de la réalisation de tels essais. Tous les essais de ce chapitre ont été réalisées dans un seul appareil, la

sphère de 20 litres. Ce chapitre constitue le cœur de cette étude et montre la grande polyvalence de la sphère de 20 L. Enfin, il a permis de mieux comprendre les facteurs d'influence sur la phénoménologie des brouillards en enceinte d'explosion fermée, avec des conditions d'injection diverses.

Chapter VI:

From flame speed to burning speed

With the limitations of the cubic law, professionals search for alternative ways to extrapolate explosion severity measurements to an industrial scale. The laminar burning velocity is an inherent parameter that could contribute to the assessment of the consequences of a mist explosion under specific conditions, particularly in the case of complex industrial geometries. The measurement of flame speeds and burning velocities has been extensively approached for hydrocarbon fuels, especially for combustion engines. Although the main focus of this study is the proposition of a complete procedure in a single apparatus, understanding the phenomenology of mist explosions and taking it a step further is pertinent. This chapter comprises group combustion discussions, flame propagation studies, and evaporation and combustion models. Even if these additional tests are not an end in themselves, they will help better understand the results and trends obtained in the previous sections.

6.1. One-by-one or together?

A short story about group combustion

In order to represent the relative tendencies of a mist cloud for either going through single droplet combustion or group combustion, the group combustion theory will be applied to average estimations of mist cloud characteristics. This theory was discussed in Subsection 2.4.4 and is based on calculating a group number, denoted G, expressed in equation II-13. G can be regarded as "strictly geometrical" as it does not incorporate the heat transfer rate and the evaporation of droplets. Nevertheless, trends are believed to still hold with increasing or decreasing G values (Law, 2006).

Figure VI-1 illustrates the total number of droplets N as a function of a non-dimensional droplet separation factor, denoted S (equation VI-1). As seen in the figure, it is divided into the four combustion regimes discussed earlier in the manuscript and which are separated according to the group number G by transition bands.

$$S = \left(\frac{0.05}{1 + 0.276 Re^{\frac{1}{2}} Pr^{\frac{1}{3}}}\right)\left(\frac{s_D}{r}\right) \qquad \text{VI-1}$$

Where Re is the Reynolds number of a droplet, Pr is the Prandtl number $\left(Pr = \frac{C_p \mu}{k}\right)$, r is the mean droplet radius, s_D is the inter-droplet distance, and N is the number of droplets inside the cloud.

A monomodal mist cloud was assumed to calculate the required parameters. Although it is not the case, and sedimentation, coalescence, and fluctuations will affect the DSD, it will give an estimation of the order of magnitude. The number of droplets was estimated by dividing the total liquid volume by a single droplet's volume. The inter-droplet distance, s_D, was estimated using equation VI-2 (Moesl, 2012). The Reynolds and Prandtl numbers were estimated from both

experimental measurements and theoretical physicochemical properties (PIV in subsection 4.1.3, properties in Table III-2). As for the droplet's radius, calculations were performed for a range of mean droplet diameters determined experimentally.

$$S = \frac{L_s}{(N)^{\frac{1}{3}}} \qquad \text{VI-2}$$

Where L_s is the size of a spherical droplet cloud (taken equal to the 20 L sphere volume, supposing a homogeneously distributed cloud).

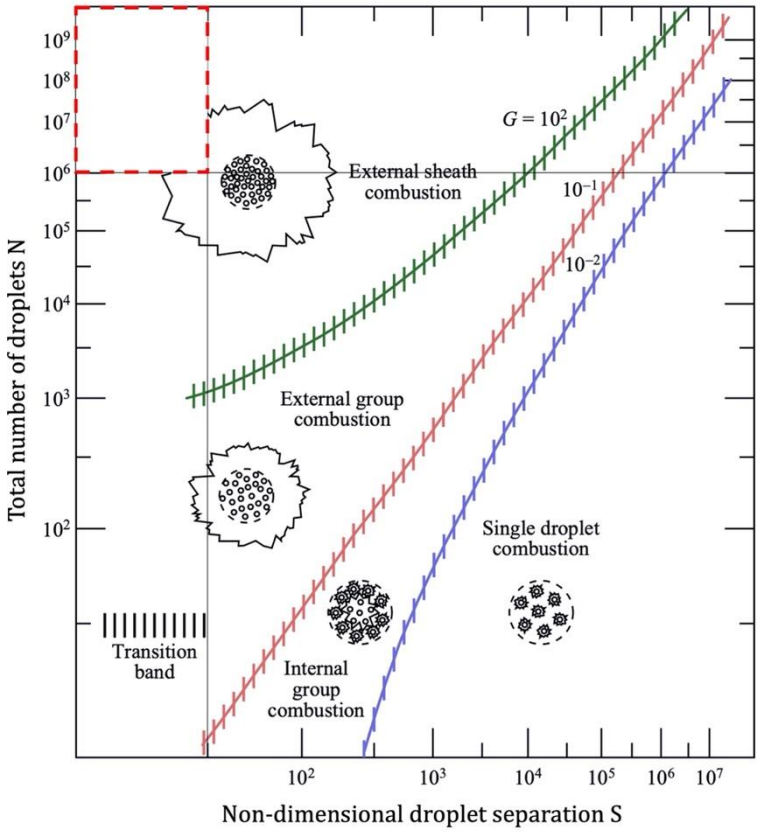

Figure VI-1: Group combustion modes for a droplet cloud - adapted from Chiu et al. (1982) and Moesl (2012)

Based on the mist generation system, calculations showed that the number of droplets could reach up to 10^{11}. As for the non-dimensional droplet separation factor, S, a maximum of about 0.1 was attained at the turbulence levels reached in this study and the physicochemical properties of the liquids. When a high percentage of sedimentation and coalescence is supposed, the inter-droplet distance might increase with an increase in droplet diameter, as seen in Subsection 4.1.2.4. *S* was therefore assumed not to exceed 50, and the number of droplets descends to 10^6. Under different configurations, the combustion of the mist cloud inside the 20 L sphere will maintain an ***external sheath combustion regime***. In such a regime, a dense spray zone would not burn with individual flames, as indicated in a classical theory of single droplet combustion. Instead, the droplets in the cloud evaporate in the dense spray zone, and the resulting fuel vapour

is carried radially outward, mixes with air, and burns with a global envelope flame that surrounds all the droplets in the cloud or dense spray region.

Due to the high density of the mist cloud, droplet clustering can take place, leading to a substantial increase in local concentrations and reducing the inter-droplet distance to a point where interaction between nearby droplets averts oxygen from penetrating. As a result, the cloud is considered a fuel-rich mixture which burns as a group. The following section will enable us to experimentally visualise the combustion of a mist cloud.

It should be noted that a multidisciplinary approach is required to fully comprehend the complex phenomenological aspects involved in the vapour-liquid explosion processes. Indeed, fluid dynamics, chemical kinetics, and mass and heat transfer are all dimensions that should be considered. If we were to include two main components to consider in the investigation of explosion processes, the rate of explosion pressure rise and the flame propagation are pertinent elements that cover all mentioned dimensions.

6.2. Flame propagation study

As explained in Section 3.9, the flame propagation was visualised in a 1-meter-long upward flame propagation tube with a square cross-section of 7 cm^2. The propagations were recorded using a high-speed video camera (MotionBLITZ EoSens®) with a frame rate of 3000 fps and 331 µs of exposure time. Moreover, as the growth of the flame kernel is limited by the tube's walls, tests were complemented by explosions in a 20 L vented sphere, providing a larger volume for the development of the flame kernel. Both configurations are discussed in this section, as well as the different operating conditions employed.

After ignition, the recorded videos underwent post-treatment using the MATLAB Image Processing Toolbox to allow better visualisation of the flame's growth and profile. The analysis of each video allowed determining the flame front's position z, which was derived in order to determine the spatial velocity S_s at instant t. Depending on the shape of the flame kernel's growth, its estimated surface area $\left(A_f = \frac{dz(t)}{dt}\right)$ and cross-section area, A_s, were also calculated. This eventually allowed determining the burning velocity, S_u, which depends on S_s, A_s, and A_f (see equation VI-3). The equation linking these parameters is valid if the following constraints are met: the flame thickness is small relative to the flame's curvature, S_s is uniform, and S_u is constant over the whole flame's surface (Andrews and Bradley, 1972).

$$S_u = S_s \frac{A_s}{A_f} \qquad \text{VI-3}$$

In general, in order to take into account the thermal expansion of the gases that could take place

near the vessel walls as the flame passes, a correction factor, χ, is added to equation VI-3 (Halter, 2005). χ is expressed as the ratio between the densities of the unburnt and burnt gases and can be estimated by calculating the ratio of the burnt gases' temperature (usually considered equal to the adiabatic temperature corresponding to a specific fuel equivalence ratio) and that of the fresh unburnt gases. This correction factor is usually unknown for mixtures containing liquid, as in our case, especially due to the supplementary evaporation phase and droplet-droplet interactions ahead of the flame, causing hydrodynamic instabilities. Such variabilities generally exist in all propagating flames. Nevertheless, as the volume increase of the flame kernel is already considered and the studied flame does not touch the vessel's walls and undergoes minimal thrust from the hot gases, this factor was first disregarded for this study.

As the flame propagates, several factors can contribute to its deformation (either by stretching or modification of its curvature). It is certainly influenced by the level of turbulence, and the chemical reactions could be modified. The Karlovitz flame stretching factor (see equation VI-4) was hence considered and is expressed as the time variation of the flame's surface area:

$$K = \frac{1}{A_f(t)} \frac{dA_f(t)}{dt} \qquad \text{VI-4}$$

For this study, flame stretching will be considered as one phenomenon and will not be decoupled into K_c and K_s (Bradley, 2000). If $K > 0$, this indicates an expansion, while the contrary signifies a compression.

As mentioned before, stretching of the reactive zones can lead to a variation in the laminar burning velocity or cause local extinctions. Clavin (1985) and Markstein (1964) have, therefore, proposed an equation that links the burning velocity to the flame stretching factor K and the unstretched burning velocity S_u^0 (equation VI-5).

$$S_u = -\delta_M K + S_u^0 \qquad \text{VI-5}$$

Where δ_M is the Markstein length. If δ_M is positive, an increase in stretching leads to decrease in the flame propagation speed. On the contrary, a negative Markstein number means that stretching increases the flame propagation speed, and therefore the flame becomes unstable.

It should be noted that equation VI-5 is only valid if the Karlovitz factor is low, meaning that the flame is weakly stretched and for a Lewis number close to unity. With a higher Karlovitz factor, this linear relation starts to lose its validity. It can also overestimate the Markstein length leading to errors of S_u^0 that can reach about 10% (Halter et al., 2010). A non-linear relation was therefore adopted by many authors (Santandrea, 2020) (equation VI-6).

$$\left(\frac{S_u}{S_u^0}\right)^2 . \ln\left(\frac{S_u}{S_u^0}\right)^2 = -\frac{2\delta_M K}{S_u^0} \qquad \text{VI-6}$$

Another point to consider is the fact that such relations were first developed for gaseous mixtures, notably for flat flames. Nevertheless, for idealised cases, such procedures can estimate the laminar burning velocity. Indeed, a mist cloud can be considered a homogeneous biphasic gas-liquid mixture, and the main limitation would be the level of turbulence.

6.2.1. Flame propagation tube

Although it is ideally preferred to test flame propagations in a quiescent environment, the mist generation system employed for this study does not function well at very low injection pressures (< 2 bar). Moreover, the sedimentation phenomenon cannot be neglected unless in microgravity conditions. Preliminary flame propagation tests were, hence, performed in the flame propagation tube in order to visualise a mist ignition, estimate the burning velocity, and eventually determine a laminar unstretched burning velocity when feasible.

One might speculate, how does a flame propagate through a turbulent mist? Will it expand spherically? Does it deform? And do droplets burn individually or as a group? As it can be seen, regarding the shape of the flame, Figures VI-2 and VI-3 present two different flame fronts. A spherical and smooth flame kernel was created for an ethanol mist ignited using 3-J spark ignition, as seen in Figure VI-2. Recordings from a few milliseconds after ignition (to avoid spark influence) to just before wall influence (10-15 ms) were analysed. Spherical growth shows a steady premixed environment with stable properties. The flame was then slightly stretched as of 9 ms and propagated in an elliptical shape, which can be caused due to the presence of the tube's walls and the gases pushing the flame. Isooctane mist was generated under the same conditions but was then flushed with one-second air injection to dilute the mixture and make it more turbulent. The initiation of the flame kernel was, therefore, less smooth with the creation of a wrinkly flame front and a cluster- or cellular-like surface (Figure VI-3). This can be explained by the action of turbulent eddies and the stronger interaction between the flame and vortices. Moreover, the "leaner" mixture ahead of the flame may have caused the creation of flame clusters reaching out towards the mixture. A final possibility is the presence of liquid droplets ahead of the flame, inducing a more pronounced cellular intensity than that of the ethanol-air mixture. The mist was, indeed, generated using nozzle set N', which may have produced droplets of different sizes. Therefore, a series of experiments will be carried out using nozzle set N1, allowing the generation of a more homogeneous and uniform mist cloud.

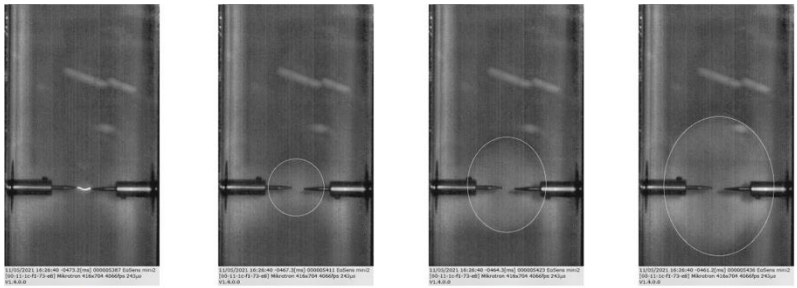

Figure VI-2: Time evolution of the flame propagation in an ethanol mist ignited by a 3 J spark ignition at t_v = 120 ms (Nozzle set N')

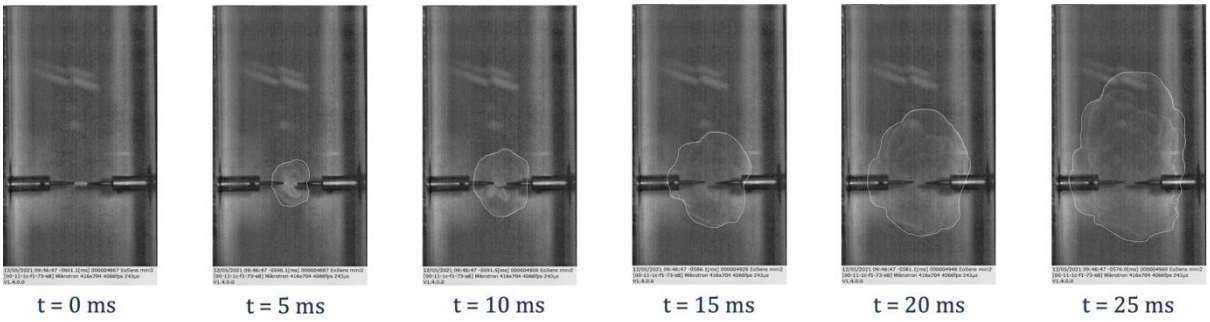

Figure VI-3: Time evolution of the flame propagation in an isooctane mist ignited by a 3 J spark ignition at t_v = 120 ms (Nozzle set N')

The aforementioned series of experiments were performed on ethanol, isooctane, and Jet A1 to evaluate the influence of the chemical nature, the DSD, the ignition energy, and the concentration on the flame propagation in the tube. It should be noted that flame wrinkling was rarely observed in this series of experiments as the generated droplets were relatively small (not exceeding 13 µm).

The flame front's position, *z*, was first determined, leading to the calculation of the spatial velocity. The experimental results were fitted using the "*smoothingspline*" function on MATLAB and were then used to estimate the burning velocity as a function of the Karlovitz factor.

Figure VI-4 shows the evolution of the flame front's position and spatial velocity of ethanol mist injected during 9 s into the flame propagation tube. As the latter is a semi-open vessel, it was not possible to indicate the exact mist concentration. Therefore, the injected quantity will be represented by its mass or the corresponding injection time. In ethanol's case, about 2.1 g were injected. The mist was ignited in turbulent conditions with an ignition delay of 3 ms to maintain close conditions to those used in the explosion sphere. It should be noted that, for most cases, the first few milliseconds after spark actuation were hard to analyse due to the small analysis window

and the influence of the spark ignition. Analysis was stopped when the propagating flame touched the tube's walls (25-40 ms for isooctane, 11-16 ms for ethanol, 18-45 ms for Jet A1).

As shown in Figure VI-4(b), varying the ignition energy between 25 J and 100 J had a slight influence on the spatial velocity, which faintly increased with decreasing energies. This can be explained by the possible destabilisation of the flame with longer spark durations. An energy of 100 J was therefore chosen to ensure the ignition of most mist clouds in the tube.

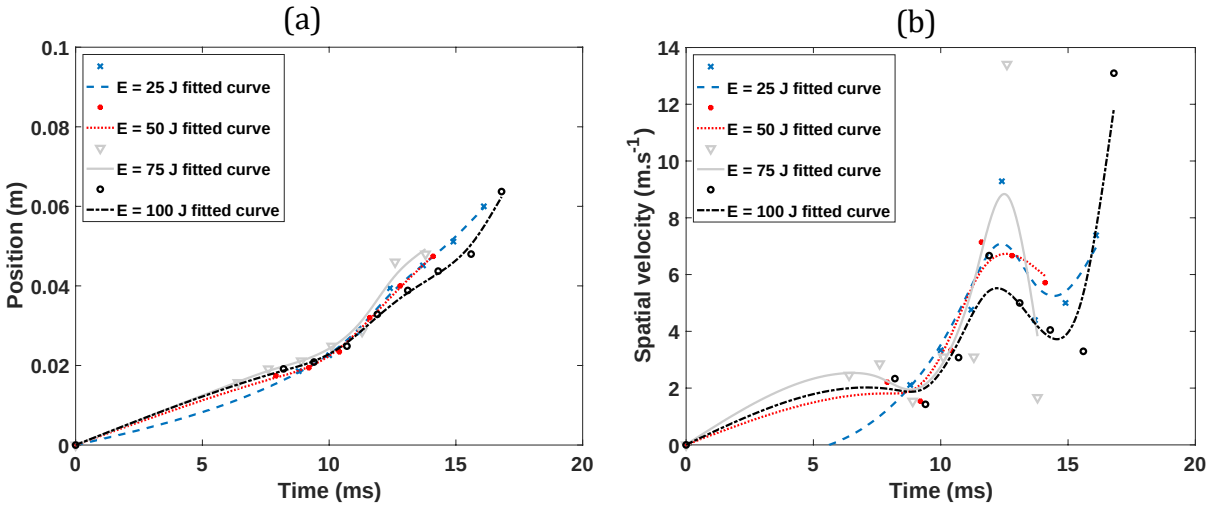

Figure VI-4: Time evolution of the flame front's (a) position and (b) spatial velocity of ethanol mist generated during t_{inj} = 9 s and ignited after t_v = 3 ms for four ignition energies

The unstretched burning velocity was determined from the linear extrapolation of the non-linear relation shown in equation VI-6 by tracing $\ln(S_u)$ as a function of K/S_u^2. The use of the linear relation (equation VI-5) was seen very far from experimental findings as it poses many requirements. Table VI-1 displays the values of S_u^0 for ethanol mist as a function of the ignition energy. As it can be seen, a slight decrease in S_u^0, from about 119 cm.s^{-1} to about 103 cm.s^{-1}, was observed as the ignition energy was increased from 25 J to 100 J, respectively.

When compared with literature, the unstretched burning velocities or the laminar burning velocities of ethanol vapours do not exceed 45 cm.s^{-1} or 50 cm.s^{-1} (Liao et al., 2007; Thimothée, 2017) at T = 358 K. On the other hand, current findings are about double the expected value and even more. Indeed, a decrease in flame propagation speed is expected when compared to a premixed environment because the characteristic evaporation time of a fuel droplet is generally larger than the characteristic chemical time scale of combustion. Nevertheless, Thimothée (2017) differentiated the laminar burning velocity and S_u^0 and obtained values between 90 cm.s^{-1} and 250 cm.s^{-1} in biphasic ethanol-air mixtures.

Several explanations can clarify these discrepancies. First, the high turbulence, which may lead to the cellular structure of the biphasic flame, as seen in Figure VI-3, increases the surface of the

flame and, consequently, the propagation speed. Indeed, acceleration of the flame can be caused by the creation of cells on a spherically expanding flame (Wu et al., 2013). Additional causes are, however, needed because not all flames exhibited the creation of cellular structures, except in the case of unclarity of the flame propagation videos. The presence of droplets ahead of the flame front may be a plausible cause as the evaporation of these droplets induces an enrichment in the local surrounding medium, causing the flame to propagate more rapidly as a whole. In general, if the droplets are small enough to create a homogeneous gaseous medium, comparable results must be found to those measured for gaseous mixtures. Nevertheless, the turbulence level should not be neglected. Although it is believed that when we remove the effect of stretching, the unstretched burning velocity is equal to the laminar burning velocity as the influence of turbulence is eliminated, one should not neglect that turbulence might affect reaction and mixing rates, droplet trajectories, and ignition delay times. In order to identify the laminar burning velocity, experiments should therefore be performed at much lower turbulence levels by increasing the ignition delay time to correspond to low v_{rms}. Until now, this was not feasible without having additional effects of sedimentation and change in the local mist concentration.

Table VI-1: Influence of the ignition energy on the unstretched burning velocity of about 2.1 g of ethanol mist ignited using 100 J spark ignition in the flame propagation tube

Fluid	Ignition energy (J)	S_u^0 (cm.s^{-1})
Ethanol	25	118.6
	50	106
	75	106.3
	100	102.8

For an injection duration of 8 s, corresponding to about 2 g of product, ethanol, isooctane, and Jet A1 were tested under the same conditions (unchanged ignition energy of 100 J). Figure VI-5 compares the position and the spatial velocity of the three fluids. A noticeable observation is the slower flame propagation of isooctane which is in agreement with the literature (Takashi and Kimitoshi, 2006; van Lipzig et al., 2011), even in the case of S_u^0 (see Table VI-2). Three factors can contribute to this phenomenon. First, the propagation speed can be linked to the oxygen content of the fuel, which is higher in the case of ethanol, and Jet A1 also contains trace amounts of oxygen. Second, radiative effects can accelerate flame propagation. Indeed, ethanol and Jet A1 flames were radiant, while isooctane flames were more “translucent”. Myers and Lefebvre (1986) shed light on this matter, stating that fuels that have a higher aromatic content tend to burn more brightly,

which affects the burning velocity. Finally, two grams of isooctane in the tube (if it were confined) correspond to a very rich fuel mixture with a fuel equivalence ratio of about 6. If we take a look back to Subsection 5.6.2, we can see that the rate of pressure rise was easily affected when the fuel-air mixture was rich (affecting the Lewis number) and exhibited weaker explosions than ethanol and Jet A1 as the nominal mist concentration increased.

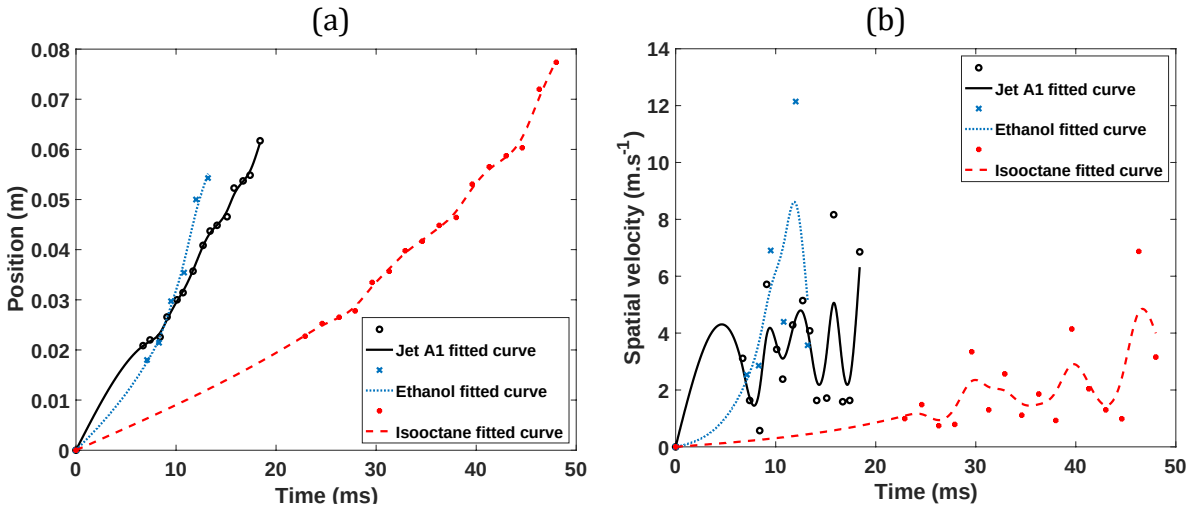

Figure VI-5: Time evolution of the flame front's (a) position and (b) spatial velocity of Jet A1, ethanol and isooctane mist generated during t_{inj} = 8 s and ignited after t_v = 3 ms – 100 J spark ignition – nozzle set N1

Table VI-2: Influence of the chemical nature on the unstretched burning velocity of about 2 g of injected mist into the flame propagation tube

Fluid	**S_u^0 (cm.s^{-1})**
Ethanol	123
Isooctane	86.1
Jet A1	108.7

Additional experiments were performed to determine the influence of the DSD on the flame propagation of ethanol and Jet A1 mist clouds. As seen in Figure VI-6, mist generation using nozzle set N2 (i.e., larger droplets) hinders the flame propagation in a Jet A1 mist as it took about 45 ms to reach the tube's walls, whereas, in the case of N1 (i.e., finer droplets), 20 ms were sufficient to reach them. Also, the unstretched burning velocity decreased from 175.7 cm.s^{-1} to 78 cm.s^{-1} for nozzle sets N1 and N2, respectively. The contrary was observed for ethanol mist clouds (see Figure VI-7), as the increase of the droplet diameter accelerated the flame propagation and increased S_u^0 from 140 cm.s^{-1} to 205.9 cm.s^{-1}.

When reflecting on the bases of diphasic flame propagation, previous studies have proven that

droplet evaporation determines the flame characteristics of an aerosol combustion (Hayashi et al., 1977; Maragkos and Bowen, 2002). As the droplet size decreases, the proportion of fuel vapour increases, and the flame propagation speed approaches that of a vapour, which is theoretically a higher value. Consequently, the amount of fuel delivered by the droplets to sustain combustion is determined by the evaporation of the droplets moving towards the flame and probably increasing the burning rate. Furthermore, seen that droplet evaporation is linked to the size of droplets, flame propagation becomes sensitive to the latter. This was observed in the case of Jet A1 mist in the flame propagation tube and the 20 L explosion sphere with an increase in flame velocity when the droplet diameters were decreased. This evolution is in agreement with findings obtained by Bowen and Cameron (1999), who stated that for droplet sizes larger than 30 µm, the burning velocity is inversely proportional to the mean droplet size in evaporation-controlled combustion.

In the case of ethanol, however, two hypotheses could be made to explain the different behaviour. Both configurations (nozzle sets N1 and N2) were on the fuel-rich side of the fuel-equivalence ratio. With a mist cloud of larger droplets, the inter-droplet distance is higher. Moreover, saturation may occur, meaning that not all liquid burns, leaving space for more oxygen to diffuse into the flame front. This phenomenon was observed by Nicoli et al. (2015), who studied flame propagation in rich sprays. A second hypothesis is that in order to generate the same amount of mist, injection durations for nozzle set N2 were shorter than in the case of nozzle set N1, meaning that the level of premixing and turbulence was different, which might have positively influenced the flame propagation speed. With this short preliminary study, none of the hypotheses can be either validated or rejected, and further examination is required. Nevertheless, the findings of Burgoyne (1963) should be reminded here. The authors stated that larger droplets increased the sedimentation speed and created longer “tails” to the surrounding diffusion flame, which enhanced the radiative heat transfer between droplets and improved flame propagation and flame stretching.

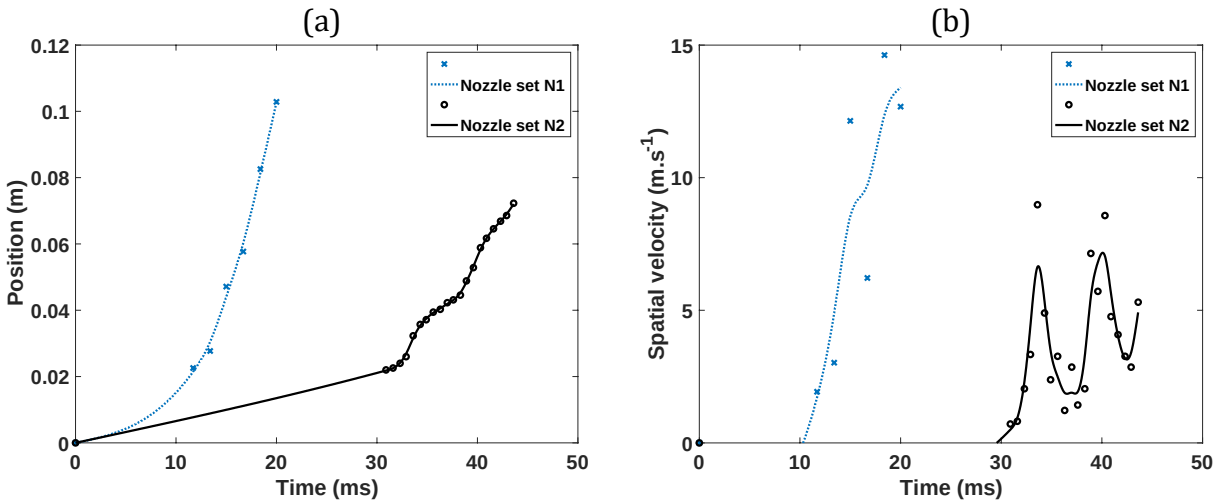

Figure VI-6: Time evolution of the flame front's (a) position and (b) spatial velocity of Jet A1 generated using nozzle set N1 and N2 and ignited after tv = 3 ms

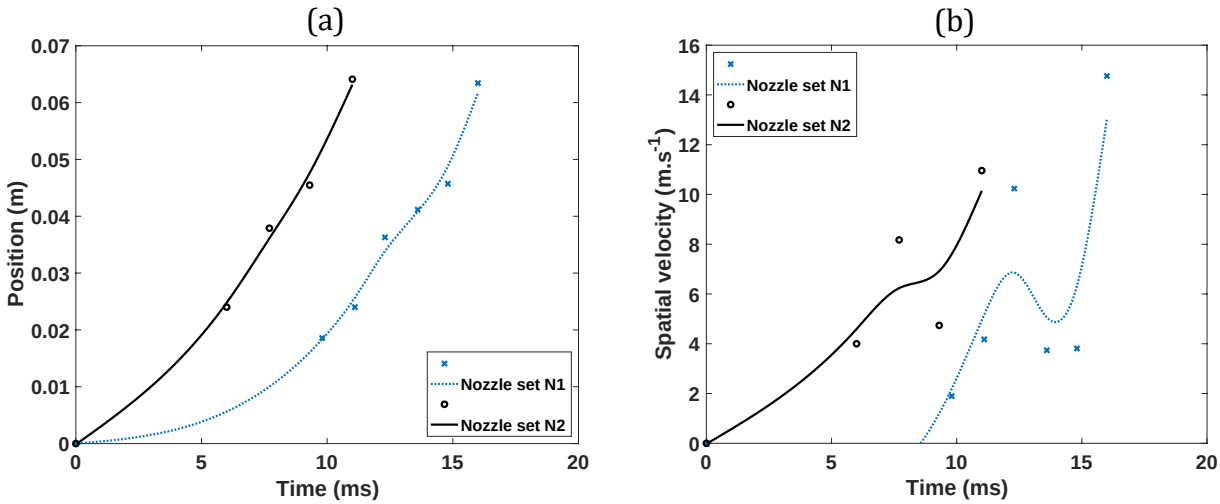

Figure VI-7: Time evolution of the flame front's (a) position and (b) spatial velocity of ethanol generated using nozzle set N1 and N2 and ignited after tv = 3 ms

An additional observation should be discussed for most of the presented findings: the oscillatory time evolution of the spatial velocity. As seen, it is recurrent in many of the performed experiments. This phenomenon can be explained as follows: with the increase of the flame's surface area, cooling (convection and radiation) becomes more significant, leading to more energy loss. The reactional volume hence decreases. Meanwhile, the amount of generated vapours is sufficient to restart burning.

6.2.2. 20 L vented sphere

Flame propagation measurements were complemented with ones performed inside the 20 L "open" sphere. This apparatus was chosen as it provides a larger observation time of the flame before being influenced by the walls' presence.

One of the windows was removed and replaced with two tungsten electrodes through which the KSEP permanent spark was generated. The latter was maintained at 100 J. Moreover, a pressure relief valve was placed on the top of the sphere to avoid any high overpressures that might break the windows. A second lateral window was equipped with a background of a colour complementary to the adiabatic flame colour of the tested fluid (e.g., a yellow background for a blue ethanol flame), and the high-speed video camera was facing it through a third window. A light source was also placed perpendicular to the camera's region of interest, illuminating the sphere's interior through the remaining fourth window. After several configurations, a frame rate of 5000 fps was found suitable as the flame propagation was significantly rapid, but sufficient lightening was needed to capture it. The shutter speed was 198 µs. The generated mist was distributed homogeneously in the pre-vacuumed sphere and then ignited just like a standard experimental sequence.

For this series of experiments, only ethanol and Jet A1 mist clouds were tested due to time constraints. The ignition delay, t_v, was first maintained at 3 ms to preserve the same turbulence level as that of the explosion sphere, but it was seen that due to the high turbulence of the cloud, video recordings were either unclear or too fast to treat as the efficient recording time was short. The t_v was hence increased to 300 ms for ethanol and 100 ms for Jet A1. A mist concentration of about 100 g.m^{-3} for both fuels, generated using nozzle set N1, was tested. Figure VI-8 (taken from behind protective Plexiglas glass) shows an explosion of the ethanol mist about 40 ms after ignition.

Figure VI-8: Ethanol mist explosion in the vented 20 L sphere

After the explosion, videos were retrieved, and their contrast was enhanced by applying CLAHE (contrast limited adaptive histogram equalisation) in order to better visualise the flame. Figure VI-9 depicts the time evolution of the flame profile each 4 ms after the actuation of the spark ignitors. The flame profile was contoured for more clarity. Nevertheless, the propagating flame exceeded the visualisation window after about 16 ms (red line). Measurements were therefore limited to the captured frames prior to this time.

Figure IV-10 presents the time evolution of the flame front's position, spatial velocity, and rate of surface change. As it can be seen, the increase of position *z* is rather linear, showing the absence of significant acceleration and a stable propagation speed through the various stages of flame growth. This validates the relevance of this approach and set-up as the rapid acceleration observed in the flame propagation tube was due to the close presence of the walls. This can also be seen in Figure VI-10(b), where the spatial velocity varied around a constant value of about 3.9 $m.s^{-1}$, aside from the first acceleration of the flame kernel. Such a phenomenon is common for stoichiometric gaseous mixtures where the velocity initially increases and then stabilises with the propagation of the flame (Zhang et al., 2019a). Flame wrinkling is evident in Figure VI-9 and is, as discussed before, linked to the high level of turbulence. However, a spherical flame growth was considered to calculate, using the procedure described in Section 6.2, an unstretched burning velocity of 108.1 $cm.s^{-1}$, which was lower than the S_u^0 measured in the tube for the same injected mass and ignition energy (123 $cm.s^{-1}$, see Table VI-2). This difference can be linked to several factors: the possible flame acceleration due to the closer walls in the tube, the vacuumed initial conditions, and the increased inter-droplet distance in the sphere.

Figure VI-11 depicts the time evolution of the flame profile of a 100 $g.m^{-3}$ Jet A1 mist cloud ignited at a t_v = 100 ms. As it can be seen at t = 3.1 ms, a flame kernel was formed. The kernel then attenuated, moved to another position, and split in two, as seen at t = 11.8 ms. This phenomenon invalidates the cubic law as no spherical propagation was observed. It also explains the presence of quenching with the splitting of the flame kernel and of a delayed ignition time, as observed in Section 5.8. Flame growth subsequently began, and a flame was established at t = 28.2 ms. A similar trend was observed by Lin et al. (2021), who studied the spark ignition and flame propagation of swirling spray flames of kerosene for aero-engine combustors. Nevertheless, the shape of the flame obtained in this study does not resemble a basic flame propagating through a premixed mixture, as seen in the previous cases. This is believed to be due to the local fast evaporation of the Jet A1 mist followed by instant burning. The mist cloud was very dense, meaning that the inter-droplet distance was much lower. This means that the combustion group number, G, is much higher than 100, implying that an external sheath combustion mode dominated the process, confirming the findings presented in Section 6.1. This led to the creation of a rich-fuel turbulent diffusion flame, the interior of which contains unburnt fuel.

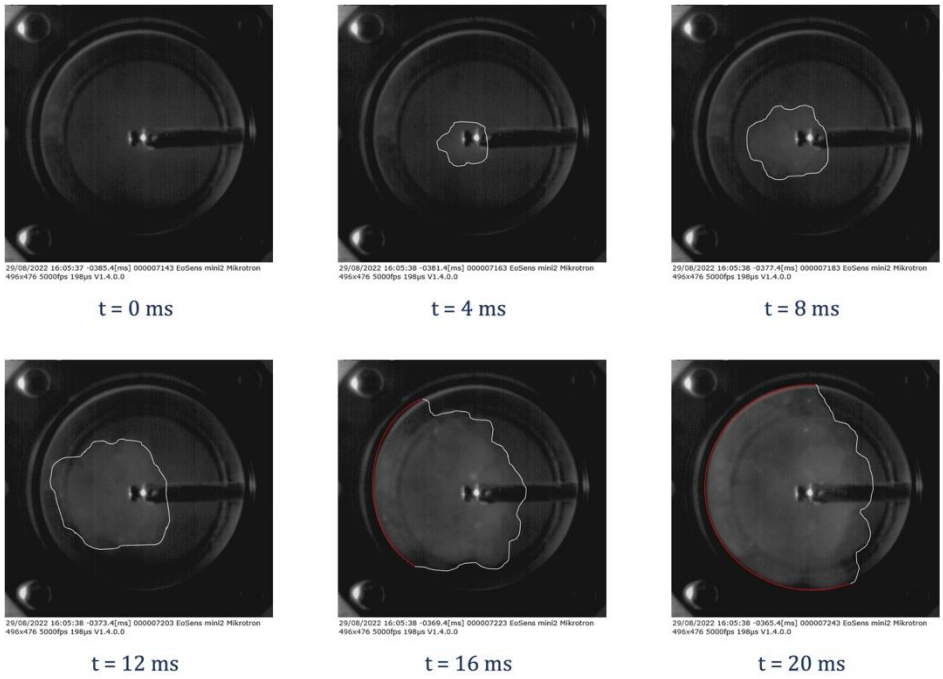

Figure VI-9: Time evolution of the flame profile of 100 g.m^{-3} ethanol mist in the 20 L vented sphere at t_v = 300 ms – 100 J spark ignition – nozzle set N1

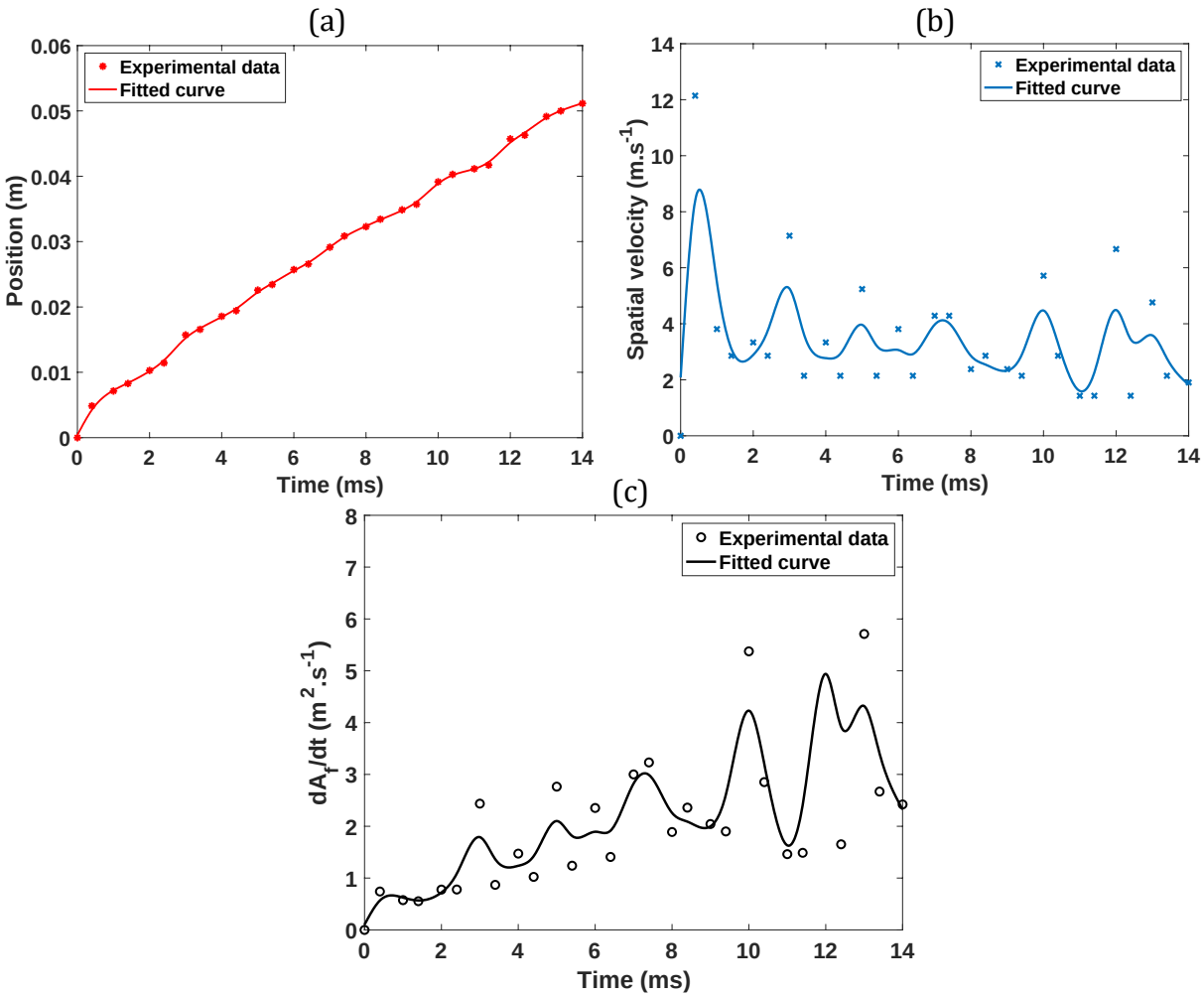

Figure VI-10: Time evolution of an ethanol flame's (a) position, (b) spatial velocity, and (c) rate of surface change

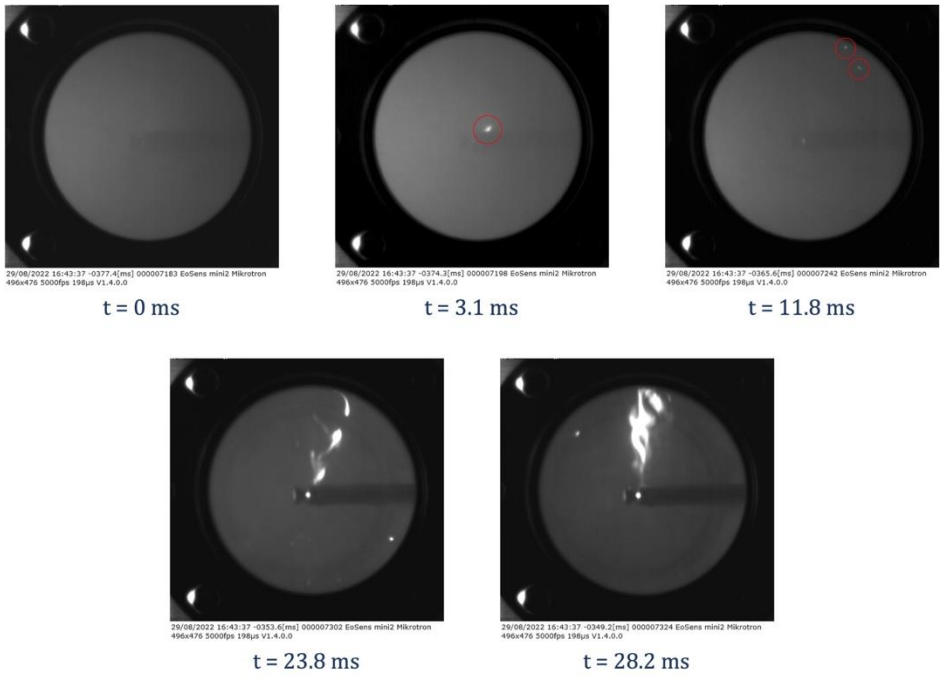

Figure VI-11: Time evolution of the flame profile of 100 g.m^{-3} Jet A1 mist in the 20 L vented sphere at t_v = 100 ms

6.2.3. 20 L explosion sphere

At a microscale level, there is quite an analogy between the behaviours of dust flames and spray flames since the oxidiser and the fuel are initially separated, and a finite rate of transport processes governs the rate of combustion of diffusion flames (Ogle, 2016). Indeed, to burn, a fuel must first evaporate and diffuse into the flame sheet. Similarly, vapours of solid fuels are formed either by pyrolysis or by melting and then evaporating. Some correlations used for dust explosions may therefore be applicable in the case of mist clouds. In order to check the validity of this statement, the correlation proposed by Silvestrini et al. (2008) was applied to explosion severity measurements to see if the calculated unstretched burning velocity has the same orders of magnitude as the current study's and literature's findings (equation III-35). It should be noted that instead of P_{max} and dP/dt_{max}, P_{ex} and dP/dt_{ex} were used (Santandrea et al., 2020). As seen in Figure VI-12, a maximum S_u^0 of 46 cm.s^{-1}, 40 cm.s^{-1}, and 33 cm.s^{-1} was found for isooctane, ethanol, and Jet A1, respectively, at concentrations close to stoichiometry. Compared to the experimental findings from the flame propagation tube (varying between 86 cm.s^{-1} and 140 cm.s^{-1} for nozzle set N1), the orders of magnitude are much lower. As for values found in the literature, the S_u^0 findings in laminar conditions were mostly performed on gaseous mixtures, hence high temperatures were used to maintain the fuel in vapour form, explaining the higher obtained results.

In addition to the level of turbulence, in standard experimental conditions in this study, it makes

sense to obtain lower S_u^0 on account of the evaporation enthalpies needed, which lead to a lower final temperature. Moreover, it should not be neglected that Silvestrini's correlation is based on several assumptions that neglect the turbulent length scale. It also relies on the cubic law and puts many strong hypotheses forward. Nevertheless, it provides values of the unstretched burning velocity closer to those found in the literature for quiescent vapours.

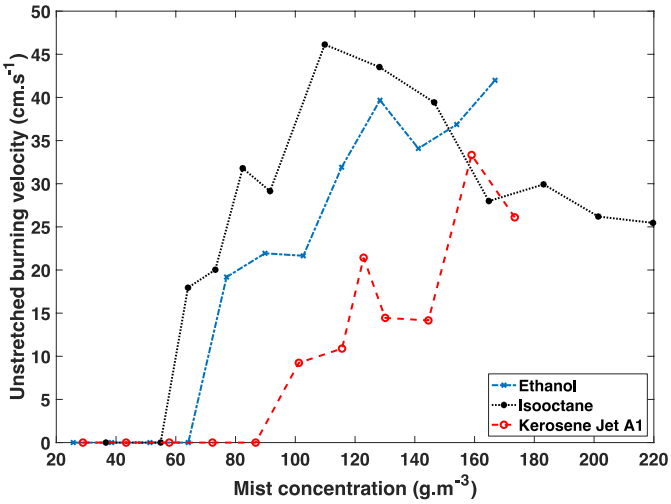

Figure VI-12: Predicted unstretched burning velocity as a function of ethanol, isooctane, and Jet A1 mist concentration from experimental explosion severity parameters determined at T = 27 °C in the 20 L explosion sphere

6.3. Evaporation and combustion modelling

As seen in the previous sections, the presence of liquid droplets ahead of the flame front modified, in many ways, the flame propagation. A key process that was used in many of the explanations is the evaporation of these droplets. Indeed, the formation of a combustible mixture through vaporisation is an essential step for igniting a mist cloud. A thorough physical understanding of the evaporation and combustion of droplets is hence required. To go back to the basics: the evaporation mechanism essentially occurs when a relatively cold droplet heats up from a warmer environment and turns into vapour. The fuel in the gas phase is transported towards the environment, where its concentration is low, through both diffusion and Stefan convection, while the droplet size is concurrently decreasing.

6.3.1. Theoretical bases

For this study, an evaporation and combustion model was developed based on the d^2 law discussed in Section 2.4.4. Hundreds of evaporation models have been developed to predict the evaporation rate of single or a group of droplets (Banerjee, 2013; Landry, 2007; Pinheiro et al., 2019; Tuntivoranukul et al., 2010); nevertheless, this model serves a calculation and estimation tool specifically for mist clouds inside the 20 L sphere. The main steps and equations on which this model was founded are as follows:

Starting with mass conservation in the gas phase with the hypothesis of a quasi-stationary regime:

$$\frac{d}{dr}(r^2 \rho v) = 0 \qquad \text{VI-7}$$

$$\dot{m}_v = 4\pi r^2 \rho v = constant \qquad \text{VI-8}$$

Where $\dot{m}_v$ is the fuel vapour mass flow rate, r the radial position, and v the radial velocity.

The convection-diffusion equations are hence written as follows:

$$\dot{m}_v \frac{dY_v}{dr} = 4\pi r^2 \rho D_v \frac{d^2 Y_v}{dr^2} \qquad \text{VI-9}$$

$$\dot{m}_v C_p \frac{dT}{dr} = 4\pi r^2 \lambda \frac{d^2 T}{dr^2} \qquad \text{VI-10}$$

Where Y_v is the fuel vapour mass fraction, D_v, the vapour mass diffusivity, and λ, the thermal conductivity.

After applying first integration and a mass and energy balance on the droplet's surface, and then solving the evaporation rate equations according to boundary conditions ($r = r_d$):

$$\dot{m} = \frac{4\pi \lambda_v r_d}{C_{p,v}} \ln(B_T + 1) = \ln(1 + B_M) \qquad \text{VI-11}$$

Where B_T and B_M are the thermal and mass transfer Spalding numbers, respectively, and are equal to the following:

$$B_T = \frac{C_{p,v}(T_\infty - T_d)}{L_v} \qquad \text{VI-12}$$

$$B_M = \frac{Y_{vs} - Y_\infty}{1 - Y_{vs}} \qquad \text{VI-13}$$

Where $C_{p,v}$ is the vapour phase heat capacity, T_∞ and T_d are the temperatures of the surrounding environment and the droplet surface, respectively, L_v is the enthalpy of vaporisation, and Y_{vs} the vapour fraction at stoichiometry, which is calculated as follows:

$$Y_{vs} = \frac{x_{vs} M_v}{x_{vs} M_v + (1 - x_{vs}) M_{air}} \qquad \text{VI-14}$$

Where x_{vs} is the molar vapour fraction at stoichiometry, that can be determined from Dalton's law of partial pressures, M_v, the molar mass.

$$x_{vs} = \frac{P_{sat}(T_s)}{P} \quad \text{VI-15}$$

Where P_{sat} is the vapour pressure, which can be determined from existing correlations in the literature (Antoine semi-empirical correlations, Clausius-Clapeyron relations…).

$$P_{sat}(T_s) = Ae^{\left(\frac{B}{T_s} - C\right)} \quad \text{VI-16}$$

A mass balance on the droplet consequently leads to (Braconnier, 2020):

$$d^2 = d_0^2 - K_v t \quad \text{VI-17}$$

Where K_v is the evaporation rate constant of the fuel droplet of initial diameter d_0 and is equal to:

$$K_v = 8D\frac{\rho}{\rho_l}\ln(1 + B_T) \quad \text{VI-18}$$

By applying equation VI-11, a relationship between both the thermal and mass transfer Spalding numbers can be obtained:

$$B_T = (1 + B_M)^{\frac{1}{Le_v}} - 1 \quad \text{VI-19}$$

where *Le* is the Lewis number representing the ratio between thermal and mass diffusivities:

$$Le_v = \frac{\lambda}{\rho C_p D} \quad \text{VI-20}$$

Solving equations VI-17 to VI-20 leads to determining the time evolution of the droplet diameter as well as the vapour/liquid ratio at different temperatures in a quiescent environment. Nevertheless, PIV measurements showed that droplet evaporation first takes place in a turbulent environment; therefore, the following equation, considering the mist aerodynamics, can be used in such a case (Gökalp et al., 1992):

$$K_{v,t} = 8D\frac{\rho}{\rho_l}\ln(1 + B_T)\left(1 + 0.0276Re^{\frac{1}{2}}Sc^{\frac{1}{3}}\right) \quad \text{VI-21}$$

Where *Re* is the droplet Reynolds number calculated from PIV data and *Sc* is the Schmidt number $\left(Sc = \frac{\mu}{\rho D}\right)$.

The fact that the 20 L sphere is a closed vessel should be taken into account. The saturation pressure at a given temperature should hence be considered to define the characteristics of the mist. Moreover, such evaporation can also be studied during droplet combustion where similar

calculations can be carried out in both quiescent and turbulent environments by including the combustion enthalpy, ΔH_{comb}, the oxygen mass fraction, $Y_{Ox,\infty}$, and the mass stoichiometric coefficient, s, as follows:

$$B_T = \frac{C_{p,v}(T_\infty - T_d) + \frac{\Delta H_{comb}}{s} Y_{Ox,\infty}}{L_v} \quad \text{VI-22}$$

$$B_M = \frac{Y_{Fs} - \frac{Y_{Ox,\infty}}{s}}{1 - Y_{Fs}} \quad \text{VI-23}$$

The model assumes a spherically symmetrical system in a quasi-stationary regime. Droplets are presumed to have uniform properties and a uniform surface temperature. These assumptions may appear too restrictive, yet they provide conclusions that are reasonably supported by actual research and experimental findings.

6.3.2. Application

In order to approach reality, the model was not based on a single initial diameter but a droplet size distribution. The user can input an experimentally measured DSD and choose the measurement time of interest (in our case, the end of the mist injection, at t_v = 3 ms). It was also based on the confined 20 L sphere to take into account any eventual saturation or fluctuation of the gas concentration. Nevertheless, the droplets were assumed to start evaporating when the mist generation stopped, which is a strong hypothesis. Figure VI-13(a) shows the time evolution at T = 27 °C (300 K) of the liquid mass ratio (number of moles of liquid in the 20 L sphere with respect to the injected liquid quantity) of unconfined mist clouds of isooctane and ethanol generated using both nozzle sets N1 and N2. Calculations were carried out under turbulent conditions but without combustion. Taking into account the confinement, Figure VI-13(b) compares the liquid mass ratio evolution under the same conditions (m_{liquid} = 4 g ➔ C_{mist} = 200 $g.m^{-3}$). As it can be seen, the ethanol and isooctane mist clouds that were generated using nozzle set N1 reach saturation very quickly (0.6 ms and 1 ms, respectively). With a t_v of 3 ms, ignition will therefore take place in a saturated mist cloud with a liquid mass ratio of 0.89 and 0.5 for ethanol and isooctane mist, respectively. Indeed, as the number of vapour molecules increases in the sphere, the pressure increases until reaching equilibrium with the liquid phase (vapour pressure of the liquid). On the other hand, a dispersion using nozzle set N2 prolongates this time to 43.5 ms for isooctane mist and 4.4 ms for ethanol mist, meaning that any delay in ignition would lead to more vapour formation. Nevertheless, none of the two configurations present a premixed fuel-air gaseous mixture, as expected.

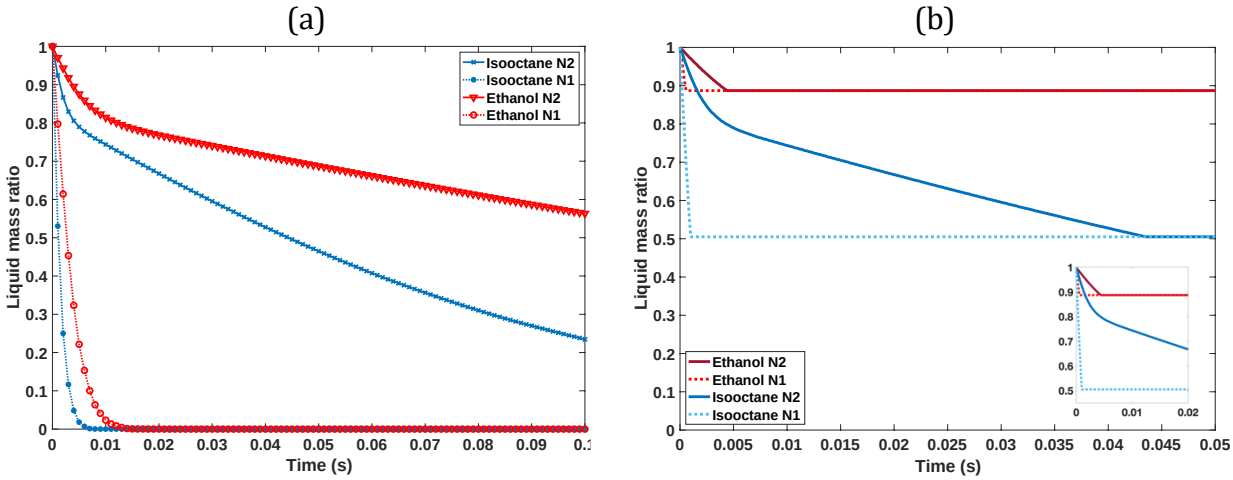

Figure VI-13: Liquid mass ratio at T = 300 K for 4 g of isooctane and ethanol as mist clouds under turbulent conditions, without combustion (a) unconfined, (b) confined in 20 L sphere, both generated using nozzle sets N1 and N2 (C_{mist} = 200 g.m^{-3})

As it is based on the d^2-law, the model assumes a single-component fuel and a one-step overall chemical reaction. Since most of the liquids selected for this study are of a multi-component nature, modifications to the evaporation model should be made. Indeed, in order to study multi-component fuel combustion, some factors should be considered. First, as the relative volatility and concentration of the constituent vary, their evaporation rates will differ. Moreover, attention should be paid to the diffusivity and miscibility of the fuel components, as in order to evaporate, they will have to circulate internally to get to the droplet surface. As a simplistic approach, the thermophysical properties of the multi-component fuels were all based on correlations and experimentally determined values from the literature.

Figure VI-14 depicts the time evolution of a droplet of ethanol, isooctane, and Jet A1 in a turbulent environment at T = 300 K, without taking combustion into account, and at T = 500 K while considering combustion. The latter was chosen arbitrarily low, but the combustion contribution to the evaporation dynamics would have been neglectable at temperatures obtained during a mist explosion. One remarkable observation can be made on ethanol droplets, which take more time to evaporate even though they have higher volatility than the other fuels. As it can be seen in Table VI-3, Jet A1 and diesel have an evaporation rate about nine times greater than that of ethanol with combustion and are also relatively higher without combustion. Isooctane has an intermediary evaporation rate with respect to the displayed fuels. This, however, does not negate the higher explosion severity measurements presented in Chapter V. Attention should be paid to the fact that both fuels remain of multi-component nature; although Jet A1 and diesel mist evaporate faster, this does not mean that the remaining liquid after saturation, is of the same volatility as those evaporated.

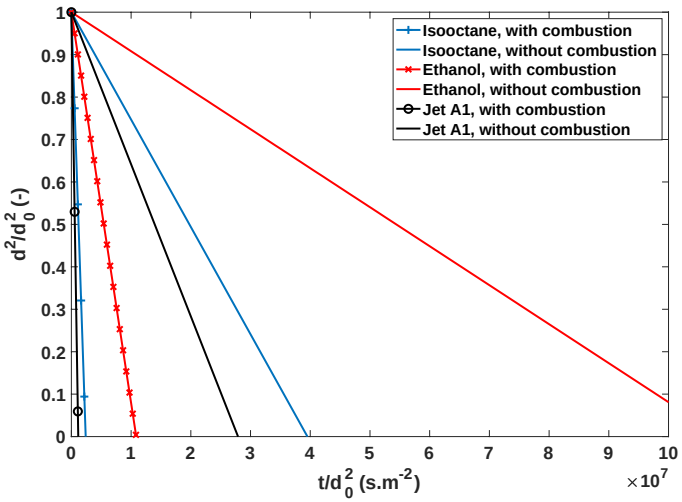

Figure VI-14: Temporal evolution of ethanol, isooctane, and Jet A1 droplets (d_0 = 13.6 µm) in a turbulent environment with combustion (T = 500 K) and without combustion (T = 300 K) - normalised axes to d_0^2

Table VI-3: Variation of the droplet evaporation rate as a function of the chemical nature and initial conditions for an initial diameter d_0 = 13.6 µm (Nozzle set N1)

Turbulent conditions	**K_v @ T = 300 K (x 10^{-7} $m^2.s^{-1}$)**	**K_v @ T = 500 K + combustion (x 10^{-7} $m^2.s^{-1}$)**
Ethanol	0.1	0.92
Isooctane	0.25	4.19
Jet A1	0.36	8.7
Diesel	0.22	8.6

In addition to the chemical nature, the initial temperature affects the droplet evaporation rate. As seen in Figure VI-15, a noticeable increase in the evaporation rate, K, takes place on an ethanol droplet in turbulent conditions without combustion when the temperature is increased from 300 K to 600 K. The rate of droplet evaporation is proportional to the initial temperature as it increased from 0.0167 $mm^2.s^{-1}$ to 0.149 $mm^2.s^{-1}$, respectively. We can also observe that the effect of the initial temperature on K decreases with increasing temperatures.

Figure VI-16 shows the evolution of K with increasing initial droplet diameters and different jet velocities (different turbulence levels) under the same conditions at T = 300 K. As seen from the figure, the droplet evaporation rate tends to increase with increasing droplet diameter (as the surface area increases) and turbulence level. Nevertheless, a quasi-linear temporal evolution was

maintained when tested under quiescent conditions, demonstrating adherence to the d^2 law, and K_v remained constant for all droplet diameters. It can also be seen that as the turbulence level increases, the slope of the evaporation rate evolution increases. The improvement of the evaporation rate of larger droplets is, therefore, strongly influenced by the level of turbulence. This finding is coherent with Verwey and Birouk (2017), who studied the evaporation of heptane and decane droplets under ambient conditions and found similar tendencies with increasing droplet diameters and turbulence levels.

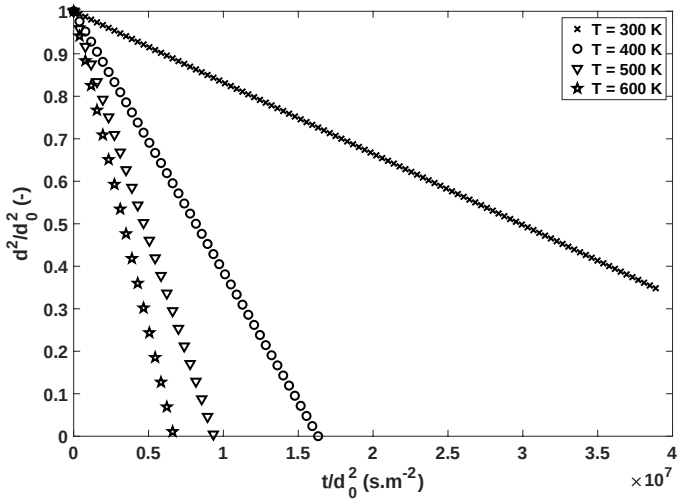

Figure VI-15: Temporal evolution of an ethanol droplet (d_0 = 160 µm) in a turbulent environment without combustion, T = 300 K - (normalised axes to d_0^2)

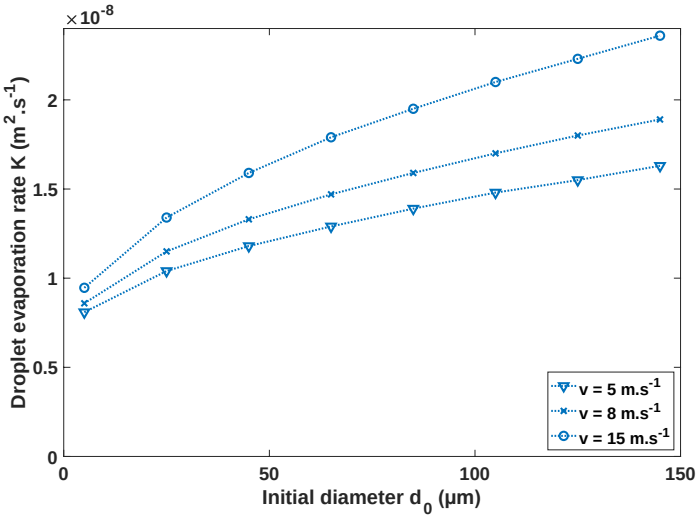

Figure VI-16: Variation of ethanol droplet evaporation rate as a function of the initial droplet diameter and the turbulence level – no combustion, T = 300 K

Until now, the influence of operating conditions on a single droplet has been discussed, but what transpires when a dense cloud of droplets is involved? Some examples that are linked to the performed explosion severity measurements (Chapter V) will be discussed hereafter to better explain certain occurrences.

Diesel fuel

Subsection 5.5.1.2 discusses the influence of the ambient sphere temperature on the explosion severity of a turbulent diesel mist cloud. The explosion severity was seen to increase with increasing initial temperatures and was explained by the increase in vapour content. To visualise this vapour content, Figure VI-17(a) plots the vapour fraction of a diesel mist cloud at t_v = 3 ms of initial liquid mass of 3.2 g (nominal mist concentration = 160 g.m^{-3}) relative to LEL of diesel vapour at 30 °C, for a range of droplet diameters and initial temperatures. For an initial droplet diameter of about 10 µm, the vapour / LEL_{vapour} ratio reaches unity at an initial temperature of about 335 K (about 62 °C), corresponding to the flashpoint of diesel fuel. However, at both 30 °C and 40 °C (303 K and 313 K), explosions took place with a P_{ex} of 0.3 bar and 4.6 bar and a dP/dt_{ex} of 24 bar.s^{-1} and 110 bar.s^{-1}, respectively, although the vapour ratio was lower than the LEL_{vapour}. It is, therefore, the total quantity of fuel present that is important, whether in liquid form or vapour form. Thus, it was clearly demonstrated that diesel could indeed ignite at a temperature below its flashpoint when dispersed as a mist. It should be kept in mind, however, that the initial mist temperature does not correspond to the local temperature at the ignition point/zone. It should also be noted that only this type of figure is based on a monomodal DSD and does not take the experimental DSD into account.

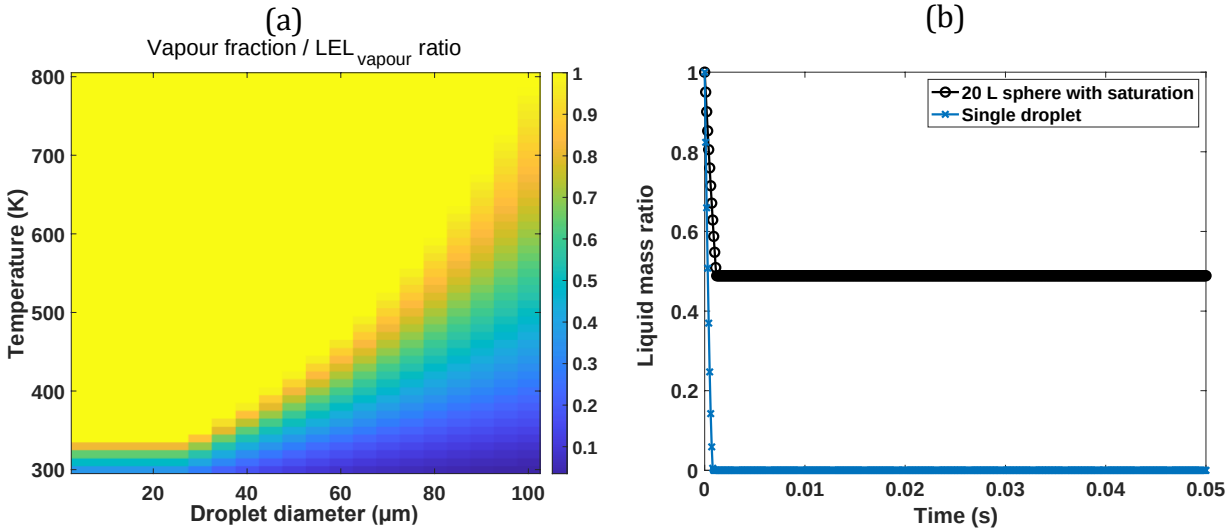

Figure VI-17: (a) Evolution of the vapour fraction / LEL ratio of 160 g.m^{-3} of diesel - threshold at 1 for a range of temperatures and droplet diameters (b) saturation of the 20 L sphere at T = 350 K for 160 g.m^{-3} of diesel mist (Nozzle set N1)

Figure VI-17 (b) demonstrates that the 160 g.m^{-3} of diesel mist generated using nozzle set N1 saturate the 20 L sphere at T = 350 K as of 1.2 ms, for a liquid mass ratio of about 0.5, meaning that 50 % of the injected mist had evaporated before ignition and was enough to exceed the LEL_{vapour} of diesel. On the other hand, it took 0.8 ms to saturate the sphere with the same mist concentration at T = 330 K due to the increase of the initial number of moles of air with the decrease in temperature. Saturation took place with 63 % of the remaining liquid. It was observed that as the injected mist concentration increased, the saturation time decreased, and the liquid mass ratio increased.

Kerosene Jet A1

Similarly, Figure VI-18 exhibits the evolution of the normalised vapour fraction as a function of both the initial temperature and droplet diameter for 120 g.m^{-3} and 350 g.m^{-3}. It can be seen from Figure VI-18(a) that at T = 40 °C (313 K), the vapour content is about half the LEL_{vapour} for a mean diameter of 8 µm. Therefore, kerosene mist would not be completely vaporised, and the DSD would have shifted to lower diameters. After 3 ms, ignition would then occur in a two-phase system: small droplets in the presence of a "layer" of kerosene vapour. Such effect, which is usually insignificant, becomes rather considerable when explosions take place at temperatures higher than 20 °C. For nozzle set N2, a d_{50} of about 62 µm was attained. As seen in Figure VI-18(b), a temperature of at least 350 K (77 °C) is required for the vapour phase to reach LEL_{vapour} in a monomodal mist cloud, not to forget coalescence phenomena that might increase the droplet sizes.

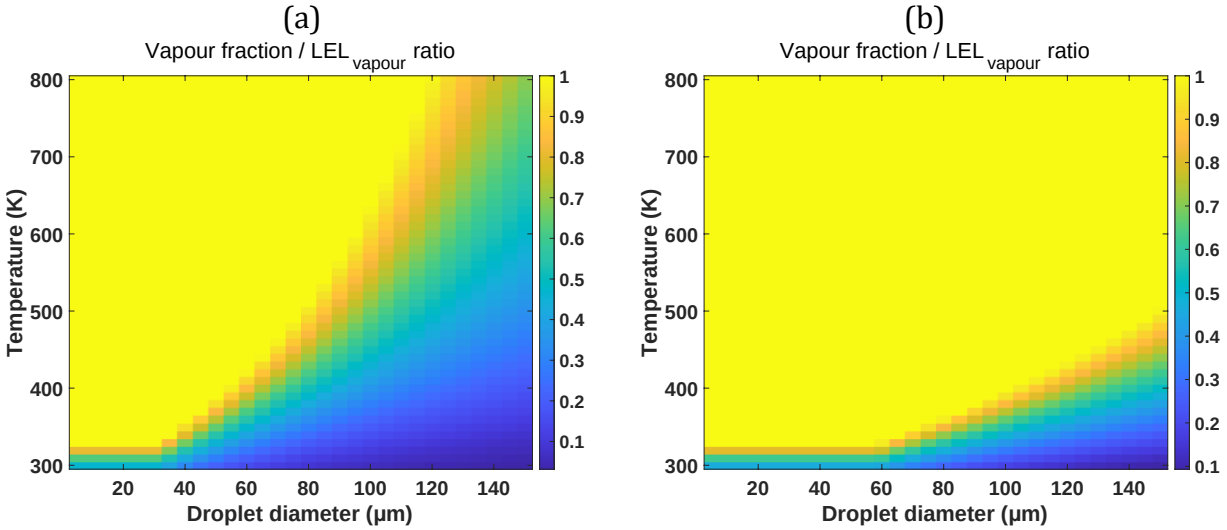

Figure VI-18: Evolution of the vapour fraction / LEL ratio of (a) 120 g.m^{-3} and (b) 350 g.m^{-3} of Jet A1 mist - threshold at 1 for a range of temperatures and droplet diameters

As seen in Figure V-5, the strongest explosion severity shifts between that obtained at 60 °C and that at 40 °C at a certain concentration for nozzle set N2. Indeed, at high concentrations, the saturation time was found to be negligible (order of magnitude of about 0.3 and 0.5 ms) for both

temperatures 40 °C and 60 °C. Nevertheless, as the mist concentration decreased, specifically below 225 $g.m^{-3}$, the saturation time became more important with respect to our 3 ms, and the difference between both temperatures increased (for 200 $g.m^{-3}$ at T = 40 °C $t_{saturation}$ = 1.6 ms, at T = 60 °C, $t_{saturation}$ =3.7 ms). This might be linked to the higher explosion severity attained at 60 °C for concentrations less than about 300 $g.m^{-3}$.

Although the developed evaporation model may seem like a simplistic approach, due to its various assumptions, it does give tendencies that support experimental findings. It is of interest to enhance this model by integrating the multi-component aspect and taking into account the amount of vapour generated during injection and not just after the end of a mist injection. This model is, therefore, the first step toward a better approach to visualising spray evaporation inside the 20 L sphere.

Summary

This chapter was dedicated to looking deeper into the phenomenology of a mist's ignition and explosion as it is a crucial step to identify intrinsic properties, such as the laminar burning velocity. The chapter was divided into three parts, comprising a group combustion discussion, flame propagation studies, and evaporation and combustion models.

In the first section, a group number, G, was calculated to represent the relative tendency of the mist clouds studied in this work to undergo single droplet or group combustion. The calculations were based on the assumption of a monomodal spray and showed that the combustion of the mist cloud inside the 20 L sphere would maintain an external sheath combustion regime. This implies that the spray zone is too dense to allow the diffusion of heat, resulting in the evaporation of the droplets close to the flame's boundary and the creation of a global envelope flame that surrounds all the droplets in the cloud.

The second section consisted of an attempt to determine the laminar burning velocity of ethanol, isooctane, and Jet A1 mist clouds in two different apparatus. Preliminary flame propagation tests were first performed in the flame propagation tube, and two types of flames were observed: a smooth spherical initiation of the flame kernel and a more wrinkly or cellular-like flame structure. The latter took place in more turbulent regimes, which was explained by the action of turbulent eddies and by the stronger interaction between the flame and the vortices. An experimental series was performed, allowing the tracking of the flame front's position and spatial velocity as a function of time. Moreover, the unstretched burning velocity was determined following a non-linear relation which links the burning velocity with the Karlovitz factor and the Markstein length. The latter is generally considered the laminar burning velocity. Nevertheless, the high levels of turbulence and the presence of droplets ahead of the flame front led to higher values than expected, in the vicinity of 100 $cm.s^{-1}$. The laminar burning velocity hence required much less turbulence which was not yet achievable.

In addition, the influence of the ignition energy was evaluated for energies starting from 25 J to 100 J, and it was seen that flame propagation was mildly influenced. Isooctane flames were found to be slower than ethanol and Jet A1 flames under the same conditions. This was linked to the lower oxygen content of isooctane, the radiative effects observed for ethanol and Jet A1 flames, and the rich fuel-air mixture that might have exceeded the UEL of isooctane. An increase in the droplet size distribution hindered the flame propagation in Jet A1 mists, but the contrary was observed in ethanol mists, a phenomenon that requires further examination. Subsequently, flame propagation measurements were complemented with ones performed inside the 20 L "open" sphere. A similar order of magnitude was obtained for the unstretched burning velocity of

ethanol. Nevertheless, a different phenomenon was observed for Jet A1 mists as a rich-fuel diffusion flame propagated upwards.

The third part of this chapter proposed an evaporation and combustion model based on the d^2 law. The model was adapted for a complete droplet size distribution of a turbulent mist cloud in a confined 20 L sphere. Although the model's assumptions may seem too restrictive, they lead to conclusions that can be reasonably justified and supported by experimental findings. It was seen that the increase of the initial temperature increased the droplet evaporation rate. In addition, it was observed that the level of turbulence strongly influenced the improvement of the evaporation rate of larger droplets. Theoretical calculations were also applied to experimental findings to link the increase of the explosion severity with increasing temperatures to the increase of the vapour phase. Nevertheless, the saturation of the 20 L sphere was proved, showing that most of the experiments occurred with at least 50 % of the initial liquid concentration in the form of liquid droplets in the sphere. This highlights the role of mist droplets in the ignition, showing that fuel vapour is not the only key indicator. The total quantity of the fuel, whether in liquid form or vapour form, is important, in addition to the droplets' initial diameters.

Résumé

Ce chapitre a été consacré à l'examen approfondi de la phénoménologie de l'inflammation et de l'explosion d'un brouillard, car il s'agit d'une étape cruciale pour identifier les propriétés intrinsèques, telles que la vitesse de combustion laminaire. Le chapitre a été divisé en trois parties, comprenant une discussion sur la combustion de groupe, des études sur la propagation de la flamme, et des modèles d'évaporation et de combustion.

Dans la première section, un nombre de groupe, G, a été calculé pour représenter la tendance relative des nuages de brouillard étudiés dans ce travail à subir une combustion de gouttelettes individuelles ou de groupe. Les calculs étaient basés sur l'hypothèse d'un spray monomodal et ont montré que la combustion du nuage de brouillard à l'intérieur de la sphère de 20 L maintiendrait un régime de combustion en gaine externe. Ceci implique que la zone du spray est trop dense pour permettre la diffusion de la chaleur, ce qui entraîne l'évaporation des gouttelettes proches de la limite de la flamme et la création d'une flamme enveloppe globale qui entoure toutes les gouttelettes du nuage.

La deuxième section consistait en une tentative de détermination de la vitesse de combustion laminaire de nuages de brouillard d'éthanol, d'isooctane et de Jet A1 dans deux appareils différents. Des tests préliminaires de propagation de la flamme ont d'abord été effectués dans le tube de propagation de la flamme, et deux types de flammes ont été observés : une initiation sphérique lisse du noyau de la flamme et une structure de flamme plus ridée ou de type cellulaire. Cette dernière a eu lieu dans des régimes plus turbulents, ce qui a été expliqué par l'action des tourbillons turbulents et par l'interaction plus forte entre la flamme et les tourbillons. Une série expérimentale a été réalisée, permettant de suivre la position et la vitesse spatiale du front de flamme en fonction du temps. De plus, la vitesse de combustion non étirée a été déterminée suivant une relation non linéaire qui lie la vitesse de combustion avec le facteur de Karlovitz et la longueur de Markstein. Cette dernière est généralement considérée comme la vitesse de combustion laminaire. Néanmoins, les niveaux élevés de turbulence et la présence de gouttelettes en avant du front de flamme ont conduit à des valeurs plus élevées que prévu, aux alentours de 100 cm.s-1. La vitesse de combustion laminaire nécessitait donc beaucoup moins de turbulence, ce qui n'était pas encore réalisable.

En outre, l'influence de l'énergie d'inflammation a été évaluée pour des énergies allant de 25 J à 100 J, et il a été constaté que la propagation de la flamme était légèrement influencée. Les flammes d'isooctane se sont avérées plus lentes que les flammes d'éthanol et de Jet A1 dans les mêmes conditions. Ceci était lié à la plus faible teneur en oxygène de l'isooctane, aux effets radiatifs observés pour les flammes d'éthanol et de Jet A1, et au mélange air-carburant riche qui aurait pu

dépasser la LSE de l'isooctane. Une augmentation de la distribution de la taille des gouttelettes a entravé la propagation de la flamme dans les brouillards de Jet A1, mais le contraire a été observé dans les brouillards d'éthanol, un phénomène qui nécessite un examen plus approfondi. Par la suite, les mesures de la propagation de la flamme ont été complétées par celles effectuées à l'intérieur de la sphère "ouverte" de 20 litres. Un ordre de grandeur similaire a été obtenu pour la vitesse de combustion non étirée de l'éthanol. Néanmoins, un phénomène différent a été observé pour les brouillards de Jet A1, une flamme de diffusion de combustible riche se propageant vers le haut.

La troisième partie de ce chapitre a proposé un modèle d'évaporation et de combustion basé sur la loi d^2. Le modèle a été adapté pour une distribution complète de la taille des gouttelettes d'un nuage de brouillard turbulent dans une sphère confinée de 20 litres. Bien que les hypothèses du modèle puissent sembler trop restrictives, elles conduisent à des conclusions qui peuvent être raisonnablement justifiées et soutenues par des résultats expérimentaux. Il a été observé que l'augmentation de la température initiale augmentait le taux d'évaporation des gouttelettes. De plus, le niveau de turbulence influençait fortement l'amélioration du taux d'évaporation des plus grosses gouttelettes. Des calculs théoriques ont également été appliqués aux résultats expérimentaux pour lier l'augmentation de la sévérité d'explosion avec l'augmentation de la température à l'augmentation de la phase vapeur. Néanmoins, la saturation de la sphère de 20 L a été prouvée, montrant que la plupart des expériences se sont déroulées avec au moins 50 % de la concentration initiale de liquide sous forme de gouttelettes liquides dans la sphère. Cela met en évidence le rôle des gouttelettes de brouillard dans l'inflammation, montrant que la vapeur de carburant n'est pas le seul indicateur clé. La quantité totale de carburant, sous forme liquide ou sous forme de vapeur, est importante, en plus du diamètre initial des gouttelettes.

Chapter VII:
Conclusions

Some of the mist has been lifted now! This study was intended to propose a new test protocol to assess the flammability and explosivity of fuel mist clouds while investigating the related phenomenology. In addition, it aimed to raise interest regarding accidental releases that might sometimes be overlooked and to lift the fog off this "misty" subject. With the manuscript ending, this chapter answers some essential questions asked throughout the study and summarises the main findings. In the following sections, the implemented procedures and mechanisms are first briefly reviewed, and a complete pre-normative protocol based on a liquid classification is proposed, followed by advised prevention measures. Some illustrative industrial cases are then analysed, and current perspectives are highlighted.

7.1. Review of the implemented mechanisms

As mentioned in the introduction of this manuscript and Chapter II, flammable mist release types are neither well classified nor assessed explicitly by the current regulations. Indeed, there is a lack of scientific data and well-established quantitative approaches to assess mist explosions correctly. Therefore, this study's objective was to fill this gap by proposing a pre-normative test method that will enable both to assess further the phenomenology in a confined environment and to provide reproducible and reliable safety data.

Several steps were taken to propose a complete test procedure (see Figure VII-1), including selecting a pertinent set of fuels and a controllable and adaptable mist generation system while producing suitable droplet sizes, concentrations, and turbulence levels. Characterisation experiments quantified such parameters before moving on to the mist ignition step. Subsequently, as existing equipment and software programs are not yet adjusted to a mist explosion test, a control and data acquisition system was developed. Some modifications were made to the explosion vessel, and a high-voltage spark ignition system was designed to evaluate the MIE of mist clouds. Also, calibration and validation tests were performed, establishing a complete modus operandi. The latter was followed, and the ignition sensitivity (MIE, LEL, and LOC) and explosion severity (P_{ex}, dP/dt_{ex}, P_{max}, dP/dt_{max}) of the selected fuels were measured under ambient and varying operating conditions in one apparatus.

The succeeding sections briefly present the main results obtained during each step of this study.

7.1.1. Set-up and operating protocol

For this study, seven fluids were selected and classified following a liquid classification system proposed by the Health and Safety Executive as follows: Jet A1, diesel, and LFO in Release Class I (more volatile and more atomising), biodiesel in Release Class IV (less volatile and more atomising), and Mobil DTE in Release Class III (less volatile and less atomising). Ethanol and

isooctane, having a flashpoint of less than 32 °C, were not classified in this system. A twin-fluid spray nozzle based on a Venturi junction was chosen as an adequate mist generation system convenient for a confined, relatively small test vessel. Three nozzle sets were mainly used, allowing the modification of the mist concentration, turbulence level, and droplet size distribution. A control and data acquisition system with customised software was used to control liquid and air injections, ignition-source activation, and the start of the data acquisition recording pressure-time evolution.

7.1.2. Ignition sensitivity

The ignition sensitivity of mist clouds was evaluated by performing three types of tests, including the determination of the minimum ignition energy (MIE), the lower explosion limit (LEL), and the limiting oxygen concentration (LOC).

At T = 27 °C and using nozzle set N1, the seven fluids could be divided into four MIE groups. Ethanol and isooctane were the easiest to ignite, with an MIE lower than 100 mJ. Kerosene Jet A1, diesel and LFO showed intermediary behaviour, depending on their ageing and storing conditions, but the three fuels exhibited ignition with MIEs less than 1 J. Finally, biodiesel and Mobil DTE were the hardest to ignite, with MIEs reaching 5000 J. Nevertheless, slightly preheating the liquid and/or the explosion vessel facilitated the ignition of all fluids, except for Mobil DTE, which did not ignite under various configurations.

The LEL was also determined under controlled conditions, and it was seen that, in most cases, it might be more conservatory to take the LEL of the fuel's vapours as a reference to evaluate the extent of a hazardous zone. Nevertheless, some fuels, such as biodiesel, are supposed as non-volatile/non-flammable with no specifications in their MSDS. Yet, an LEL of 103 $g.m^{-3}$ was obtained. It is, therefore, interesting to evaluate the LEL in all cases.

The LOC was an additional parameter that was determined for ethanol and Jet A1 mist clouds of 8-10 µm droplets for a range of concentrations. Findings showed that Jet A1 mists generated with nozzle set N1 have a LOC of 15.8 $\%_{v/v}$, corresponding to a mist concentration of 144 $g.m^{-3}$; whereas ethanol mists have a LOC of 13.1 $\%_{v/v}$, corresponding to a mist concentration of 110 $g.m^{-3}$.

7.1.3. Explosion severity

The assessment of the explosion severity of the fuel mist clouds was also carried out in the 20 L explosion sphere under varying conditions. It was seen that for most of the fuels, plateau-like severity curves were obtained, showing that it would be difficult to determine the upper explosion limit (UEL) using this apparatus due to the eventual recirculation and rain-

out/vaporisation concurrent phenomena of the injected mist. It also appeared that the chemical nature of the fuels significantly affected explosivity measurements, which led to a classification based on the deflagration index. Indeed, if we were to apply the cubic law, fuels were classified into four deflagration classes.

After validating that the maximum explosion overpressure, P_{max}, and the maximum rate of explosion pressure rise, dP/dt_{max}, were attainable using the employed test apparatus and equipment, the influence of several factors was studied. It appeared that the explosion severity, as well as the ignition sensitivity, decreased with increasing droplet diameters. The most noticeable effect was observed on the rate of pressure rise, showing that the dynamics of the mist flow easily influenced the reaction kinetics. In addition to the DSD, the initial temperature affected the explosion severity to a certain extent. Indeed, when the sphere was preheated to temperatures higher than the flashpoint, the influence on the explosion overpressure started to decrease. This phenomenon was linked to saturation inside the 20 L sphere and was proved using the proposed evaporation model. However, a more significant influence continued to occur on the rate of pressure rise.

The influence of the ignition energy on the explosion severity was also assessed by comparing 100-J and 5-kJ chemical ignitors. It was seen that for fuel mists that ignited using the 100-J ignitors, increasing the energy to 5 kJ led to similar or lower values of the explosion severity parameters. It was linked to the high turbulence created by the 5-kJ ignitors, which may have altered the concentration distribution in the mist cloud. Nevertheless, in the case of biodiesel, for instance, no ignition occurred at 100 J, contrary to when using 5 kJ. This implies that the increase of the ignition energy is only required when no ignition occurs at 100 J.

Other influencing factors, such as the turbulence level, the vapour content, and the addition of flammable gases, were also examined and showed considerable effects on the explosion severity. Consequently, it is vital to ensure a well-controlled environment when performing such experiments.

Flame propagation tests were also performed in two apparatus: the flame propagation tube and the open sphere. These tests allowed understanding the phenomenology of mist explosions better. Moreover, they helped confirm the influence of radiation and flame stretching on the explosion severity. Such tests can be used to determine intrinsic properties, complementing those determined in the 20 L sphere, as seen in Figure VII-1.

This study has therefore succeeded in developing a device that is able to test the ignition sensitivity and explosion severity and benchmark mist clouds in a potentially standardisable way, which has never been done to our knowledge.

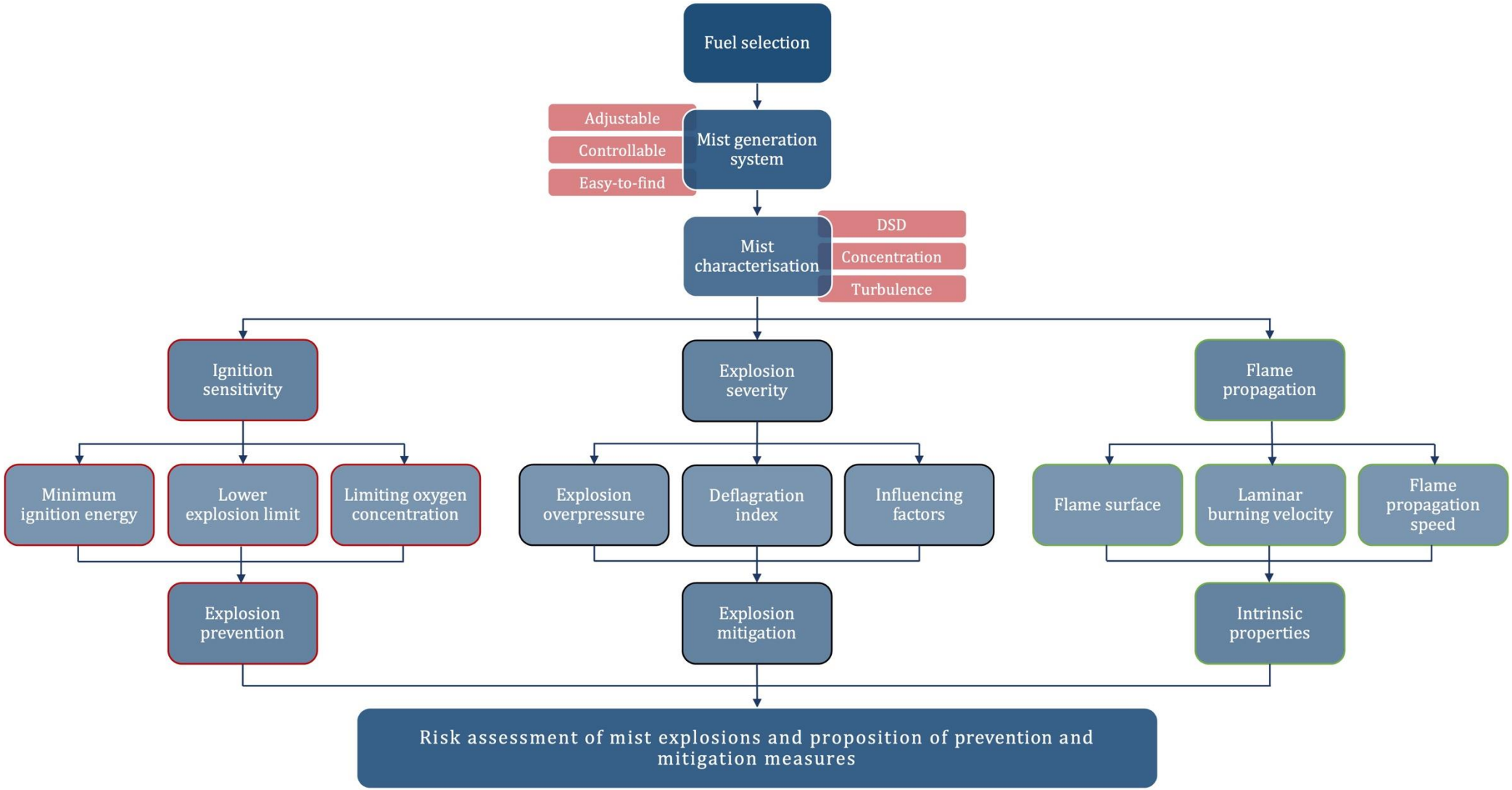

Figure VII-1: A systematic approach to study the flammability and explosivity of fuel mist clouds

7.2. Proposition of a standard

When predicting a fuel mist cloud's explosion severity and ignition sensitivity, it is safer to imagine a worst-case scenario. As observed throughout the manuscript, the increase of the DSD did not lead to a more sensitive mist cloud or a severer explosion. Moreover, when a plateau was reached, the influence of increasing the mist concentration weakened. As for the turbulence level, its influence varied from one fuel class to another. Therefore, it is advised to use nozzle set N1 for the standard test method as it is sufficient to evaluate the required parameters with a DSD that does not surpass 15 µm and concentrations reaching 200 or 250 g.m^{-3} for an air injection pressure of 3 bar.

7.2.1. Fuel classification

In order to classify fuels, it was seen as appropriate to start from the liquid classification proposed by the HSE as a foundation (Section 2.3). Nevertheless, seen that the current classification concerns testing on a laboratory-scale test bench and that the liquid exits the spray nozzle atomised, only secondary atomisation should be considered to see if the droplet resists aerodynamic and internal instabilities. Following the steps proposed by Burrell and Gant (2017), the droplet Weber number was first calculated according to equation VII-1:

$$We = \frac{\rho_l v^2 d_d}{\sigma_l} \qquad \text{VII-1}$$

Where ρ_l is the liquid's density in kg.m^{-3}, v is the relative velocity of the droplet in m.s^{-1}, d_d is the diameter of the droplet in m, and σ_l is the surface tension of the liquid in kg.s^{-2}.

The authors then identified a critical Weber number as the "upper limit" of stability following equation VII-2, and liquids were classified according to the ratio We/We_c.

$$We_c = 12\left(1 + 1.077{Oh_d}^{1.6}\right) = 12\left(1 + 1.077\left(\frac{\mu_l}{\sqrt{\rho_l d_d \sigma_l}}\right)^{1.6}\right) \qquad \text{VII-2}$$

The authors based their calculations on reference conditions of a 10-bar pressure drop and a 30 µm droplet and classified the liquids of interest as a function of the flashpoint, obtaining the same classification as the one based on primary atomisation. Nevertheless, for this fuel classification, a reference mean droplet diameter d_{50} of 9 µm will be considered, as well as a velocity of 5 m.s^{-1} (value determined from PIV experiments as a velocity magnitude at the centre of the sphere during injection).

Calculations of the ratio We/We_c are presented in Table VII-1. As seen, a droplet generated using nozzle set N1 is considered stable.

Table VII-1: Calculated Weber ratio for the seven liquids for d_{50} = 9 µm and v = 5 m.s^{-1}

	Ethanol	**Isooctane**	**Jet A1**	**Diesel B7**	**LFO**	**Biodiesel B100**	**Mobil DTE**
$\frac{We}{We_c}$	0.71	0.7	0.6	0.55	0.61	0.45	0.01

A dimensional analysis of the ignition of a mist cloud was presented in Section 3.8. In order to classify the fuels, the Spalding number presented in equation III-29 $\left(B_T = \frac{IE}{\Delta H_{vap} {d_c}^3 C_m}\right)$ was selected out of the remaining dimensionless numbers as droplet evaporation was seen to be one of the main factors contributing to the explosion severity and sensitivity of the mist cloud. The ignition energy, IE, was equal to the MIE of each fluid. Approximate values of the enthalpy of vaporisation, ΔH_{vap}, were extracted from the literature as they can differ from one study to another. The Spalding number was evaluated for a range of critical diameters, d_c, and concentrations, C_m, and, when plotted as a function of the Weber ratio, the liquids were divided into four quadrants, each containing the same liquids as the ones presented in Figure III-1. This implies that the classification presented by the HSE and adapted to the current study's reference conditions is sufficient to divide liquids according to their atomisation and volatility, simultaneously reflecting on their flammability and explosivity.

An example is presented in Appendix A, Figure A-6, for a critical diameter of 1 cm and a mist concentration of 100 g.m^{-3}. The five multi-component liquids are therefore classified as shown in Table VII-2:

Table VII-2: Updated liquid classification based on that proposed by the HSE

	***We* Ratio < 0.3**	***We* Ratio ≥ 0.3**
32 °C < FP < 125 °C *FP < 32 °C*	Quadrant **II** -	Quadrant **I** *Jet A1, diesel, and biodiesel* *ethanol, isooctane*
FP ≥ 125 °C	Quadrant **III** *Mobil DTE*	Quadrant **IV** *Biodiesel*

Although ethanol and isooctane belong to Class I of the Energy Institute's liquid classification and may vaporise quickly upon release (see Table II-1), they may still form a mist hazard, especially in confined environments. It was, therefore, of interest to add them to the current classification and to remove the lower FP boundary.

7.2.2. Test procedures

In order to commence the experimental procedure, the flashpoint and the parameters required to calculate the Weber ratio should be known. Experimenters can suppose that the reference diameter remains unchanged if the tested liquids are of very similar properties to those tested for this study. Otherwise, as shown in Subsection 4.1.4, correlations may be used, and the liquid class can, therefore, be identified.

This section details the steps to take for each liquid class (quadrants I to IV), followed by detailed procedures (I, II, and A). If it is wished to preheat the liquid and test it at ambient temperatures, it is advised to re-evaluate its physicochemical properties at the required temperature and recalculate its Weber ratio to verify to which class it belongs.

Moreover, if possible, it is preferred that mass flow rate and pressure increase calibration tests be performed before the experimental cycle to determine the mist concentration and the vacuum pressure accurately. If not possible, it is advised to refer to Table IV-1. Furthermore, performing each test at least three times for repeatability is recommended. The sphere should be thoroughly cleaned between each experiment to avoid impurities.

Quadrant I liquid

Among the other liquids, this fuel class is relatively easy to ignite. Figure VII-2 depicts a flowchart detailing a standard procedure to determine the ignition sensitivity and explosion severity of a liquid of Quadrant I.

- If the operating temperature exceeds 27 °C, ***Procedure II*** should be followed using a 100-J spark ignition. If ignition occurs, the experimenter should obtain the LEL, the explosion severity curves, and the P_{max} and dP/dt_{max} at the end of the experiment. In this case, the LEL of the liquids tends to be greater than that of their vapours. According to the predetermined requirements, the experimenter can either suppose that the MIE is less than or equal to 100 J or perform ***Procedure A*** to determine the MIE at a chosen optimal concentration. If no ignition occurs at 100 J, it is advised to perform the same procedure using 5-kJ chemical ignitors and, if it is of interest, assess the optimal concentration at 1 kJ to obtain an MIE approximation. Seen that the sphere is preheated, it is generally unnecessary to test at 10 kJ in the case of no ignition at 5 kJ.
- If the liquid is operated at ambient temperature, ***Procedure I*** should be followed using 100-J spark ignition. The subsequent steps are similar to those mentioned above, except that testing at 10 kJ is advised if no ignition occurs at 5 kJ. This generally does not happen in the case of Quadrant I liquids.

Quadrant II liquid

None of the selected seven liquids fell into this class; therefore, no exact procedure can be given. Nonetheless, such liquids are of the same level of volatility and have more stable droplets than those of quadrant I. Therefore, it is advised to follow the recommendations given for quadrant I liquids to cover all the bases.

Quadrant III liquid

The liquid that belongs to this quadrant (Mobile DTE) did not exhibit any ignition under different configurations. Nevertheless, accidental releases and fires have occurred in cases involving hydraulic oils that might fall into this category (see Section 2.2). Most of such cases occurred at high operating temperatures. It is therefore advised to perform the right half of the flowchart proposed for a Quadrant IV liquid (framed in red) (Figure VII-3).

Quadrant IV liquid

Figure VII-3 portrays a flowchart detailing a proposed experimental cycle to follow for liquids belonging to this quadrant. This proposal was based on the trends observed by biodiesel mist clouds. Nevertheless, additional information may be required. Starting energy of 5 kJ (if handled at ambient temperatures) is advised to test such liquids. If no ignition occurs using 5 kJ and 10 kJ ignitors, it is advised to preheat the sphere to a temperature below the flashpoint to increase the vapour content mildly.

If the operating temperature is above 27 °C, a regular experimental series following procedure II and starting at 100 J is proposed.

Procedure I

This procedure takes place at a controlled ambient temperature. The sphere should be equipped with an insulating system or a temperature control apparatus. Moreover, with some modifications, the experimental cycle should follow the proposed modus operandi introduced in Section 4.6. The turbulence level is set to that corresponding to a compressed air injection pressure, P_{inj}, equal to 3 bar. To cover a complete range of concentrations it is advised to start with 1-s injections (1-s steps) with a maximum t_{inj} of 10 or 12 s, depending on the mass flow rate.

Procedure II

For this procedure, the operating temperature of the liquid should be known. In order to perform the tests at the same temperature, the 20 L sphere should be equipped with a heating system. It is advised to perform temperature calibration tests before the experimental series to ensure that the sphere's centre is heated to the required temperature after a specific time *t*.

A similar procedure should be followed for the experimental cycle, except for preheating the

sphere to the required temperature at which the liquid operates. Between each test, it is recommended to wait at least 5 minutes or the predetermined required time to stabilise the temperature in the sphere.

Procedure A

An optimal mist concentration should be identified first for determining the MIE of the liquid. Explosion severity tests should therefore be conducted before. In the case of a plateau curve, the first concentration corresponding to P_{max} should be considered the optimum. Once the concentration is identified, the high-voltage spark ignition system, presented in Section 3.10, can be installed to determine the MIE. If heating is required, procedure II should be followed for a single concentration. Otherwise, procedure I should be respected. If no ignition occurs at a specific energy, it is advised to redo the same test at least ten times. If no ignition takes place for ten consecutive times, the last tested energy at which ignition occurred is considered the MIE. Attention should be paid to the distance between the two electrodes (6 mm) and the temperature rise between tests. The relative level of humidity of the atmospheric air and the quality of the pressurised air may also affect findings.

The same procedure can be carried out at any other concentration if needed.

7.2.3. Test report

Following the procedures mentioned above should allow the experimenter to determine:

- The explosion severity of the mist cloud, comprising the evolution of P_{ex} and dP/dt_{ex} as a function of the mist concentration, as well as P_{max}, dP/dt_{max}, and their corresponding concentration C_{opt}.
- The LEL of the mist cloud at the operating conditions. This parameter should be determinable from the evolution of P_{ex} and dP/dt_{ex} as a function of the mist concentration.
- The MIE of the mist cloud at the operating conditions.

7.2.4. What is next?

As the previous chapters show, P_{max} and dP/dt_{max} are not absolute values. Moreover, the validity of the cubic law may be doubted due to its various assumptions and requirements, especially regarding the flame thickness. The laminar burning velocity might therefore be determined. To do so, lower turbulence level than those mentioned in Chapter VI should be attained. The fuel-air mixture should also switch to the leaner side. Further investigations are hence required. In addition, liquids belonging to Quadrant II should be tested as no validation has yet been made for the proposed procedure.

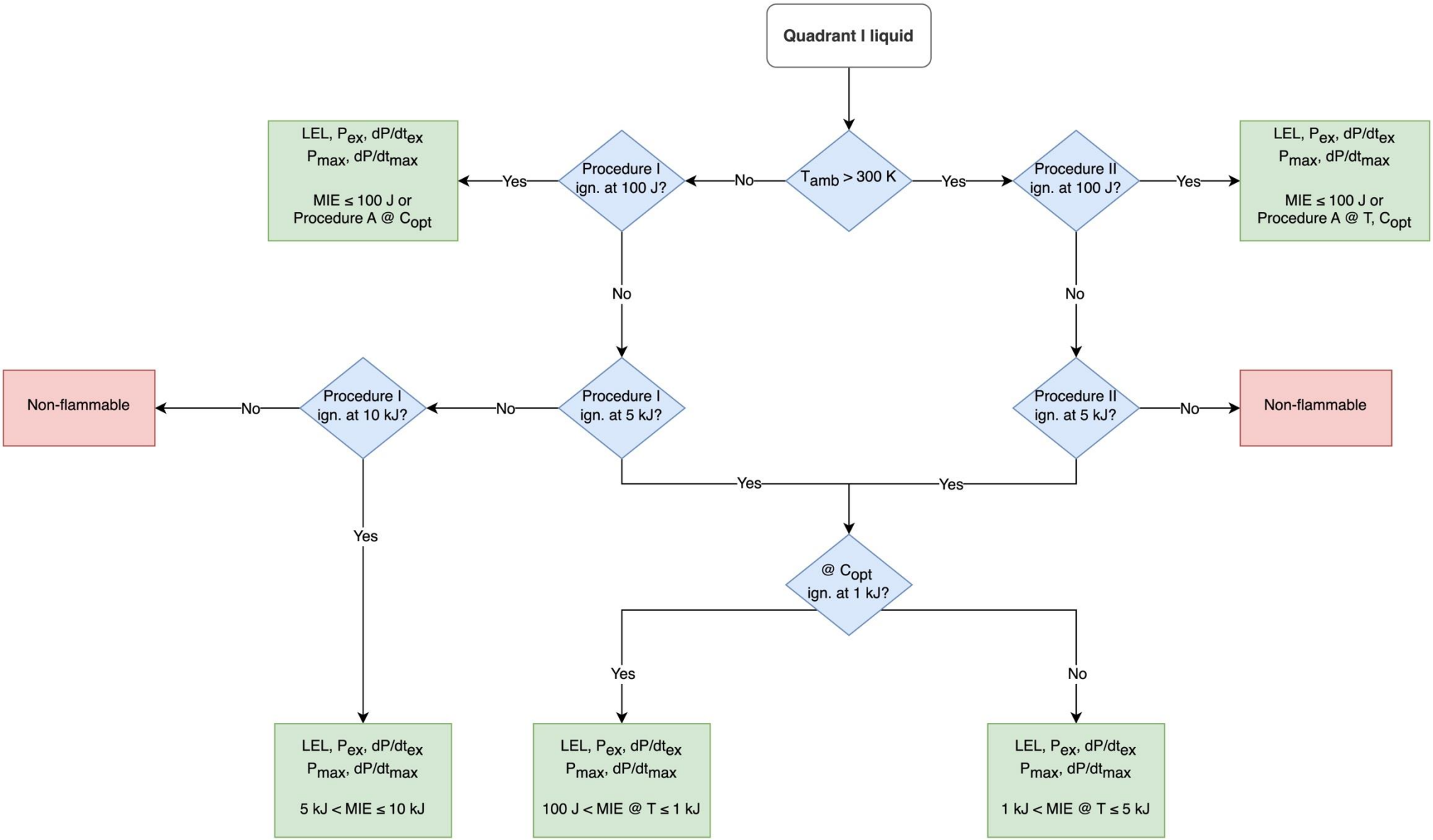

Figure VII-2: Flowchart of a standard procedure to determine the ignition sensitivity and explosion severity of a liquid of Quadrant I

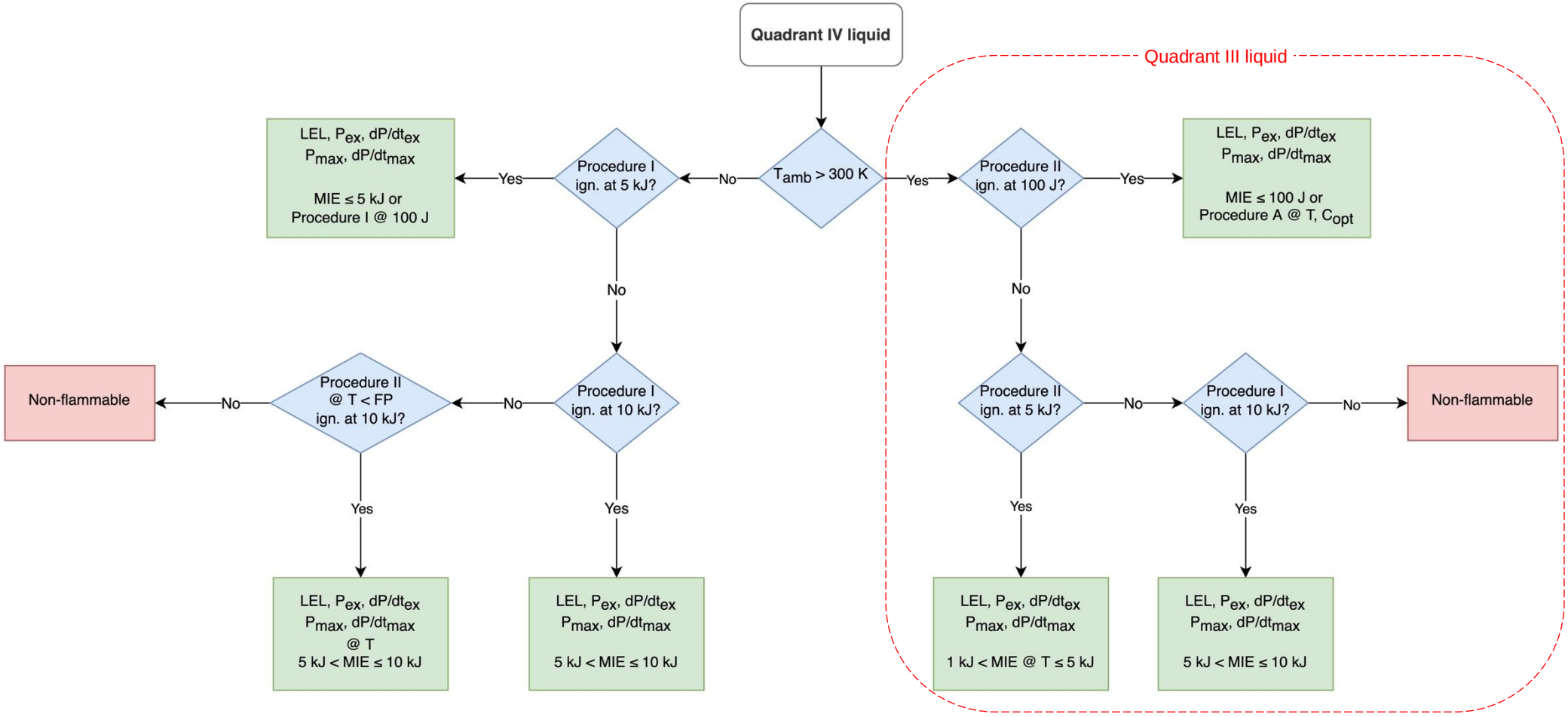

Figure VII-3: Flowchart of a standard procedure to determine the ignition sensitivity and explosion severity of a liquid of Quadrant IV

7.3. Case studies

Since the formation of a mist cloud involves numerous possibilities, the assessment of a mist hazard is given for specific scenarios. The three cases below comprise different ways a mist release can occur under varying conditions. Nevertheless, they are not intended to be practically applied but are only for illustration purposes.

- **Case 1:** a rotary fuel pump filling a **Jet A1** supply tank exhibited corrosion, which led to a Jet A1 mist release. The pump was functioning at 15 bar and was located indoors.
- **Case 2:** an indoor high-pressure injection pipe for a **diesel** engine operating at 800 bar punctured.
- **Case 3:** a ruptured control valve installed in a closed pipe-work system transporting **biodiesel** at 10 bar in an unobstructed heated environment of 80 °C.

Table VII-3 presents the release and location characteristics of the three cases. A succinct hazardous area classification procedure was followed, as proposed by IEC 60079-10-1 (2020), with additional considerations concerning the presence of droplets in the flammable clouds.

The release sources were classified as secondary grade releases because they were accidental discharges that were not expected to occur in regular operations. The LEL values of the liquids were those identified experimentally at the corresponding temperatures. The liquid release rate was determined depending on the orifice shape and size and the pressure differential. Subsequently, it was possible to determine the released jet's atomisation degree by calculating the Ohnesorge ratio discussed in Section 3.3. The HSE Release Class (RC) of each liquid was consequently reattributed. Jet A1 and diesel belonged to RC I and biodiesel to RC III. Following the findings of Gant et al. (2016), releases belonging to RC I with a pressure above 1 bar can be considered prone to creating a hazardous zone; whereas releases of RC III, having an orifice size ≥ 1 mm and a pressure below 20 barg, are believed not capable of creating a hazardous zone.

Depending on the grade of release and the LEL of the clouds, a characteristic ventilation flow rate was determined, supposing that the clouds are formed of fuel vapours. It can be seen that for cases 1 and 2, this characteristic flow rate is much higher than the available air flow rate in the building (0.085 $m^3.s^{-1}$), implying that the degree of dilution is low and classifying the hazardous areas in both cases as Zone 1; while for case 3, as biodiesel belongs to RC III and the degree of dilution is medium, Zone 2 suits as a classification. However, as the clouds would consist of both liquid droplets and a vapour phase, the characteristic ventilation flow rate may not be sufficient to decrease the cloud's concentration to less than its corresponding LEL (here, we note that a

decrease of at least 50 % of the LEL_{mist} should take place. Otherwise, the concentrations can still exceed the LEL_{vapour} in case of heating and evaporation). Ventilation may also increase coalescence or induce more turbulence. Moreover, mist clouds may absorb heat from the surroundings, adding to the vapour cloud. Several scenarios can take place, but it is clear that the LEL is insufficient to classify a hazardous area for mists, and other parameters, such as the ease of ignition, should be considered.

Table VII-3: Release and location characteristics for hazardous area classification

	Case 1	**Case 2**	**Case 3**
Leaked liquid	Jet A1	Diesel B7	Biodiesel B100
LEL ($kg.m^{-3}$) *($\%_{v/v}$)*	0.06 *0.88*	0.08 *0.98*	0.1
Release source	Secondary	Secondary	Secondary
Release rate ($kg.s^{-1}$)	0.19 *5 mm^2 sharp orifice – discharge coefficient 0.75*	1.13 *3 mm^2 rounded orifice – discharge coefficient 0.95*	0.08 *2.5 mm^2 sharp orifice – discharge coefficient 0.75*
Oh/Oh_c	5.5	43.2	1.7
HSE Release Class	I	I	III
Minimum required ventilation flow rate* ($m^3.s^{-1}$)	6 *safety factor 0.5*	28.85 *safety factor 0.5*	1.9 *safety factor 0.5*
Ventilation velocity ($m.s^{-1}$)	0.003 *naturally ventilated building*	0.003 *naturally ventilated building*	0.3 *calm conditions*
Volume under consideration (m^3)	150	150	-
Degree of dilution	Low	Low	Medium
Zone type	Zone 1 or 0	Zone 1 or 0	Zone 2
Zone extent (m)	25	40	15

** safety factor as defined in IEC 60079-10-1 (2020)*

In order to reduce the danger of the zones of cases 1 and 2, inerting could be performed. In the case of Jet A1, for instance, the oxygen percentage can be decreased to values lower than 15.8 $\%_{v/v}$, corresponding to the experimentally-determined LOC. Furthermore, in the context of the study of the fire and explosion risks of mist clouds, the compliance of electrical equipment must be considered cautiously when assessing the ignition probability of an explosive atmosphere created by mists. Industrially, ignition sources such as hot surfaces, sparks of mechanical origin, electrical equipment, flames and static electricity can be encountered, having different ranges of generated energies. In the case of Jet A1, an ignition energy of less than 1 J was identified experimentally, but it can still be considered high (> 200 mJ). Therefore, electrostatic cone discharges, sparks, and propagating brush discharges can easily ignite a Jet A1 mist cloud. These ignition modes must consequently be considered when implementing the ATEX directives. However, corona or single-corona electrostatic discharges, capable of igniting gas clouds that are more sensitive to ignition, are unlikely to ignite such mists. Diesel mists can exhibit the same behaviours as they were ignited with energies as low as 300 mJ. It is, therefore, interesting to list some general principles of prevention and protection against the mentioned potential ignition hazards, such as using conductive, earthed equipment to promote the flow of charges, inserting conductive grounded rods/cables, and maintaining low levels of electrification. As for case 3, the risk of ignition is very low as the MIE of biodiesel is 5 kJ at 27 °C. However, the environment is heated to 80 °C, which means that biodiesel mist might ignite at 100 J. Propagating brush discharges can generate as high as such energies.

Attention should be paid to the possible presence of solvents of more volatile products that, when mixed with the ejected liquid, can considerably decrease its minimum ignition energy. Moreover, because it is not always feasible to completely regulate all potential ignition sources, explosive atmospheres in the supply tank must not be allowed to accumulate, and measurements must be taken constantly. When possible, it is advised to add anti-misting additives, use warning and fluid-stopping systems, and ensure suitable ventilation.

For protection, with the explosion severity parameters determined experimentally, it is also possible to calculate the size of explosion relief vents for a specific volume that needs protection. For comparative purposes, the EN 14491 (2012) standard was used to calculate a vent area for a rectangular enclosure filled with particles, here, mist droplets. An area of 2.4 m^2 was calculated for case 1 and 0.3 m^2 for case 2. The higher explosion severity can explain this difference for Jet A1 mist clouds found in the 20 L sphere. Nevertheless, as the diesel release was more turbulent and concentrated, it would be expected to obtain higher risks. The level of expected turbulence should therefore be taken into account when vent sizing, in addition to the explosion severity.

7.4. Perspectives

Although this study proposes a complete procedure to assess the flammability and explosivity of fuel mists, further work is required.

First, the biphasic flow analysis launched on CFD could carry on in order to predict the local mist concentration in the vicinity of the ignition source. Such computations could also estimate the quantity of liquid lost by sedimentation or sticking to the sphere's walls. Subsequently, a more exact estimate of the maximum injection duration can be identified.

Second, as the 20 L sphere is a relatively small, confined vessel, testing at very high turbulence levels and concurrently avoiding significant rain-out phenomena is not evident. Nevertheless, industrial mist releases tend to start at high turbulence, and then their dispersion becomes somewhat unclear as droplets can get entrained with passing air streams, for instance. This does not eliminate the high fluctuations that can take place at industrial scale releases where non-homogeneous concentration distributions can occur, rain-out phenomena with liquid releases, and impacts on walls and equipment are all possible scenarios. This balance between the industrial level of turbulence and the level employed in a laboratory-scaled apparatus could be discussed further as it may affect the prevention and mitigation measures to be taken. An experimental approach that can cover as many scenarios as possible while remaining controllable and comprehensible is suitable. More nozzle combinations with higher injection pressures could also be tested to explore higher or lower DSDs and turbulence levels.

In addition, difficulty in determining the laminar burning velocity of a mist cloud was perceived in this study. It would therefore be of interest to generate mists at lower levels of turbulence and concentrations in the flame propagation tube to estimate this intrinsic and fundamental parameter that can be used in complex simulations to evaluate the consequences of a mist explosion, especially through the use of CFD codes – FLACS (Liu et al., 2019).

Furthermore, hazardous area classification for mist clouds should depend on not only the corresponding LEL but also the ease of ignition of the liquid in question. Chapter V showed that the fuels can have relatively close LEL but do not readily ignite at the same energies or under the same conditions. Moreover, the ageing and storing conditions should be considered as they affect both the ignition sensitivity and the explosion severity of the cloud.

Concerning multi-component liquids, pre-characterisation could be performed to predict their behaviours better. For instance, nuclear magnetic resonance (NMR) spectroscopy could be performed to approximate their carbon content better, and thermogravimetric analysis (TGA) could be interesting to examine the volatility characteristics as they directly influence the ignition

behaviour of the fuel mist. An explosion model can therefore be developed based on such characteristics to predict better the pressure-time evolution encountered when the mist is ignited.

Finally, the evaporation model presented in this study was based on several assumptions that might not entirely reflect reality. One interesting approach would be to consider the presence of fuel vapour in the sphere before the beginning of the simultaneous evaporation phase. Indeed, as a mist injection can last for 10 seconds, for instance, initially-injected droplets would start evaporation before, increasing the vapour content and the possibility of saturation before the calculated time. Moreover, the model should be more accommodating to multi-component liquids by integrating their compositions (approximately) in calculations of the Spalding number and the Sherwood number, as the components would have different diffusivities.

As it is difficult to define the limits of a mist cloud, it is also challenging to define a standard without limitations, but one has to start somewhere! This study can therefore be the starting point through which future studies can pass to establish better understandings and procedures to evaluate the flammability and explosivity of fuel mists.

CONCLUSION (VERSION FRANÇAISE)

Cette étude avait pour but de proposer un nouveau protocole d'essai pour évaluer l'inflammabilité et l'explosivité des nuages de brouillard d'hydrocarbures tout en examinant la phénoménologie connexe. En outre, elle visait à susciter l'intérêt pour les rejets accidentels qui pourraient parfois être négligés et à lever le brouillard sur ce sujet " brumeux ". Le manuscrit étant terminé, ce chapitre répond à certaines questions essentielles posées tout au long de l'étude et résume les principaux résultats. Dans les sections suivantes, les procédures et mécanismes mis en œuvre sont d'abord brièvement examinés, et un protocole prénormatif complet basé sur une classification des liquides est proposé, suivi de mesures de prévention conseillées. Quelques cas industriels illustratifs sont ensuite analysés, et les perspectives actuelles sont mises en évidence.

Révision des mécanismes mis en œuvre

Comme mentionné dans l'introduction de ce manuscrit et dans le chapitre II, les types de dégagement de brouillard inflammable ne sont ni bien classés ni évalués explicitement par les réglementations actuelles. En effet, il y a un manque de données scientifiques et d'approches quantitatives bien établies pour évaluer correctement les explosions de brouillard. L'objectif de cette étude était donc de combler cette lacune en proposant une méthode d'essai pré-normative qui permettra à la fois d'évaluer plus précisément la phénoménologie dans un environnement confiné et de fournir des données de sécurité reproductibles et fiables.

Plusieurs étapes ont été franchies pour proposer une procédure d'essai complète (figure VII 1), notamment la sélection d'un ensemble pertinent de combustibles et d'un système de génération de brouillard contrôlable et adaptable tout en produisant des tailles de gouttelettes, des concentrations et des niveaux de turbulence appropriés. Les expériences de caractérisation ont permis de quantifier ces paramètres avant de passer à l'étape d'inflammation du brouillard. Par la suite, comme les équipements et les logiciels existants ne sont pas encore adaptés à un essai d'explosion de brouillard, un système de contrôle et d'acquisition de données a été développé. Certaines modifications ont été apportées au récipient d'explosion, et un système d'inflammation par étincelle à haute tension a été conçu pour évaluer l'EMI des nuages de brouillard. De plus, des tests de calibration et de validation ont été effectués, établissant un modus operandi complet. Ce dernier a été suivi, et la sensibilité à l'inflammation (EMI, LIE et CLO) et la sévérité d'explosion (P_{ex}, dP/dt_{ex}, P_{max}, dP/dt_{max}) des combustibles sélectionnés ont été mesurées dans des conditions ambiantes et des conditions de fonctionnement variables dans un seul appareil.

Les sections suivantes présentent brièvement les principaux résultats obtenus à chaque étape de cette étude.

Mise en place et protocole opératoire

Pour cette étude, sept fluides ont été sélectionnés et classés suivant un système de classification des liquides proposé par le Health and Safety Executive comme suit : Jet A1, diesel et LFO dans la classe de rejet I (plus volatile et plus atomisant), biodiesel dans la classe de rejet IV (moins volatile et plus atomisant), et Mobil DTE dans la classe de rejet III (moins volatile et moins atomisant). L'éthanol et l'isooctane, dont le point d'éclair est inférieur à 32 °C, n'ont pas été classés dans ce système. Une buse de pulvérisation à deux fluides basée sur une jonction Venturi a été choisie comme système adéquat de génération de brouillard convenant à un récipient d'essai confiné et relativement petit. Trois jeux de buses ont été principalement utilisés, permettant de modifier la concentration du brouillard, le niveau de turbulence et la distribution de la taille des gouttelettes. Un système de contrôle et d'acquisition de données avec un logiciel personnalisé a été utilisé pour contrôler les injections de liquide et d'air, l'activation de la source d'allumage et le début de l'acquisition de données enregistrant l'évolution pression-temps.

Sensibilité à l'inflammation

La sensibilité à l'inflammation des nuages de brouillard a été évaluée en réalisant trois types d'essais, dont la détermination de l'énergie minimale d'inflammation (EMI), de la limite inférieure d'explosion (LIE) et de la concentration limite en oxygène (CLO).

À T = 27 °C et en utilisant le jeu de buses N1, les sept fluides ont pu être divisés en quatre groupes d'EMI. L'éthanol et l'isooctane étaient les plus faciles à enflammer, avec une EMI inférieure à 100 mJ. Le kérosène Jet A1, le diesel et le LFO ont montré un comportement intermédiaire, dépendant de leurs conditions de vieillissement et de stockage, mais les trois carburants ont présenté une inflammation avec des EMI inférieurs à 1 J. Enfin, le biodiesel et Mobil DTE ont été les plus difficiles à enflammer, avec des EMI atteignant 5000 J. Néanmoins, un léger préchauffage du liquide et/ou du récipient d'explosion a facilité l'inflammation de tous les fluides, à l'exception de Mobil DTE, qui ne s'est pas enflammé sous différentes configurations.

La LIE a également été déterminée en conditions contrôlées, et il a été vu que, dans la plupart des cas, il serait plus conservateur de prendre la LIE des vapeurs du combustible comme référence pour évaluer l'étendue d'une zone dangereuse. Néanmoins, certains hydrocarbures, tels que le biodiesel, sont supposés être non volatils/non inflammables sans aucune spécification dans leur FDS. Pourtant, une LIE de 103 $g.m^{-3}$ a été obtenue. Il est donc intéressant d'évaluer la LIE dans tous les cas.

La CLO était un paramètre supplémentaire qui a été déterminé pour l'éthanol et Jet A1 de gouttelettes de 8-10 µm pour une gamme de concentrations. Les résultats ont montré que les brouillards de Jet A1 générés avec le jeu de buses N1 ont une CLO de 15,8 $\%_{v/v}$, correspondant à

une concentration de brouillard de 144 $g.m^{-3}$; alors que les brouillards d'éthanol ont une CLO de 13,1 $\%_{v/v}$, correspondant à une concentration de brouillard de 110 $g.m^{-3}$.

Sévérité d'explosion

L'évaluation de la sévérité d'explosion des nuages de brouillard d'hydrocarbures a également été effectuée dans la sphère d'explosion de 20 L dans des conditions variables. On a constaté que pour la plupart des combustibles, des courbes de sévérité en forme de plateau ont été obtenues, ce qui montre qu'il serait difficile de déterminer la limite supérieure d'explosivité (LSE) à l'aide de cet appareil en raison de la recirculation éventuelle et des phénomènes simultanés de rain-out et de vaporisation du brouillard injecté. Il est également apparu que la nature chimique des combustibles affectait significativement les mesures d'explosivité, ce qui a conduit à une classification basée sur l'indice de déflagration. En effet, si l'on appliquait la loi cubique, les hydrocarbures étaient classés en quatre classes de déflagration.

Après avoir validé que la surpression maximale d'explosion, P_{max}, et la vitesse maximale de montée en pression d'explosion, dP/dt_{max}, étaient atteignables avec les appareils et équipements d'essai employés, l'influence de plusieurs facteurs a été étudiée. Il est apparu que la gravité de l'explosion, ainsi que la sensibilité à l'inflammation, diminuaient avec l'augmentation du diamètre des gouttelettes. L'effet le plus notable a été observé sur la vitesse de montée en pression, ce qui montre que la dynamique de l'écoulement du brouillard influence facilement la cinétique de la réaction. En plus du DSD, la température initiale a affecté la gravité de l'explosion dans une certaine mesure. En effet, lorsque la sphère a été préchauffée à des températures supérieures au point d'éclair, l'influence sur la surpression de l'explosion a commencé à diminuer. Ce phénomène était lié à la saturation à l'intérieur de la sphère de 20 L et a été prouvé en utilisant le modèle d'évaporation proposé. Cependant, une influence plus significative a continué à se produire sur la vitesse de montée en pression.

L'influence de l'énergie d'inflammation sur la sévérité d'explosion a également été évaluée en comparant des amorceurs chimiques de 100 J et de 5 KJ. On a constaté que pour les brouillards d'hydrocarbures qui se sont enflammés avec des inflammateurs de 100 J, l'augmentation de l'énergie à 5 kJ a conduit à des valeurs similaires ou inférieures des paramètres de sévérité d'explosion. Cela était lié à la forte turbulence créée par les inflammateurs de 5 kJ, qui a pu modifier la distribution de la concentration dans le nuage de brouillard. Néanmoins, dans le cas du biodiesel, par exemple, aucune inflammation ne s'est produite à 100 J, contrairement à l'utilisation de 5 kJ. Cela implique que l'augmentation de l'énergie d'inflammation n'est nécessaire que lorsque aucune inflammation ne se produit à 100 J.

D'autres facteurs d'influence, tels que le niveau de turbulence, la teneur en vapeur et l'ajout de

gaz inflammables, ont également été examinés et ont montré des effets considérables sur la sévérité d'explosion. Par conséquent, il est vital d'assurer un environnement bien contrôlé lors de la réalisation de telles expériences.

Des tests de propagation de flamme ont également été réalisés dans deux appareils : le tube de propagation de flamme et la sphère ouverte. Ces tests ont permis de mieux comprendre la phénoménologie des explosions de brouillard. De plus, ils ont permis de confirmer l'influence du rayonnement et de l'étirement de la flamme sur la sévérité d'explosion. Ces tests peuvent être utilisés pour déterminer les propriétés intrinsèques, en complément de celles déterminées dans la sphère de 20 L, comme le montre la figure VII-1.

Cette étude a donc permis de développer un dispositif capable de tester la sensibilité à l'inflammation et la sévérité d'explosion et de benchmarker les nuages de brouillard de manière potentiellement standardisable, ce qui n'a jamais été fait à notre connaissance.

Proposition d'un standard

Un système de classification des liquides a été proposé sur la base de la classification du HSE. Ce système divisait les liquides en quatre quadrants en fonction de leur point d'éclair et de la stabilité des gouttelettes lors de l'atomisation secondaire (Tableau VII-2). Les étapes à suivre pour chaque classe de liquide (quadrants I à IV) et les procédures détaillées (I, II et A) pour évaluer la sensibilité à l'inflammation et la sévérité d'explosion des nuages de brouillard ont été détaillées et représentées dans les Figures VII-2 et VII-3.

Pour commencer la procédure expérimentale, il faut connaître le point d'éclair et les paramètres nécessaires au calcul du rapport Weber. Les expérimentateurs peuvent supposer que le diamètre de référence reste inchangé si les liquides testés ont des propriétés très similaires à celles des liquides testés pour cette étude. Dans le cas contraire, comme indiqué dans la sous-section 4.1.4, des corrélations peuvent être utilisées, et la classe de liquide peut donc être identifiée.

De plus, si cela est possible, il est préférable que des tests d'étalonnage du débit massique et de l'augmentation de la pression soient effectués avant le cycle expérimental afin de déterminer avec précision la concentration du brouillard et la pression du vide. Si ce n'est pas possible, il est conseillé de se référer au tableau IV 1. En outre, il est recommandé d'effectuer chaque test au moins trois fois pour assurer la répétabilité. La sphère doit être soigneusement nettoyée entre chaque expérience pour éviter les impuretés.

Perspectives

Bien que cette étude propose une procédure complète pour évaluer l'inflammabilité et l'explosivité des brouillards d'hydrocarbures, des travaux supplémentaires sont nécessaires.

Tout d'abord, l'analyse de l'écoulement biphasique lancée sur CFD pourrait être poursuivie afin de prédire la concentration locale du brouillard à proximité de la source d'inflammation. Ces calculs pourraient également estimer la quantité de liquide perdue par sédimentation ou collage aux parois de la sphère. Par la suite, une estimation plus précise de la durée maximale d'injection peut être identifiée.

Deuxièmement, la sphère de 20 litres étant un récipient relativement petit et confiné, il n'est pas évident d'effectuer des essais à des niveaux de turbulence très élevés tout en évitant des phénomènes de rain-out importants. Néanmoins, les rejets de brouillard industriel ont tendance à commencer à des niveaux de turbulence élevés, puis leur dispersion devient quelque peu incertaine, car les gouttelettes peuvent être entraînées par les courants d'air qui passent, par exemple. Cela n'élimine pas les fortes fluctuations qui peuvent avoir lieu lors de rejets à l'échelle industrielle où des distributions de concentration non homogènes peuvent se produire, des phénomènes de rain-out avec des rejets liquides, et des impacts sur les murs et les équipements sont tous des scénarios possibles. Cet équilibre entre le niveau industriel de turbulence et le niveau employé dans un appareil à l'échelle du laboratoire pourrait faire l'objet d'une discussion plus approfondie car il peut affecter les mesures de prévention et d'atténuation à prendre. Une approche expérimentale qui peut couvrir autant de scénarios que possible tout en restant contrôlable et compréhensible est appropriée. Davantage de combinaisons de buses avec des pressions d'injection plus élevées pourraient également être testées pour explorer des distributions de taille de gouttelettes et des niveaux de turbulence plus ou moins élevés.

En outre, la difficulté de déterminer la vitesse de combustion laminaire d'un nuage de brouillard a été perçue dans cette étude. Il serait donc intéressant de générer des brouillards à des niveaux de turbulence et de concentrations plus faibles dans le tube de propagation de flamme afin d'estimer ce paramètre intrinsèque et fondamental qui peut être utilisé dans des simulations complexes pour évaluer les conséquences d'une explosion de brouillard, notamment par l'utilisation de codes CFD - FLACS (Liu et al., 2019).

En outre, la classification des zones dangereuses pour les nuages de brouillard devrait dépendre non seulement de la LIE correspondante, mais aussi de la facilité d'inflammation du liquide en question. Le chapitre V a montré que les combustibles peuvent avoir des LIE relativement proches mais ne s'enflamment pas facilement aux mêmes énergies ou dans les mêmes conditions. De plus, les conditions de vieillissement et de stockage doivent être prises en compte car elles

affectent à la fois la sensibilité à l'inflammation et la gravité de l'explosion du nuage.

En ce qui concerne les liquides multi-composants, une pré-caractérisation pourrait être effectuée afin de mieux prévoir leur comportement. Par exemple, la spectroscopie de résonance magnétique nucléaire (RMN) pourrait être réalisée pour mieux évaluer leur teneur en carbone, et l'analyse thermogravimétrique (ATG) pourrait être intéressante pour examiner les caractéristiques de volatilité, car elles influencent directement le comportement d'inflammation du brouillard. Un modèle d'explosion peut donc être développé sur la base de ces caractéristiques pour mieux prédire l'évolution pression-temps rencontrée lors de l'inflammation du brouillard.

Enfin, le modèle d'évaporation présenté dans cette étude était basé sur plusieurs hypothèses qui pourraient ne pas refléter entièrement la réalité. Une approche intéressante serait de considérer la présence de vapeur de carburant dans la sphère avant le début de la phase d'évaporation simultanée. En effet, comme une injection de brouillard peut durer 10 secondes, par exemple, les gouttelettes initialement injectées commenceraient à s'évaporer avant, ce qui augmenterait la teneur en vapeur et la possibilité de saturation avant le temps calculé. En outre, le modèle devrait être plus accommodant pour les liquides multi-composants en intégrant leurs compositions (approximativement) dans les calculs du nombre de Spalding et du nombre de Sherwood, car les composants auraient des diffusivités différentes.

Comme il est difficile de définir les limites d'un nuage de brouillard, il est également difficile de définir une norme sans limites, mais il faut bien commencer quelque part ! Cette étude peut donc être le point de départ par lequel les études futures pourront passer pour établir de meilleures compréhensions et procédures pour évaluer l'inflammabilité et l'explosivité des brouillards d'hydrocarbures.

References

Addai, E.K., 2016. Investigation of explosion characteristics of multiphase fuel mixtures with air. Western Engineering, Inc, Powell, Wyoming.

Addai, E.K., Clouthier, M., Amyotte, P., Safdar, M., Krause, U., 2019. Experimental investigation of limiting oxygen concentration of hybrid mixtures. Journal of Loss Prevention in the Process Industries 57, 120–130. https://doi.org/10.1016/j.jlp.2018.11.016

Addai, E.K., Gabel, Dieter, Krause, Ulrich, 2016. Models to estimate the lower explosion limits of dusts, gases and hybrid mixtures. Chemical Engineering Transactions 48, 313–318. https://doi.org/10.3303/CET1648053

Aggarwal, S.K., 1998. A review of spray ignition phenomena: Present status and future research. Progress in Energy and Combustion Science 24, 565–600. https://doi.org/10.1016/S0360-1285(98)00016-1

Aggarwal, S.K., Sirignano, W.A., 1986. Ignition of Polydisperse Sprays: Importance of D20. Combustion Science and Technology 46, 289–300. https://doi.org/10.1080/00102208608959804

Alkidas, A.C., 1981. The influence of size-distribution parameters on the evaporation of polydisperse dilute sprays. International Journal of Heat and Mass Transfer 24, 1913–1923. https://doi.org/10.1016/0017-9310(81)90114-9

Andrews, G.E., Bradley, D., 1972. Determination of burning velocities: A critical review. Combustion and Flame 18, 133–153. https://doi.org/10.1016/S0010-2180(72)80234-7

Antony, J., 2014. 6 - Full Factorial Designs, in: Antony, J. (Ed.), Design of Experiments for Engineers and Scientists (Second Edition). Elsevier, Oxford, pp. 63–85. https://doi.org/10.1016/B978-0-08-099417-8.00006-7

Ashgriz, N. (Ed.), 2011. Handbook of Atomization and Sprays: Theory and Applications. Springer US.

ASTM D3278-21, 2021. Standard Test Methods for Flash Point of Liquids by Small Scale Closed-Cup Apparatus.

ASTM E582-21, 2021. Standard Test Method for Minimum Ignition Energy and Quenching Distance in Gaseous Mixtures.

ASTM E659-15, 2015. Standard Test Method for Autoignition Temperature of Chemicals.

ASTM E681-09, 2015. Standard Test Method for Concentration Limits of Flammability of Chemicals (Vapors and Gases).

ASTM E1226-19, 2019. Standard Test Method for Explosibility of Dust Clouds.

ASTM E1491-06, 2019. Standard Test Method For Minimum Autoignition Temperature Of Dust Clouds.

ASTM E1515-14, 2014. Standard Test Method for Minimum Explosible Concentration of Combustible Dusts.

ASTM E2019-03, 2019. Standard Test Method for Minimum Ignition Energy of a Dust Cloud in Air.

Atkinson, G., 2017. Buncefield: Lessons learned on emergency preparedness. Loss Prevention Bulletin 23–28.

Avvaru, B., Patil, M.N., Gogate, P.R., Pandit, A.B., 2006. Ultrasonic atomization: Effect of liquid phase properties. Ultrasonics 44, 146–158. https://doi.org/10.1016/j.ultras.2005.09.003

Bai, C., Wang, Y., 2015. Study of the explosion parameters of vapor–liquid diethyl ether/air mixtures. Journal of Loss Prevention in the Process Industries 38, 139–147. https://doi.org/10.1016/j.jlp.2015.09.007

Ballal, D.R., Lefebvre, A.H., 1981a. A general model of spark ignition for gaseous and liquid fuel-air mixtures. Symposium (International) on Combustion, Eighteenth Symposium (International) on Combustion 18, 1737–1746. https://doi.org/10.1016/S0082-0784(81)80178-6

Ballal, D.R., Lefebvre, A.H., 1981b. Flame propagation in heterogeneous mixtures of fuel droplets, fuel vapor and air. Symp. (Int.) Combust., (Proc.); (United States).

Ballal, D.R., Lefebvre, A.H., 1978. Ignition and flame quenching of quiescent fuel mists. Proceedings of the Royal Society of London. A. Mathematical and Physical Sciences 364, 277–294. https://doi.org/10.1098/rspa.1978.0201

Bane, S.P.M., Ziegler, J.L., Boettcher, P.A., Coronel, S.A., Shepherd, J.E., 2013. Experimental investigation of spark ignition energy in kerosene, hexane, and hydrogen. Journal of Loss Prevention in the Process Industries, Selected Papers from the Eighth International Symposium on Hazards, Prevention, and Mitigation of Industrial Explosions (Yokohama, Japan, 5–10 September 2010) 26, 290–294. https://doi.org/10.1016/j.jlp.2011.03.007

Banerjee, R., 2013. Numerical investigation of evaporation of a single ethanol/iso-octane droplet. Fuel 107, 724–739. https://doi.org/10.1016/j.fuel.2013.01.003

Bettis, R., Burrell, G., Gant, S., Coldrick, S., 2017. Area classification for oil mists - final report of a Joint Industry Project. RR1107 HSL report, UK.

Birch, A.D., Brown, D.R., Dodson, M.G., 1981. Ignition probabilities in turbulent mixing flows. Symposium (International) on Combustion, Eighteenth Symposium (International) on Combustion 18, 1775–1780. https://doi.org/10.1016/S0082-0784(81)80182-8

Boileau, M., 2007. Simulation aux grandes échelles de l'allumage diphasique des foyers aéronautiques 237.

Borghi, R., Champion, M., 2000. Modélisation et théorie des flammes. Editions TECHNIP.

Bowen, P.J., Bull, D.C., Prothero, A., Rowson, J.J., 1997. Deflagration of Hydrocarbon Aerosol Fuels. Combustion Science and Technology 130, 25–47. https://doi.org/10.1080/00102209708935736

Bowen, P.J., Cameron, L.R.J., 1999. Hydrocarbon Aerosol Explosion Hazards: A Review. Process Safety and Environmental Protection 77, 22–30. https://doi.org/10.1205/095758299529749

Bowen, P.J., Shirvill, L.C., 1994. Pressurised atomisation of high flashpoint liquids - implications for hazardous area classification, in: IChemE Symposium Series No. 134. p. 15.

Braconnier, A., 2020. Étude expérimentale de la combustion d'une particule d'aluminium isolée : influence de la pression et de la composition de l'atmosphère oxydante (These de doctorat). Orléans.

Bradley, D., 2000. Flame Propagation in a Tube: The Legacy of Henri Guenoche. Combustion Science and Technology 158, 15–33. https://doi.org/10.1080/00102200008947325

Bradley, D., Lawes, M., Liao, S., Saat, A., 2014. Laminar mass burning and entrainment velocities and flame instabilities of i-octane, ethanol and hydrous ethanol/air aerosols. Combustion and Flame 161, 1620–1632. https://doi.org/10.1016/j.combustflame.2013.12.011

Britton, L.G., 2002. Using heats of oxidation to evaluate flammability hazards. Proc. Safety prog. 21, 31–54. https://doi.org/10.1002/prs.680210108

Britton, L.G., Harrison, B.K., 2018. Minimum explosible concentrations of mist and dust clouds. Process Safety Progress 37, 4–17. https://doi.org/10.1002/prs.11959

Buckingham, E., 1914. On Physically Similar Systems; Illustrations of the Use of Dimensional Equations. Phys. Rev. 4, 345–376. https://doi.org/10.1103/PhysRev.4.345

Burgoyne, J.H., 1963. The flammability of mists and sprays. Proc. 2nd Symp. on Chemical Process Hazards 1–5.

Burgoyne, J.H., 1957. Mist and spray explosions. Chemical Engineering Progress 53, 121–124.

Burgoyne, J.H., Cohen, L., 1954. The Effect of Drop Size on Flame Propagation in Liquid Aerosols. Proceedings of the Royal Society of London. Series A, Mathematical and Physical Sciences 225, 375–392.

Burrell, G., Gant, S., 2017. Liquid classification for flammable mists (No. RR1108). Health and Safety Executive.

Cameron, L.R.J., Bowen, P.J., 2001. Novel Cloud Chamber Design for 'Transition Range' Aerosol Combustion Studies. Process Safety and Environmental Protection 79, 197–205. https://doi.org/10.1205/095758201750362235

Cammarota, F., Di Benedetto, A., Di Sarli, V., Salzano, E., 2019. Influence of initial temperature and pressure on the explosion behavior of n-dodecane/air mixtures. Journal of Loss Prevention in the Process Industries 62, 103920. https://doi.org/10.1016/j.jlp.2019.103920

Čekalin, E.K., 1961. Propagation of flame in turbulent flow of two-phase fuel-air mixture. Symposium (International) on Combustion, Eighth Symposium (International) on Combustion 8, 1125–1129. https://doi.org/10.1016/S0082-0784(06)80610-7

CEN/TR 15281, 2006. Guidance on Inerting for the Prevention of Explosions.

Chan, S.H., 1996. Transport Phenomena in combustion. Taylor & Francis.

Chiu, H.H., Kim, H.Y., Croke, E.J., 1982. Internal group combustion of liquid droplets. Symposium (International) on Combustion 19, 971–980. https://doi.org/10.1016/S0082-0784(82)80273-7

Chiu, H.H., Liu, T.M., 1977. Group Combustion of Liquid Droplets. Combustion Science and Technology 17, 127–142. https://doi.org/10.1080/00102207708946823

Chomiak, J., Jarosiński, J., 1982. Flame quenching by turbulence. Combustion and Flame 48, 241–249. https://doi.org/10.1016/0010-2180(82)90131-6

Chong, C.T., Ng, J.-H., 2021. Chapter 4 - Combustion performance of biojet fuels, in: Chong, C.T., Ng, J.-H. (Eds.), Biojet Fuel in Aviation Applications. Elsevier, pp. 175–230. https://doi.org/10.1016/B978-0-12-822854-8.00002-0

Chot-Plassot, P., Vignes, A., Murillo, C., Lacome, J.-M., El-Zahlanieh, S., Bardin-Monnier, N., Dufaud, O., 2022. Combining CFD and experimental approaches to optimize a spray release in a 20 L sphere. Chemical Engineering Transactions 90, 397–402. https://doi.org/10.3303/CET2290067

Clavin, P., 1985. Dynamic behavior of premixed flame fronts in laminar and turbulent flows. Progress in Energy and Combustion Science 11, 1–59. https://doi.org/10.1016/0360-1285(85)90012-7

Cook, S.J., Cullis, C.F., Good, A.J., 1977. The measurement of the flammability limits of mists. Combustion and Flame 30, 309–317. https://doi.org/10.1016/0010-2180(77)90079-7

Coward, H., Jones, G., 1952. Limits of Flammability of Gases and Vapors. undefined.

Cracknell, R., Head, B., Remmert, S., Wu, Y., Prakash, A., Luebbers, M., 2013. Laminar burning velocity as a fuel characteristic: Impact on vehicle performance, in: Internal Combustion Engines: Performance, Fuel Economy and Emissions. Woodhead Publishing, pp. 149–156. https://doi.org/10.1533/9781782421849.4.149

Dahoe, A.E., Cant, R.S., Scarlett, B., 2001. On the Decay of Turbulence in the 20-Liter Explosion Sphere. Flow, Turbulence and Combustion 67, 159–184. https://doi.org/10.1023/A:1015099110942

Dahoe, A.E., de Goey, L.P.H., 2003. On the determination of the laminar burning velocity from closed vessel gas explosions. Journal of Loss Prevention in the Process Industries 16, 457–478. https://doi.org/10.1016/S0950-4230(03)00073-1

Danis, A., 1987. Spark Ignition of Monodisperse Fuel Sprays.

Davis, S., Kelly, S., Somandepalli, V., 2010. Hot Surface Ignition of Performance Fuels. Fire Technol 46, 363–374. https://doi.org/10.1007/s10694-009-0082-z

Di Benedetto, A., Russo, P., 2008. Explosion properties of aerosol/air mixtures 7.

DIN 51794, 2003. Determining the Ignition Temperature of Petroleum Products.

DIN 53015, 2019. Viscometry - Measurement of viscosity using the Hoeppler Falling-Ball Viscometer.

Directive 1999/92/EC, 2000. Directive 1999/92/EC of the European Parliament and of the Council of 16 December 1999 on minimum requirements for improving the safety and health protection of workers potentially at risk from explosive atmospheres (15th individual Directive within the meaning of Article 16(1) of Directive 89/391/EEC), 023.

Directive 2014/34/EU, 2014. Directive 2014/34/EU of the European Parliament and of the Council of 26 February 2014 on the harmonisation of the laws of the Member States relating to equipment and protective systems intended for use in potentially explosive atmospheres (recast) Text with EEA relevance, 096.

Dombrowski, N., Fraser, R.P., 1954. A photographic investigation into the disintegration of liquid sheets. Philosophical Transactions of the Royal Society of London. Series A, Mathematical and Physical Sciences 247, 101–130. https://doi.org/10.1098/rsta.1954.0014

Dombrowski, N., Horne, W., Williams, A., 1974. The Formation and Combustion of Iso-octane Sprays in Hot Gases. Combustion Science and Technology 9, 247–254. https://doi.org/10.1080/00102207408960362

Dufaud, O., Charvet, A., Mougel, G., Luthun, S., Molière, M., Brunello, D., Perrin, L., Delimoges, S., Couchot, M., 2015. Generation, Characterization and Ignition of Lube Oil Mists, in: Volume 4B: Combustion, Fuels and Emissions. American Society of Mechanical Engineers, Montreal, Quebec, Canada. https://doi.org/10.1115/GT2015-43524

Eckhoff, R.K., 2005. Chapter 3 - Explosions in Clouds of Liquid Droplets in Air (Spray/Mist), in: Eckhoff, R.K. (Ed.), Explosion Hazards in the Process Industries. Gulf Publishing Company, pp. 149–173.

Eckhoff, R.K., 1995. Generation, ignition, combustion and explosion of sprays and mists of flammable liquids in air: a literature survey, Offshore Technology Report OTN 95 260, Health and Safety Executive, Bootle, UK.

Eckhoff, R.K., 1984. Use of (dPldt)max from Closed-Bomb Tests for Predicting Violence o f Accidental Dust Explosions in Industrial Plants 10.

Eichhorn, J., 1955. Careful! Mist can explode. Petroleum Refiner 34(11), 194–196.

Elkotb, M.M., Mahdy, M., Montaser, M.E., 1982. Investigation of External-Mixing Air-blast Atomizers, in: Proceedings of the 2nd International Conference on Liquid Atomization and Sprays. Madison, Wisconsin, pp. 107–115.

El-Zahlanieh, S., Dos Santos, I.S., Brunello, D., Tribouilloy, B., Blanchard, C., Koenig, C., Vignes, A., Dufaud, O., 2022a. Mist can explode, but still no standard! Proposal of a combustible sprays test method. Chemical Engineering Transactions 90, 79–84. https://doi.org/10.3303/CET2290014

El-Zahlanieh, S., Dos Santos, I.S., Sivabalan, S., Brunello, D., Tribouilloy, B., Vignes, A., Dufaud, O., 2022b. Finding a way through the “misty” evaluation of the flammability and explosivity of kerosene aerosols. Fuel 328, 125275. https://doi.org/10.1016/j.fuel.2022.125275

El-Zahlanieh, S., Sivabalan, S., Dos Santos, I.S., Tribouilloy, B., Brunello, D., Vignes, A., Dufaud, O., 2022c. A step toward lifting the fog off mist explosions: Comparative study of three fuels. Journal of Loss Prevention in the Process Industries 74, 104656.

https://doi.org/10.1016/j.jlp.2021.104656

EN 1127-1, 2019. Explosive atmospheres - Explosion prevention and protection - Part 1 : basic concepts and methodology.

EN 1839, 2017. Determination of the explosion limits and the limiting oxygen concentration (LOC) for flammable gases and vapours.

EN 13463-1, 2009. Non-electrical equipment for potentially explosive atmospheres - Part 1 : basic method and requirements.

EN 14034-1, 2004. Determination of explosion characteristics of dust clouds - Part 1: Determination of the maximum explosion pressure pmax of dust clouds.

EN 14034-2, 2006. Determination of explosion characteristics of dust clouds - Part 2: Determination of the maximum rate of explosion pressure rise (dp/dt)max of dust clouds.

EN 14034-3, 2006. Determination of explosion characteristics of dust clouds - Part 3: Determination of the lower explosion limit LEL of dust clouds.

EN 14034-4, 2011. Determination of explosion characteristics of dust clouds - Part 4: Determination of the limiting oxygen concentration LOC of dust clouds.

EN 14491, 2012. Dust explosion venting protective systems.

EN 14994, 2007. Gas explosion venting protective systems.

EN 15967, 2022. Determination of maximum explosion pressure and the maximum rate of pressure rise of gases and vapours.

Energy Institute, 2015. Model code of safe practice: Area classification code for installations handling flammable fluids.

Fraser, R.P., Eisenklam, P., 1956. Liquid Atomization and the Drop Size of Sprays. Institution of Chemical Engineers.

Freeston, H.G., Roberts, J.D., Thomas, A., 1956. Crankcase Explosions: An Investigation into Some Factors Governing the Selection of Protective Devices. Proceedings of the Institution of Mechanical Engineers 170, 811–824. https://doi.org/10.1243/PIME_PROC_1956_170_072_02

Friedman, R., Johnston, W.C., 1952. Pressure Dependence of Quenching Distance of Normal Heptane, Iso-Octane, Benzene, and Ethyl Ether Flames. J. Chem. Phys. 20, 919–920. https://doi.org/10.1063/1.1700600

Fuller, L.E., Parks, D.J., Fletcher, E.A., 1969. Flat flames in tubes—easy fundamental flame speed measurements. Combustion and Flame 13, 455–460. https://doi.org/10.1016/0010-2180(69)90084-4

Galmiche, B., 2014. Caractérisation expérimentale des flammes laminaires et turbulentes en expansion. Université d'Orléans.

Gant, S., 2013. Generation of flammable mists from high flashpoint fluids: literature review. Health and Safety Executive, Research Report RR980.

Gant, S., Bettis, R., Coldrick, S., Burrell, G., Santon, R., Fullam, B., Hill, H., Mouzakitis, K., Giles, A., Bowen, P., 2016. Area classification of flammable mists: summary of joint-industry project findings 12.

Gant, S., Giles, A., Bettis, R., Bowen, P., 2020. Flammable mist hazards involving high-flashpoint fluids.

Gieras, M., Klemens, R., Kuhl, A., Oleszczak, P., Trzciński, W., Wolański, P., 2008. Influence of the chamber volume on the upper explosion limit for hexane–air mixtures. Journal of Loss Prevention in the Process Industries 21, 423–436. https://doi.org/10.1016/j.jlp.2008.02.006

Giles, A.P., Kay, P.J., Mouzakitis, K., Bowen, P.J., Crayford, A.P., 2017. On flammability hazards from pressurised high-flashpoint liquid releases. Journal of Loss Prevention in the Process Industries 46, 185–194. https://doi.org/10.1016/j.jlp.2017.01.024

Godsave, G.A.E., 1953. Studies of the combustion of drops in a fuel spray—the burning of single drops of fuel. Symposium (International) on Combustion 4, 818–830. https://doi.org/10.1016/S0082-0784(53)80107-4

Gökalp, I., Chauveau, C., Simon, O., Chesneau, X., 1992. Mass transfer from liquid fuel droplets in turbulent flow. Combustion and Flame 89, 286–298. https://doi.org/10.1016/0010-2180(92)90016-I

Guiberti, T.F., Belhi, M., Damazo, J.S., Kwon, E., Roberts, W.L., Lacoste, D.A., 2020. Quenching distance of laminar methane-air flames at cryogenic temperatures and implications for flame arrester design. Applications in Energy and Combustion Science 1–4, 100001. https://doi.org/10.1016/j.jaecs.2020.100001

Halter, F., 2005. Caractérisation des effets de l'ajout d'hydrogène et de la haute pression dans les flammes turbulentes de prémélange méthane/air (phdthesis). Université d'Orléans.

Halter, F., Tahtouh, T., Mounaïm-Rousselle, C., 2010. Nonlinear effects of stretch on the flame front propagation. Combustion and Flame 157, 1825–1832. https://doi.org/10.1016/j.combustflame.2010.05.013

Han, J., Yamashita, H., Hayashi, N., 2010. Numerical study on the spark ignition characteristics of a methane–air mixture using detailed chemical kinetics: Effect of equivalence ratio, electrode gap distance, and electrode radius on MIE, quenching distance, and ignition delay. Combustion and Flame 157, 1414–1421. https://doi.org/10.1016/j.combustflame.2010.02.021

Hansen, O.R., Gavelli, F., Davis, S.G., Middha, P., 2013. Equivalent cloud methods used for explosion risk and consequence studies. Journal of Loss Prevention in the Process Industries, Papers presented at the 2011 Mary Kay O'Connor Process Safety Center International Symposium 26, 511–527. https://doi.org/10.1016/j.jlp.2012.07.006

Hattwig, M., Steen, H., 2004. Handbook of Explosion Prevention and Protection.

Hayashi, S., Kumagai, S., 1975. Flame propagation in fuel droplet-vapor-air mixtures. Symposium

(International) on Combustion, Fifteenth Symposium (International) on Combustion 15, 445–452. https://doi.org/10.1016/S0082-0784(75)80318-3

Hayashi, S., Kumagai, S., Sakai, T., 1977. Propagation Velocity and Structure of Flames in Droplet-Vapor-Air Mixtures. Combustion Science and Technology 15, 169–177. https://doi.org/10.1080/00102207708946782

IEC 60079-10-1, 2020. Explosive atmospheres – Part 10-1: Classification of areas – Explosive gas atmospheres.

IEC 60079-10-2, 2015. Explosive atmospheres – Part 10-2: Classification of areas – Explosive dust atmospheres.

IEC 60079-32-2, 2015. Explosive atmospheres - Part 32-1: Electrostatic hazards - guidance.

IEC TS 60079-32-1:2013+AMD1:2017, n.d. Explosive atmospheres - Part 32-1: Electrostatic hazards - guidance.

Inamura, T., Nagai, N., 1985. The relative performance of externally and internally-mixed twin-fluid atomizers, in: Proceedings of the 3rd International Conference on Liquid Atomization and Sprays. London, p. IIC/2/1-11.

ISO/IEC 80079-20-1, 2020. Explosive atmospheres — Part 20-1: Material characteristics for gas and vapour classification — Test methods and data.

ISO/IEC 80079-20-2, 2016. Explosive atmospheres — Part 20-2: Material characteristics — Combustible dusts test methods.

Jaworek, A., 2007. Micro- and nanoparticle production by electrospraying. Powder Technology 176, 18–35. https://doi.org/10.1016/j.powtec.2007.01.035

Jespen, T., 2016. ATEX—Explosive Atmospheres: Risk Assessment, Control and Compliance. Springer.

Jones, G.W., Zabetakis, M.G., 1952. RESEARCH ON THE FLAMMABILITY CHARACTERISTICS OF AIRCRAFT FUELS: Defense Technical Information Center, Fort Belvoir, VA.

Karlovitz, B., Denniston, D.W., Wells, F.E., 1951. Investigation of Turbulent Flames. J. Chem. Phys. 19, 541–547. https://doi.org/10.1063/1.1748289

Ko, Y., Anderson, R.W., Arpaci, V.S., 1991. Spark ignition of propane-air mixtures near the minimum ignition energy: Part I. An experimental study. Combustion and Flame 83, 75–87. https://doi.org/10.1016/0010-2180(91)90204-O

Kooij, S., Sijs, R., Denn, M.M., Villermaux, E., Bonn, D., 2018. What Determines the Drop Size in Sprays? Phys. Rev. X 8, 031019. https://doi.org/10.1103/PhysRevX.8.031019

Krishna, K., 2003. Measurement and Prediction of Aerosol Formation for the Safe Utilization of Industrial Fluids.

Krishna, K., Rogers, W.J., Mannan, M.S., 2003. The use of aerosol formation, flammability, and

explosion information for heat-transfer fluid selection. Journal of Hazardous Materials 104, 215–226. https://doi.org/10.1016/S0304-3894(03)00273-5

Kuchta, J., 1968. Review of Ignition and Flammability Properties of Lubricants. U.S. Bureau of Mines.

Kurata, O., Takahashi, S., Uchiyama, Y., 1994. Influence of Preheat Temperature on the Laminar Burning Velocity of Methane-Air Mixtures. SAE Transactions 103, 1766–1772.

Labowsky, M., Rosner, D.E., 1978. "Group" Combustion of Droplets in Fuel Clouds. I. Quasi-steady Predictions, in: Evaporation—Combustion of Fuels, Advances in Chemistry. AMERICAN CHEMICAL SOCIETY, pp. 63–79. https://doi.org/10.1021/ba-1978-0166.ch004

Landry, X., 2007. Étude sur un modèle d'évaporation multicomposants appliqué aux gouttelettes de carburant dans des conditions de moteur diesel. École de technologie supérieure.

Law, C.K., 2006. Combustion Physics. Cambridge University Press, Cambridge.

Lawes, M., Saat, A., 2011. Burning rates of turbulent iso-octane aerosol mixtures in spherical flame explosions. Proceedings of the Combustion Institute 33, 2047–2054. https://doi.org/10.1016/j.proci.2010.05.094

Lee, T.-W., Jain, V., Kozola, S., 2001. Measurements of minimum ignition energy by using laser sparks for hydrocarbon fuels in air: propane, dodecane, and jet-A fuel. Combustion and Flame 125, 1320–1328. https://doi.org/10.1016/S0010-2180(01)00248-6

Lees, P., Gant, S., Bettis, R., Vignes, A., Lacome, J.-M., Dufaud, O., 2019. Review of recent incidents involving flammable mists. IChemE Hazards 29 Conference, Birmingham, UK 23.

Lefebvre, A.H., McDonell, V.G., 2017. Atomization and sprays, Second edition. ed. CRC Press, Taylor & Francis Group, CRC Press is an imprint of the Taylor & Francis Group, an informa business, Boca Raton.

Lemkowitz, S.M., Pasman, H.J., 2014. A Review of the Fire and Explosion Hazards of Particulates. KONA 31, 53–81. https://doi.org/10.14356/kona.2014010

Lewis, B., Elbe, G. von, 2012. Combustion, Flames and Explosions of Gases. Elsevier.

Lewis, B., von Elbe, G., 1961. Combustion, Flames, and Explosions of Gases. Academic Press, New York, London.

Li, Q., Cheng, Y., Huang, Z., 2015. Comparative assessment of the explosion characteristics of alcohol–air mixtures. Journal of Loss Prevention in the Process Industries 37, 91–100. https://doi.org/10.1016/j.jlp.2015.07.003

Lian, P., 2011. Flammability and Combustion Behaviors in Aerosols Formed by Industrial Heat Transfer Fluids Produced by the Electrospray Method.

Lian, P., Mejia, A.F., Cheng, Z., Sam Mannan, M., 2010. Flammability of heat transfer fluid aerosols produced by electrospray measured by laser diffraction analysis. Journal of Loss Prevention in the Process Industries 23, 337–345. https://doi.org/10.1016/j.jlp.2009.11.003

Liao, S.Y., Jiang, D.M., Huang, Z.H., Zeng, K., Cheng, Q., 2007. Determination of the laminar burning velocities for mixtures of ethanol and air at elevated temperatures. Applied Thermal Engineering 27, 374–380. https://doi.org/10.1016/j.applthermaleng.2006.07.026

Lin, B., Wu, Y., Xu, M., Chen, Z., 2021. Experimental investigation on spark ignition and flame propagation of swirling kerosene spray flames. Fuel 303, 121254. https://doi.org/10.1016/j.fuel.2021.121254

Lin, Y.-R., Chen, H., Mashuga, C., Mannan, M.S., 2015. Improved electrospray design for aerosol generation and flame propagation analysis. Journal of Loss Prevention in the Process Industries 38, 148–155. https://doi.org/10.1016/j.jlp.2015.09.011

Liu, E., Liao, Q., Xu, S., 2020. Aerosol Shock Tube Designed for Ignition Delay Time Measurements of Low-Vapor-Pressure Fuels and Auto-Ignition Flow-Field Visualization. Energies 13, 683. https://doi.org/10.3390/en13030683

Liu, W., Ren, H., Cheng, K., 2019. Simulation Analysis of Tunnel Diesel Oil Explosion Based on FLACS. IOP Conf. Ser.: Mater. Sci. Eng. 563, 022045. https://doi.org/10.1088/1757-899X/563/2/022045

Liu, X., Wang, Y., Zhang, Q., 2016. A study of the explosion parameters of vapor–liquid two-phase JP-10/air mixtures. Fuel 165, 279–288. https://doi.org/10.1016/j.fuel.2015.10.081

Liu, X., Zhang, Q., Wang, Y., 2015. Influence of Vapor-Liquid Two-Phase n-Heptane on the Explosion Parameters in Air. Combustion Science and Technology 187, 1879–1904. https://doi.org/10.1080/00102202.2015.1069282

Liu, X., Zhang, Q., Wang, Y., 2014. Influence of Vapor–Liquid Two-Phase n-Hexane/Air Mixtures on Flammability Limit and Minimum Ignition Energy. Ind. Eng. Chem. Res. 53, 12856–12865. https://doi.org/10.1021/ie5023496

M. de Oliveira, P., 2019. Ignition and propagation mechanisms of spray flames. https://doi.org/10.17863/CAM.44744

Ma, T., 2015. Ignitability and Explosibility of Gases and Vapors. Springer New York, New York, NY. https://doi.org/10.1007/978-1-4939-2665-7

Mandato, S., Rondet, E., Delaplace, G., Barkouti, A., Galet, L., Accart, P., Ruiz, T., Cuq, B., 2012. Liquids' atomization with two different nozzles: Modeling of the effects of some processing and formulation conditions by dimensional analysis. Powder Technology 224, 323–330. https://doi.org/10.1016/j.powtec.2012.03.014

Maragkos, A., Bowen, P.J., 2002. Combustion hazards due to impingement of pressurized releases of high-flashpoint liquid fuels. Proceedings of the Combustion Institute, Proceedings of the Combustion Institute 29, 305–311. https://doi.org/10.1016/S1540-7489(02)80041-4

Markstein, G.H., 1964. Nonsteady flame propagation. Published for and on behalf of Advisory Group for Aeronautical Research and Development, North Atlantic Treaty Organization by Pergamon Press; [distributed in the Western Hemisphere by Macmillan, New York, Oxford; New York.

Mashuga, C.V., Crowl, D.A., 2000. Derivation of Le Chatelier's mixing rule for flammable limits. Process Safety Progress 19, 112–117. https://doi.org/10.1002/prs.680190212

McBride, B.J., Gordon, S., 1996. Computer Program for Calculation of Complex Chemical Equilibrium Compositions and Applications II. Users Manual and Program Description.

Mikami, M., Mizuta, Y., Tsuchida, Y., Kojima, N., 2009. Flame structure and stabilization of lean-premixed sprays in a counterflow with low-volatility fuel. Proceedings of the Combustion Institute 32, 2223–2230. https://doi.org/10.1016/j.proci.2008.08.009

Mitu, M., Brandes, E., 2017. Influence of pressure, temperature and vessel volume on explosion characteristics of ethanol/air mixtures in closed spherical vessels. Fuel 203, 460–468. https://doi.org/10.1016/j.fuel.2017.04.124

Mizutani, Y., Nishjmoto, T., 1972. Turbulent Flame Velocities in Premixed Sprays Part I. Experimental Study. Combustion Science and Technology 6, 1–10. https://doi.org/10.1080/00102207208952297

Moesl, K., 2012. On the Formation of Nitrogen Oxides During the Combustion of Partially Pre-Vaporized Droplets.

Motily, A.H., Ryu, J.I., Kim, Keunsoo, Kim, Kenneth, Kweon, C.-B.M., Lee, T., 2021. High-pressure fuel spray ignition behavior with hot surface interaction. Proceedings of the Combustion Institute 38, 5665–5672. https://doi.org/10.1016/j.proci.2020.08.041

Murillo, C., 2016. Experimental and numerical approaches to particles dispersion in a turbulent flow: application to dust explosions 278.

Myers, G.D., Lefebvre, A.H., 1986. Flame propagation in heterogeneous mixtures of fuel drops and air. Combustion and Flame 66, 193–210. https://doi.org/10.1016/0010-2180(86)90091-X

Nakamura, M., Akamatsu, F., Kurose, R., Katsuki, M., 2005. Combustion mechanism of liquid fuel spray in a gaseous flame. Physics of Fluids 17, 123301. https://doi.org/10.1063/1.2140294

Nasr, G.G., Yule, A.J., Bendig, L., 2002. Industrial Sprays and Atomization: Design, Analysis and Applications. Springer-Verlag, London.

Neophytou, A., Mastorakos, E., 2009. Simulations of laminar flame propagation in droplet mists. Combustion and Flame 156, 1627–1640. https://doi.org/10.1016/j.combustflame.2009.02.014

NF/BS CEI EN 50281-2-1, 2000. Electrical apparatus for use in the presence of combustible dust -- Part 2-1: Test methods - Methods for determining the minimum ignition temperatures of dust.

NFPA 68, 2018. Standard on Explosion Protection by Deflagration Venting.

Nicoli, C., Denet, B., Haldenwang, P., 2015. Rich spray-flame propagating through a 2D-Lattice of alkane droplets in air. Combustion and Flame 162, 4598–4611. https://doi.org/10.1016/j.combustflame.2015.09.018

Nolan, D.P., 2014. Chapter 4 - Physical Properties of Hydrocarbons and Petrochemicals, in: Nolan, D.P. (Ed.), Handbook of Fire and Explosion Protection Engineering Principles (Third Edition).

William Andrew Publishing, pp. 55–77. https://doi.org/10.1016/B978-0-323-31301-8.00004-0

Nomura, H., Koyama, M., Miyamoto, H., Ujiie, Y., Sato, J., Kono, M., Yoda, S., 2000. Microgravity experiments of flame propagation in ethanol droplet-vapor-air mixture. Proceedings of the Combustion Institute 28, 999–1005. https://doi.org/10.1016/S0082-0784(00)80307-0

Nunome, Y., Kato, S., Maruta, K., Kobayashi, H., Niioka, T., 2002. Flame propagation of n-decane spray in microgravity. Proceedings of the Combustion Institute 29, 2621–2626. https://doi.org/10.1016/S1540-7489(02)80319-4

Ogle, R.A., 2016. Dust Explosion Dynamics. Elsevier Science.

O'Rourke, P.J., 1981. Collective drop effects on vaporizing liquid sprays. Los Alamos National Lab., NM (USA).

Pande, S.G., Romans, J.B., Little, R.C., 1984. Mist Flammability Studies of Candidate Fire-Resistant Hydraulic Fluids.

Peters, J.E., Mellor, A.M., 1980. An ignition model for quiescent fuel sprays. Combustion and Flame 38, 65–74. https://doi.org/10.1016/0010-2180(80)90037-1

Pinheiro, A.P., Vedovoto, J.M., da Silveira Neto, A., van Wachem, B.G.M., 2019. On ethanol droplet evaporation in the presence of background fuel vapor. Presented at the 29th Conference on Liquid Atomization and Spray Systems, Paris, France, p. 8.

Polymeropoulos, C.E., Das, S., 1975. The effect of droplet size on the burning velocity of kerosene-air sprays. Combustion and Flame 25, 247–257. https://doi.org/10.1016/0010-2180(75)90091-7

Puttick, S., 2008. Liquid mists and sprays flammable below the flash point: the problem of preventative bases of safety 13.

Raffel, M. (Ed.), 2007. Particle image velocimetry: a practical guide, 2nd ed. ed. Springer, Heidelberg ; New York.

Rao, K.V.L., Lefebvre, A.H., 1976. Minimum ignition energies in flowing kerosine-air mixtures. Combustion and Flame 27, 1–20. https://doi.org/10.1016/0010-2180(76)90002-X

Razus, D., Brinzea, V., Mitu, M., Movileanu, C., Oancea, D., 2011. Temperature and pressure influence on maximum rates of pressure rise during explosions of propane–air mixtures in a spherical vessel. Journal of Hazardous Materials 190, 891–896. https://doi.org/10.1016/j.jhazmat.2011.04.018

Richards, G.A., Lefebvre, A.H., 1989. Turbulent flame speeds of hydrocarbon fuel droplets in air. Combustion and Flame 78, 299–307. https://doi.org/10.1016/0010-2180(89)90019-9

Rochette, B., Riber, E., Cuenot, B., 2019. Effect of non-zero relative velocity on the flame speed of two-phase laminar flames. Proceedings of the Combustion Institute 37, 3393–3400. https://doi.org/10.1016/j.proci.2018.07.100

Russo, P., Benedetto, A.D., Sanchirico, R., 2012. Theoretical evaluation of the explosion regimes of

hybrid mixtures. https://doi.org/10.3303/CET1226009

Saat, A., 2010. Fundamental Studies of Combustion of Droplet and Vapour Mixtures.

Sánchez, A.L., Urzay, J., Liñán, A., 2015. The role of separation of scales in the description of spray combustion. Proceedings of the Combustion Institute 35, 1549–1577. https://doi.org/10.1016/j.proci.2014.08.018

Santamaría Ramiro, J.M., Braña Aísa, P.A., 1998. Risk Analysis and Reduction in the Chemical Process Industry. Springer Netherlands, Dordrecht. https://doi.org/10.1007/978-94-011-4936-5

Santandrea, A., 2020. New insights on the explosion severity of nanopowders: a nano-grain of sand in the gears of the standards (phdthesis). Université de Lorraine.

Santandrea, A., Gavard, M., Pacault, S., Vignes, A., Perrin, L., Dufaud, O., 2020. 'Knock on nanocellulose': Approaching the laminar burning velocity of powder-air flames. Process Safety and Environmental Protection 134, 247–259. https://doi.org/10.1016/j.psep.2019.12.018

Santon, R.C., 2009. Mist fires and explosions - an incident survey. IChemE Hazards XXI Symposium & Workshop, Manchester, UK 5.

Schick, R., 2006. Spray Technology Reference Guide: Understanding Drop Size. Spraying System Co.

Schwenzfeuer, K., Glor, M., Gitzi, A., 2001. T5-16 - Relation between Ignition Energy and Limiting Oxygen Concentration for powders, in: Pasman, H.J., Fredholm, O., Jacobsson, A. (Eds.), Loss Prevention and Safety Promotion in the Process Industries. Elsevier Science B.V., Amsterdam, pp. 909–916. https://doi.org/10.1016/B978-044450699-3/50011-2

Scull, W.E., 1951. Relation between inflammables and ignition sources in aircraft environments (Report No. 1091). National Advisory Committee for Aeronautics.

Shaw, A., Epling, W., McKenna, C., Weckman, B., 2010. Evaluation of the Ignition of Diesel Fuels on Hot Surfaces. Fire Technol 46, 407–423. https://doi.org/10.1007/s10694-009-0098-4

Shepherd, J.E., Krok, J.C., Lee, J.J., 1997. Spark Ignition Energy Measurements in Jet A 87.

Shepherd, J.E., Nuyt, C.D., Lee, J.J., 2000. Flash Point and Chemical Composition of Aviation Kerosene (Jet A) 38.

Silvestrini, M., Genova, B., Leon Trujillo, F.J., 2008. Correlations for flame speed and explosion overpressure of dust clouds inside industrial enclosures. Journal of Loss Prevention in the Process Industries 21, 374–392. https://doi.org/10.1016/j.jlp.2008.01.004

Singh, A.K., Polymeropoulos, C.E., 1988. Spark ignition of aerosols. Symposium (International) on Combustion, Twenty-First Symposuim (International on Combustion) 21, 513–519. https://doi.org/10.1016/S0082-0784(88)80280-7

Sirignano, W.A., 2014. Advances in droplet array combustion theory and modeling. Progress in Energy and Combustion Science 42, 54–86. https://doi.org/10.1016/j.pecs.2014.01.002

Sirignano, W.A., 2007. Liquid-fuel burning with nonunitary Lewis number. Combustion and Flame 148, 177–186. https://doi.org/10.1016/j.combustflame.2006.09.009

Sirignano, W.A., Wu, G., 2008. Multicomponent-liquid–fuel vaporization with complex configuration. International Journal of Heat and Mass Transfer 51, 4759–4774. https://doi.org/10.1016/j.ijheatmasstransfer.2008.02.018

Siwek, R., Cesana, C., 1995. Ignition behavior of dusts: Meaning and interpretation. Proc. Safety Prog. 14, 107–119. https://doi.org/10.1002/prs.680140205

Skjold, T., 2014. Flame propagation in dust clouds: Numerical simulation and experimental investigation 46.

Skjold, T., 2003. Selected aspects of turbulence and combustion in 20-litre explosion vessels : development of experimental apparatus and experimental investigation.

Snee, T., Braddock, R., Allen, J., 2016. Spontaneous ignition of gas turbine lubricants at temperatures below their standard auto-ignition temperatures. Health and Safety Executive.

Spalding, D.B., 1979. CHAPTER 3 - DROPLET VAPORISATION I, in: Spalding, D.B. (Ed.), Combustion and Mass Transfer. Pergamon, pp. 59–69. https://doi.org/10.1016/B978-0-08-022106-9.50007-3

Spitzer, S., Askar, E., Krietsch, A., Schröder, V., 2021. Comparative study on standardized ignition sources used for explosion testing. Journal of Loss Prevention in the Process Industries 71, 104516. https://doi.org/10.1016/j.jlp.2021.104516

ST/SG/AC.10/30/Rev.8, 2019. Globally harmonized system of classification and labelling of chemicals (GHS)., 8th revised version. ed. UNITED NATIONS, New York and Geneva.

Sulaiman, S.A., 2006. Burning Rates and Instabilities in the Combustion of Droplet and Vapour Mixtures 222.

Sullivan, M.V., Wolfe, J.K., Zisman, W.A., 1947. Flammability of the Higher Boiling Liquids and Their Mists. Ind. Eng. Chem. 39, 1607–1614. https://doi.org/10.1021/ie50456a021

Sun, K., Zhang, Q., Wang, W., Niu, S., 2022. Experimental study on explosion parameters of ethanol aerosol under high-temperature source ignition. Fuel 311, 122610. https://doi.org/10.1016/j.fuel.2021.122610

Sung, K., Zhang, Q., 2021. Experimental study of the explosion characteristics of isopropyl nitrate aerosol under high-temperature ignition source. Journal of Hazardous Materials 415, 125634. https://doi.org/10.1016/j.jhazmat.2021.125634

Szabová, Z., Kuracina, R., Sahul, M., Mynarz, M., Lepík, P., Kosár, L., 2021. Influence of the Pyrotechnic Igniter Composition Aging on Explosion Parameters of Dispersed Dusts. Applied Sciences 11, 10728. https://doi.org/10.3390/app112210728

Takashi, H., Kimitoshi, T., 2006. LAMINAR FLAME SPEEDS OF ETHANOL, n-HEPTANE, ISO-OCTANE AIR MIXTURES.

Tascón, A., 2018. Influence of particle size distribution skewness on dust explosibility. Powder Technology 338, 438–445. https://doi.org/10.1016/j.powtec.2018.07.044

Taylor, G.I., 1964. Disintegration of water drops in an electric field. Proceedings of the Royal Society of London. Series A. Mathematical and Physical Sciences 280, 383–397. https://doi.org/10.1098/rspa.1964.0151

Thielicke, W., 2021. PIVlab - particle image velocimetry (PIV) tool with GUI [WWW Document]. GitHub. URL https://github.com/Shrediquette/PIVlab/releases/tag/2.53 (accessed 7.1.21).

Thimothée, R., 2017. Experimental characterization of a laminar flame propagation in a two-phase medium (aerosol) in microgravity conditions (Theses). Université d'Orléans.

Torrado, D., 2017. Effect of carbon black nanoparticles on the explosion severity of gas mixtures. Université de Lorraine.

Tuntivoranukul, K., Vallikul, P., Fungtammasan, B., Yongyingsakthavorn, P., Dumouchel, C., 2010. Application of the D2-Law to Determine Time Evolution and Burn-Out Time of Evaporating Biodiesel Spray Drop-Size Distribution 5.

van Lipzig, J.P.J., Nilsson, E.J.K., de Goey, L.P.H., Konnov, A.A., 2011. Laminar burning velocities of n-heptane, iso-octane, ethanol and their binary and tertiary mixtures. Fuel 90, 2773–2781. https://doi.org/10.1016/j.fuel.2011.04.029

Verwey, C., Birouk, M., 2017. Experimental investigation of the effect of droplet size on the vaporization process in ambient turbulence. Combustion and Flame 182, 288–297. https://doi.org/10.1016/j.combustflame.2017.04.027

von Pidoll, U., 2001. The ignition of clouds of sprays, powders and fibers by flames and electric sparks. Journal of Loss Prevention in the Process Industries 14, 103–109. https://doi.org/10.1016/S0950-4230(00)00035-8

Vukadinovic, V., Habisreuther, P., Zarzalis, N., 2013. Influence of pressure and temperature on laminar burning velocity and Markstein number of kerosene Jet A-1: Experimental and numerical study. Fuel 111, 401–410. https://doi.org/10.1016/j.fuel.2013.03.076

Wang, L., Wu, Z., Ahmed, A., Badra, J.A., Sarathy, S.M., Roberts, W.L., Fang, T., 2019. Auto-ignition of direct injection spray of light naphtha, primary reference fuels, gasoline and gasoline surrogate. Energy 170, 375–390. https://doi.org/10.1016/j.energy.2018.12.144

Wang, Y., Lu, W., Zhang, Q., Liu, X., 2017. An Experimental Study of the Explosion Parameters of Vapor-Liquid Mixtures of Nitroethane/Air. Journal of Energetic Materials 35, 458–473. https://doi.org/10.1080/07370652.2016.1271838

Willauer, H.D., Ananth, R., Hoover, J.B., Mushrush, G.W., Williams, W., 2006. Methods of quantifying and mitigating aerosol fire and explosion hazards associated with low vapor pressure liquids 9.

Williams, A., 1990. Combustion of Liquid Fuel Sprays. Butterworth-Heinemann.

Williams, F.A., 1975. Recent Advances in Theoretical Descriptions of Turbulent Diffusion Flames,

in: Murthy, S.N.B. (Ed.), Turbulent Mixing in Nonreactive and Reactive Flows. Springer New York, Boston, MA, pp. 189–208. https://doi.org/10.1007/978-1-4615-8738-5_5

Wong, S.-C., Chang, J.-C., Yang, J.-C., 1993. Autoignition of droplets in nondilute monodisperse clouds. Combustion and Flame 94, 397–406. https://doi.org/10.1016/0010-2180(93)90122-J

Wu, F., Jomaas, G., Law, C.K., 2013. An experimental investigation on self-acceleration of cellular spherical flames. Proceedings of the Combustion Institute 34, 937–945. https://doi.org/10.1016/j.proci.2012.05.068

Wu, F., Pan, X., Wang, H., Hua, M., Yu, H., Zang, X., Jiang, J., 2022. Experimental study on the explosion characteristic and flame propagation of methanol spray at different injection pressures. Fuel 325, 124746. https://doi.org/10.1016/j.fuel.2022.124746

Wunsch, D., 2009. Theoretical and numerical study of collision and coalescence - Statistical modeling approaches in gas-droplet turbulent flows. Université de Toulouse.

Yao, J., Tanaka, K., Kawahara, A., Sadatomi, M., 2013. Performance Evaluation of an Air Assisted Atomizer with Liquid Siphon. Journal of Applied Sciences 13, 4985–4993. https://doi.org/10.3923/jas.2013.4985.4993

Yuan, L., 2006. Ignition of hydraulic fluid sprays by open flames and hot surfaces. Journal of Loss Prevention in the Process Industries 19, 353–361. https://doi.org/10.1016/j.jlp.2005.09.001

Yuan, S., Ji, C., Han, H., Sun, Y., Mashuga, C.V., 2021. A review of aerosol flammability and explosion related incidents, standards, studies, and risk analysis. Process Safety and Environmental Protection 146, 499–514. https://doi.org/10.1016/j.psep.2020.11.032

Yuan, S., Ji, C., Monhollen, A., Kwon, J.S.-I., Mashuga, C., 2019. Experimental and thermodynamic study of aerosol explosions in a 36 L apparatus. Fuel 245, 467–477. https://doi.org/10.1016/j.fuel.2019.02.078

Zabetakis, M.G., 1964. Flammability characteristics of combustible gases and vapors (No. BM-BULL-627). Bureau of Mines, Pittsburgh, PA (United States).

Zhang, L., Ma, H., Pan, J., Shen, Z., Wang, L., Liu, R., Zhao, K., 2019a. Effects of hydrogen addition on the explosion characteristics of n-hexane/air mixtures. International Journal of Hydrogen Energy 44, 2029–2038. https://doi.org/10.1016/j.ijhydene.2018.11.085

Zhang, L., Ma, H., Shen, Z., Wang, L., Liu, R., Pan, J., 2019b. Influence of pressure and temperature on explosion characteristics of n-hexane/air mixtures. Experimental Thermal and Fluid Science 102, 52–60. https://doi.org/10.1016/j.expthermflusci.2018.11.004

Zhou, C.Q., S. Fleeter, Houstis, E., Rice, J., 1999. Gas Turbine Spray Dynamics and Combustion Simulation Design. undefined.

Appendix A: Complementary information

LIQUID CLASSIFICATION

Table A-1: Oil fluid categories (Jespen, 2016)

Category	Definition
A	A flammable liquid that would evaporate quickly and significantly if released
B	Any flammable liquid that is not in category A but is handled at a high enough temperature to cause boiling on release
C	Any flammable liquid that is not in category A or B but can reach a temperature beyond its flash point or create a **flammable mist or spray** when released
G(i)	A methane-rich natural gas
G(ii)	Refinery hydrogen

HIGH-VOLTAGE SPARK IGNITION SYSTEM

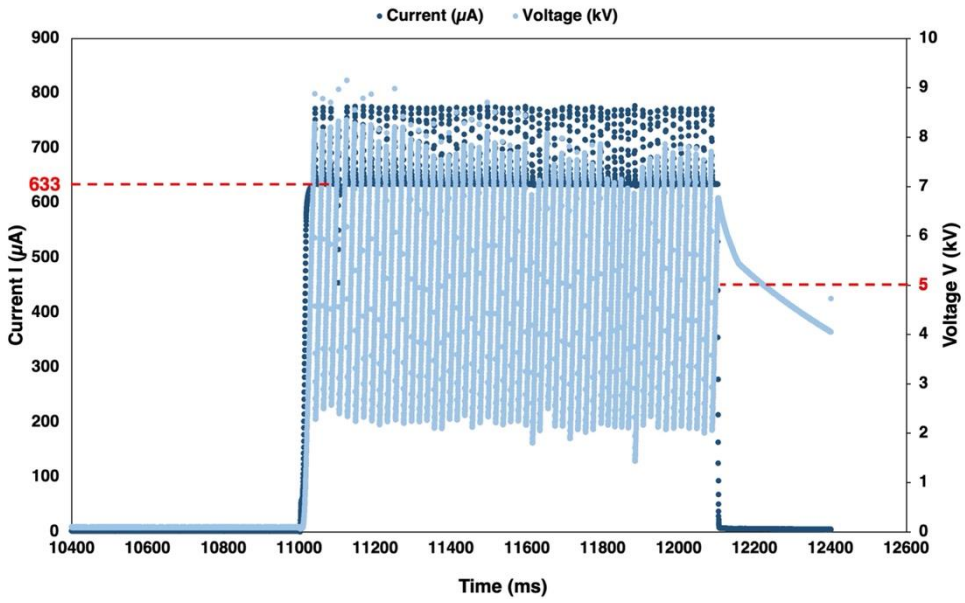

Figure A-1: Time evolution of the voltage and current during a long spark ignition

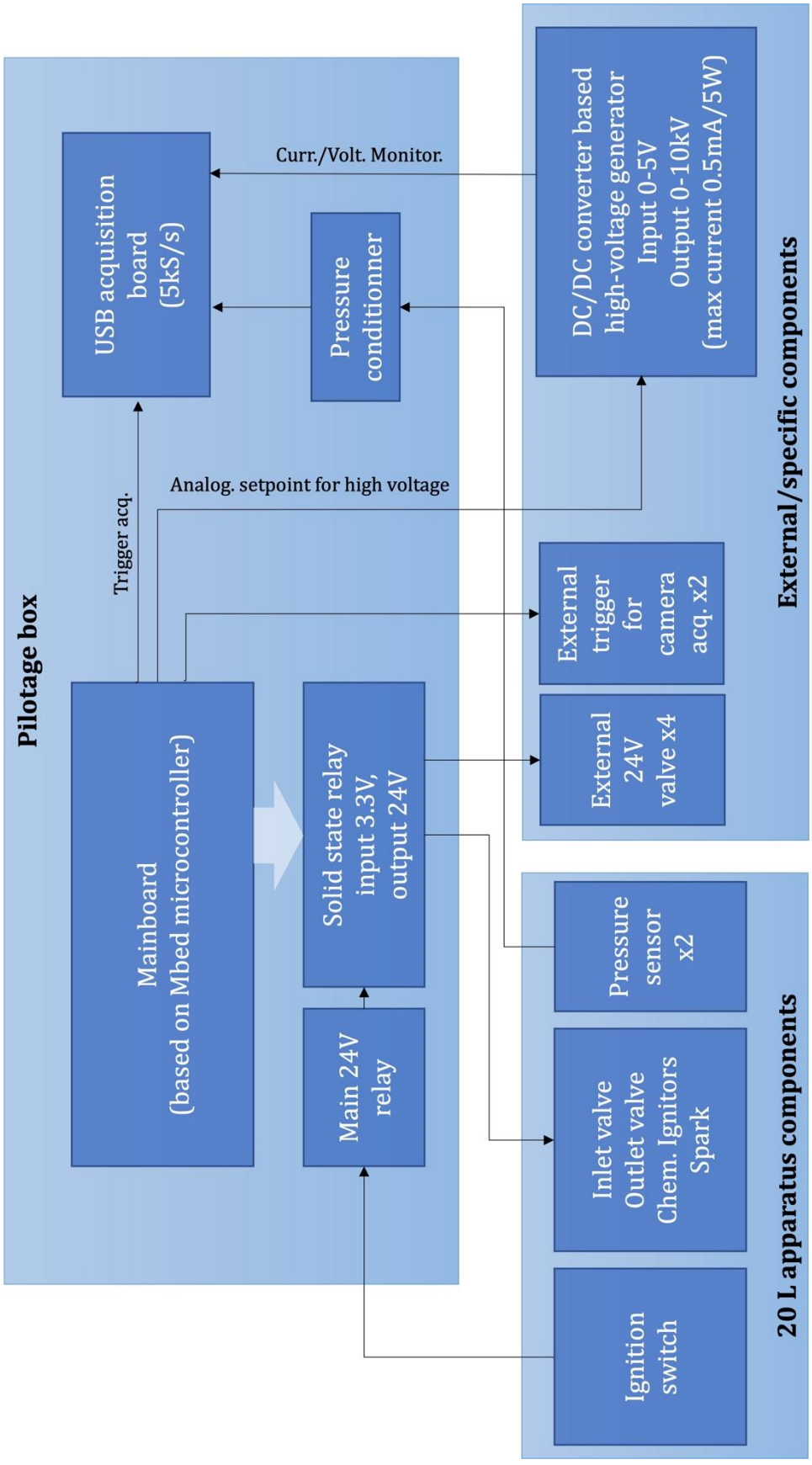

Figure A-2: Control scheme of the high-voltage spark ignition system and the control and data acquisition unit

PARTICLE IMAGE VELOCIMETRY

Table A-2: Calculated relaxation time per fluid and mass median diameter

	Relaxation time τ_s (ms)						
d_{50} (µm)	**Ethanol**	**Isooctane**	**Jet A1**	**Diesel B7**	**LFO**	**Biodiesel B100**	**Mobil DTE**
9	0.22	0.17	0.21	0.22	0.22	0.23	0.23
50	6.64	5.27	6.49	6.72	6.72	7.02	7.10
80	17.00	13.48	16.61	17.19	17.19	17.97	18.17

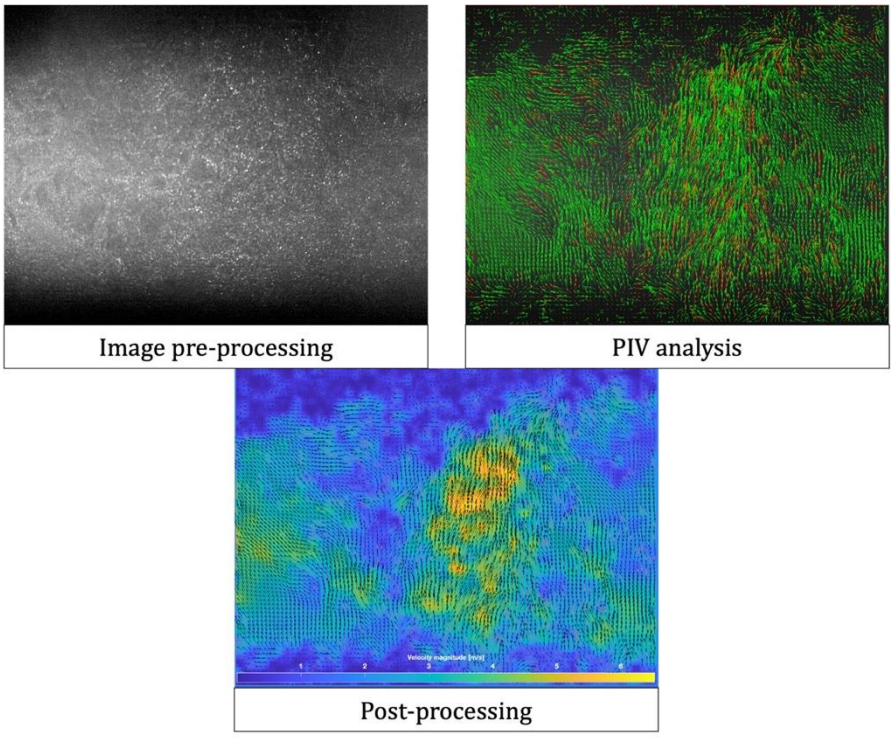

Figure A-3: Steps for the Particle Image Velocimetry analysis of illuminated ethanol droplets

THERMODYNAMIC PROPERTIES OF THE FUELS

Table A-3: Thermodynamic properties of the seven fuels

Fuel	Boiling point* (°C)	ΔH_{vap} (J.mol^{-1})
Ethanol	78	42300
Isooctane	99	35100
Kerosene Jet A1	130 - 300	50000
Diesel B7	163 - 357	53380
Light Fuel Oil	150 - 380	56290
Biodiesel B100	> 350	90000
Mobil DTE VG68	> 316	80000

* *Determined from fuels' MSDS*

INFLUENCE OF IGNITION ENERGY ON BIODIESEL MIST EXPLOSIVITY

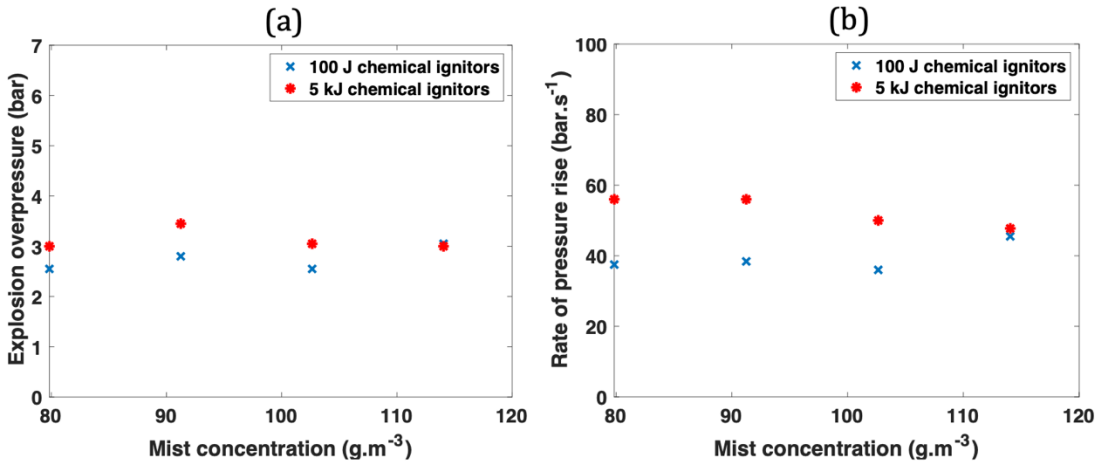

Figure A-4: Influence of the ignition energy on the explosion severity of biodiesel at T = 80 °C

USUAL SPRAY PERFORMANCE IN TWIN-FLUID NOZZLES

The table below presents supplementary information on the performance of a spray generated using twin-fluid spray nozzles. It was copied from the catalogue of the nozzles' supplier and should reflect the same behaviour as the mist generation system proposed in this study. Nevertheless, discrepancies may occur as the system as a whole was modified and the siphon and feed line distance may differ.

Table A-4: Spray performance considerations - copied from the Spraying Systems Co.® catalogue 76a

Nozzle characteristics	Increase in operating pressure	Increase in specific gravity	Increase in viscosity	Increase in fluid temperature	Increase in surface tension
Pattern quality	Improves	Negligible	Deteriorates	Improves	Negligible
Drop size	Decreases	Negligible	Increases	Decreases	Increases
Spray angle	Increases then decreases	Negligible	Decreases	Increases	Decreases
Capacity	Increases	Decreases	Full/hollow cone - increases flat - decreases	Depends on fluid sprayed and nozzle used	No effect
Impact	Increases	Negligible	Decreases	Increases	Negligible
Velocity	Increases	Decreases	Decreases	Increases	Negligible
Wear	Increases	Negligible	Decreases	Depends on fluid sprayed and nozzle used	No effect

ADDITIONAL FLAME PROPAGATION RESULTS

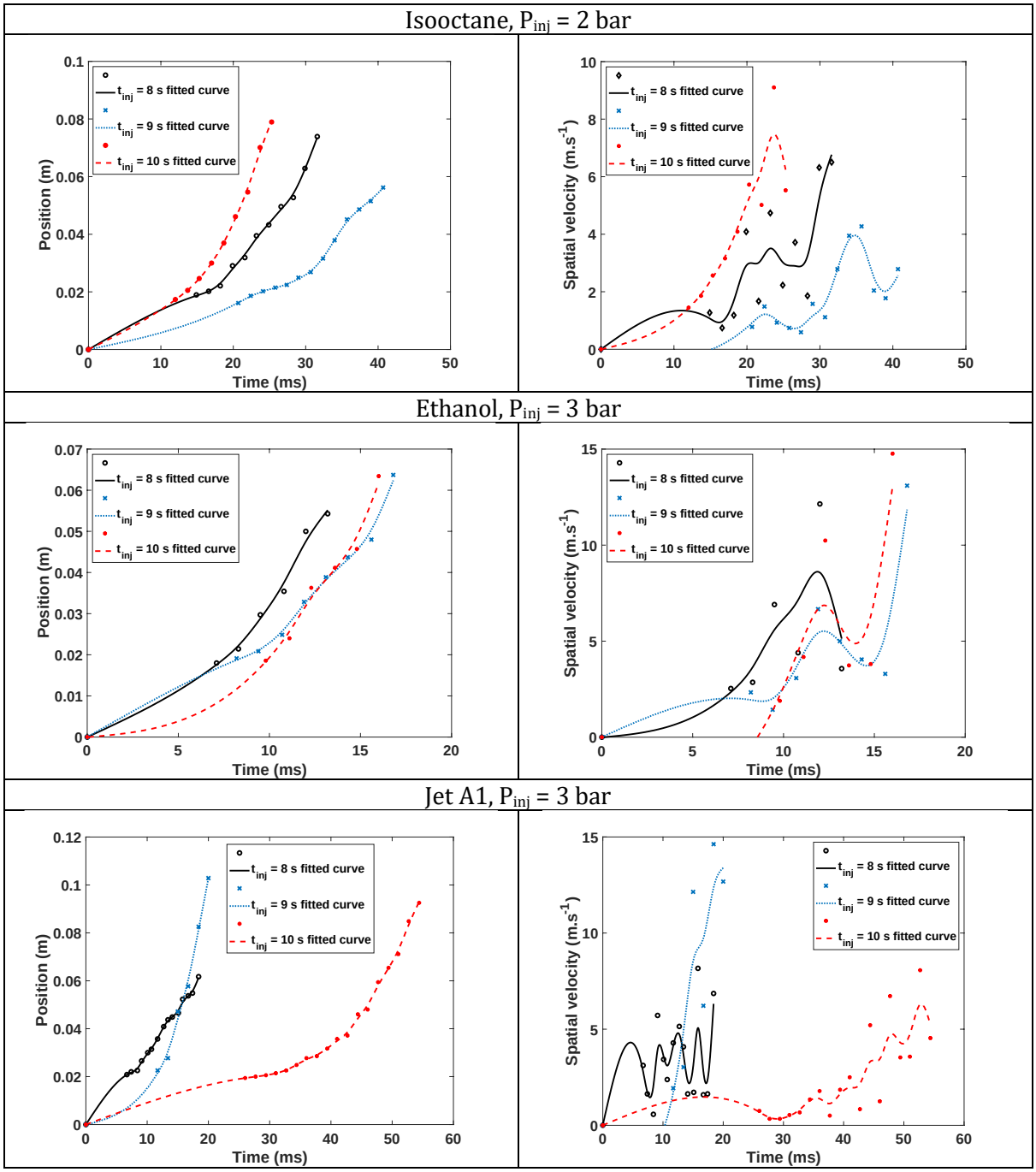

Figure A-5: Time evolution of the flame's position and spatial velocity for isooctane, ethanol, and Jet A1 mists generated with nozzle set N1 and ignited using 100 J spark ignition

LIQUID CLASSIFICATION EXAMPLE

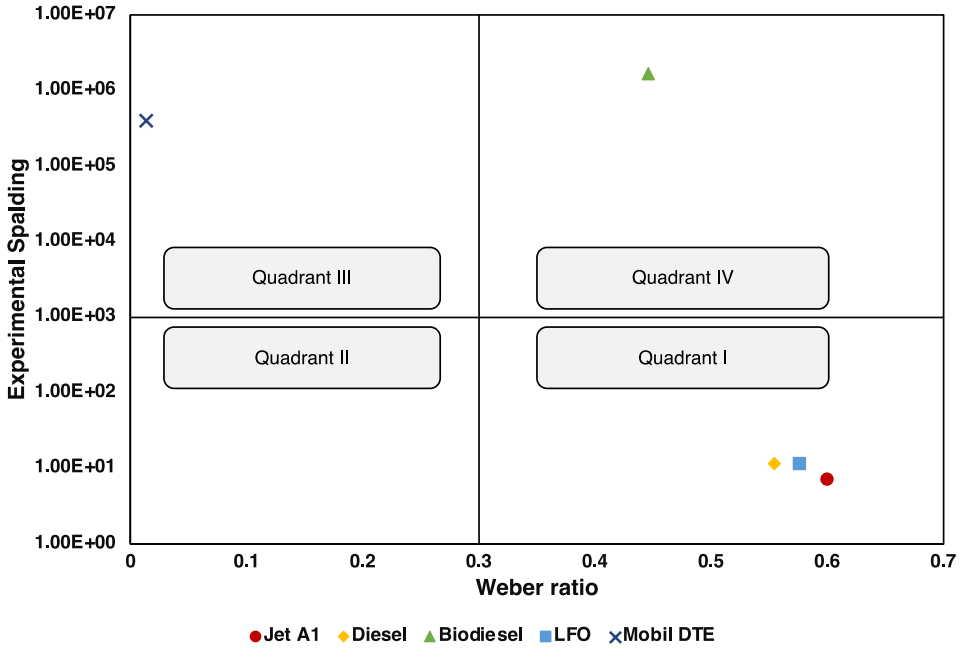

Figure A-6: Experimental Spalding number as a function of the Weber ratio for d_c = 1 cm and C_m = 100. g.m^{-3}

APPENDIX B:
EXPLOSION MODELLING

This work was performed on a pre-existing code developed by the LRGP during a master's internship in the framework of this study.

In an attempt to model mist explosions, a MATLAB program was developed to predict the explosion pressure-time evolution allowing the determining of P_{ex} and dP/dt_{ex} for a specific mist concentration. This was achieved by calculating the temperature increase due to exothermic reactions. The model was based on a perfectly spherical flame that propagates from the centre of the sphere towards the inner walls. The position of the flame front over time and the flame propagation velocity were calculated according to the model proposed by Dahoe and de Goey (2003). Some of the assumptions taken for this program were as follows:

- The thickness of the flame is equal to zero, meaning that the explosion model consists only of two zones: burnt and unburnt
- Heat is transferred from the flame to the medium via convection and radiation
- Heat is accumulated on the walls by conduction in an isotropic and homogeneous medium
- Heat transfer is unidirectional
- The emissivity of the droplets is constant and is equal to that of the flame
- The surface of the radiation emission is that of the flame and not the sum of the droplet surfaces

Four differential equations that govern the reaction system were the basis of the model, including flame heat balance, wall heat balance, the ideal gas law, and a conversion equation, detailed below (from equations B-1 to B-18). To estimate the reaction conversion rate, X, as a function of time, two models were selected and tested: a reaction limitation model based on the shrinking core mode used for dust explosions (equation B-10), and an evaporation model based on the d^2 law (equation B-9).

The MATLAB program was based on a combustion model governed by:

- ***Flame heat balance:***

$$\sum_{g,i} C_{v,i}\frac{dT}{dt} + m_{s,0}C_{p,s}(1-X)\frac{dT}{dt} = n_{s,0}\Delta H_{comb}\frac{dX}{dt} - hS_{flame}(T-T_{wall}) - \varepsilon\sigma\left(T^4 - T_{wall}^4\right) + \frac{EI}{\Delta t_{ignition}} \quad \text{B-1}$$

Where n_i is the number of moles, C_v and C_p, the heat capacities at constant volume and pressure,

respectively, S_{flame}, the surface of the flame, T_{wall}, the temperature of the sphere's wall, $n_{s,0}$ and $m_{s,0}$, the initial number of moles and mass of the fuel, X, the reaction conversion, ε, the emissivity, σ, the Stefan-Boltzmann constant, IE, the ignition energy, and $\Delta t_{ignition}$, the ignition duration.

- ***Wall heat balance:***

$$\frac{dT_{wall}}{dt} = \frac{\varepsilon\sigma\left(T^4 - T_{wall}^4\right) + hS_{int}(T - T_{wall})}{m_{sphere}C_{v,sphere}} \quad \text{B-2}$$

Where S_{int} is the internal surface of the sphere and $C_{v,sphere}$ and m_{sphere} are the heat capacity and mass of the sphere

- ***The ideal gas law:***

$$V\frac{dP}{dt} = d_g n_{s,0} RT\frac{dX}{dt} + n_g R\frac{dT}{dt} \quad \text{B-3}$$

Where d_g is the change in the quantity of gas during combustion, and n_g is the total number of gas moles in the sphere

- ***Conversion equation***

This equation was based either on the evaporation model (d^2-law of combustion) or the reaction limitation model, both presented below.

The evaporation model:

$$d^2 = d_0^2 - k_e t \quad \text{B-4}$$

$$d = \sqrt{d_0^2 - k_e t} \quad \text{B-5}$$

$$X = \frac{V_0 - V}{V_0} = \frac{d_0^3 - d^3}{d_0^3} \quad \text{B-6}$$

$$X = 1 - \frac{(d_0^2 - k_e t)^{3/2}}{d_0^3} \quad \text{B-7}$$

$$\frac{dX}{dt} = \frac{3}{2}k_e\frac{(d_0^2 - k_e t)^{1/2}}{d_0^3} \quad \text{B-8}$$

$$\frac{dX}{dt} = \frac{3}{2}\frac{k_e}{d_0^2}(1 - X)^{1/3} \quad \text{B-9}$$

The shrinking-core model:

$$\frac{dX}{dt} = \frac{4\pi r_0^2 k_{cin}}{n_{s,0}} (1-X)^{\frac{2}{3}} \left(\frac{n_{O2}}{V}\right)^n \quad \text{B-10}$$

Where V is the volume of the sphere, k_{cin}, the reaction rate constant, and n, the partial order of reaction for oxygen.

The conversion rate constants k_e and k_{cin} can be determined following the equations presented in Table B-1. To do so, the optimisation MATLAB function "*fminsearch*" was used to determine the activation energy and the pre-exponential factor if both rate constants were based on the Arrhneius equations, for instance.

Table B-1: Available equations that can be used to determine the conversion rate constants k_{cin} and k_e

Equations for k_{cin} (B-11)	**Equations for k_e (B-12,15)**
Arrhenius equation: $k_{cin} = A \exp\left(-\frac{E}{RT}\right)$	Arrhenius equation: $k_e = A \exp\left(-\frac{E}{RT}\right)$
	Linear equation: $k_e = A + ET$
	Sigmoid function: $k_e = \frac{A}{1+\exp(-ET)}$
	d² law: $k_e = 8\left(\frac{\lambda}{C_p \rho_l}\right)\ln\left(1+B_{h,v}\right)$

Where λ is the thermal conductivity, R, the universal gas constant, A, the pre-exponential factor, and E, the activation energy

The heat transfer coefficient and the flame radius are recalculated for each iteration. The flame radius is estimated using the model proposed by Dahoe and de Goey (2003). As for the heat transfer coefficient, it is determined using the Nusselt correlation (equation B-16) applied to an annular space.

$$Nu_{Dh} = \frac{hD_h}{\lambda} = 0.023 Re_{Dh}^{0.8} Pr^{\frac{1}{3}} \left(\frac{d_o}{d_i}\right)^{0.14} \quad \text{B-16}$$

Where d_o and d_i are the outer and inner diameters of the annular space (between the sphere and the flame), respectively

$$Pr = \frac{\mu C_p}{\lambda} \quad \text{B-17}$$

$$Re = \frac{\rho S_u D_h}{\mu} \qquad \text{B-18}$$

Where μ is the dynamic viscosity and S_u is the burning velocity

Figure B-1 depicts some modelling results for isooctane, ethanol, and Jet A1 mist explosions using the two conversion models proposed previously. As it can be seen, until now, the reaction limitation model delivers the closest pressure-time evolution to the experimental findings. This model was found more adequate for single component liquids of relatively high volatility. Nevertheless, improvements should be made by considering a tri-zone explosion model for instance. Indeed, as seen through the manuscript, the flame thickness is not negligible and should be taken into account when conducting calculations of the laminar burning velocity.

It can also be seen that the evaporation model did not present satisfactory results as the predicted pressure-time evolution was very far from the experimental one. Indeed, the various assumptions of the d2 law do not reflect a deflagration phenomenon of a mist cloud. First, as the droplet is treated as a constant source of single-component fuel vapour with a constant and uniform temperature, this make the d2 law less adequate for multi-component liquids. Moreover, it imposes the non-existence of heat and mass transfer within the droplet, which is not the case in real conditions. Second, assuming spherical symmetry removes convection; however, as seen in this study, the turbulence level and the effect of the initial temperature cannot be neglected. In addition, droplet-droplet interactions are not taken into consideration in this model, while coalescence has been clearly observed in DSD measurements.

Further investigation and improvements are required to better predict the explosion behaviours of mist clouds. An appropriate start would be to consider the multi-component nature of the liquids and to incorporate droplet-droplet interactions as the mist clouds are rather dense in the 20 L sphere and interactions are inevitable.

Isooctane – evaporation model	Isooctane – reaction model
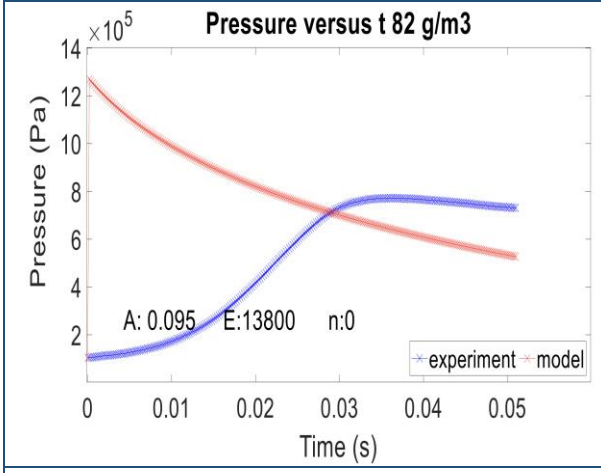	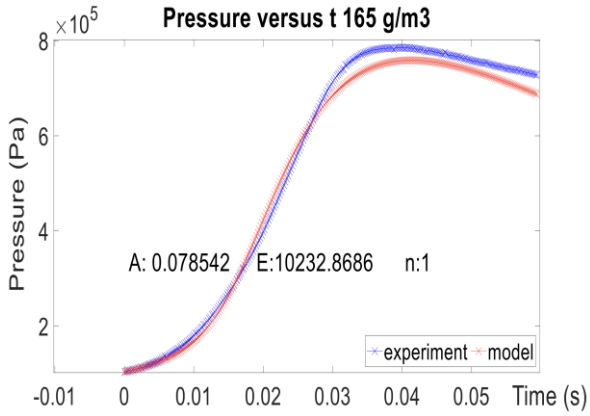
Ethanol – reaction model	**Jet A1 – reaction model**
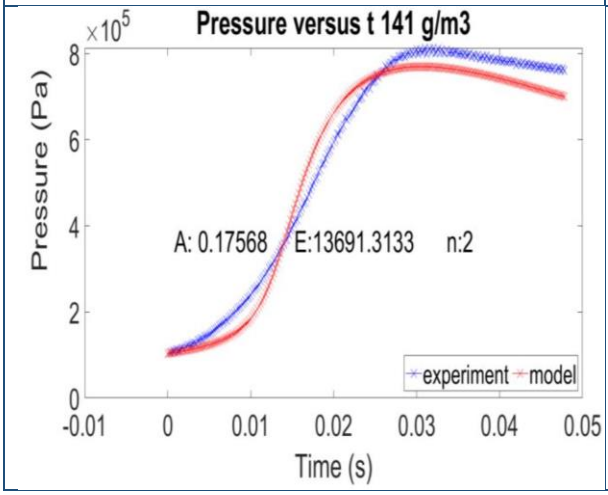	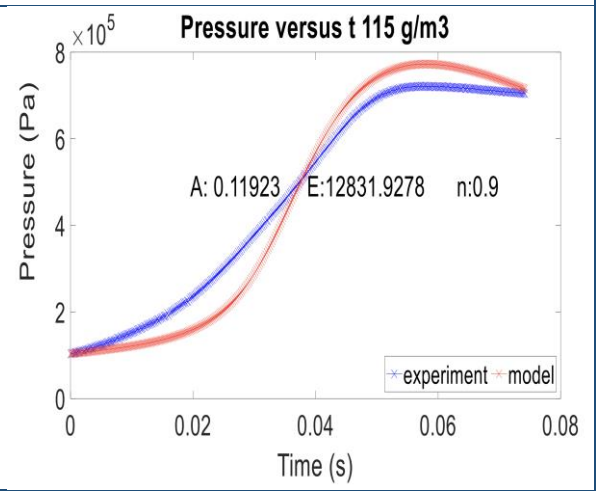

Figure B-1: Modelling results for isooctane, ethanol, and Jet A1 mist explosions using the evaporation and the reaction limitation models

Lifting the fog off fuel mist explosions:
a new procedure to determine the ignitability and explosivity of mist releases

---

Stephanie El-Zahlanieh